Biomedical Applications and Strategies using Boronic Acids

By

Thomas P. Smith

A dissertation submitted in partial fulfillment of

the requirements for the degree of

Doctor of Philosophy

(Chemistry)

at the

UNIVERSITY OF WISCONSIN–MADISON

2016

Date of final oral examination: December 12th, 2016

This dissertation is approved by the following members of the Final Oral Committee:

Ronald T. Raines, *Henry Lardy Professor of Biochemistry*, Biochemistry and Chemistry
Jennifer E. Golden, Assistant Professor, Pharmaceutical Sciences
Glen S. Kwon, *Jens T. Carstensen Distinguished Chair*, Professor, Pharmaceutical Sciences
Sandro Mecozzi, Associate Professor, Pharmaceutical Sciences and Chemistry
Regina M. Murphy, *Smith-Bascom Professor*, Chemical and Biological Engineering

Table of Contents

Abstract

Biomedical Applications and Strategies using Boronic Acids

Thomas P. Smith

Under the supervision of Professor Ronald T. Raines

at the University of Wisconsin–Madison

Boronic acids have been shown to interact with biological molecules including carbohydrates and reactive oxygen species (ROS). This variety of biological targets is due to the unique reactivity of boron that, within a physiological pH range, can adopt two electronically and structurally distinct forms that differ in Lewis acidity. This type of reactivity can be exploited for the design of novel biomedical tools and strategies for biological-based therapeutics.

The development of therapeutic proteins is generating considerable interest. This interest is due to the high selectivity of proteins for a target and the high enzymatic activity a protein-based therapeutic can possess. There are, however, a number of challenges that need to be met. The delivery of peptides and proteins to the site of action is notoriously difficult. This challenge is due, in part, to the difficulty of molecules of peptidic size and complexity to reach the site of action, primarily the cytosol of a cell, and still maintain function. Although there is considerable effort to develop better ways to facilitate uptake into the cytosol, many of these strategies have

serious limitations related to toxicity or physiological stability.

In chapter 2, I describe the development of a discreet, small-molecule boronic acid-based delivery strategy for the delivery of native protein into the cytosol of a cell. This was accomplished by appending a specialized boronic acid directly to solvent-exposed lysine residues of a protein of interest via an immolative linker possessing esterase sensitivity. The boronic acid, benzoxaborole, has enhanced affinity for the non-reducing saccharides that are prevalent on the surface of a cell. By increasing the number and affinity of interactions with the cell surface, this strategy was shown to significantly improve cellular uptake of both green fluorescent protein (GFP) and a cytotoxic variant of RNase A. Most importantly, these boronic acid appendages are quantitatively cleaved when exposed to endosomal and cytosolic esterases, releasing completely native, unmodified protein.

Another challenge with biologic therapeutics is overcoming the potential pleiotropic nature of the particular protein or enzyme. This challenge is explicit in the use of angiogenin (ANG) as a potential treatment of amyotrophic lateral sclerosis (ALS). ANG has been shown to be a powerful neuroprotectant and recovery agent in mouse models for ALS. Nonetheless, treatment with wild-type angiogenin can also promote undesired angiogenesis and tumor growth in the systemic system.

In chapter 3, I highlight a specific masking strategy that silences the catalytic activity of ANG under normal physiological conditions. When exposed to reactive oxygen species (ROS) leading to oxidative stress, this mask is removed, and catalytic activity is reconstituted. Oxidative stress is a key component in a number of disease states including cancer, cardiomyopathy, inflammation, diabetes, and many neurodegenerative diseases.

In ALS, the up-regulation of ROS in the central nervous system (CNS) is primarily

responsible for the motor neuron degeneration characteristic of the disease. The presence of a boronic acid-masking agent engenders ANG with pro-drug characteristics, which not only expands the potential use of this protein as a therapeutic for ALS, but also offers a novel way of fine-tuning enzyme activity in a controlled fashion.

Boronic acids have also been utilized as important functional groups in medicinal chemistry. For example, Velcade® (bortezomib), is a first-in-class boronic acid-containing protease inhibitor and the first boronic acid drug to be approved by the FDA. Another potential target is the homotetrameric protein transthyretin (TTR). The misfolding of TTR leads to amyloid fibril formation in the peripheral nervous system or cardiac tissue, leading to several known human amyloidogenic diseases. Current treatment for TTR amyloidosis requires a high-risk and costly liver transplant to remove the primary source of a deleterious TTR variant. Alternative strategies use small-molecules to stabilize the TTR quaternary structure and thereby preventing fibril formation.

In chapter 4, I discuss the development and characterization of a targeted library of small-molecule boronic acids that bind to the thyroxin (T_4) binding pockets and strongly inhibit fibril formation in both wild-type and a common disease variant, V30M–TTR. Structural data has shown that two molecules from this library bind in a covalent fashion with polar residues within the T_4 binding pocket. These are the first boronic acids to interact covalently with a non-catalytic residue within a protein-binding site and opens new avenues for the use of boronic acids in the design of small-molecule therapeutics.

Acknowledgements

There are many without whom this body of work would not have been possible. Foremost among them, I want to thank my advisor, Professor Ronald Raines. I am grateful for the unquestionable freedom and opportunity that Ron as provided to do research, which has allowed me to pursue my scientific interests, no matter the directions they may have taken. It was very rare that Ron ever told me "no". I am also thankful for the highly collaborative lab environment that Ron encourages. This setting has allowed me to easily reach out to and seek advice from many different experts who were always just down the hall. For these reasons, I don't think there is another place where I could have so confidently pursued challenging and exciting research projects.

I would like to acknowledge my immediate collaborators within the Raines group whose unparalleled support and patience has allowed many of my core projects to come to full fruition. In particular, I would like to thank Dr. Kristen Andersen and Dr. Trish Hoang for their constant help and willingness to carry more than their fair share of the effort. I would also like to thank Ian Windsor not only for his extensive collaborative help, including multiple road-trips to Argonne National Laboratory, but also for his friendship through the years. I am also deeply grateful to Professor Katrina Forest for her helpful insights and constructive criticisms in regards to our ambitious pursuits in structural biology.

I sincerely thank the members of my thesis committee for their time and support. Thanks very much to Professor Jennifer Golden, Professor Glen Kwon, Professor Sandro Mecozzi, and

Professor Regina Murphy for their invaluable insights and allowing me to drop-in from time to time. Thanks also to my undergraduate research advisors Professor Sherry Chemler, Professor Mark Kristal, and Professor Gabriella Popescu, who all played important roles in my scientific development and independence. I still appreciate many of the lessons from those early forays into basic research. Very special thanks to Professor Richard Cheng who saw the potential in a wayward philosophy student who accidently took his honors organic chemistry class, and convinced me that chemistry is a far more engaging subject of study.

I would also like to thank the former colleagues who were instrumental in making sure I was off to a good start early in my graduate career. I am grateful to Dr. Mike Palte, who was not only one of the first people to welcome me into the Raines lab, but also for taking me under his wing and introducing me to the unique research opportunities associated with boronic acids. I will always appreciate the deep scientific conversations that we had, and continue to have, up to this day. I am also thankful to Dr. John Lukesh who was a constant presence early on and always made sure I never got into anything over my head. I would also like to extend my thanks to Aubrey Ellison, Dr. Robert Newberry, Dr. Çağlar Tanrikulu, and Dr. James Vasta for their support and friendship.

I would also like to acknowledge the world-class staff at the UW–Madison. I would first like to thank Dr. Mark Anderson of the NMRFAM, who not only got me out of trouble a couple of times, but was always willing to pass along helpful advice concerning “life, the universe, and everything”. I also have deep gratitude for Dr. Martha Vestling and Dr. Stephanie Knezz of the mass spectrometry facility in the UW–chemistry department. Mass spec characterization of boronic acids, especially free boronic acids, is very challenging. Despite many obstacles, which

pushed their skills and the equipment to the limit, Martha and Stephanie always pulled through for me.

Thanks very much to the chemistry department and the graduate school, especially Arietta Clauss, Kat Myhre, and Karen Stephens for all of their help and administrative assistance. I also need acknowledge the support staff in the biochemistry department including Julie Kennedy and Brenda Renaud, who constantly made sure that things ran smoothly, as well as Robin Davies and Laura Vanderploeg in the media lab, who always made it a priority that I had a polished product.

Last but certainly not least, I thank my friends and family from outside the lab for their unwavering support though all of the highs and lows of graduate school. I would not have been able to weather the storms without you.

List of Figures

List of Schemes

List of Tables

1

Modern boradeption: Boronic acid as a dynamic functional group for biomedical applications

1.1 Abstract

Boronic acids are small-molecule Lewis acids that can adopt two structurally and electronically distinct forms. This unique property has led to near ubiquitous adoption of boronic acids throughout the fields of chemistry and chemical biology. More recently, boronic acids have gained momentum as an important functional group in medicinal and pharmaceutical chemistry. Researchers are borrowing principles from diverse fields such as molecular recognition, analytical chemistry, and saccharide- and ROS-sensing, to develop functionalized boronic acids as alternative delivery, targeting, and activating agents for small-molecule therapeutics and biopharmaceuticals. Herein, I present a brief overview of the development of boronic acids as transport and delivery agents for therapeutic molecules.

1.2 Introduction

Boronic acid was first synthesized and isolated by Frankland in the mid-19th century[1] and characterized by Loland, Edwards, and others in the mid-20th century.[2-4] Since that time, boronic acids have become almost ubiquitous in many areas of chemistry. This widespread adoption is due to its unique properties. Structurally, boronic acid is sp^2-hybridized with a single B–C bond and two B–OH bonds to fill out the valence. As such, boronic acid has six valence electrons and an empty *p*-orbital that lies perpendicular to the plane of the molecule.

Despite its name, a boronic acid is not a Brønsted–Lowry acid in the same sense as its carbon analog, a carboxylic acid. The empty *p*-orbital instills the boron center with Lewis acidic character, which can accept electrons from a Lewis base, such as water. This leads to a conversion from a neutral, sp^2-hybridized species to an anionic, sp^3-hybridized species and releases a proton. Accordingly, this transformation is pH-dependent; at a pH greater than the pK_a of the boronic acid, the tetravalent form predominates (Scheme 1.1).[5]

At more alkaline pH, boronic acids have been found to readily interact with 1,2- and 1,3-cis diols to form stable 5- and 6-membered boronate esters.[3,6,7] The stability of the boronate ester is also pH- and solvent-dependent. At a pH lower than the pK_a of the boronic acid, the trivalent boronate is the prominent species. Due to increased ring strain, the boronate ester will hydrolyze back to the free boronic acid (Scheme 1.1).[7] The trivalent form of both the free acid as well as the boronate ester can coordinate water and release a proton. In many cases, the boronate ester is considered more acidic than the free acid.[5,8]

The exact mechanism as to how boronic acids react with diols to form boronate esters is still under investigation. Effective boronic acid–diol interaction is now generally believed to be dependent on a number of factors including steric strain, the pK_a of both the boronic acid and the

diol of interest, and the pH of the solution.[5,7-11] Attempts have been made to describe optimal binding conditions, but many exceptions defy any observed trends.[8,11,12]

Although mechanistic details are still being debated, empirically, this selective and dynamic diol–boronic acid interaction has led to an incursion into subfields of supramolecular chemistry,[13-15] including saccharide sensing,[16] analytical separations,[17-19] drug delivery,[20,21] materials science,[22] and molecular recognition.[23,24] Boronic acids have also earned a special place in medicinal chemistry due to their low toxicity and ability to coordinate with Lewis basic amino acids such as serine. Small-molecule boronic acids have been developed as transition-state protease and proteasome inhibitors, as well as anti-cancer and anti-bacterial agents.[25-28] A new and promising application of boronic acid is the cellular delivery of large macromolecules. In particular, boronic acids are being developed to facilitate the internalization of protein-based biopharmaceuticals across biological membranes.

1.3 Challenges faced by biopharmaceuticals

Nature has developed efficient and selective mechanisms for the bi-directional transport of ions, small molecules, peptides, and proteins across cellular membranes.[29, 30,31] These active and passive transport processes are crucial for maintaining homeostasis and allowing cellular communication and protection.[29] The development of artificial transporters to move molecules across biological membranes has both academic and clinical interest; such transporters not only aid the study of cellular function, but also allow for the effective delivery of therapeutic molecules to the site of action, primarily the cytosol of the cell.[31]

The high therapeutic value of biopharmaceuticals is based on their specific mechanisms of action, high potency, low dosing, and the opportunity for replacement therapy. Still, the delivery

of protein-based therapeutics to a site of action is notoriously difficult.[32-35] Proteins are structurally diverse and complex molecules that are easily hydrolyzed and metabolized *in vivo,* leading to poor bioavalibility.[33] Additionally, the natural immune response from the body could potentially neutralize the protein therapeutic and, in some cases, negatively affect the patient. Finally, due to their large size and hydrophilic nature, protein therapeutics are often unable to easily cross biological membranes.[32-35]

Efforts to design strategies to overcome challenges associated with protein delivery and stability are ongoing. Current approaches to alter or mask the physical properties of a biologic to improve pharmacokinetic attributes such as bioavailability and cellular uptake typically include cationic peptides,[36] liposomes,[37] polyethyleneimine derivatives,[38] nanoparticles,[39] dendrimers,[40,41] and antibody- or viral-based methods.[42,43] Many of these strategies possess inherent limitations, including instability, off-site reactivity, toxicity, immunogenicity, or poor bio-degradability.[32,44,45] Boronic acids offer an alternative approach to current delivery and protecting strategies that avoids many of these pitfalls.

1.4 Boradeption: Boronic acid as an artificial membrane transporter

In 1982, Henson and coworkers discovered that under certain conditions, insoluble boronic acid functionalized reporter molecules, such as *m*-dansylamido phenylboronic acid (**1.1**), could be solubilized in buffered solution at neutral pH (Figure 1.1). These hydrophobic molecules were found to be taken up by living cells and stained different cellular components.[46] These authors coined this process "boradeption" to signify *boronic acid-dependent phase transfer of water-insoluble agents.*[46-48]

The "boronate-carrying buffer" typically contained a "receptor" agent, such as

diethyanolamine (DEA), known to complex with boronic acids. The authors hypothesized that the boronic acid–DEA adduct allowed the molecule to become more hydrophilic overall, possibly due to the charged tetravalent boronate. The proposed mechanism involves contact of the boronate complex with the cell surface, leading to dissociation and transfer of the free boronic acid into the lipid regions of the cell membrane and leaving the "carrier buffer" behind (Scheme 1.2). This approach offers a mild and non-toxic alternative to "shocking" cells with high levels of organic solvent in order to deliver insoluble, hydrophobic molecules.

These authors believed that this strategy could be used to produce reagents to stain living cells, as well as to solubilize and deliver drugs, enzyme substrates, heavy metal containing organic molecules, and radioactive reagents.[46] Structural modification to install a linker sensitive to enzymatic cleavage between a cargo of interest and boronic acid was hypothesized to allow for selective cleavage and the subsequent release of the cargo from the boronic acid-carrier agent. Many of these predictions have now been realized, and in some cases, have led to distinct areas of research that will be touched upon throughout this thesis.

1.4.1 Boronic acid-mediated transport through bulk liquid membranes

There is considerable interest in developing efficient transporter systems to deliver therapeutic molecules into living cells.[31] The complex and highly heterogeneous nature of the cell membrane has, however, made studying the mechanism of boronic acid-mediated transport challenging. After the concept of boradeption was introduced, a number of research groups looked to study this mechanism in detail using artificial bulk liquid membranes (BLM).[17,49]

This simplified system uses a "U-tube" apparatus for the study of solute movement through an organic solvent, usually dichloroethane (DCE), which is flanked by two buffered

aqueous phases. These aqueous phases serve as "departure" and "receiving" points for the molecule being transported (Scheme 1.3). BLM experiments are easy and inexpensive to operate but require an excess of material and suffer from low reproducibility.[49]

Shinbo and co-workers were the first to use BLMs to study boronic acid-mediated transport of monosaccharides.[50] Instead of using a "carrier buffer" containing DEA, the aim was to transport the saccharide-boronate ester itself. In this initial study, the boronic acid investigated is the prototypical phenylboronic acid (**1.2**). Monosaccharides were added to the departure phase, and the pH of the system was maintained at 10 to facilitate boronate ester formation. Because the tetravalent form of the boronate was believed to exist at high pH, the transfer catalyst trioctylmethylammonium chloride (TOMA–Cl) was also added to both aqueous phases to provide an ammonium co-transport ion.

Under these conditions, a number of reducing monosaccharides were successfully transported from the departure phase, across the BLM, and then extracted from the receiving phase. The rate at which these saccharides were transported are as follows: fructose > mannose > galactose > glucose. This trend is due to the increased stability of the boronic acid–saccharide complex wherein boronate esters formed with syn-periplanar 1,2-diols are considerably more favorable.[5,16,51,52] A similar observation was made for non-reducing *p*-nitrophenyl glycosides in which the rate of transport was determined to be: *cis*-α,γ-diol > *cis*-α,β-diol > *trans*-α,γ-diol >> *trans*-α,β-diol.[53]

In the absence of TOMA–Cl or when the pH of the system was acidified, no saccharide transport was observed. This result suggests that the primary transport pathway utilizes an "ion-pair" mechanism via the tetravalent boronate (Scheme 1.3 b). This ion-pair mechanism of boronic acid-mediated transport was also determined for other biologically relevant molecules,

including ribonucleosides,[54-56] catecholamines,[57,58] sialic acid derivatives,[59] amino acids,[60,61] as well as galacto- and glucopyranosides.[62-65]

An alternative mechanism, in which transport is mediated by the neutral trigonal boronate, was also proposed (Scheme 1.3a).[53,64] This mechanism was suggested based on the observation that a small amount of glucoside transport occurred using compound **1.2** at neutral pH and in the absence of TOMA. The rate of transport was only 4-fold faster than baseline diffusion when the boronic acid transporter was absent. Yet, the same experiment in the presence of TOMA saw a 25-fold increase in transport rate. Although seemingly unimpressive, these studies are significant in that they show it is possible to achieve boron-mediated transport without a co-transporting agent such as TOMA.

This result prompted the development of structurally diverse boronic acids that can form net-neutral, lipophilic complexes to transport biomolecules effectively at a physiologically relevant pH. One of the first attempts to design an independent boronate-transporter was done by Smith and coworkers. Their initial aim was to complex a sodium ion with a crown ether for co-transport with the boronate ester.[62,63]

Their model utilizes a "cleft" linker between the boronic acid and the crown ether (**1.3**), which positions the sodium ion ~5.5 Å from the boron center. This strategy was proven successful in transporting *p*-nitrophenyl *β*-D-glucopyranoside at a rate of 2-fold above baseline diffusion at pH 6.3. This rate is considerably less than that of the PBA-TOMA system, which had a 21-fold increase in transport under the same conditions. Decreased transport efficiency could be due to design limitations including steric occlusion of the monosaccharide and the placement of the sodium counter-ion too far from the boron center.

Interestingly, a change in the linker leading to compound **1.4** led to both an efficient and selective strategy to transport the neurotransmitter dopamine.[57] This selectivity comes from simultaneous interactions between the boronic acid and catechol motif, and between the crown ether and primary amine on dopamine. These interactions lead to a net-neutral complex that does not need a co-transporting ion. This transporter shows significant preference for dopamine (160-fold rate increase) and norepinephrine (60-fold rate increase) over other catecholamines such as epinephrine due to the crown ether affinity for primary amines.

Czarnick and coworkers expanded upon this idea to develop *N*-alkylated pyridine boronates.[55] These molecules exist as a zwitterionic species under neutral conditions, with pK_a values of 4 and 8. This new class of boronate transporters was able to transport nucleosides effectively at pH 6.5.[55] The best transporter, compound **1.5**, contained a cholanyl group and was found to transport uridine 140-fold faster than passive diffusion. The TOMA–Cl system only showed a 17-fold increase in transport rate. Structural modeling suggests that this rate enhancement might be due to additional hydrophobic interactions between the cholanyl group and the uridine. Other versions of this transporter used a smaller alkyl tail and still showed up to a 110-fold increase in transport rate.[55]

1.4.2 Boronic acid-mediated transport through artificial lipid bilayers

Additional experiments were performed to study boron-mediated transport through artificial bilayers using liposomes.[66-68] The rationale for studying transport across a lipid bilayer is that liposomes are also being developed as potential delivery agents.[37] As such, efficiently transporting a therapeutic molecule out of its liposome carrier would be desirable. Smith and coworkers were able to show that boronic acids **1.4** and **1.5** were able to transport

monosaccharides, glucopyranosides, and nucleosides selectively and effectively in both directions across liposomal membranes. Interestingly, this transport process is believed to occur via the reversible trivalent boronate pathway (Scheme 1.3a).

This conclusion is based on the observation that the addition of different lipophilic cations did not affect influx or efflux rates of glucose at neutral pH.[66,67] The neutral pH is significant because boronic acids **1.4** and **1.5** have pK_a values of 7.4 and 7.2, respectively, which would lead to an equilibrium of trivalent and tetravalent forms of the boronate. Previously, with BLM experiments, transport rates were highly dependent on the presence of a co-transport ion. This result suggests that the mechanism of transport is context dependent.

1.5 The role of boronic acid in protein delivery systems

As stated previously, there are many potential delivery strategies that have been explored for the intracellular delivery and release of both small-molecule and protein therapeutics. More recently, there has been interest in dendritic and micelle forming complexes due to the ease of chemical functionalization and subsequent cargo loading.[45] In many cases, boronic acids have been structurally incorporated into these systems as "smart" technology to engender a stimuli-responsive release mechanism. The stimuli correspond to different physiological contexts, such as pH,[69-71] saccharide,[72-75] and reactive oxygen species (ROS) sensitivity.[76] Most of these examples involve encapsulating small-molecule therapeutics to improve pharmacokinetic properties through release under a particular physiological condition.

Boronic acid is typically employed as a "handle" for reversible attachment of additional delivery and micelle forming components such as lipids, dendritic polymers,[77-80] nanoparticle cores,[73,81] PEGylated co-polymers,[70,82-84] or ligands for receptor-mediated uptake[85] via a

boronate-catechol complex. When a micelle or other therapeutic carrier containing a therapeutic of interest encounters a change in the environment, such as a decrease in pH, the boronate-catechol complex will dissociate. This process leads to the break-up of the micelle and release of the therapeutic cargo.

1.5.1 Boronic acid-protein conjugates for cellular delivery

There are relatively few examples of using a boronic acid to "decorate" a protein of interest as a direct boronic acid-protein conjugate. Pillay and Arriatti published one of the first examples of protein conjugate formation with a boronic acid.[86] These authors were able to reversibly coordinate DNA fragments to the surface of human serum albumin (HSA) via a boronic acid linker. This boronic acid was attached covalently to the protein surface via peptide coupling with solvent-exposed carboxylates. More recent examples utilize a bioconjugated boronic acid as a handle for further modification with either a lipid[76] or dendritic polymers[77] that encapsulate and protect a protein from its extracellular environment.

This approach requires the attachment of the boronic acid directly to the surface of the protein via now routine bioconjugation techniques.[87,88] Although the extra delivery components can be removed with a decrease in pH, the boronic acid itself is attached covalently to the protein surface, usually through non-specific conjugation. Since protein function is highly sensitive to such changes in structure,[88] any viable delivery or masking strategy must be reversible or traceless in nature, delivering only native protein.

Gois and co-workers have recently published an interesting way to label proteins reversibly with boronic acids for additional functionalization and bioconjugation. These researchers developed small-molecule boronic acids that can target surface-exposed lysine

residues and form stabilized imines that are not prone to hydroyisis.[72,85,89] These boronic acids can be functionalized with different components such as fluorescent tags, azides for click chemistry, or folic acid for folate receptor-mediated uptake.[85] These boronic acid appendages can be removed in the presence of fructose, which has a high affinity for boronic acid, or the intracellular reducing agent glutathione (GSH). This strategy has also been employed to selectively label N-terminal cysteine residues of peptides via a thiazolidino boronate complex.[90]

1.5.2 Targeting boronic acids to the cell surface-glycocalyx

Boronic acids can also be used as the main functional group to facilitate cellular uptake by interaction with glycans present on the cell surface.[91-93] In 1980, Hageman and coworkers were one of the first groups to target the cell surface with a boronic acid.[94] This group targeted fluorescent boronic acid **1.1** to the surface of bacterial cells. Evidence of boronate ester formation was confirmed by adding a competitive binder such as mannitol, which leads to a drastic decrease in fluorescence.

This idea was expanded to target cargo-carrying liposomes to the cell surface.[95] The incorporation of phenylboronic acid linked phospho-lipids into liposomes allows for the encapsulation of a reporter agent or therapeutic. The free boronic acid on the liposome surface initiates cell-surface recognition. These investigators hoped to target the glycocalyx of red blood cells, where enhanced interactions with the cell surface would lead to a lipid fusion event that delivers fluorogenic or therapeutic cargo. Although this fusion strategy worked *in vitro* between two liposomal carriers,[96,97] these experiments failed to produce viable therapeutic delivery *in cellulo*. Even though high-affinity binding was observed between the liposome and cell surface, the liposomal carrier was positioned too far from the surface for a fusion event to occur.[95]

Currently, a similar strategy that uses a specialized boronic acid known as benzoxaborole (**1.8**) is being explored. This type of boronic acid was first described by Torssell in 1957[27] and then characterized further by Hall and coworkers in the mid-2000's and found to have higher affinity for the non-reducing saccharides prevalent in the glycocalyx.[98-100] This enhanced affinity is believed to be due in part to the intramolecular 5-membered ring, which both depresses the pK_a of the boronic acid to 7.4 and also pre-organizes the tetravalent form of the boronic acid.[98]

Raines and co-workers have exploited this enhanced affinity for non-reducing glycosides and have shown that boronic acid **1.8** conjugated to the surface of RNase A enhanced cellular uptake.[93] Aida and co-workers also showed that boronic acid **1.8** can be incorporated into larger nanocarrier systems for efficient delivery.[92] In chapter two, I describe an expansion on this strategy to develop a discreet and modular boronic acid for the traceless delivery of protein into cells.

1.6 Outlook for boronic acid-mediated delivery

Boronic acids compose a very unique functional group that has been shown to have important roles in a variety of biomedical applications. Boronic acids have been utilized as transport agents for small organic molecules as well as important structural components in therapeutic nanocarrier systems. In addition, specialized boronic acids are currently being developed for improved recognition of complex carbohydrates and biomarkers present within the glycocalyx.[23,24,100,101]

Researchers are utilizing multidentate boronic acids on peptide or polymeric backbones to achieve unprecedented selectivity not only for monosaccharides, but also for bi- and tri-saccharides. This new class of boronates, known as borolectins, are being optimized for

enhanced affinity for antigens associated with cancer such as sialic acid,[102] Lewis X,[103] and Thomsen-Friedenrich (TF) antigen.[104,105] It is not hard to imagine that the next generation of protein delivery strategies will incorporate borolectins for improved cell-type specificity.

1.7 Boronic acid as a chemoselective trigger

The potential of boronic acid in biomedical research is only just being realized. In addition to forming stable and reversible complexes with biologic polyols, boronic acids are also known to be oxidized chemoselectively by the reactive oxygen specie (ROS) hydrogen peroxide (H_2O_2).[106,107] This mechanism, known as "hydroboration oxidation", has also been well developed as a stimuli-responsive trigger for sensing and drug release applications.

ROS, including H_2O_2, are important biomolecules utilized by the cell for both protection and communication.[106,107] Endogenous antioxidant enzymes such as the peroxiredoxin class of enzymes, are important regulators of intercellular ROS concentrations.[107] An accumulation of ROS leads to conditions of oxidative stress that can be deleterious to cellular function.[107] Oxidative stress is associated with many different disease states including cancer,[108,109] neurodegenerative disorders,[110] diabetisis,[111] and inflammation,[111] as well as physical trauma.[112] Because of the potential causative role of ROS in many different disease conditions, significant research has been conducted to develop selective probes for ROS.[106] This strategy has also been adopted for prodrug activation.[113-117]

In chapter 3, I describe our design of a new type of biologic prodrug that exploits the chemoselectivity of boronic acid for H_2O_2. We have developed a boronic acid–angiogenin conjugate for the selective neuroprotection of astroglial cells under disease conditions. This

strategy could be geared to the targeted treatment of neurodegenerative diseases such as amyotrophic lateral sclerosis (ALS).

1.8 Small-molecule boronic acid-based therapeutics

There is no shortage of small-molecule boronic acids that have been designed for therapeutic proposes. In fact, new molecules that contain boronic acid functional groups with therapeutic potential are published on almost a weekly basis. Currently there are two boronic acid based drugs that have been approved by the FDA (Figure 1.2).

Boronic acids have been known for a long time to act as transition state mimics of hydrolytic enzymes, particularly of serine proteases.[25,26,118] Arguably, the most famous boronic acid therapeutic is the dipeptide proteasome inhibitor bortezomib (Velcade®) (**1.9**).[119] Bortezomid is the first boronic acid proteasome inhibitor to be approved by the FDA and is currently used to treat multiple myeloma.[120] Recently, the FDA also approved the anti-fungal AN2690 (Kerydin®) (**1.10**), and there are additional compounds in clinical trials for the treatment of psoriasis as well as African sleeping sickness.[27] There are currently small-molecule boronic acids being developed as anti-bacterial, anti-viral, and anti-cancer agents[27, 28,120,121] as well as inhibitors of β-lactamase that could combat bacterial resistance to β-lactam drugs such as penicillin.[122,123]

In chapter 4, I describe the synthesis and characterization of a small library of boronic acid-functionalized stilbenes for the treatment of transthyretin amyloidosis. Unlike many of the current examples of boronic acid therapeutics that target activated residues within a catalytic active site, we instead target serine residues in a non-catalytic binding site in order to engender enhanced protein stability. This work offers a new perspective in the design of small-molecule

boronic acid-based therapies.

The potential biomedical applications of boronic acids are broad. In chapter 5, I discuss some future directions associated with a few of the developments described above. In addition, much of how boronic acid behaves *in vivo* is relatively unknown. I propose a couple of experiments, which may help further describe the pharmacokinetic attributes of boronic acid such as distribution and metabolism.

Scheme 1.1

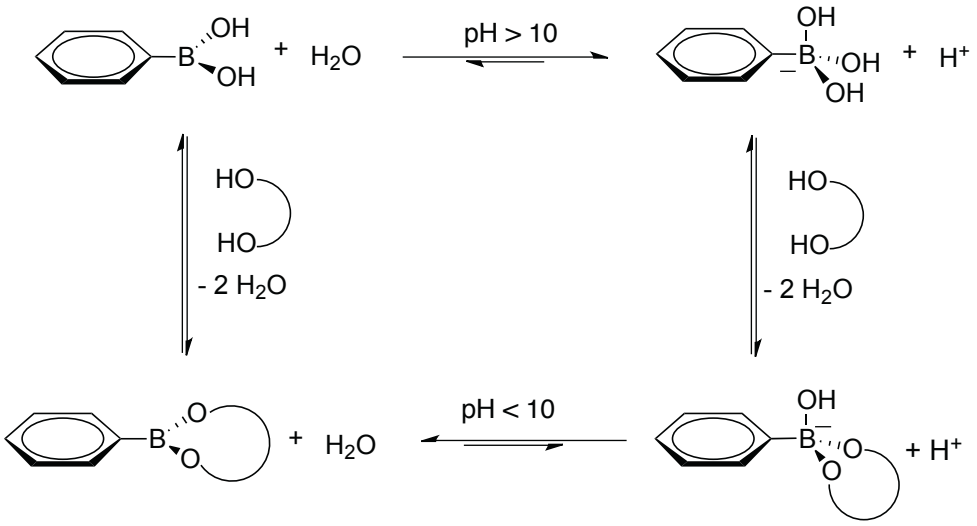
OH
B
OH
+ H2O
pH > 10
OH
B
OH
OH
+ H+
HO
HO
- 2 H2O
HO
HO
- 2 H2O
O
B
O
+ H2O
pH < 10
OH
B
O
O
+ H+

Scheme 1.1 Boronic acid equilibrium with polyols is a complex process dependent on factors including the pK_a values of the boronic acid and the diol as well as the pH of the solution.

Scheme 1.2

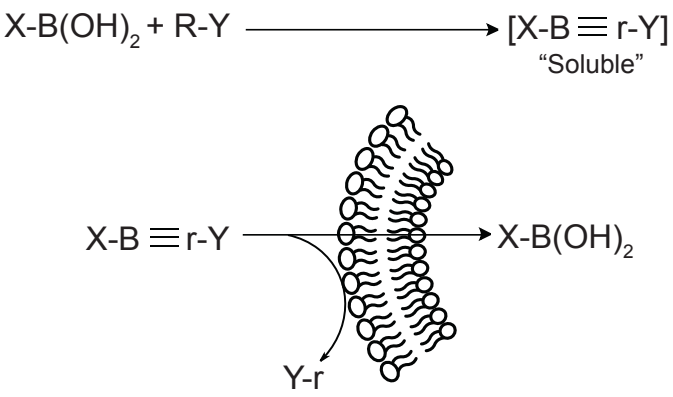

Scheme 1.2 Proposed mechanism of boronic acid-mediated transport of insoluble molecules via boradeption.

Scheme 1.3

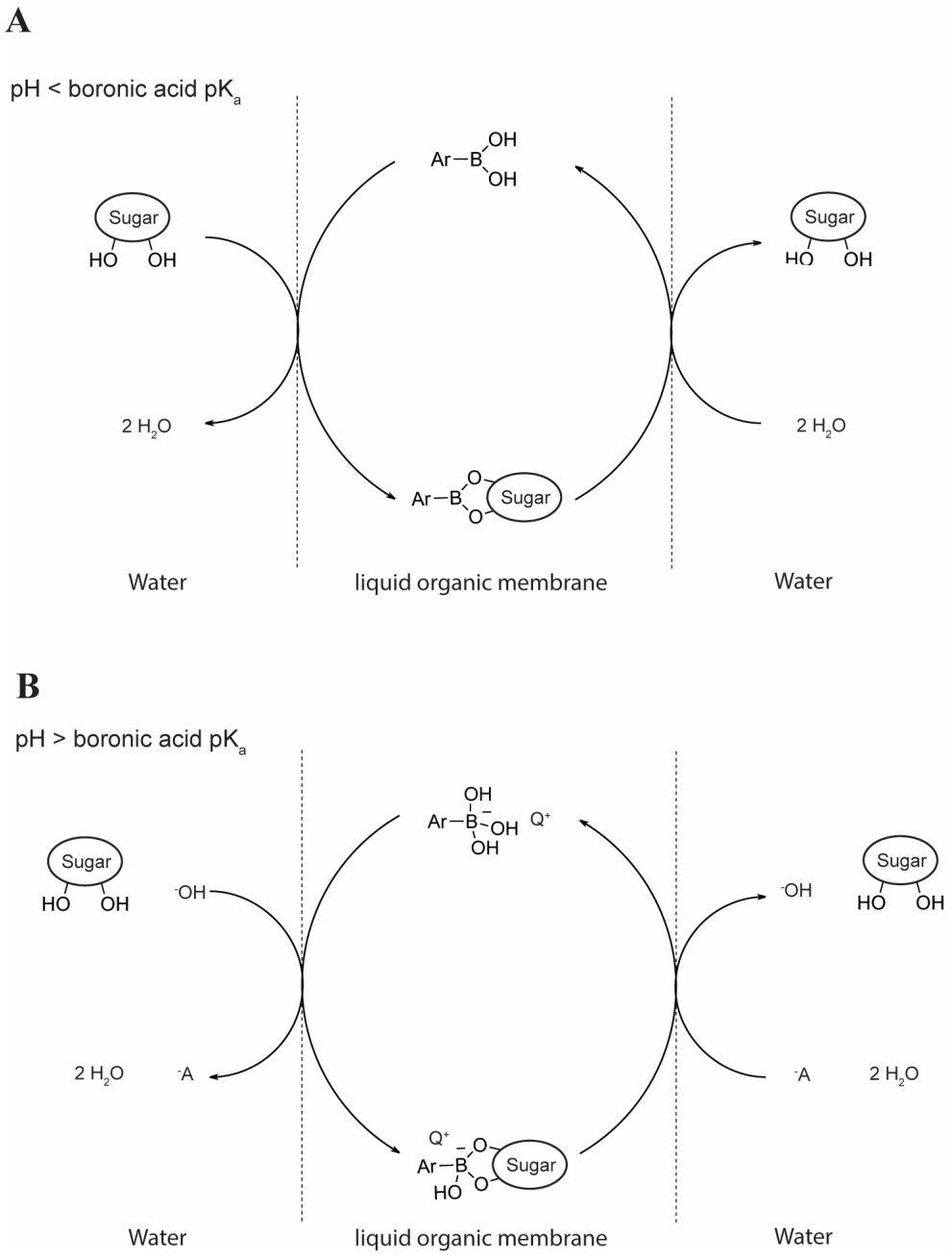
A
pH < boronic acid pK$_a$
Ar—B(OH)$_2$
Sugar
HO OH
2 H$_2$O
Ar—B(O)$_2$Sugar
Water
liquid organic membrane
Water
B
pH > boronic acid pK$_a$
Ar—B$^-$(OH)$_3$ Q$^+$
Sugar
HO OH
$^-$OH
2 H$_2$O
$^-$A
Q$^+$ Ar—B(O)$_2$(HO)Sugar
Water
liquid organic membrane
Water

Scheme 1.3 Proposed mechanisms of boronic acid mediated transport across bulk liquid membranes. (A) At pH lower than the pK_a of the boronic acid, the neutral trivalent boronate will transport a diol-containing molecule. (B) At higher pH, the tetravalent boronate with the aid of a lipophilic cation will transport a diol-containing molecule.

Figure 1.1

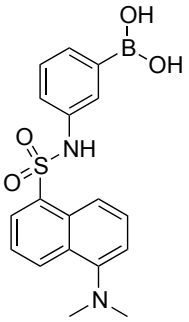

1.1

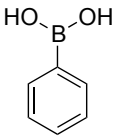

1.2

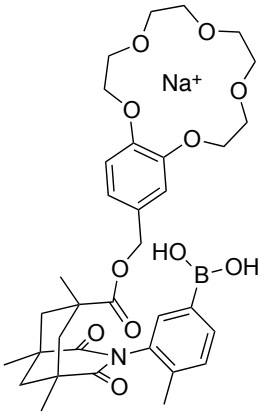

1.3

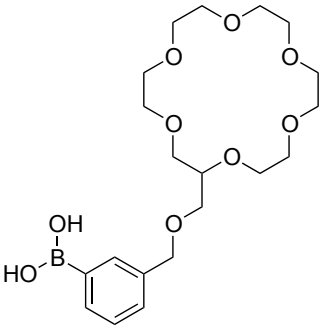

1.4

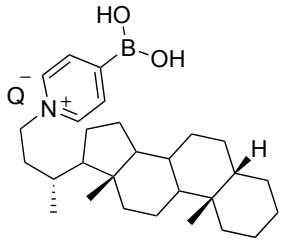

1.5

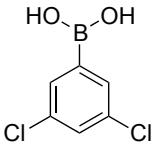

1.6

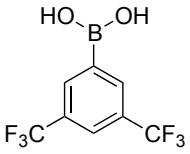

1.7

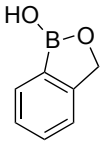

1.8

Figure 1.1 Boronic acids for the transport of biomolecules across artificial and natural membranes.

Figure 1.2

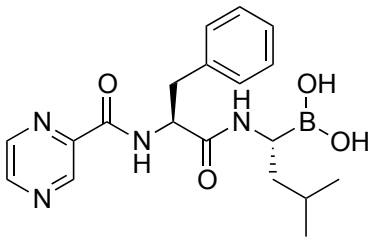

1.9

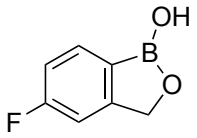

1.10

Figure 1.2 FDA approved boronic acid therapeutics, bortezomib (Velcade®) (**1.9**) and AN2690 (Kerydin®) (**1.10**).

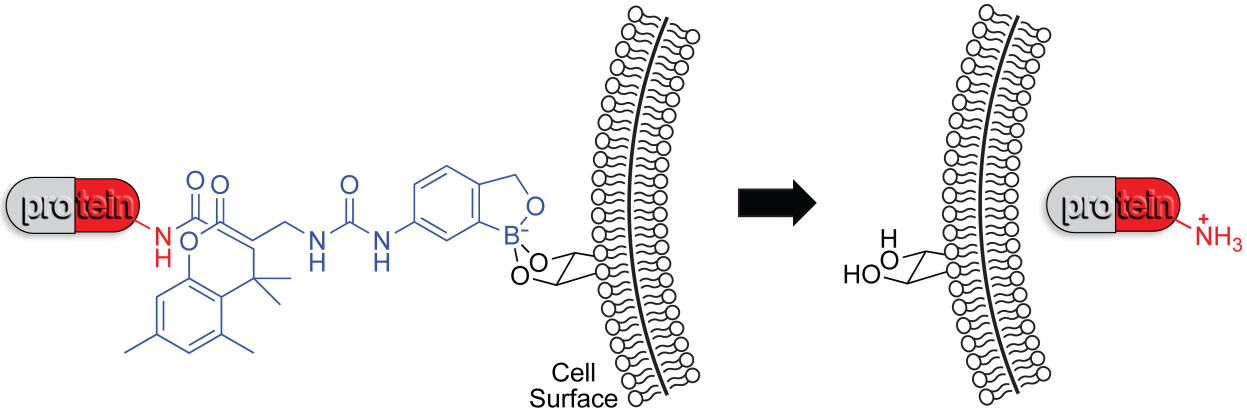
protein
N
H
O
O
O
N
H
N
H
B
O
O
Cell
Surface
H
O
HO
protein
NH3

2

Boronic acid for the traceless delivery of proteins into cells*

2.1 Abstract

The use of exogenous proteins as intracellular probes and therapeutic agents is in its infancy. A major hurdle has been the delivery of native proteins to an intracellular site of action. Herein, we report on a compact delivery vehicle that employs the intrinsic affinity of boronic acids for the carbohydrates that coat the surface of mammalian cells. In the vehicle, benzoxaborole is linked to protein amino groups via a "trimethyl lock". Immolation of this linker is triggered by cellular esterases, releasing native protein. Efficacy is demonstrated by enhanced delivery of green fluorescent protein and a cytotoxic ribonuclease into mammalian cells. This versatile strategy provides new opportunities in chemical biology and pharmacology.

2.2 Author Contributions

K.A.A., T.P.S., and R.T.R. conceived the project and designed the experiments. T.P.S. designed, synthesized, and characterized the organic compounds and protein conjugates. K.A.A. designed and performed the *in cellulo* assays and confocal microscopy. J.E.L. provided protein substrate. K.A.A., T.P.S., and R.T.R. analyzed data and wrote the manuscript.

*This chapter has been published, in part, under the same title. Reference:

Andersen, K. A.; Smith, T. P.; Lomax, J. E.; Raines, R. T. *ACS Chemical Biology* **2016**, *11*, 319–323.

Highlighted in ACS Chemical Research in Toxicology (February 28, 2016).

ACS Chemical Research in Toxicology **2016**, *29,* 134–135.

2.3 Introduction

The delivery of proteins and other macromolecules to an intracellular site is made difficult by cellular membranes.[32] Extensive efforts have led to the development of effective delivery systems that invoke cell-penetrating peptides,[36,124-127] antibodies,[128] ligands for natural receptors,[129] dendrimers,[40] functionalized polymers,[130,131] liposomes,[132] or nanoparticles,[133,134] and even enable targeting to sub-cellular organelles.[135,136] Nonetheless, extant strategies often inflict proteins with low biological activity,[87,88,93,130] instability in a physiological context,[137,138] or immunogenicity *in vivo*,[139,140] or employ vehicles that are recalcitrant to biodegradation.[44]

Boronic acids are physiologically benign Lewis acids that react spontaneously and reversibly with 1,2- and 1,3-diols to form five- and six-membered cyclic boronic esters, respectively.[5,141] The dynamic covalent bonding of boronic acids/esters can facilitate the delivery of cargo into cells, which are coated with a diol-rich glycocalyx. To exploit that attribute, polymers, nanoparticles, and noncovalent assemblies have been decorated with phenylboronic acid and other arylboronic acids.[21,27]

Recently, we showed that boronic acids can be advantageous when conjugated *directly* to a protein.[93] The ensuing formation of transient boronate esters with the glycocalyx enhances cellular delivery. To date, this approach has relied on the irreversible modification of a target protein, with ensuing compromises. For example, our previous work installed boronic acids by the irreversible amidation of enzymic carboxyl groups, which led to the loss of 83% of catalytic activity.[93] An ideal delivery system based on boronic acids (or, indeed, any moiety) conveys native cargo, and is thus “traceless”.

We sought to use a boronic acid and an immolative linker to promote the delivery of native proteins into a cell. As a boronic acid, we chose 2-hydroxymethylphenylboronic acid

(benzoxaborole), which has higher affinity than does phenylboronic acid for the glycopyranosides that are abundant in the glycocalyx.[27,93,98] As an immolative linker, we chose the *o*-hydroxydihydrocinnamic acid derivative known as the trimethyl lock (TML). After being triggered, the TML exhibits extremely high lactonization rates to release a cargo of interest (Scheme 2.1).[142-146] The TML has been used for a wide variety of applications in chemistry and pharmacology,[147] but not as an immolative linker on a protein. We chose ester hydrolysis as the means to trigger lactonization of the TML, as esterases are abundant inside, but not outside, of human cells[148-150] and underlie the action of numerous prodrugs.[151] We equipped our TML scaffold with an *N*-hydroxysuccinimide ester for chemoselective conjugation to amino groups,[88] such as those at the N terminus and on the side chain of lysine residues, which have a ~6% abundance in proteins.[152] Thus, our delivery vehicle (B-TML–NHS ester) has three modules: benzoxaborole, an esterase-activated TML linker, and an NHS ester (Figure 2.1a).

2.4 Results and Discussion

We synthesized B-TML–NHS ester convergently in 10 steps by extending a known procedure.[153] Then, we characterized its ability to enhance the cellular internalization of green fluorescent protein (GFP) (Scheme 2.2), which has distinctive fluorescence and an inability to enter mammalian cells.[154] Overnight incubation at ambient temperature with 100-fold excess of B-TML–NHS ester in 3:1 PBS/acetonitrile yielded 3 ± 1 labels per protein (Figures 2.1b and Figure 2.2). The number of labels in the B-TML–GFP conjugate did not decrease after a month of storage in PBS (Figure 2.3), consistent with the stability observed for other TML conjugates.[155-157] Labeling was, however, “bioreversible”. Incubation with a lysate from Chinese hamster ovary (CHO) K1 cells removed all of the labels from B-TML–GFP (Figure 2.1b).

Next, we compared the uptake of B-TML–GFP and unlabeled GFP by CHO K1 cells. After a 4-h incubation, we observed a dramatic increase in the cellular uptake of B-TML–GFP (Figure 2.1c). The fluorescence in microscopy images was largely punctate, suggesting that B-TML–GFP was taken up via an endosomal pathway (Figure 2.1d). Co-localization of this bright punctate staining with a stain for transferrin was consistent with this conclusion (Figure 2.4). After a 24-h incubation, the fluorescence intensity had increased significantly beyond the level measured at 4 h, indicating that the conjugate was stable in the presence of serum, which was a component of the cell-culture medium (Figure 2.5).

To confirm that the boronic acid moiety was responsible for the difference in cellular entry, we performed two control experiments. First, we modified GFP with a vehicle (Ac-TML–NHS ester) that lacks the benzoxaborole functionality (Figure 2.1a), yielding a level of labeling similar to that from B-TML–NHS ester (Figure 2.2c). When incubated with cells for 4 h, Ac-TML–GFP was taken up comparably to unlabeled GFP rather than to B-TML–GFP (Figures 2.1c and 2.1d). These data indicate that the enhanced delivery upon treatment with B-TML–NHS ester is not due to the mere modification of lysine residues or to interactions with the TML portion of B-TML. Next, we repeated the cellular uptake experiments with B-TML–GFP in the presence of fructose, which has a K_a of 336 M^{-1} for benzoxaborole.[93] We observed a significant decrease in GFP uptake in the presence of fructose, apparent with both confocal microscopy and flow cytometry (Figures 2.6a and 2.6b). Again, these data indict the boronic acid portion of B-TML–GFP as being responsible for cellular uptake.

Finally, we sought to test the efficacy of B-TML as a delivery vehicle to the cytosol. To do so, we employed an enzymic cytotoxin—the G88R variant of ribonuclease A, which must reach cytosolic RNA to manifest its toxic activity.[158,159] After labeling the ribonuclease by the

same procedure used to label GFP, we observed an average of 1.6 ± 0.7 labels per molecule of protein (Figure 2.7). This lower labeling is consistent with GFP (19 lysine residues) having more amino groups than does the ribonuclease (12 lysine residues). Again, we found that the labeling was bioreversible, as incubation with a CHO K1 cell lysate removed all of the labels (Figure 2.8). Finally, we assayed the ability of B-TML–ribonuclease and unlabeled ribonuclease to inhibit the proliferation of K-562 cells, which are derived from a human myelogenous leukemia line. We found that the pendant boronic acids resulted in a decrease in the IC_{50} value (Figure 2.9), indicative of more cytotoxin reaching the cytosol.

2.5 Conclusions

We conclude that covalent modification of proteins with B-TML–NHS ester can increase their ability to enter mammalian cells. Importantly, this modification is bioreversible. The irreversible modification of a protein can compromise its utility.[87,88,93,130,137-140] In contrast, endogenous cellular enzymes revert modification with B-TML.

The bioreversibility of our delivery vehicle provides new opportunities. The sulfhydryl groups of cysteine residues have long been used for this purpose because their mixed disulfides suffer reduction within the cytosol.[160,161] Recently, we found that appropriately tuned diazo compounds can esterify protein carboxyl groups, providing a second type of bioreversible modification.[162,163] In this work, we report on a bioreversible modification of protein amino groups that is distinct from others[72,76,164] in its being removable by an enzyme-catalyzed reaction. With its traceless utility in promoting cellular uptake, B-TML–NHS ester provides new opportunities in chemical biology and pharmacology.

2.6 Acknowledgements

We are grateful to I. Ç. Tanrikulu (University of Wisconsin–Madison) for technical advice. K.A.A. was supported by a predoctoral fellowship from the PhRMA Foundation and Molecular and Cellular Pharmacology Training Grant T32 GM008688 (NIH). J.E.L. was supported by a National Science Foundation Graduate Research Fellowship. This work was supported by grants R01 GM044786 and R01 CA073808 (NIH), and made use of the National Magnetic Resonance Facility at Madison, which is supported by Grant P41 GM103399 (NIH), and the University of Wisconsin Carbone Cancer Center, which is supported by Grant P30 CA014520 (NIH).

2.7 Materials and Methods

2.7.1 General Information

All chemicals were from Sigma–Aldrich (Milwaukee, WI) and were used without further purification. All glassware was flame-dried, and all reactions were performed under an atmosphere of N_2(g). Reagent grade solvents, *i.e.*, dichloromethane (DCM), tetrahydrofuran (THF), triethylamine (TEA), and dimethylformamide (DMF), were dried over a column of alumina and were accessed under an atmosphere of N_2 (g). The removal of solvents "under reduced pressure" refers to the use of a rotary evaporator with water-aspirator pressure (<20 torr) and a water bath of <40 °C. Column chromatography was performed with Silicycle 40–63 Å silica (230–400 mesh); thin-layer chromatography (TLC) was performed with EMD 250-μm silica gel 60-F254 plates. PBS contained Na_2HPO_4 (10 mM), KH_2PO_4 (1.8 mM), NaCl (137 mM), and KCl (2.7 mM) at pH 7.3. All procedures were performed at room temperature (~22 °C) unless noted otherwise.

^{1}H and ^{13}C NMR spectra were acquired at ambient temperature with a Bruker Avance III 500i spectrometer at the National Magnetic Resonance Facility at Madison (NMRFAM) and referenced to residual protic solvent. Electrospray ionization (ESI) mass spectrometry of small molecules was performed with a Micromass LCT in the Mass Spectrometry Facility in the Department of Chemistry at the University of Wisconsin–Madison. Matrix-assisted laser desorption ionization–time-of-flight (MALDI–TOF) mass spectrometry of proteins was performed with a Voyager DE-Pro instrument at the Biophysics Instrumentation Facility at the University of Wisconsin–Madison. Absorbance measurements were made with an infinite M1000 plate reader from Tecan (Männedorf, Switzerland). Confocal microscopy was performed with an Eclipse TE2000-U laser scanning confocal microscope from Nikon (Tokyo, Japan), equipped with an AxioCam digital camera from Zeiss (Jena, Germany). Flow cytometry was performed at the University of Wisconsin–Madison Carbone Cancer Center Flow Cytometry Facility with a FACS Calibur instrument from BD Biosciences (San Jose, CA). Cytometry data were analyzed by using the program FlowJo 8.7 from Treestar (Ashland, Oregon). Calculations were performed with Prism version 6 software from GraphPad Software (La Jolla, CA).

2.7.2 Chemical Synthesis

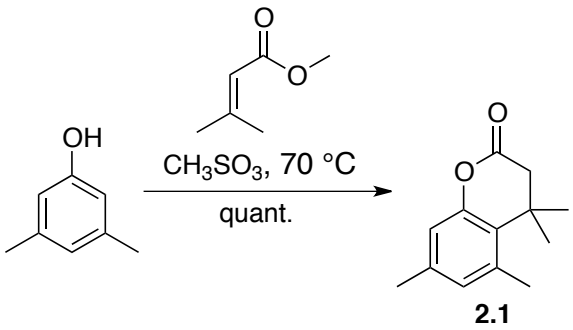

2.1

3,5-Dimethylphenol (5.0 g, 40.9 mmol) was dissolved in methanesulfonic acid (10 mL). Methyl-3,3-dimethylacrylate (5.61 g, 49.1 mmol) was added, and the resulting solution was heated to 70 °C for 24 h. The reaction mixture was then allowed to cool to room temperature and poured into separating funnel with 250 mL of water. The mixture was then extracted with ethyl acetate (3 × 100 mL). The organic layer was washed with saturated aqueous $NaHCO_3$ followed by brine. The organic layers were combined and dried over $NaSO_4$(s). The solvent was removed under reduced pressure and the crude product was purified by chromatography on a column of silica gel (2:8 EtOAc/hexanes) to afford **2.1** as an off-white solid (7.6 g, 92%).

^{1}H NMR (500 MHz, $CDCl_3$, δ): 1.45 (s, 6H), 2.27 (s, 3H), 2.46 (s, 3H), 2.60 (s, 2H), 6.83 (d, J = 6.86 Hz, 1H), 6.99 (d, J = 6.85 Hz, 1H); **^{13}C NMR (125 MHz, $CDCl_3$, δ)**: 16.28, 23.10, 27.63, 35.35, 45.61, 124.56, 127.98, 129.10, 129.49, 133.54, 149.75, 168.43; **HRMS** (ESI) calculated for $[C_{13}H_{16}O_2]^+$ $(M+NH_4)^+$ requires m/z 222.1489; found m/z 222.1486

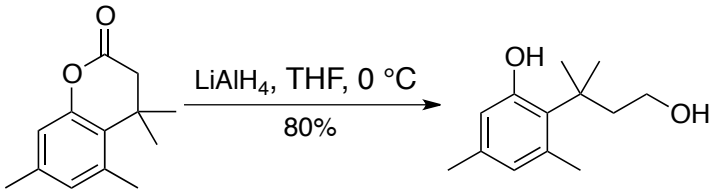

2.1 **2.2**

Compound **2.1** (3.5 g, 17.1 mmol) was dissolved in anhydrous THF (20 mL). The resulting solution was added dropwise to a suspension of $LiAlH_4$ (0.971 g, 25.6 mmol) in anhydrous THF (170 mL) that had been cooled to 0 °C. The reaction mixture was allowed to warm to room temperature and stirred overnight. The reaction was quenched by the slow addition of ethyl acetate (20 mL) followed by the slow addition of water (20 mL). The mixture was filtered to remove the aluminum salts, and the filtrate was dried over $NaSO_4$(s). The solvent was removed under reduced pressure, and the crude product was purified by chromatography on a column of silica gel (4:6 EtOAc/hexanes) to afford compound **2.2** as a colorless oil (2.8 g, 80%).

^{1}H NMR (500 MHz, $CDCl_3$, δ): 1.45 (s, 6H), 2.18 (s, 3H), 2.22 (t, *J* = 7.12 Hz, 2 H), 2.48 (s, 3H), 3.59 (t, *J* = 7.11 Hz, 2H), 5.31 (s, 1H), 6.59 (d, *J* = 7.60 Hz, 1H), 6.86 (d, *J* = 7.58 Hz, 1H); **^{13}C NMR (125 MHz, $CDCl_3$, δ)**: 16.24, 25.69, 32.06, 39.90, 44.93, 61.36, 121.82, 125.57, 127.98, 131.55, 135.88, 153.54; **HRMS** (ESI) calculated for $[C_{13}H_{20}O_2]^+$ ($M^{+\bullet}$) requires *m*/*z* 208.1458; found *m*/*z* 208.1453

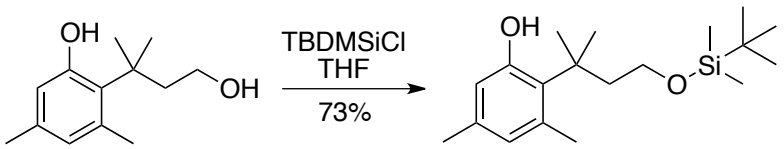

2.2 **2.3**

Compound **2.2** (2.5 g, 12 mmol) and *tert*-butyl dimethylchlorosilane (3.6 g, 24 mmol) were dissolved in DCM (120 mL). Triethylamine (5 mL, 36 mmol) was then added, and the reaction mixture was allowed to stir overnight. The solvent was removed under reduced pressure, and the crude product was purified by chromatography on a column of silica gel (2:8 EtOAc/hexanes) to afford compound **2.3** as a white solid (2.8 g, 73%).

^{1}H NMR (500 MHz, $CDCl_3$, δ): 0.03 (s, 6H), 0.89 (s, 9H), 1.59 (s, 6H), 2.15 (t, J = 6.76 Hz, 2H), 2.21 (s, 3H), 2.48 (s, 3H), 3.61 (t, J = 6.77 Hz, 2H), 5.82 (s, 1H), 6.60 (d, J = 7.63 Hz, 1H), 6.88 (d, J = 7.57 Hz, 1H); **^{13}C NMR (125 MHz, $CDCl_3$, δ)**: 5.41, 16.43, 18.30, 25.62, 25.92, 32.27, 39.68, 44.91, 61.75, 122.88, 125.17, 127.79, 132.07, 135.53, 153.87; **HRMS** (ESI) calculated for $[C_{19}H_{34}O_2Si]^+$ ($M+H^+$) requires m/z 323.2401; found m/z 323.2394

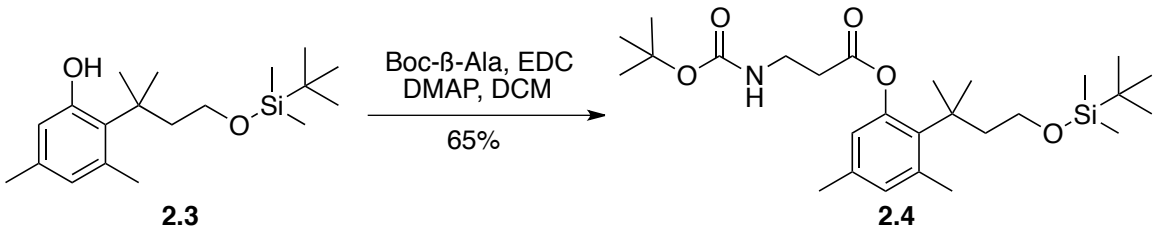

2.3 **2.4**

Boc-protected β-alanine (1.75 g, 9.3 mmol), EDC (2.3 g, 18.6 mmol), and DMAP (2.28 g, 18.6 mmol) were added to a flame-dried 250-mL round-bottom flask. The flask was evacuated and flushed with N_2(g), and DCM (42 mL) was added. Compound **2.3** (2.0 g, 6.2 mmol) was dissolved in dry DCM (20 mL), and the resulting solution was added drop-wise. The reaction mixture was allowed to stir overnight. The reaction mixture was diluted with 10% w/v aqueous $NaHCO_3$ and then washed with 1 N HCl. The solution was dried over $NaSO_4$(s), and solvent was removed under reduced pressure. The crude product was purified by chromatography on a column of silica gel (1:9 EtOAc/hexanes) to afford compound **2.4** as a white solid (1.98 g, 65%).

^{1}H NMR (500 MHz, $CDCl_3$, δ): 0.03 (s, 6H), 0.84 (s, 9H), 1.49–1.44 (m, 18H) 2.02 (s, 3H), 2.09–2.08 (m, 2H), 2.53 (s, 3H); 3.48–3.44 (m, 4H), 5.15–5.12 (bs, 1H), 6.92 (d, J = 7.71 Hz, 1H), 6.96 (d, J = 7.64 Hz, 1H); **^{13}C NMR (125 MHz, $CDCl_3$, δ)**: 5.36, 17.21, 18.24, 25.26, 25.92, 28.38, 31.88, 34.87, 35.94, 39.40, 46.06, 60.72, 79.39, 128.46, 128.95, 131.26, 136.34, 137.29, 148.57, 155.85, 171.28; **HRMS** (ESI) calculated for $[C_{27}H_{47}NO_5Si]^+$ ($M+H^+$) requires m/z = 494.3297; found m/z = 494.3294

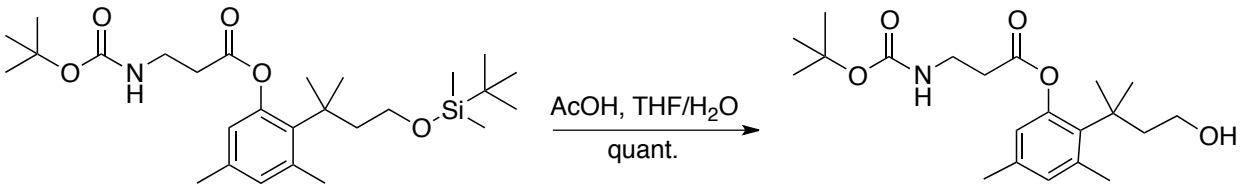

2.4 **2.5**

Compound **2.4** (1.5 g, 3.0 mmol) was dissolved in a mixture of THF (6 mL), H_2O (6 mL), and concentrated glacial acetic acid (18 mL). The reaction mixture was stirred and reaction progress was monitored with TLC. After 2 h, solvent was removed under reduced pressure, and the crude product was purified by passage through a short (2-in) plug of silica gel (2:8 EtOAc/hexanes) to afford compound **2.5** as a colorless oil (1.34 g, quant).

^{1}H NMR (500 MHz, $CDCl_3$, δ): 1.43 (s, 9H), 1.46 (s, 3H), 1.51 (s, 3H), 1.93–1.89 (m, 2H), 2.02 (s, 3H), 2.53 (s, 3H), 2.84–2.82 (m, 2H) 3.57–3.45 (m, 4H), 5.20 (bs, 1H), 6.92–6.91 (d, J = 7.70 Hz, 1H), 6.97–6.95 (d, J = 7.73 Hz, 1H); **^{13}C NMR (125 MHz, $CDCl_3$, δ)**: 17.22, 25.39, 28.41, 32.20, 34.94, 35.93, 39.50, 45.77, 60.38, 79.54, 128.65, 129.14, 131.43, 136.47, 137.09, 148.58, 155.86, 171.78; **HRMS** (ESI) calculated for $[C_{21}H_{33}NO_5]^+$ ($M+H^+$) requires *m*/*z* 380.2432; found *m*/*z* 380.2437

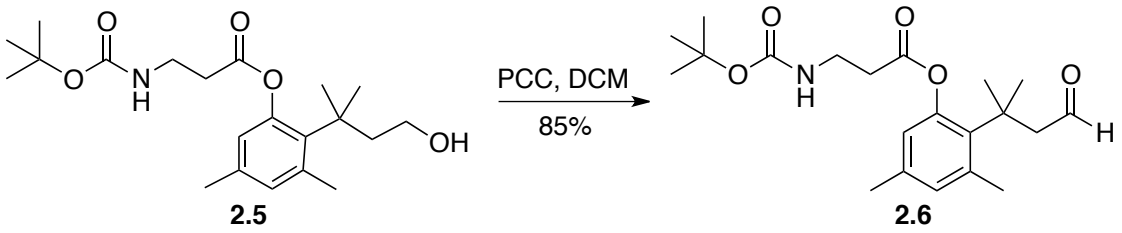

2.5 **2.6**

A solution of compound **2.5** (1.0 g, 2.6 mmol) in anhydrous DCM (5 mL) was added slowly to a suspension of PCC (2.2 g, 10.4 mmol) in DCM (21 mL), and the reaction mixture was allowed to stir overnight. The reaction mixture was then filtered, and solvent was removed under reduced pressure. The crude product was purified by chromatography on a column of silica gel (4:6 EtOAc/hexanes) to afford compound **2.6** as a clear oil (0.83 g, 85%).

^{1}H NMR (500 MHz, $CDCl_3$, δ): 1.52–1.44 (s, 16H), 2.04 (s, 3H), 2.55 (s, 3H), 2.93–2.55 (m, 4H), 3.51–3.48 (s, 2H), 5.08 (t, J = 6.40 Hz, 1H), 6.97 (d, J = 7.72 Hz, 1H), 7.02 (d, J = 7.73 Hz, 1H), 9.51 (t, J = 2.63 Hz, 1H); **^{13}C NMR (125 MHz, $CDCl_3$, δ)**: 17.18, 25.35, 28.37, 34.88, 35.90, 38.42, 56.70, 79.50, 129.23, 129.42, 131.70, 135.78, 135.91, 148.21, 155.80, 171.20, 202.81; **HRMS** (ESI) calculated for $[C_{21}H_{31}NO_5]^+$ ($M+H^+$) requires m/z 378.2275; found m/z 378.2280

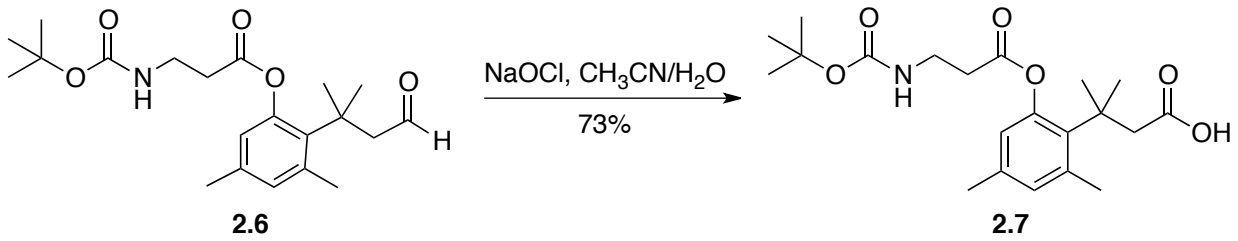

Compound **2.6** (0.8 g, 2.1 mmol) and NaH_2PO_4 (0.26 g, 1.59 mmol) were dissolved in CH_3CN (10 mL), and the resulting solution was cooled to –10 °C. A solution of 80% w/v sodium chlorite (0.6 g, 6.3 mmol) in water (10 mL) was added dropwise. The reaction mixture was stirred for 1 h at –10 °C and then allowed to warm to room temperature. Saturated sodium sulfite solution (2 mL) was added, and the reaction mixture was acidified to pH 2.0 with 1 N HCl followed by extraction with ethyl acetate (3 × 15 mL). The organic layer was washed with brine and then dried over $NaSO_4$(s). The solvent was removed under reduced pressure, and the crude product was purified by chromatography on a column of silica gel (5–10% v/v MeOH/DCM) to afford compound **2.7** as a clear oil (0.61 g, 73%)

^{1}H NMR (500 MHz, $CDCl_3$, δ): 1.43 (s, 9H), 1.54 (s, 3H), 1.63 (s, 3H), 2.02 (s, 3H), 2.55 (s, 3H), 2.85–2.74 (m, 4H), 3.48 (s, 2H), 5.16 (t, J = 6.14 Hz, 1H), 6.93 (d, J = 7.76 Hz, 1H), 6.98, (d, J = 7.78 Hz, 1H); **^{13}C NMR (125 MHz, $CDCl_3$, δ)**: 17.19, 25.23, 28.36, 31.23, 31.55, 34.87, 35.92, 39.00, 47.48, 79.50, 128.82, 131.44, 136.04, 136.69, 148.26, 155.89, 171.27, 175.98; **HRMS** (ESI) calculated for $[C_{21}H_{31}NO_6]^+$ ($M+H^+$) requires m/z 394.2225; found m/z 394.2219

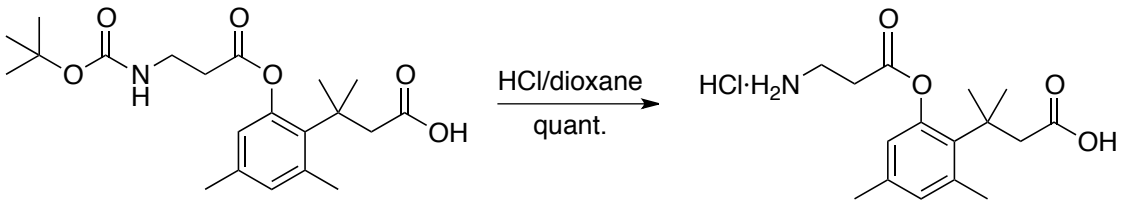

2.7 **2.8**

Compound **2.7** (0.5 g, 1.2 mmol) was dissolved in a solution of 4 M HCl in dioxane (8.4 mL) and allowed to stir for 1 h. N_2(g) was then bubbled though the solution for 15 min to remove excess HCl, and solvent was removed under reduced pressure. Diethyl ether was added to precipitate compound **2.8** as its HCl salt (0.4 g; quant).

^{1}H NMR (500 MHz, CD_3OD, δ): 1.54 (s, 6H), 2.18 (s, 3H), 2.53 (s, 3H), 2.77 (s, 2H), 2.99–3.01 (t, J = 6.52 Hz, 2H), 3.25–3.28 (m, 6H), 6.65 (s, 1H), 6.83 (s, 1H); **^{13}C NMR (125 MHz, CD_3OD, δ)**: 20.22, 25.50, 32.09, 33.08, 36.21, 39.80, 124.01, 133.41, 134.86, 137.33, 139.54, 150.55, 171.46, 175.54; **HRMS** (ESI) calculated for $[C_{16}H_{24}NO_4]^+$ $(M–Cl)^+$ requires m/z 294.1779; found m/z 294.1793

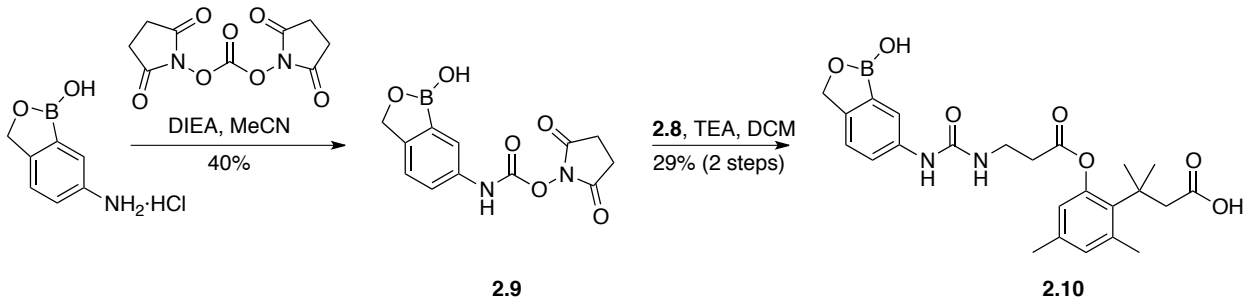

2.9 **2.10**

5-Amino-2-hydroxymethylphenylboronic acid (0.200 g, 1.07 mmol) was dissolved in 10.4 mL of dry acetonitrile. *N*,*N*-Disuccinimidyl carbonate (0.303 g, 1.18 mmol) was then added to the solution, followed by the dropwise addition of DIEA (0.20 mL, 2.14 mmol). The reaction mixture was allowed to stir overnight. The reaction mixture was then filtered to remove the insoluble *N*-hydroxysuccinimide (NHS) byproduct. The solvent from the filtrate was removed under reduced pressure to give the crude product as a yellow solid. The crude solid was dissolved in chloroform and cooled to –20 °C in the freezer for 1 h. The solution was filtered, and solvent was removed under reduced pressure to give compound **2.9** as a light yellow solid. Compound **2.9** was used in the next step without further purification.

Compound **2.8** (0.080 g, 0.244 mmol) was dissolved in dry THF (2.4 mL). Compound **2.9** (0.078 g, 0.268 mmol) was then added to the solution, followed by the dropwise addition of DIEA (0.06 mL, 0.73 mmol). The reaction mixture was allowed to stir overnight. The reaction mixture was then filtered, and solvent was removed under reduced pressure. The crude product was purified by chromatography on a column of silica gel (3–5% v/v MeOH:DCM) to afford compound **2.10** as a white solid (0.083 g, 73%).

^{1}H NMR (500 MHz, CD_3OD, δ): 1.56 (s, 3H), 2.20 (s, 3H), 2.55 (s, 3H), 2.80 (s, 2H), 2.87–2.85 (t, J = 6.16 Hz, 2H), 3.60–3.67 (t, J = 6.18 Hz, 2H), 5.03 (s, 2H), 6.63 (s, 2H), 6.68 (s, 1H),

7.28–7.29 (d, J = 8.22 Hz, 1H), 7.50–7.52 (d, J = 8.24 Hz, 1H), 7.62 (s, 1H); **^{13}C NMR (125 MHz, CD_3OD, δ)**: 18.66, 24.00, 24.73, 30.45, 35.16, 38.22, 70.56, 119.96, 120.95, 122.28, 122.62, 131.62, 133.49, 135.96, 137.84, 138.42, 147.83, 149.29, 156.70, 171.60, 173.36, 174.05; note: the signal for the carbon attached to boron was not observable due to quadrupolar relaxation; **HRMS** (ESI) calculated for the methyl boronic ester $[C_{25}H_{31}{}^{11}BN_2O_7]^+$ $(M+H)^+$ requires m/z 483.2298; found m/z 483.2308

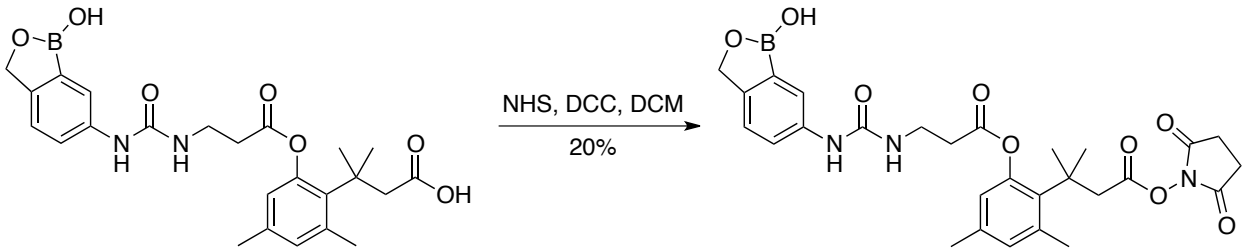

2.10 **2.11**

Compound **2.10** (0.068 g, 0.129 mmol) was dissolved in dry DCM (1.3 mL). The reaction mixture was then cooled to 0 °C and DCC (0.032 g, 0.155 mmol) followed by *N*-hydroxysuccinimide (0.016 g, 0.142 mmol) were added. The reaction mixture was allowed to warm to room temperature and stir over night. The reaction mixture was then cooled to 0 °C and the solid was removed by filtration. The solvent was removed under reduced pressure, and the resulting reside and dissolved in ethyl acetate and chilled to –20 °C in a freezer for 3 h. The solids were removed by filtration, and the filtrate was extracted with water to remove any residual urea byproduct. The organic layers were combined, and the solvent was removed under reduced pressure to afford the compound **2.11** as a white solid (0.012 g, 20%).

^{1}H NMR (500 MHz, CD_3OD, δ): 1.61 (s, 6H), 2.20 (s, 3H), 2.55 (s, 3H), 2.75 (s, 4H), 2.93–2.90 (t, J = 5.76 Hz, 2H), 3.15 (s, 2H), 3.61–3.58 (t, J = 6.74 Hz, 2H), 5.03 (s, 2H), 6.66 (s, 1H), 6.84 (s, 1H), 7.28–7.29 (d, J = 8.21 Hz, 1H), 7.51–7.49 (d, J = 8.19 Hz, 1H), 7.61 (s, 1H); **^{13}C NMR (125 MHz, CD_3OD, δ)**: 20.24, 25.50, 26.45, 31.56, 36.54, 36.72, 40.04, 45.15, 72.11, 121.51, 122.51, 123.84, 124.29, 133.32m 133.95, 137.71, 139.17, 139.99, 149.38, 150.86, 158.22, 168.16, 171.79, 173.13; note: the signal for the carbon attached to boron was not observable due to quadrupolar relaxation; **HRMS** (ESI) calculated for the methyl boronic ester $[C_{29}H_{34}{}^{10}BN_3O_9]^+$ $(M+Na)^+$ requires m/z 602.2286; found m/z 602.2290

2.7.3 Cell Culture

Cell lines were obtained from American Type Culture Collection (Manassas, VA) and were maintained according to the recommended procedures. Medium and added components were the Gibco® brand from Thermo Fisher Scientific (Waltham, MA). Cells were grown in flat-bottomed culture flasks in a cell-culture incubator at 37 °C under CO_2 (g) (5% v/v). Chinese hamster ovary (CHO K1) cells were grown in F12K nutrient medium and K562 cells were grown in RPMI 1640 medium, both supplemented with fetal bovine serum (FBS) (10% v/v), penicillin (100 units/mL), and streptomycin (100 μg/mL). Cells were counted with a hemocytometer to determine the seeding density in 12-well plates from Corning Costar (Lowell, MA) or microscopy dishes from Ibidi (Madison, WI). All flow cytometry and confocal microscopy was performed with live cells, incubated on ice at the time of analysis.

2.7.4 Labeling of GFP

2.7.4.1 Preparation of Green Fluorescent Protein (GFP)

The gene encoding the eGFP variant GFP was inserted into the pET22b vector (Novagen), along with an N-terminal His_6 tag followed by a spacer region and a TEV protease recognition sequence. The GFP gene was modified with the following 17 substitutions to generate a "superfolding" variant that folds readily when produced in *Escherichia coli*: F64L, S65T, F99S, M153T, V163A, S30R, Y145F, I171V, A106V, Y39I, N105K, E111V, I128T, K166T, I167V, S205T, L221H, F223Y, T225N.[165-169] The vector also contained a T7 promoter and ampicillin resistance gene.

The expression vector was transformed into electrocompetent BL21(DE3) *E. coli* cells from New England Biolabs (Ipswich, MA), then plated on LB agar containing ampicillin

(200 μg/mL). On the following day, a single colony was used to inoculate 50 mL of LB medium, and the resulting culture was grown overnight at 37 °C in a shaking incubator. On the following day, 10 mL of starter culture was used to inoculate 1.00 L of Terrific Broth medium from Research Products International (Mt. Prospect, IL) in a 3.8-L glass flask with ampicillin at a final concentration of 200 μg/mL. Flasks were shaken at 200 rpm at 37 °C in a shaking incubator until cells reached log phase (*OD* 0.6–0.8 at 600 nm). The production of GFP was induced by adding IPTG to a final concentration of 1 mM, and cells were grown overnight at 37 °C in a shaking incubator.

Cells were harvested by centrifugation for 20 min at 5,000 rpm at 4 °C. Cell pellets, which were bright yellow in color, were collected and resuspended in 15 mL of lysis buffer per 2 L of liquid growth, which was 50 mM Tris–HCl buffer, pH 7.0, containing NaCl (100 mM) and imidazole (30 mM). Cell pellets were vortexed and stored frozen at –20 °C overnight.

Cells were lysed with a TS Series cell disrupter from Constant Systems (Kennesaw, GA), and the lysate was subjected to centrifugation immediately for 1 h at 11,000 rpm at 4 °C. The supernatant was filtered through 5-μM syringe filters from EMD Millipore (Billerica, MA) and solid, pelleted material was discarded. Filtered cell lysates were purified by chromatography on Ni–NTA resin from GE Healthcare (Little Chalfont, UK) and eluted using a linear gradient of imidazole. The binding and wash buffer was 30 mM sodium phosphate buffer, pH 7.4, containing NaCl (0.50 M) and imidazole (20 mM). The elution buffer was 30 mM sodium phosphate buffer, pH 7.4, containing NaCl (0.50 M) and imidazole (0.50 M). Eluted fractions were collected, pooled, and dialyzed against 4 L of 20 mM Tris–HCl buffer, pH 7.0, containing EDTA (1 mM).

The dialyzed solution was purified again using anion-exchange chromatography on a hiTrap Q column from GE Healthcare. The protein was eluted by using a linear gradient of NaCl (0–1.00 M) in 20 mM Tris–HCl buffer, pH 7.0, containing EDTA (1.0 mM). Upon elution, colored fractions were pooled and concentrated (if necessary). The overall yield of GFP was ~120 mg per L of culture.

2.7.4.2 Labeling of GFP with TMLB-NHS Ester

TMLB–NHS ester (2.2 mg, 4 μmol, 100 equiv) was added to a 150-μL solution of GFP (300 μM, 0.04 μmol) in PBS. The vial was placed on a nutator in foil overnight at room temperature. The solution was transferred to 10,000 MWCO dialysis tubing and dialyzed twice against 4 L of PBS for 4 h at 4 °C. The extent of labeling was characterized by MALDI–TOF mass spectrometry. To determine the extent of labeling, the average mass of labeled protein was taken as a weighted average for all events within the defined peak range on the background-corrected MALDI–TOF spectra. The molecular weight of non-labeled protein was then subtracted from the given value to give the average total mass of all labels. This value was then divided by the molecular weight of the modifying small molecule minus the mass of *N*-hydroxysuccinimide (565.38 Da – 115.09 Da = 450.29 Da), which was lost during conjugation, to give the average number of labels per molecule of protein. On average we determined there to be approximately 3 ± 1 labels per GFP. The labeled protein is referred to as TMLB–GFP. An identical procedure was used with non-boronated TML (TMLOAc) commercially available from sigma Aldrich (Milwaukee, WI) in which the phenolic oxygen is protected as acetate. The TMLOAc–GFP was also decorated with 3 ± 1 labels.

2.7.4.3 Hydrolysis of labeled GFP by CHO K1 cell lysate

CHO K1 cells were grown to confluence in a 10-cm^2 dish before their collection and lysis with M-PER (Thermo Fisher Scientific). The presence of esterase activity in the lysate was verified by a colorimetric assay using *p*-nitrophenyl acetate. A solution of TMLB–GFP (10 μg) was added to 200 μL of CHO K1 cell lysate, and the reaction mixture was nutated at ambient temperature for 12 h. The GFP was subsequently purified with HisPur™ Ni-NTA Magnetic Beads (Thermo Fisher Scientific). The regeneration of native GFP was confirmed with MALDI–TOF mass spectrometry (Figure 2.1b).

2.7.5 Analysis of TMLB–GFP Internalization

2.7.5.1 Flow Cytometry

CHO K1 cells were seeded at a density of 50,000 cells/well in 12-well plates. Cells were incubated with GFP (10 μM), TMLB–GFP (10 μM), or TMLOAc–GFP (10 mM) for 4 h. Cells were then rinsed twice with Dulbecco's PBS (DPBS) from Thermo Fisher Scientific and released from the plate with 250 μL of trypsin/EDTA (0.25% w/v). Cells were resuspended in an additional 500 μL of medium and incubated on ice until analyzed by flow cytometry. The fluorescence intensity of at least 20,000 events was measured by flow cytometry. Alexa Fluor488® was excited with a 488-nm solid-state laser, and the emission was measured through a 530/30 bandpass filter (Figure 2.1c).

2.7.5.2 Microscopy

CHO K1 cells were seeded at a density of 50,000 cells/dish in 35-mm μ-dish microscopy imaging dishes from Ibidi. Cells were incubated with GFP (10 μM), TMLB–GFP (10 μM), or TMLOAc–GFP (10 μM) for 4 h. Cells were then rinsed twice with DPBS and cell nuclei were stained with Hoechst 33342 (2 μg/mL) for 5 min at 37 °C and cell membrane was stained with WGA-594 (5.0 μg/mL) (Invitrogen) for 15 min on ice. Cells were then washed twice with wash buffer, and examined live using a scanning confocal microscope (Figure 2.1d).

2.7.6 Colocalization with Organelles

2.7.6.1 Microscopy

CHO K1 cells were seeded at a density of 50,000 cells/dish in 35-mm μ-dish microscopy imaging dishes from Ibidi. Cells were incubated with 10 μM TMLB–GFP for 4 h, then rinsed twice with DPBS, and cell nuclei were stained with Hoechst 33342 (2 μg/mL) for 5 min at 37 °C and cell membranes were stained with either WGA-594 (5.0 μg/mL) for 15 min on ice, CellTracker™ Orange CMTMR dye (1 μM) at 37 °C for 15 min, Transferrin-594 (25 μg/mL) at 37 °C for 15 min or LysoTracker Red (50 nM) at 37 °C for 30 min (all from Invitrogen). Cells were then washed twice with wash buffer, and examined live using a scanning confocal microscope.

2.7.7 Internalization over time

2.7.7.1 Microscopy

CHO K1 cells were seeded at a density of 50,000 cells/dish in an 8-well μ-slide microscopy-imaging dish from Ibidi. Cells were incubated with GFP (10 μM) or TMLB–GFP (10 μM) for 4 or 24 h. Cells were then rinsed twice with DPBS, and cell nuclei were stained with Hoechst 33342 (2 μg/mL) for 5 min at 37 °C, and cell membranes were stained with WGA-594 (5.0 μg/mL) for 15 min on ice. Cells were then washed twice with wash buffer, and examined live using a scanning confocal microscope.

2.7.8 Fructose Competition

10 μM TMLB–GFP was preincubated in an aqueous solution of fructose (175 mM) for 30 min, then used to treat CHO K1 cells for 4 h before analysis by either confocal microscopy or flow cytometry as described above and shown in Figure 2.6.

2.7.9 Ribonuclease A Protein Labeling

2.7.9.1 Preparation of FLAG-Ribonuclease A (RNase A) and G88R RNase A

FLAG–RNase A and G88R RNase A were produced and purified by methods described previously.[158,163]

2.7.9.2 Labeling of FLAG–RNase A and G88R RNase A

The labeling of FLAG–RNase A and G88R RNase A with TMLB–NHS ester, and characterization of the extent of labeling was carried out as described for GFP. On average, there were 1.6 ± 0.7 labels per FLAG–RNase A, and 2 ± 1 labels per G88R RNase A.

2.7.9.3 Hydrolysis of labeled FLAG-RNase A by K562 cell lysate

K-562 cells were grown to confluence in a T75 flask before their collection and lysis with M-PER from Thermo Fisher Scientific. The presence of esterase activity in the lysate was verified by a colorimetric assay using *p*-nitrophenyl acetate. A solution of esterified FLAG–RNase A (10 μg) was added to 200 μL of K-562 cell lysate, and the reaction mixture was nutated at ambient temperature for 12 h. FLAG–RNase A was purified with anti-FLAG® M2 Magnetic Beads from Sigma–Aldrich. The regeneration of native FLAG-RNase A was confirmed with MALDI–TOF mass spectrometry.

2.7.9.4 Cell-Proliferation Assays

The effect of unmodified G88R RNase A and TMLB-G88R RNase A on the proliferation of K-562 cells was assayed using a CyQUANT® NF Cell Proliferation Assay Kit (Invitrogen). Briefly, 5×10^4 cells/mL were added to each well of a 96-well plate in 100 µL of serum-free RPMI 1640 medium. Cells were incubated with G88R RNase A or TMLB–G88R RNase A for 48 h, with PBS and H_2O_2 serving as negative and positive controls, respectively. Cells were then washed and incubated in CyQUANT® reagent for 30 min and fluorescence intensity was measured with excitation at ~485 nm and emission detection at ~530 nm. Data are the average of two measurements for each concentration, and the entire experiment was repeated in triplicate. The results are shown as the percentage of dye incorporated relative to control cells treated with PBS. Values for IC_{50} were calculated by fitting the curves by nonlinear regression to the equation: $y = 100\% / (1 + 10^{(\log(IC50) - \log[\text{ribonuclease}])h})$, where y is the total DNA synthesis following the CyQUANT dye pulse and h is the slope of the curve (Figure 2.9).

2.8 NMR Spectra

^{1}H NMR ($CDCl_3$) and ^{13}C NMR ($CDCl_3$) of Compound **2.1**

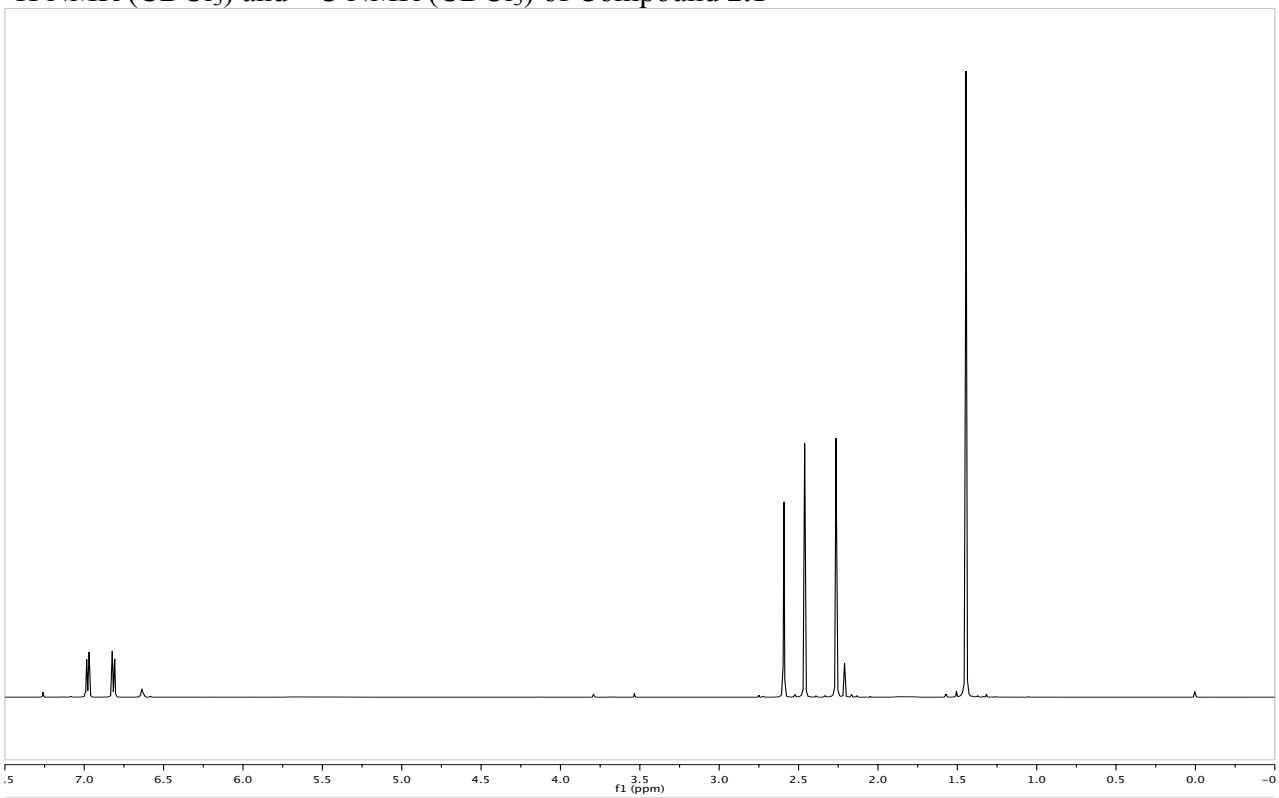

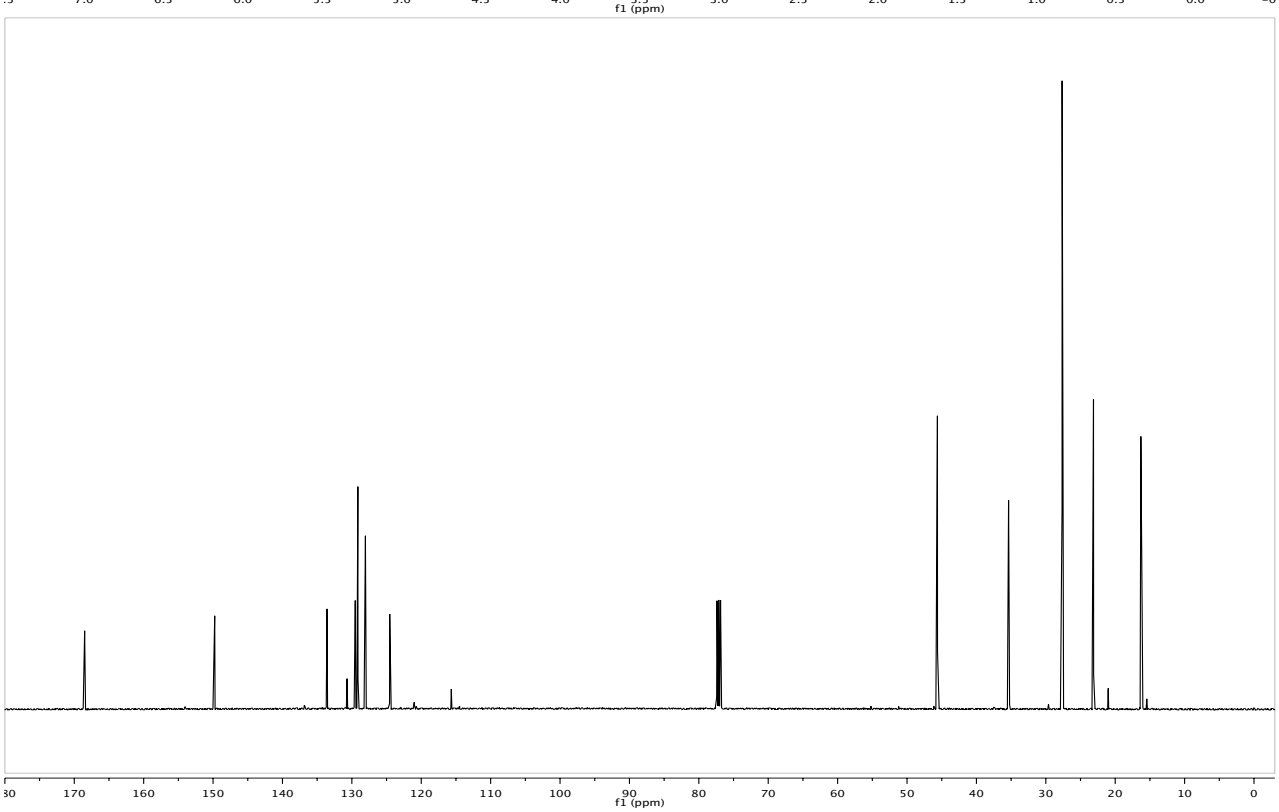

^{1}H NMR ($CDCl_3$) and ^{13}C NMR ($CDCl_3$) of Compound **2.2**

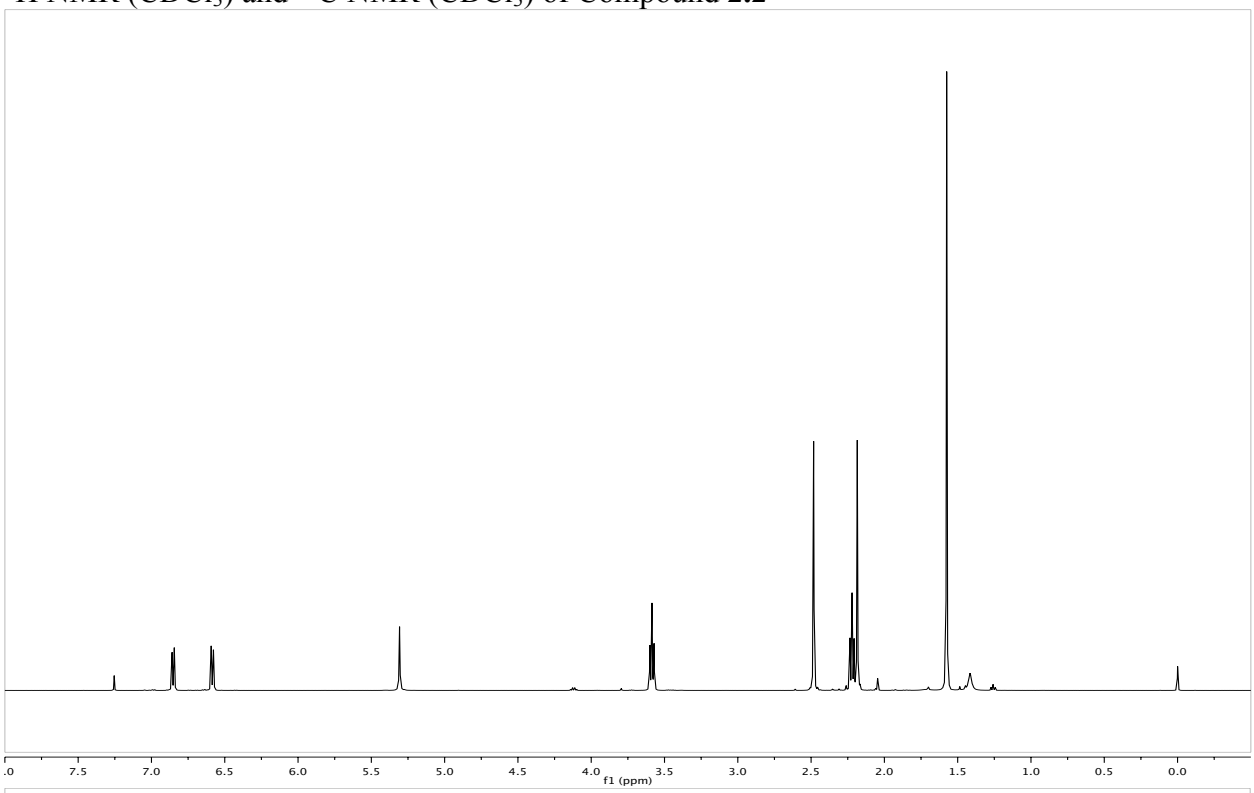

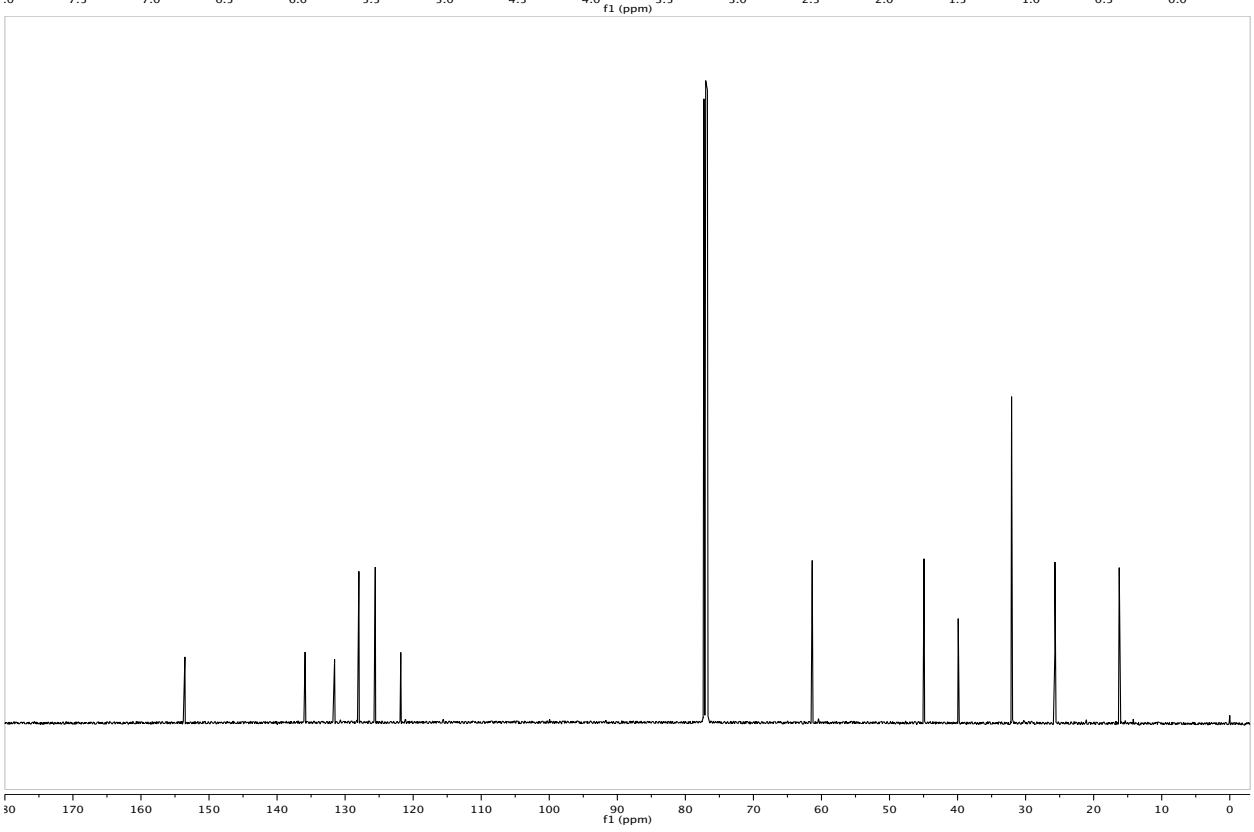

^{1}H NMR ($CDCl_3$) and ^{13}C NMR ($CDCl_3$) of Compound **2.3**

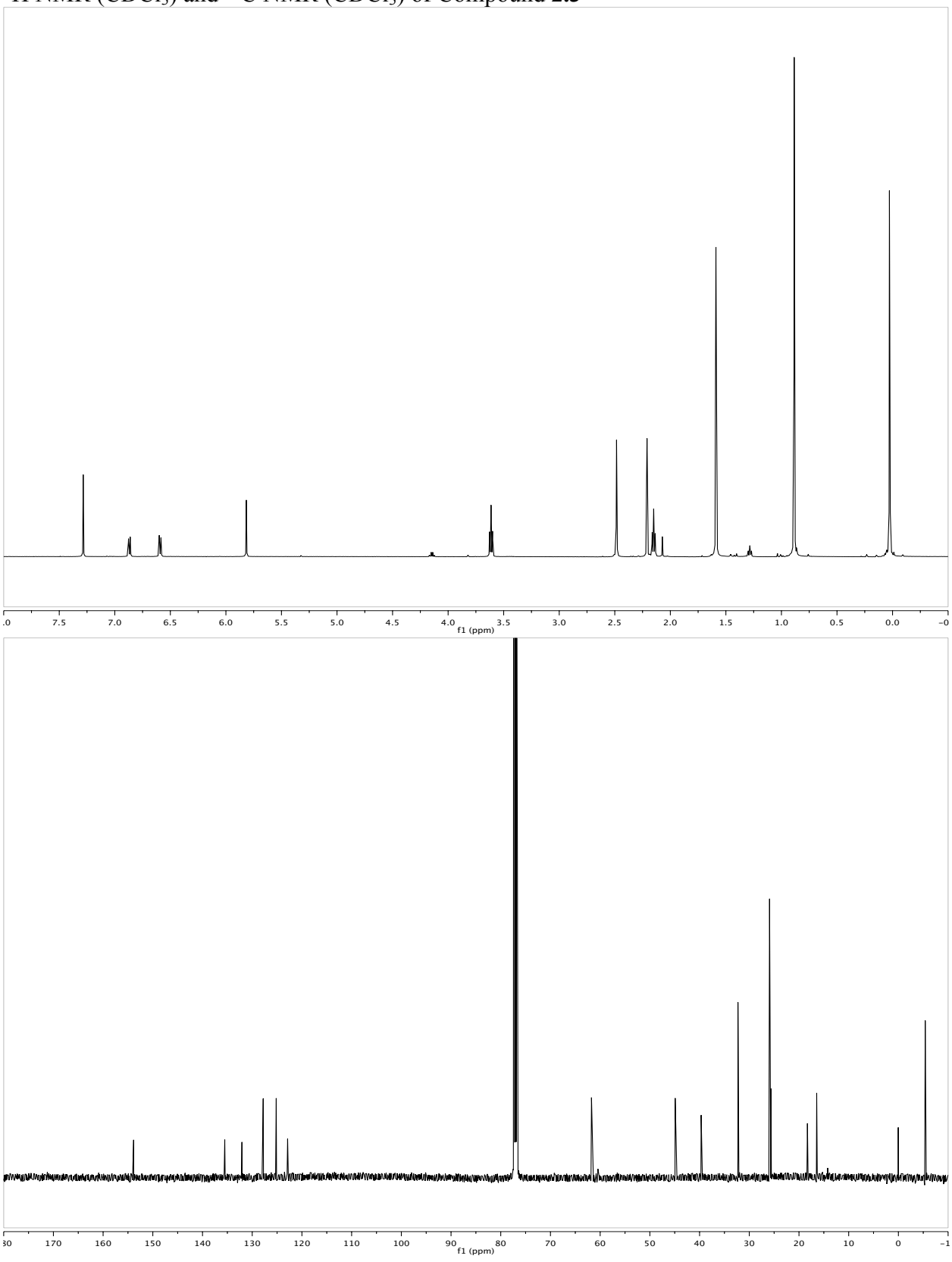

^{1}H NMR ($CDCl_3$) and ^{13}C NMR ($CDCl_3$) of Compound **2.4**

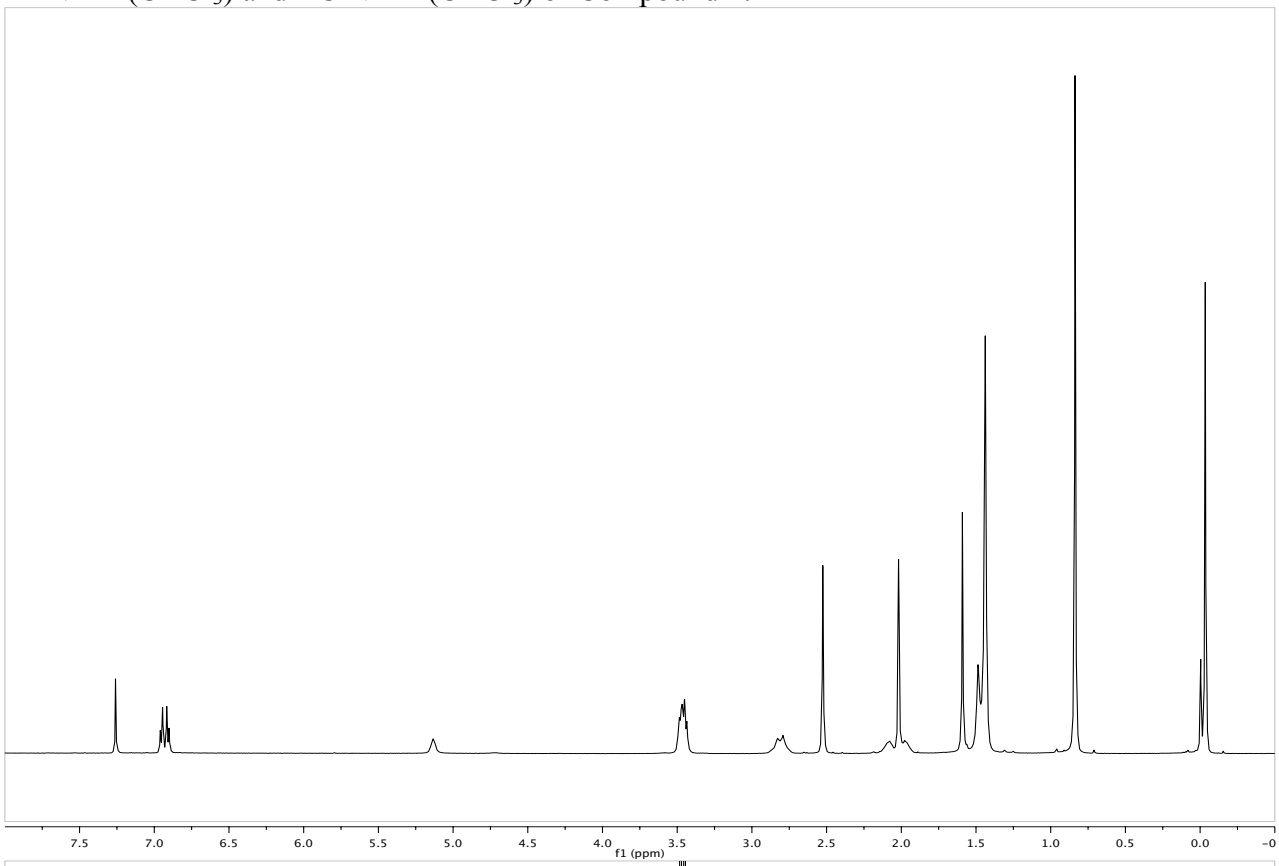

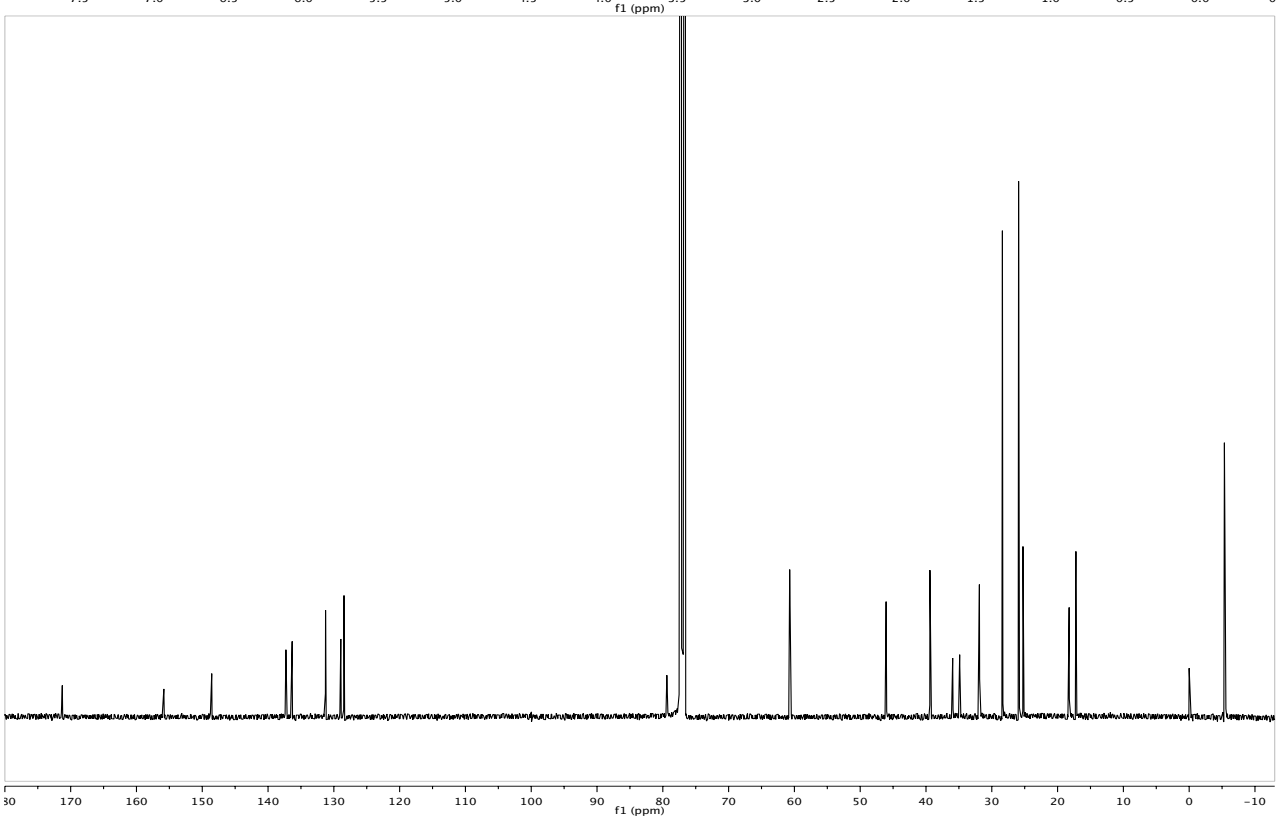

^{1}H NMR ($CDCl_3$) and ^{13}C NMR ($CDCl_3$) of Compound **2.5**

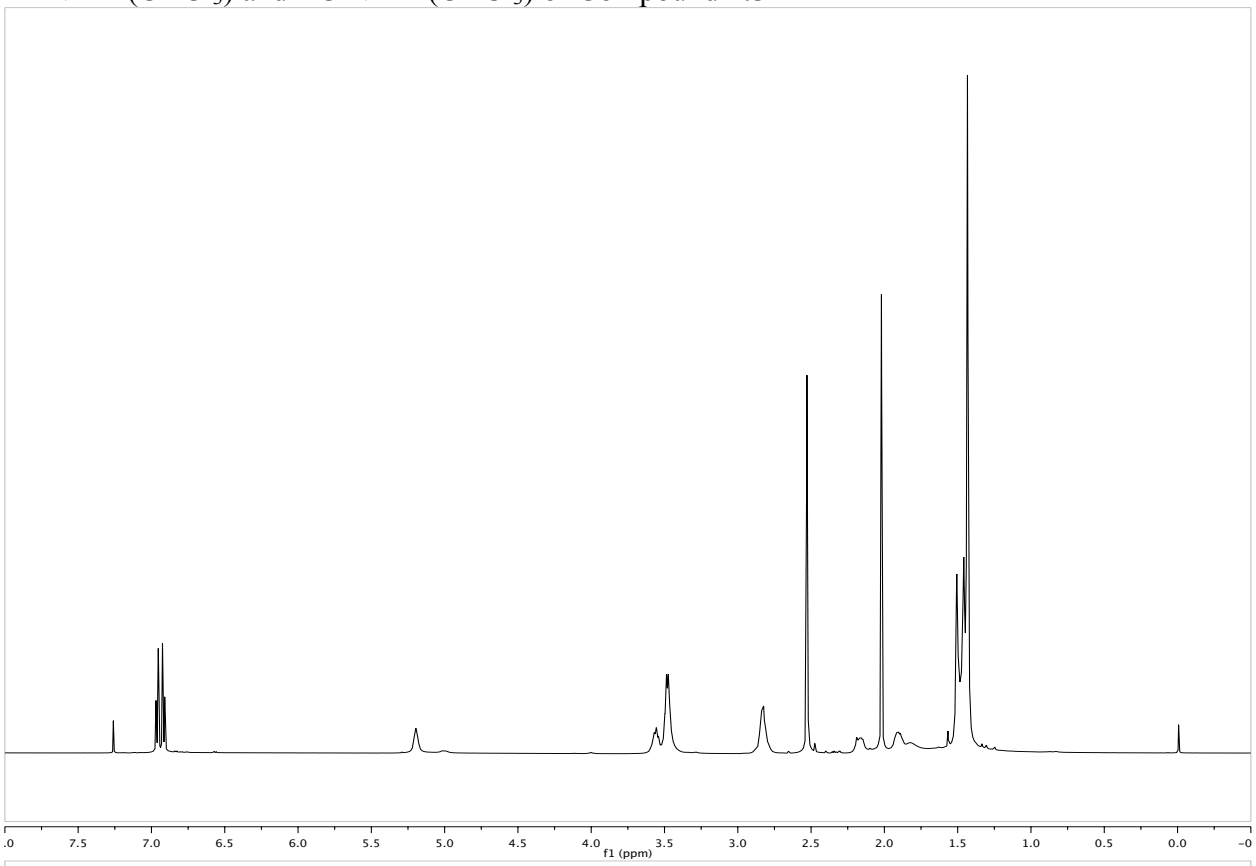

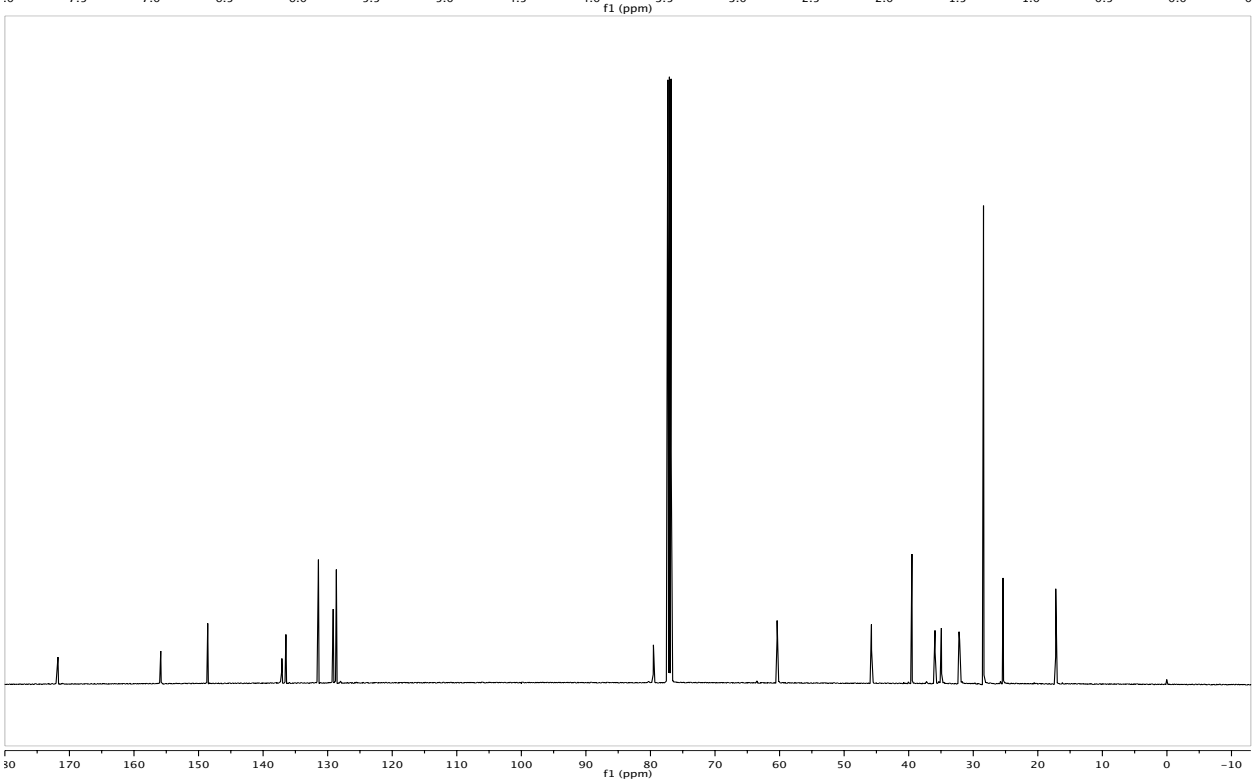

^{1}H NMR ($CDCl_3$) and ^{13}C NMR ($CDCl_3$) of Compound **2.6**

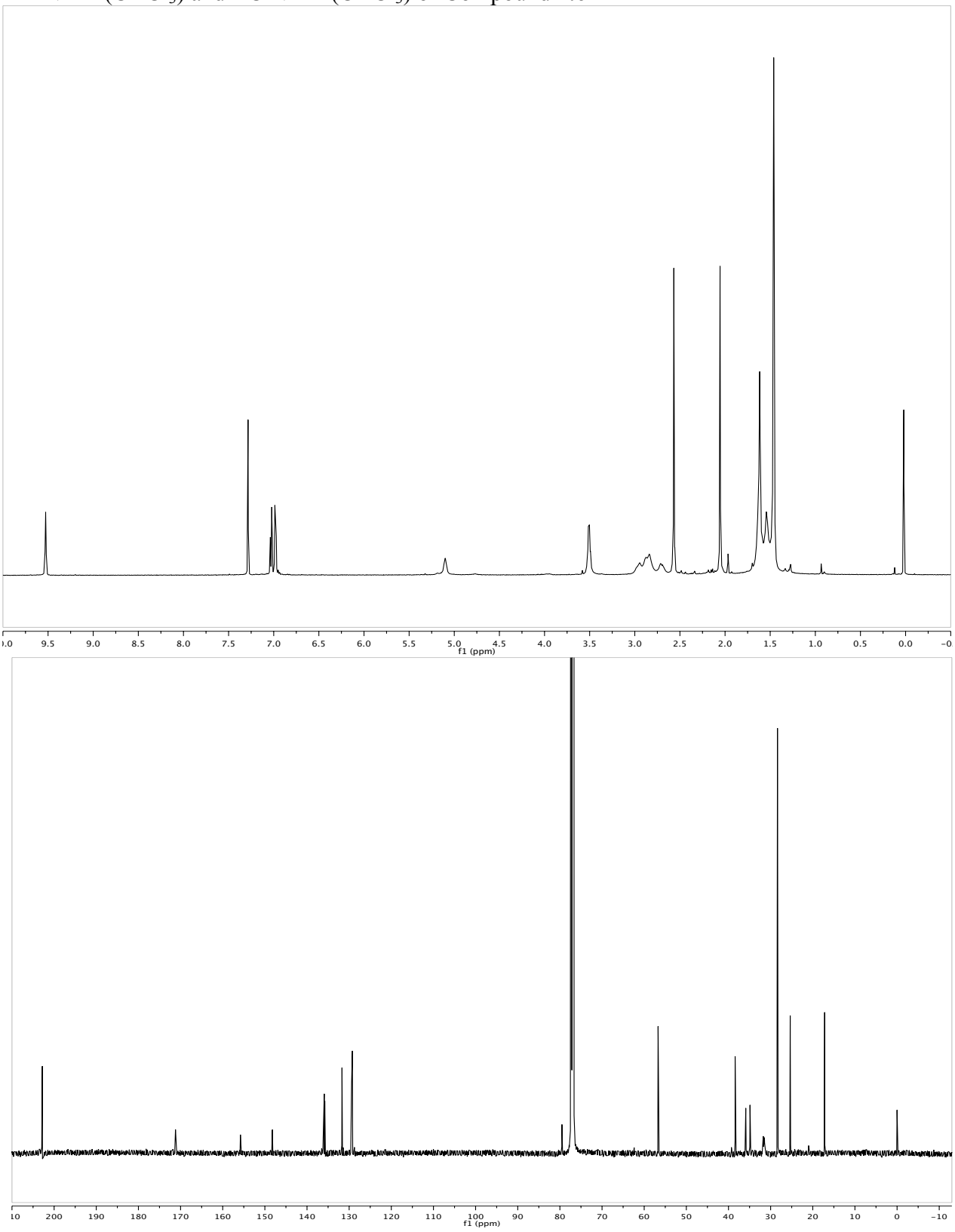

^{1}H NMR ($CDCl_3$) and ^{13}C NMR ($CDCl_3$) of Compound **2.7**

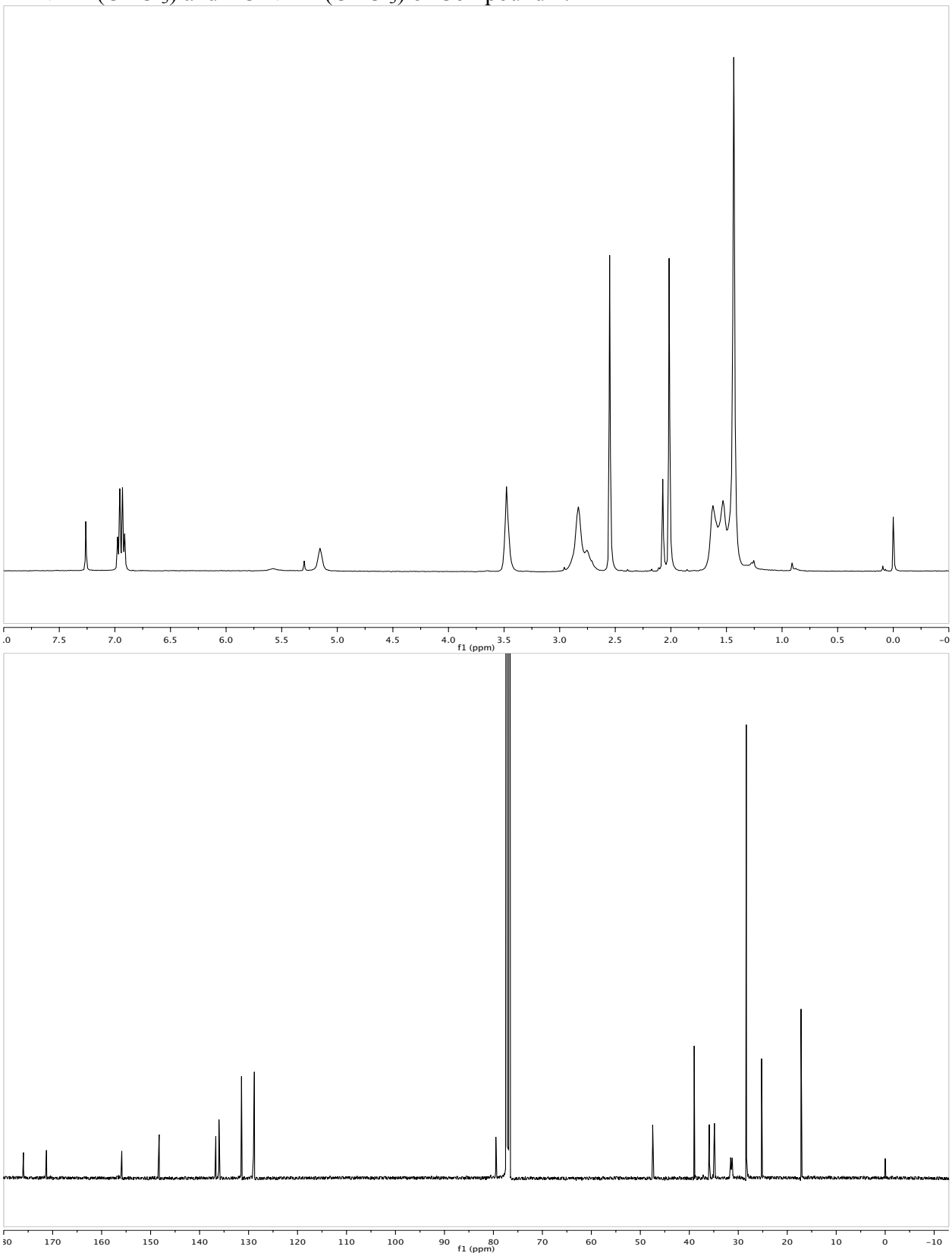

^{1}H NMR (CD_3OD) and ^{13}C NMR (CD_3OD) of Compound **2.8**

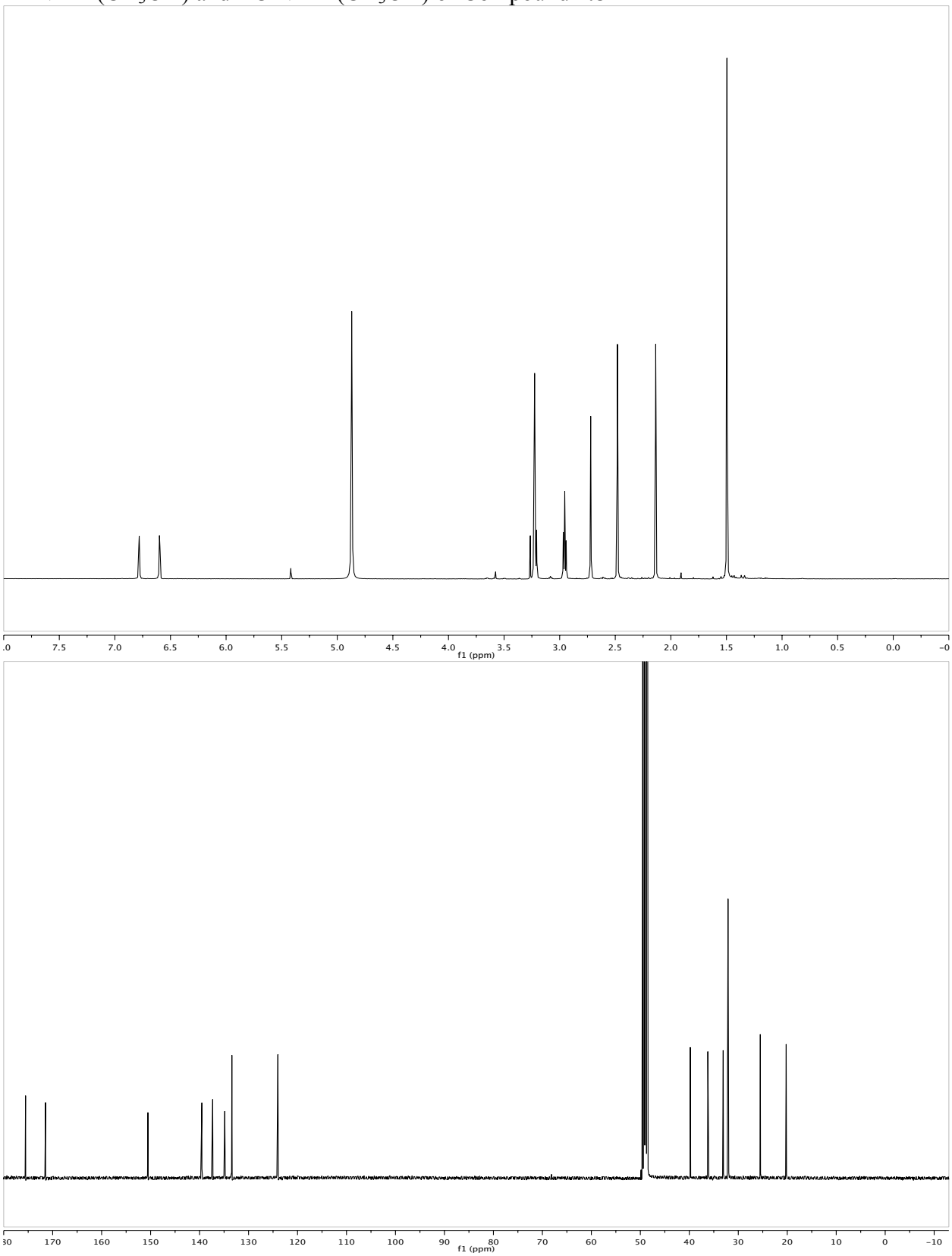

^{1}H NMR (CD_3OD) and ^{13}C NMR (CD_3OD) of Compound **2.10**

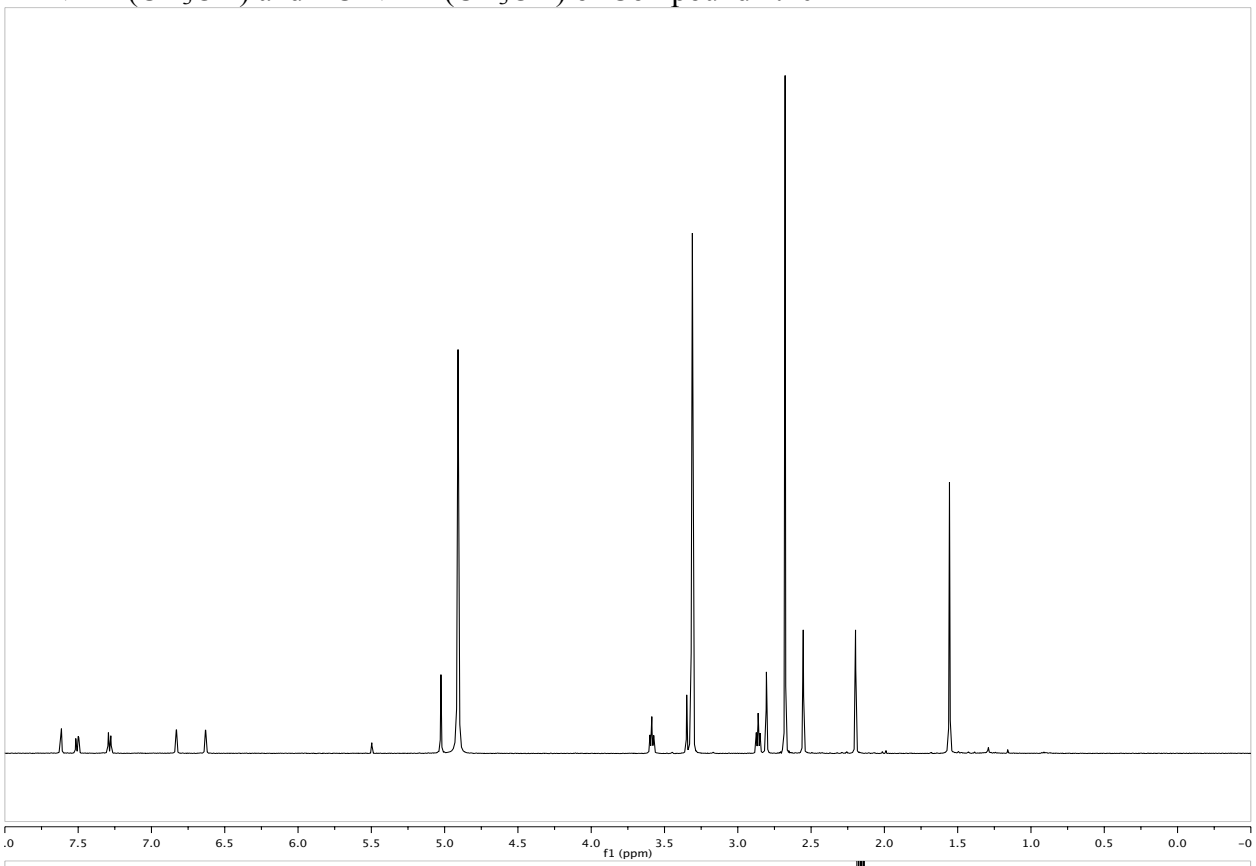

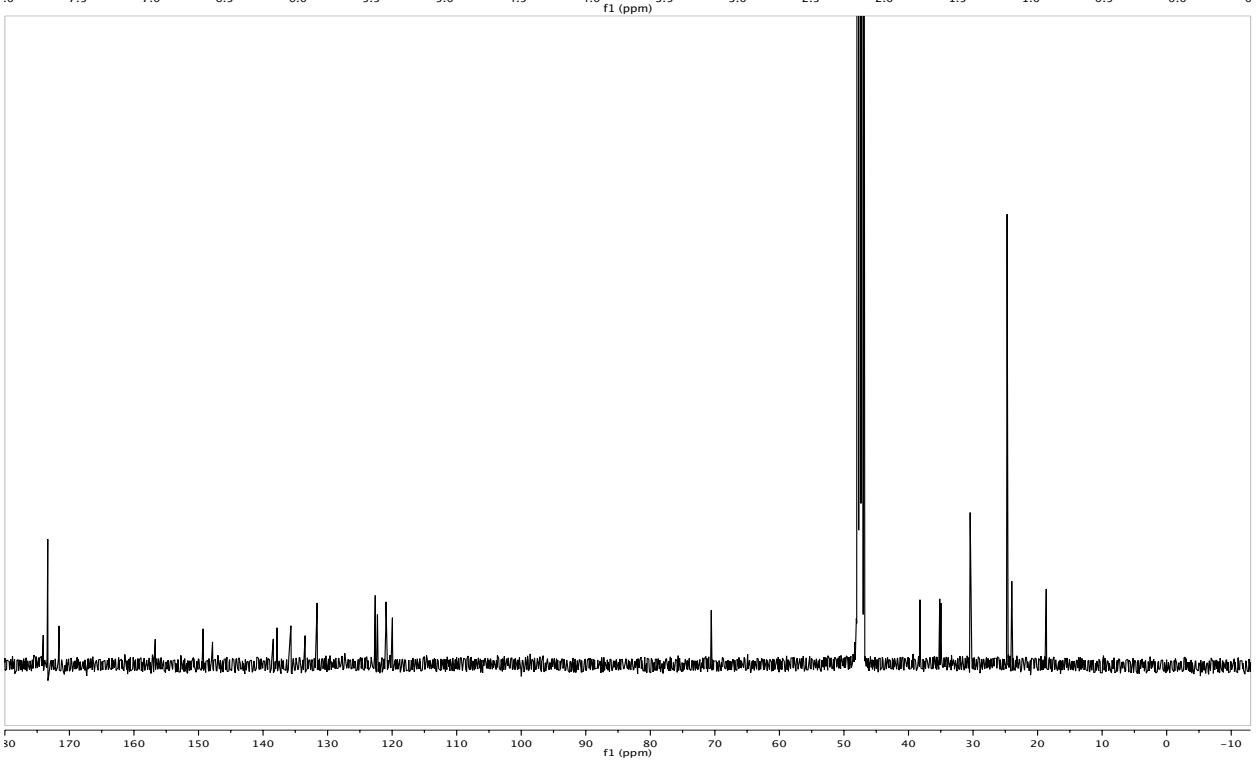

^{1}H NMR (CD_3OD) and ^{13}C NMR (CD_3OD) of Compound **2.11**

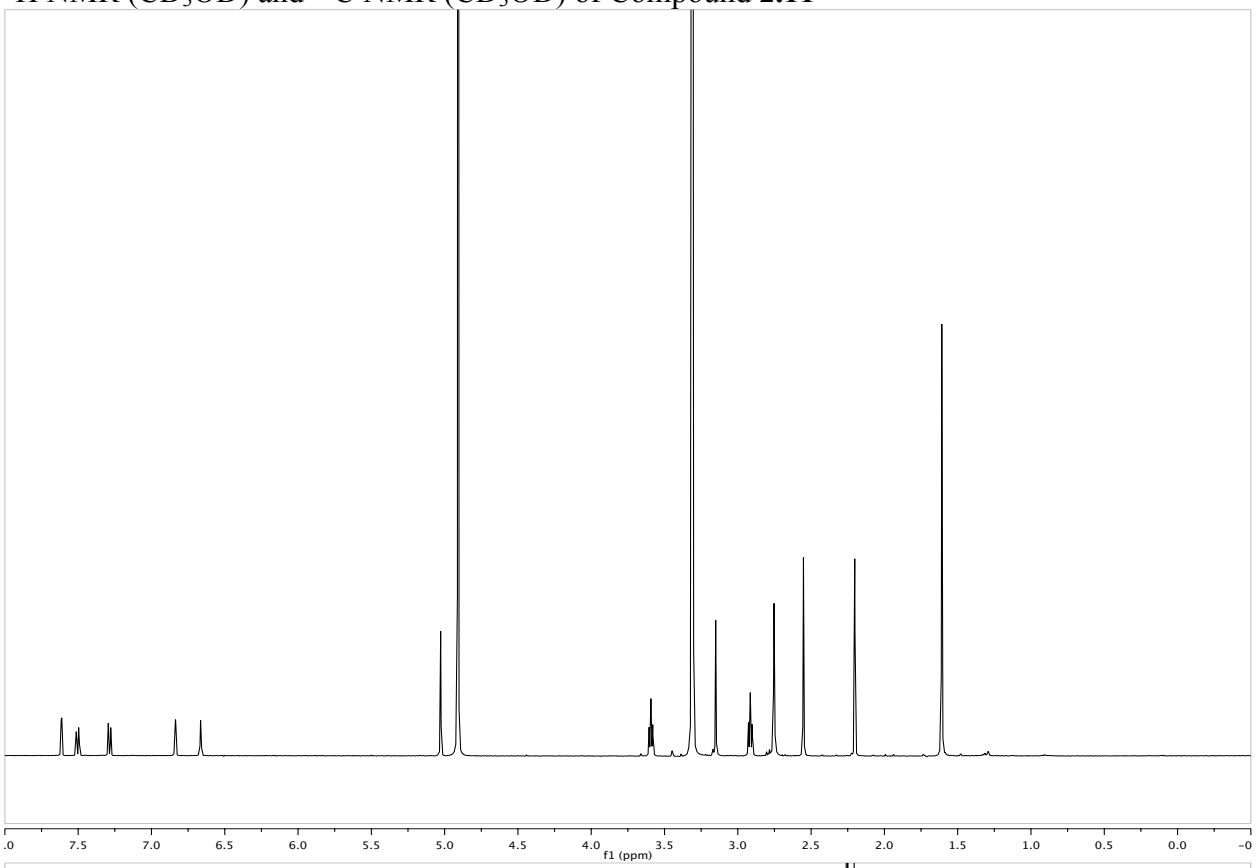

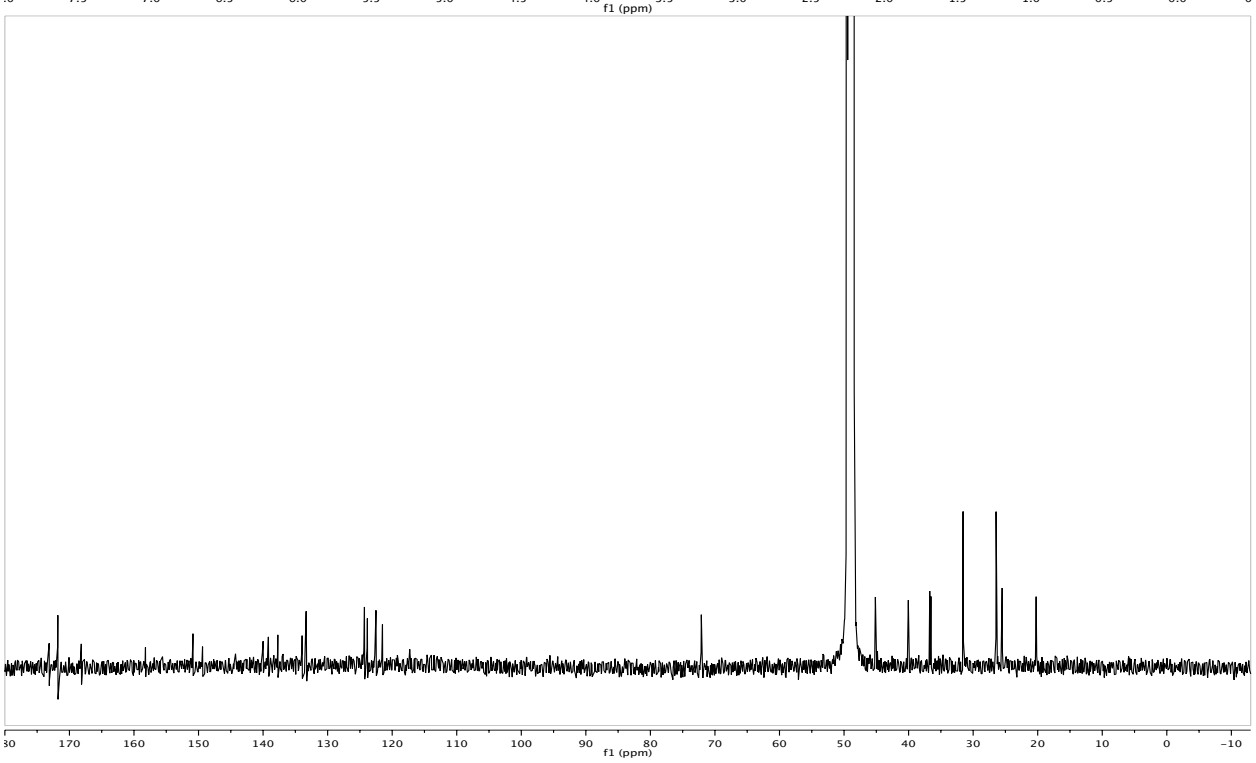

Scheme 2.1

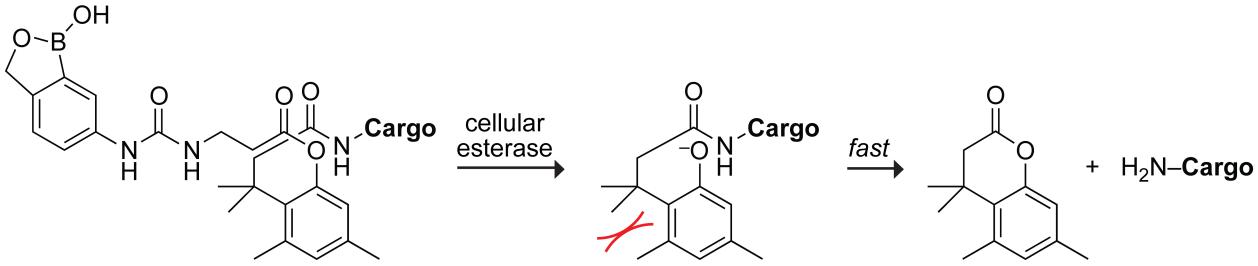
OH
B
O
N
H
O
N
H
O
O
O
N
H
Cargo
cellular
esterase
O
−O
N
H
Cargo
fast
O
O
+
H2N–Cargo

Scheme 2.1 Putative mechanism of esterase cleavage and immolative release of a protein cargo. Exposure of the phenolate leads to an irreversible lactonization reaction driven by high effective concentration and steric strain associated with the tri-methyl lock motif.

Scheme 2.2

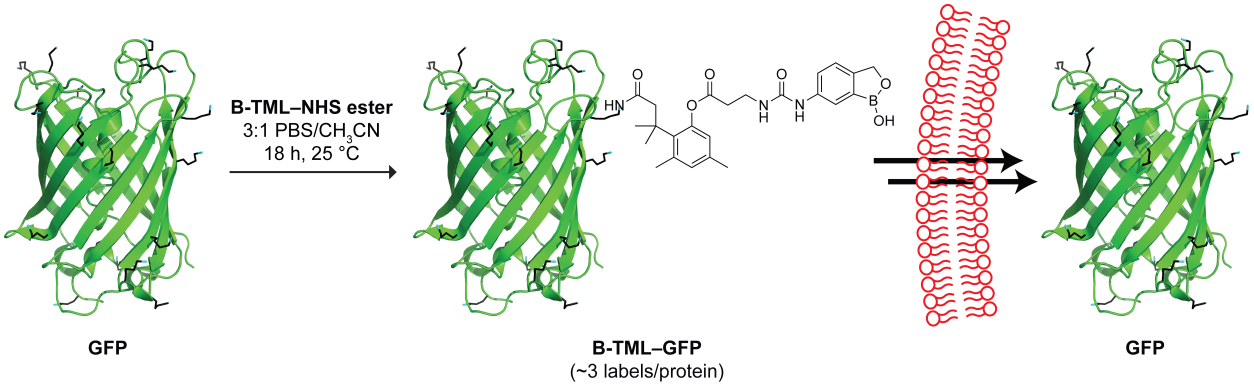
B-TML–NHS ester
3:1 PBS/CH3CN
18 h, 25 °C
HN
O
O
O
N
H
N
H
B
O
OH
GFP
B-TML–GFP
(~3 labels/protein)
GFP

Scheme 2.1 Formation of B-TML–GFP conjugate. Under mild bioconjugation conditions (3:1 PBS/ACN at room temperature overnight), 3-4 boronic acid labels are conjugated to the surface of GFP. These labels are removed once exposed to intracellular esterases, releasing unmodified protein.

Figure 2.1

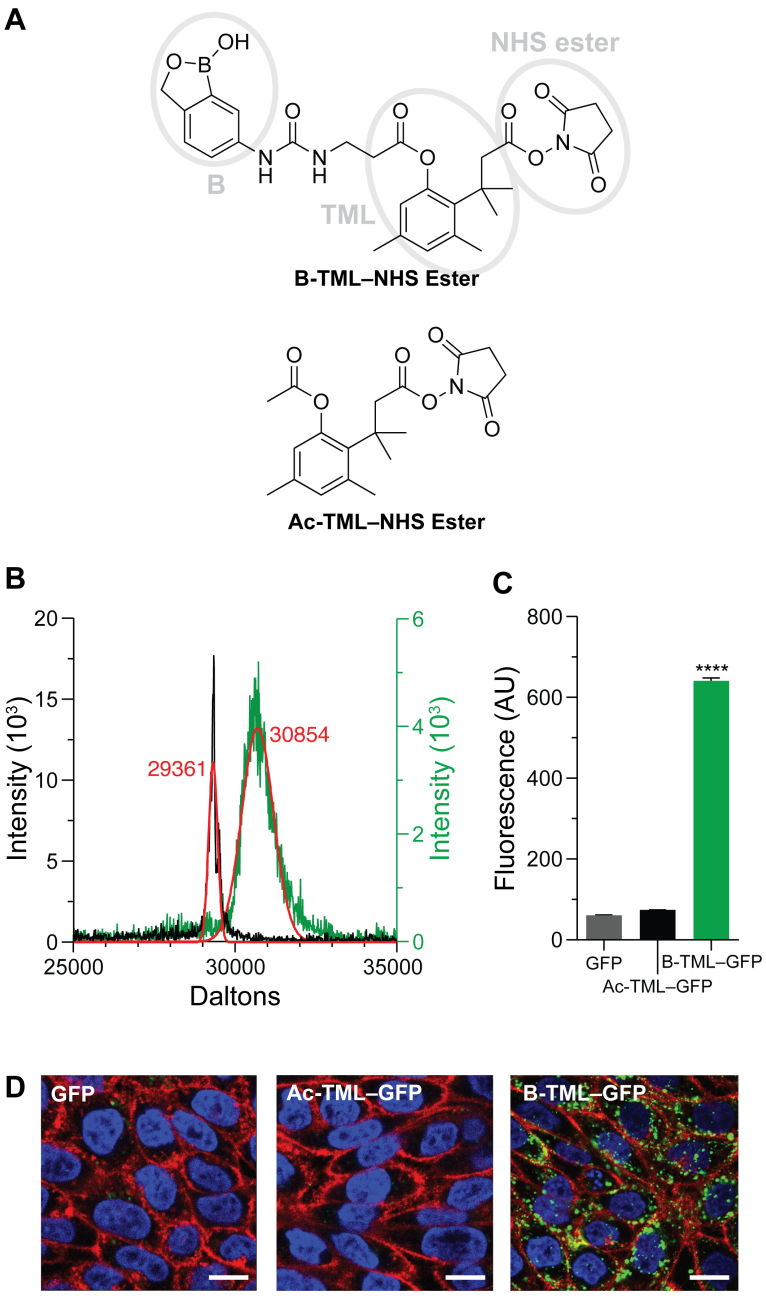
A
NHS ester
B
TML
B-TML–NHS Ester
Ac-TML–NHS Ester
B
Intensity (10³)
Daltons
29361
30854
C
Fluorescence (AU)
****
GFP
B-TML–GFP
Ac-TML–GFP
D
GFP
Ac-TML–GFP
B-TML–GFP

Figure 2.1 Cellular internalization of B-TML-labeled GFP. (A) Structures of B-TML-NHS ester and Ac-TML-NHS ester. Ellipses denote the three distinct modules within B-TML-NHS ester. (B) MALDI−TOF mass spectra of B-TML-GFP (green), conjugated to ~3 boronic acid moieties per molecule and the same protein after exposure to CHO K1 cell lysate and purification (gray). Expected m/z: GFP, 29361; each B-TML moiety, 450. (C) Flow cytometry analysis of CHO K1 cells incubated with 10 μM unlabeled GFP, GFP labeled with a control vehicle (Ac-TML), or GFP labeled with the boronate vehicle (B-TML) for 4 h ($p < 0.0001$). (D) Confocal microscopy of CHO K1 cells grown as in panel C. Cells were stained with WGA-594 (red) and Hoechst 33342 (blue). Scale bars: 10 μm.

Figure 2.2

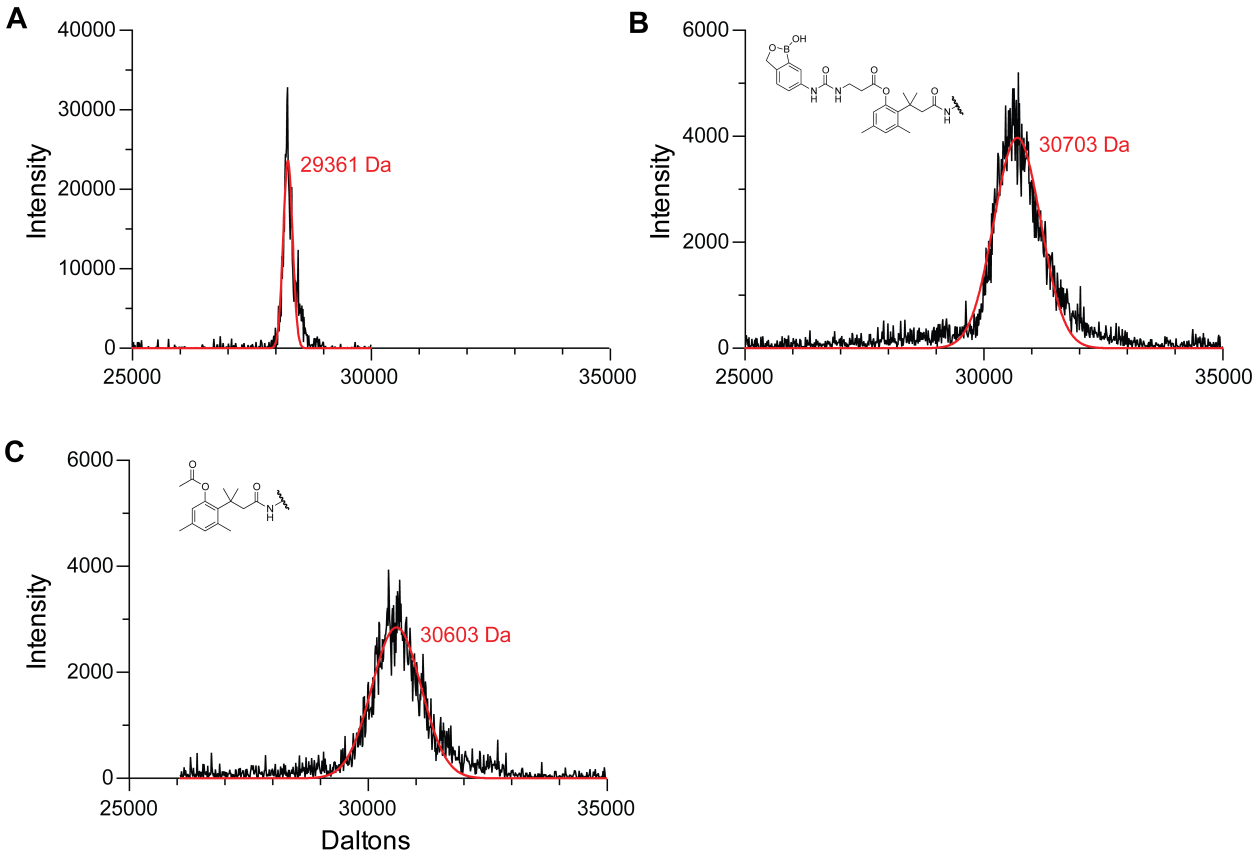
A
40000
30000
20000
10000
0
Intensity
29361 Da
25000
30000
35000
B
6000
4000
2000
0
Intensity
30703 Da
25000
30000
35000
C
6000
4000
2000
0
Intensity
30603 Da
25000
30000
35000
Daltons

Figure 2.2 MALDI–TOF spectra of (A) unmodified GFP, (B) TMLB–GFP, and (C) TMLOAc–GFP. Data for each spectrum were fitted to a Gaussian curve (red line).

Figure 2.3

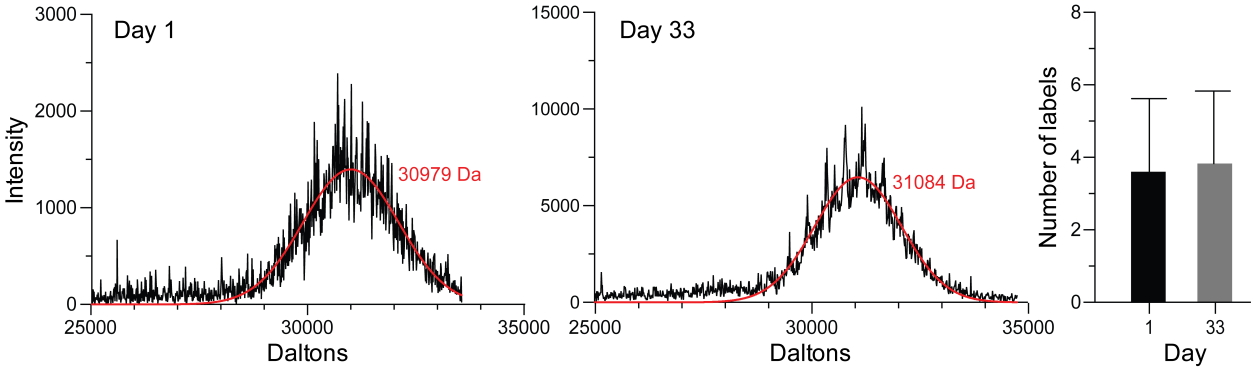
Day 1
Intensity
3000
2000
1000
0
30979 Da
25000
30000
35000
Daltons
Day 33
15000
10000
5000
0
31084 Da
25000
30000
35000
Daltons
Number of labels
8
6
4
2
0
1
33
Day

Figure 2.3 MALDI-TOF of B-TML-GFP on day 1 and day 33 post bioconjugation. Data for each spectrum were fitted to a Gaussian curve (red line).

Figure 2.4

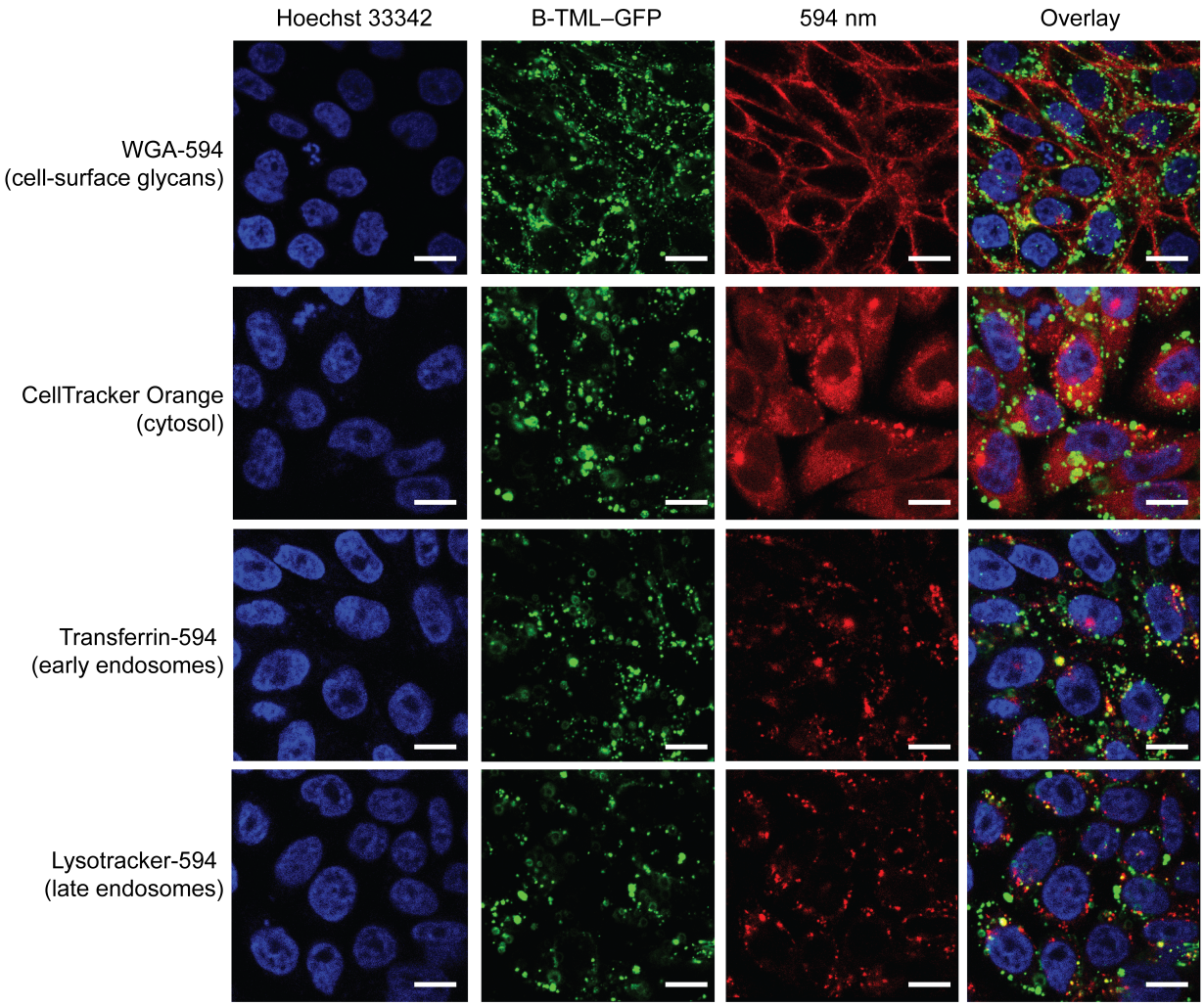
Hoechst 33342
B-TML–GFP
594 nm
Overlay
WGA-594
(cell-surface glycans)
CellTracker Orange
(cytosol)
Transferrin-594
(early endosomes)
Lysotracker-594
(late endosomes)

Figure 2.4 Confocal microscopy images of live cells after a 4-h incubation of CHO K1 cells with TMLB–GFP, subsequently costained with various organelle markers. Scale bars: 10 μm.

Figure 2.5

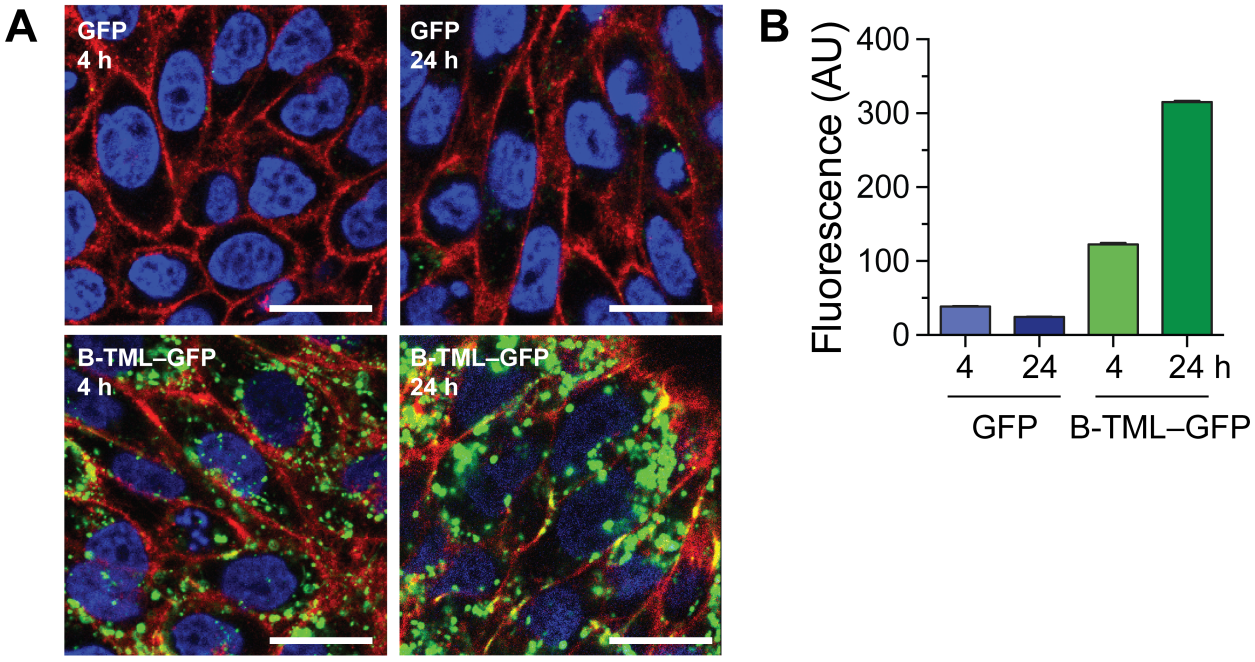
A
GFP
4 h
GFP
24 h
B-TML–GFP
4 h
B-TML–GFP
24 h
B
Fluorescence (AU)
400
300
200
100
0
4
24
4
24 h
GFP
B-TML–GFP

Figure 2.5 Internalization of TMLB–GFP at 4 and 24 h. (A) Confocal microscopy of CHO K1 cells incubated with unlabeled GFP or TMLB–GFP (10 μM) for 4 or 24 h. Cells were stained with WGA-594 (red) and Hoechst 33342 (blue). Scale bars: 10 μm. (B) Flow cytometry analysis of CHO K1 cells incubated with either unlabeled GFP or TMLB–GFP (10 μM) for 4 or 24 h.

Figure 2.6

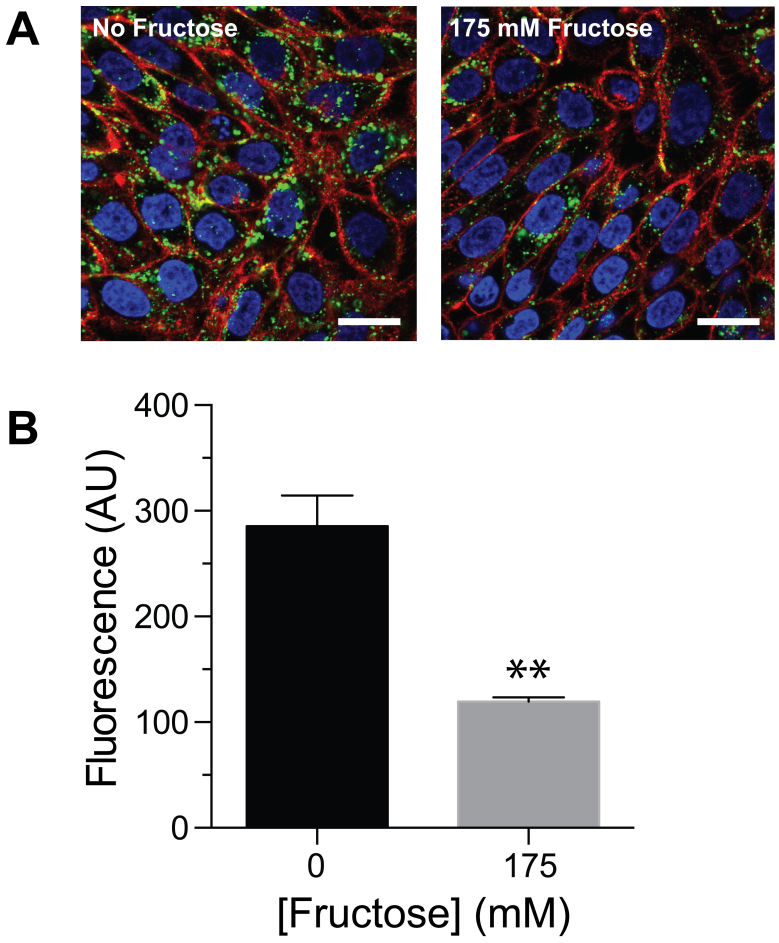
A
No Fructose
175 mM Fructose
B
Fluorescence (AU)
400
300
200
100
0
**
0
175
[Fructose] (mM)

Figure 2.6 Effect of fructose on the cellular internalization of B-TML labeled GFP. (A) Confocal microscopy of B-TML-GFP (10 μM) preincubated with PBS or 175 mM fructose for 30 min, then used to treat CHO K1 cells for 4 h. Cells were stained with WGA-594 (red) and Hoechst 33342 (blue). Scale bars: 20 μm. (B) Flow cytometry analysis of CHO K1 cells treated as in panel A ($p < 0.01$).

Figure 2.7

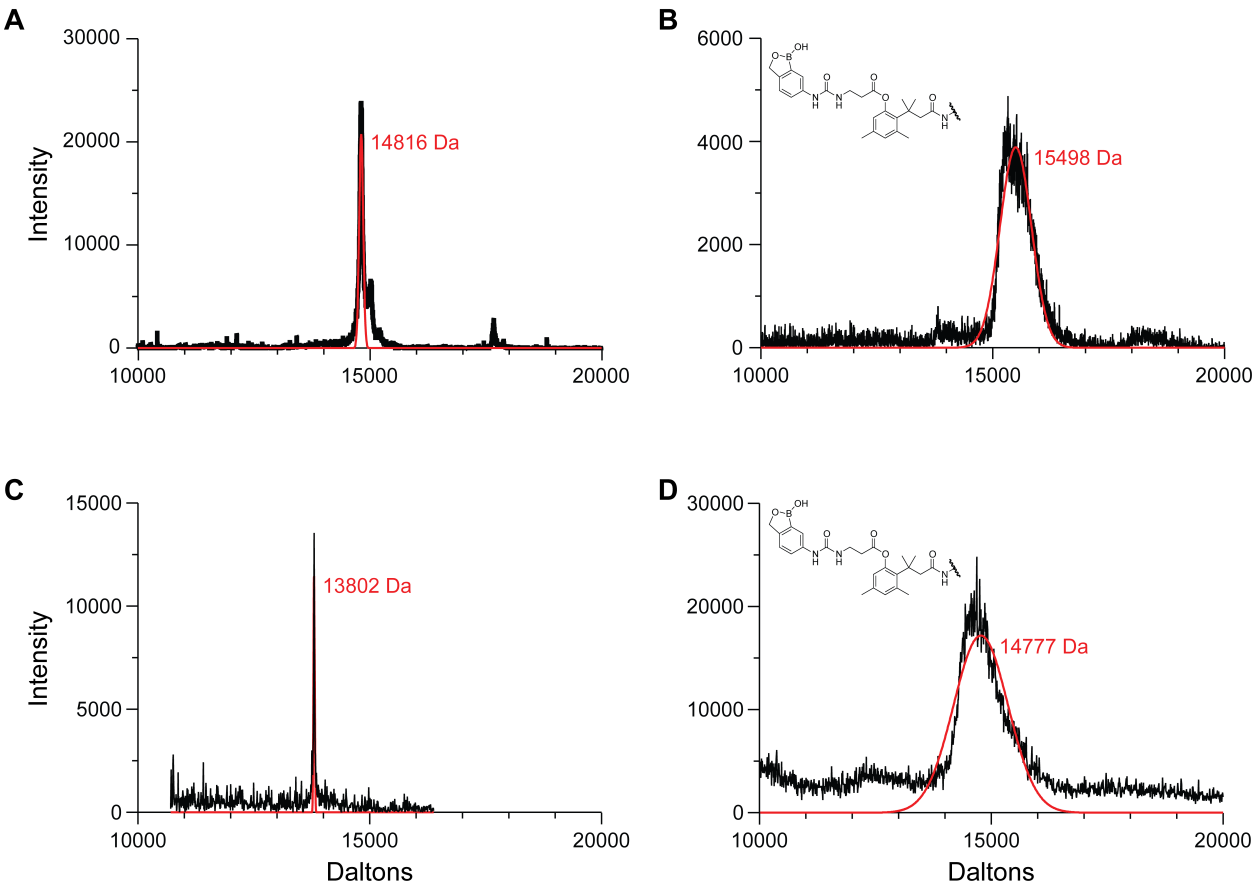
A
30000
20000
10000
0
Intensity
14816 Da
10000
15000
20000
B
6000
4000
2000
0
15498 Da
10000
15000
20000
C
15000
10000
5000
0
Intensity
13802 Da
10000
15000
20000
Daltons
D
30000
20000
10000
0
14777 Da
10000
15000
20000
Daltons

Figure 2.7 MALDI–TOF mass spectra of (A) unmodified FLAG–RNase A (B) TMLB-modified FLAG–RNase A (C) G88R RNase A and (D) TMLB-modified G88R RNase A. Data for each spectra were fitted to a Gaussian curve (red line).

Figure 2.8

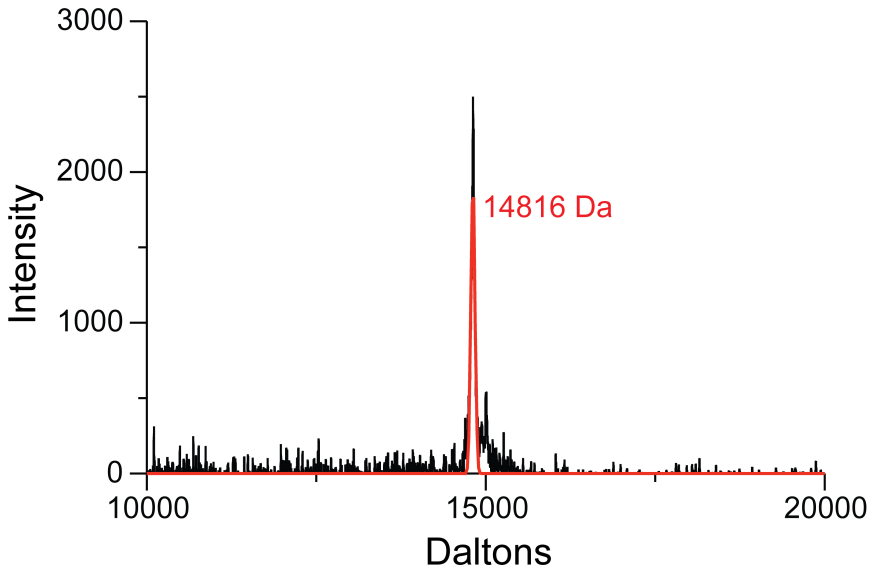
3000
2000
1000
0
Intensity
14816 Da
10000
15000
20000
Daltons

Figure 2.8 K562 cell lysate-treated FLAG–RNase A originally decorated with TML.

Figure 2.9

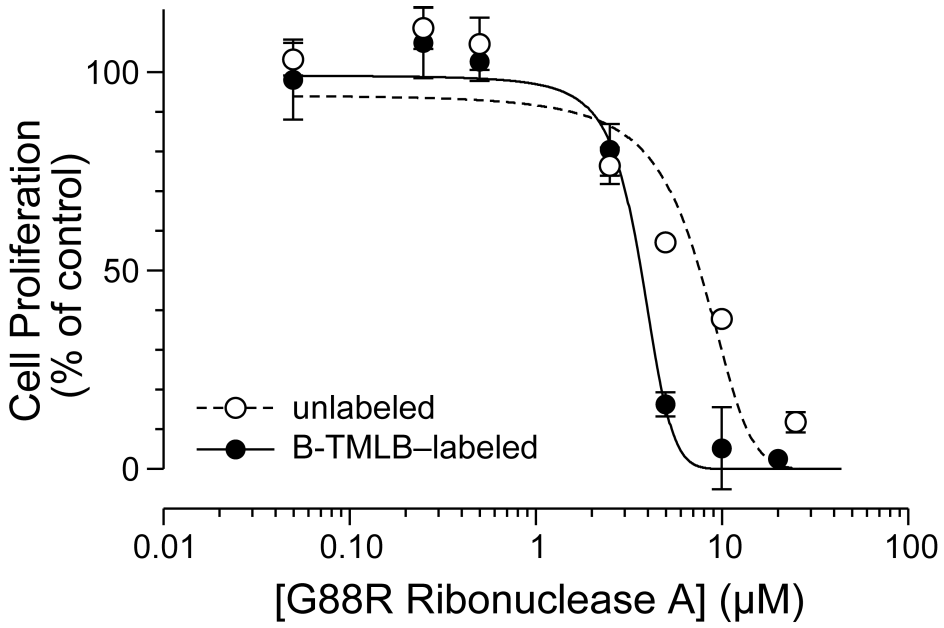
Cell Proliferation
(% of control)
100
50
0
unlabeled
B-TMLB–labeled
0.01
0.10
1
10
100
[G88R Ribonuclease A] (μM)

Figure 2.9 Effect of B-TML-labeling on the inhibition of K-562 cell proliferation by a ribonuclease. Unlabeled G88R ribonuclease A, IC50 = 6.4 ± 0.1 μM; B-TML-labeled G88R ribonuclease A, IC50 = 3.5 ± 0.8 μM. Each data point represents the mean ± SE for three separate experiments, each performed in duplicate.

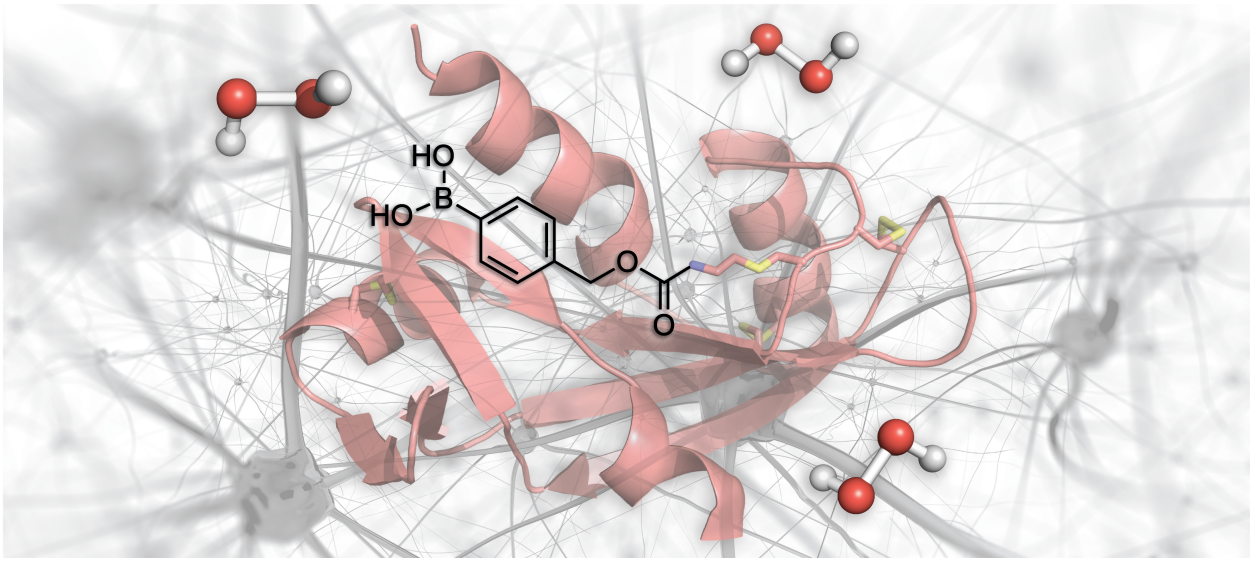
HO
B
HO
O
O

3

Angiogenin–boronic acid conjugate with selective neuroprotection activity*

3.1 Abstract

Angiogenin (ANG) is a human ribonuclease that is compromised in patients with amyotrophic lateral sclerosis (ALS). ANG also promotes neovascularization, and can induce hemorrhage and encourage tumor growth. The causal neurodegeneration of ALS is associated with reactive oxygen species, which are also known to elicit the oxidative cleavage of carbon─boron bonds. We have developed a boronic acid mask that restrains the ribonucleolytic activity of ANG. The masked ANG does not stimulate endothelial cell proliferation but protects astrocytes from oxidative stress. By differentiating between the two dichotomous biological activities of ANG, this strategy predicates a viable pharmacological approach for the treatment of ALS.

3.2 Author Contributions

T.T.H., T.P.S., and R.T.R. conceived the project and designed the experiments. T.P.S. designed, synthesized, and characterized organic compounds. T.T.H. designed and performed *in vitro* and *in cellulo* assays. T.T.H., T.P.S., and R.T.R. analyzed data and wrote the manuscript.

*This chapter has been published, in part, under the same title. Reference:

Hoang, T.T.; Smith, T. P.; Raines, R. T. *Angewandte Chemie International Edition* **2017**, In Press.

3.3 Introduction

Amyotrophic lateral sclerosis (ALS) is an aggressive, fatal disease that is characterized by the selective destruction of motor neurons in the motor cortex, brain stem, and spinal cord.[170] Although the fundamental cause of ALS is not clear, its pathogenesis arises from several mechanisms, including oxidative stress.[171] The only approved chemotherapeutic agent for ALS is a sodium-channel-blocking agent, Riluzole®, that extends survival by only 2–3 months and does not improve motor function.[172,173]

Loss-of-function mutations in the human gene encoding a secretory ribonuclease, angiogenin (ANG), are associated with the progression of ALS.[174,175] In accord, the administration of human ANG increases the lifespan and improves the motor function of ALS-like transgenic mice.[176] Nevertheless, ANG has a well-known adverse effect as a potential chemotherapeutic agent for ALS. As its name implies, ANG induces the proliferation of endothelial cells to form, ultimately, new blood vessels. Accordingly, long-term treatment with ANG could engender hemorrhage and tumor growth.[177-179]

The neurodegeneration that is characteristic of ALS correlates with an abundance of reactive oxygen species (ROS), which are cytotoxic.[110,171,180] Moreover, ALS is linked to the hyperactivity of superoxide dismutase (SOD1).[181,182] This enzyme catalyzes the conversion of superoxide ion (O_2^-) to hydrogen peroxide (H_2O_2), which is the major physiological ROS.

The chemical reactivity of H_2O_2 can be exploited in a physiological context. For example, H_2O_2 has long been known to effect the oxidative cleavage of the boron–carbon bond in phenylboronic acid, leading to phenol and boric acid ($B(OH)_3$).[183] This reaction has served as the basis of chemoselective probes for H_2O_2 and in cancer prodrug strategies.[106,184,185]

ANG relies on the intracellular manifestation of its ribonucleolytic activity to mediate neuroprotection.[186] We envisioned the oxidative cleavage of a boronic acid as a means to generate active ANG *only* in cells suffering from ROS-mediated toxicity.

3.4 Results and Discussion

To install an ROS-sensitive trigger in ANG, we chose to target a key active-site residue: Lys40 (Scheme 3.1). This residue is essential for the ribonucleolytic activity of ANG.[187,188] We replaced Lys40 with a cysteine residue, which serves as a reactive handle for conjugation of a boronic acid containing a latent amino group that is poised to reconstitute catalytic activity. We synthesized the boronic acid **3.1**, as well as a control molecule lacking the boronic acid moiety **3.2**, from an azide precursor via a Curtius rearrangement.

An ROS-activatable phenylboronic acid conjugate (B-thiaK40 ANG) or an inactivatable phenyl conjugate (P-thiaK40 ANG) were made by a radical-initiated thiol-ene reaction (Scheme 3.1).[189,190] Notably, the common method of creating γ-thialysine derivatives by *S*-alkylation with a haloethylamine failed with K40C ANG, despite working with a ribonuclease A, which is an ANG homolog.[191] The integrities of the K40C variant and its conjugation products were confirmed with LC-MS/MS after trypsin digestion (Figure 3.1).

Exposure to an ROS reconstitutes the enzymatic activity of B-thiaK40 ANG *in vitro*. A zymogram assay of ribonucleolytic activity revealed that P-thiaK40 ANG was inactive, even after treatment with H_2O_2 (Figure 3.2a). In contrast, this ROS did elicit activity from B-thiaK40 ANG (Figure 3.2a and 3.2b), which was quantified in solution to be (16 ± 4)% that of the wild-type enzyme (Figure 3.2c). This relative level of activity is similar to that of a variant of ribonuclease A in which γ-thialysine replaces the active-site lysine residue.[191]

The intrinsic catalytic activity of ANG is low.[192] In the three-dimensional structure of ANG, the side chain of Gln117 obstructs a nucleobase-binding pocket in the active site.[193] A Q117G substitution increases the catalytic activity of ANG toward conventional substrates by 30-fold.[194] Accordingly, we generated an ROS-activatable phenylboronic acid conjugate with K40C/Q117G ANG, and we observed enhanced catalytic activity upon its unmasking with H_2O_2, both in a zymogram assay (Figure 3.2a and 3.2b) and in solution (Fig. 3.2c). Moreover, in the context of Q117G ANG, having a lysine or γ-thialysine as residue 40 affects catalytic activity by less than twofold.

ANG promotes endothelial cell proliferation, unlike its P-thiaK40, P-thiaK40/Q117G, B-thiaK40, or B-thiaK40/Q117G variants (Figure 3.3). Thus, conjugation eliminates this biological activity of ANG. Exposure to H_2O_2 does enable B-thiaK40 ANG and B-thiaK40/Q117G ANG to induce cell proliferation. The unmasked variants that have a γ-thialysine as residue 40 are, however, less potent than their isosteres with lysine as residue 40, consistent with relative enzymatic activities observed *in vitro* (Fig. 3.2).

Finally, we asked whether the ROS-activatable masked ANG conjugates elicit a phenotype that could benefit an ALS patient. Astrocytes are prevalent glial cells in the central nervous system that support neuronal plasticity and recovery after injury.[181,195-197] Under stress like that imposed by ALS, motor neurons secrete ANG, which is taken up selectively by astrocytes.[198] Within astrocytes, ANG stimulates pro-survival signals, which are transmitted to motor neurons to afford protection from oxidative damage.[199]

Oxidative stress was imposed upon astrocytes by treatment with either phorbol 12-myristate 13-acetate (PMA) or H_2O_2. PMA activates protein kinase C, stimulating the catalytic production of O_2^- by nicotinamide adenine dinucleotide phosphate oxidase.[200] To begin, we

determined the toxicity of each agent to human astrocytes (Figure 3.4a) and found a dose–response correlation between doses that led to 25%, 50%, and 75% cell survival and intracellular ROS levels (Figure 3.4b).

Like wild-type ANG, B-thiaK40 ANG and B-thiaK40/Q117G ANG protect human astrocytes from ROS-mediated toxicity. This protection was evident for cells challenged with all three doses of PMA or H_2O_2 (Figure 3.5). In contrast, no benefit was observed upon treatment of astrocytes with P-thiaK40 ANG or P-thiaK40/Q117G ANG. Importantly, our data indicate that the neuroprotection afforded by B-thiaK40/Q117G ANG is comparable to that of the wild-type enzyme.

The byproducts that form upon unmasking of the ANG conjugates are not cytotoxic. The immolative mechanism of unmasking produces boric acid and 4-hydroxybenzyl alcohol (Scheme 3.2). Millimolar levels of boric acid or 4-hydroxybenzyl alcohol, alone or in combination, did not lead to detectable toxicity for human astrocytes (Figure 3.6).

3.5 Conclusions

In conclusion, we have described a semisynthetic ANG that is inactive under normal physiological conditions but becomes active in the presence of the most prevalent ROS—H_2O_2. ALS is an incurable disease that is linked to hypoactive ANG[174,175] and hyperactive SOD1,[181,182] which catalyzes the formation of H_2O_2. The accumulating H_2O_2 could serve to unmask our semisynthetic ANG selectively in contexts relevant for the treatment of ALS.

3.6 Acknowledgements

We are grateful to M. Wickens for use of his ultraviolet light box, G. Sabat for help in the analysis of mass spectra, and C. L. Jenkins for contributive discussions. T.T.H. was supported by an Advanced Opportunity/Graduate Research Scholar Fellowship and by Molecular Biosciences Training Grant T32 GM007215 from the National Institutes of Health (NIH). This work was supported by grants R01 CA073808 and R01 GM044786 (NIH), and made use of the National Magnetic Resonance Facility at Madison, which is supported by Grant P41 GM103399 (NIH).

3.7 Materials and Methods

3.7.1 General Information

All chemicals and reagents were from Sigma–Aldrich Chemical (St. Louis, MO) unless indicated otherwise, and were used without further purification. All glassware was flame-dried, and all synthetic chemical reactions were performed under N_2 (g). Dichloromethane (DCM), tetrahydrofuran (THF), triethylamine (TEA), and dimethylformamide (DMF) were dried with columns of alumina. Removal of solvents "under reduced pressure" refers to the use of a rotary evaporator with water-aspirator pressure (<20 torr) and water bath at <40 °C. Flash column chromatography was performed with 40–63 Å silica (230–400 mesh) from Silicycle (Québec City, Canada); thin-layer chromatography (TLC) was performed with EMD Millipore 250-μm silica gel 60 F_{254} plates from Sigma–Aldrich. Poly(cytidylic acid) was from Sigma–Aldrich; 6-FAM–dArUdAdA–6-TAMRA was from IDT (Coralville, IA).

All procedures were performed in air at ambient temperature (~22 °C) and pressure (1.0 atm) unless indicated otherwise. ^{1}H and ^{13}C NMR spectra were acquired with a Bruker Avance III 500i spectrometer at the National Magnetic Resonance Facility at Madison and referenced to

residual protic solvent. Mass spectrometry was performed with a Micromass LCT (electrospray ionization, ESI) instrument at the Mass Spectrometry Facility in the Department of Chemistry at the University of Wisconsin–Madison. Fluorescence and absorbance measurements were made with an M1000 fluorescence plate reader from Tecan (Männedorf, Switzerland). Statistical analyses were performed with Prism 5 from GraphPad Software (La Jolla, CA). All data are shown as the mean ± standard error of the mean (SEM).

Human cells were from Lonza (Walkersville, MD) and were maintained according to recommended procedures. Medium and added components, trypsin (0.25% w/v), and Dulbecco's PBS (DPBS) were the Gibco® brand from ThermoFisher Scientific (Waltham, MA). Cells were grown in flat-bottomed culture flasks in a cell-culture incubator at 37 °C under CO_2 (g) (5% v/v). Human umbilical vein endothelial cells (HUVEC) were grown in EGM™-2; human astrocytes were grown in AGM™. The Corning 96-well microplates used in experiments were from Sigma–Aldrich.

3.7.2 Chemical Synthesis

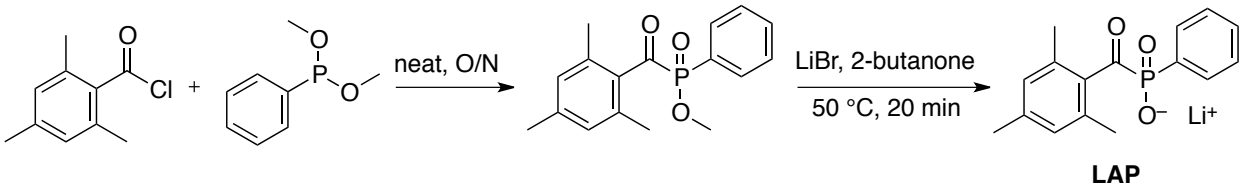

LAP

The water-soluble photoactivatable radical initiator, lithium phenyl-2,4,6-trimethylbenzoylphosphinate (**LAP**), was synthesized as reported previously.[1] Briefly, dimethyl phenylphosphonite (0.186 mL, 1.17 mmol) was added to neat 2,4,6-trimethylbenzoyl chloride, and the reaction mixture was stirred overnight. A solution of LiBr (0.406 g, 4.68 mmol) in 2-butanone (10 mL) was added to the reaction mixture, which was then heated to 50 °C for 20 min as a white precipitate formed. The reaction mixture was cooled and filtered to afford **LAP** as a white solid (0.325 g, 97%).

^{1}H NMR (500 MHz, D_2O, δ): 1.97 (s, 6H), 2.26 (s, 3H), 6.81 (s, 2H), 7.39–7.42 (t, J = 7.65 Hz, 2H), 7.48–7.51 (t, J = 7.20 Hz, 1H), 7.66–7.68 (d, J = 11.25 Hz, 1H), 7.67–7.70 (d, J = 11.23 Hz, 1H); **^{13}C NMR (125 MHz, D_2O, δ)**: 21.16, 22.77, 130.72, 130.97, 131.07, 134.70, 134.73, 134.75, 134.83, 134.91, 135.77, 136.31, 140.26, 140.57, 142.53; **HRMS** (ESI) calculated for $[C_{16}H_{16}O_3P]$ $(M - H)^-$ requires m/z 287.0843; found m/z 287.0841

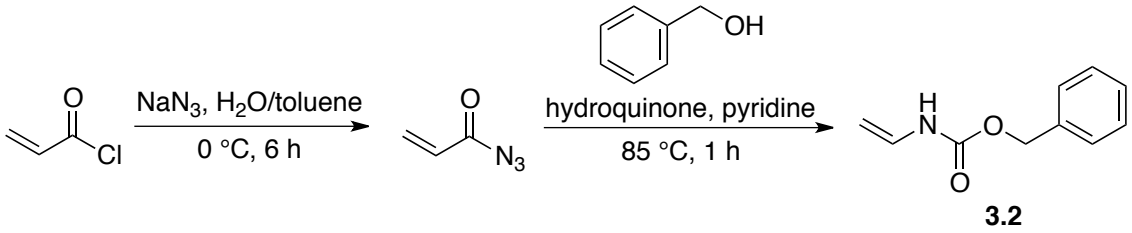

3.2

Carbamate **3.2** was accessed via a Curtius rearrangement as reported previously.[2] Briefly, sodium azide (0.430 g, 5.52 mmol) was dissolved in water (3.75 mL), and the resulting solution was cooled to 0 °C. A solution of acryloyl chloride (0.500 mL, 5.52 mmol) in toluene (2.25 mL) was then added dropwise to the reaction mixture, which was stirred at 0 °C for 6 h. The layers were separated quickly, and the organic layer was washed with Na_2CO_3 (2 × 3 mL) and dried with $MgSO_4$(s). The reaction mixture was then filtered and added dropwise to a stirring solution of benzyl alcohol (0.776 g, 7.17 mmol), pyridine (0.218 g, 2.76 mmol), and hydroquinone (0.031 g, 0.286 mmol) at 85 °C. The reaction mixture was stirred at 85 °C for 1 h. The reaction mixture was then washed with saturated aqueous Na_2CO_3 and dried with Na_2SO_4(s). The solvent was removed under reduced pressure, and the crude product was purified with by flash chromatography (30% v/v EtOAc in hexanes) to afford compound **3.2** as a white solid (0.610 g, 62%).

^{1}H NMR (500 MHz, $CDCl_3$, δ): 4.30–4.31 (d, J = 8.78 Hz, 1 H), 4.47–4.50 (d, J = 15.83 Hz, 1H), 5.15 (s, 2H), 6.44 (bs, 1 H), 6.68–6.76 (m, 1 H), 7.26–7.38 (m, 5H); **^{13}C NMR (125 MHz, $CDCl_3$, δ)**: 67.35, 93.51, 128.42, 128.54, 128.75, 129.88, 135.98, 153.55; **HRMS** (ESI) calculated for $[C_{10}H_{11}NO_2]^+$ $(M + H)^+$ requires m/z 178.0863; found m/z 178.0860

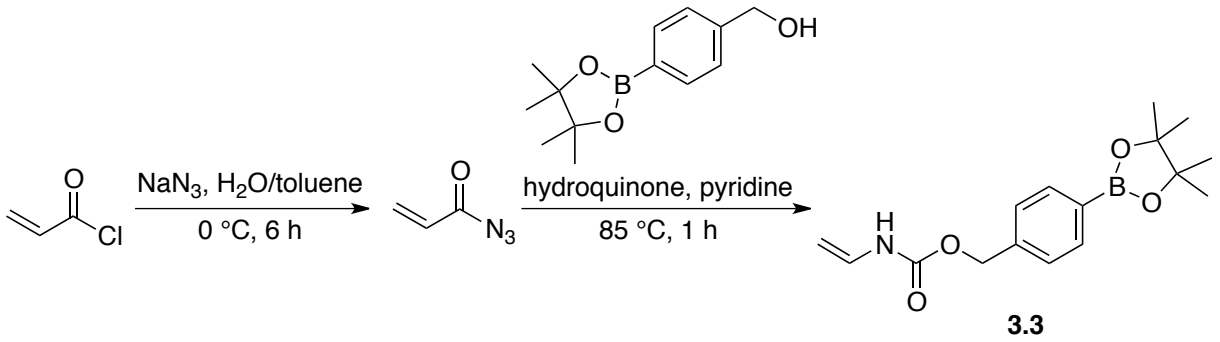

Pinacol-protected boronated carbamate **3.3** was accessed in the same manner as was carbamate **3.2**. Briefly, sodium azide (0.430 g, 5.52 mmol) was dissolved in water (3.75 mL), and the resulting solution was cooled to 0 °C. A solution of acryloyl chloride (0.500 mL, 5.52 mmol) in toluene (2.25 mL) was added dropwise, and the reaction mixture was allowed to stir at 0 °C for 6 h. The layers were separated quickly, and the organic layer was washed with Na_2CO_3 (2 × 3 ml) and dried with $MgSO_4$(s). The reaction mixture was then filtered and added dropwise to a stirring solution of 4-(hydroxymethyl)phenylboronic acid pinacol ester (1.60 g, 7.17 mmol), pyridine (0.218 g, 2.76 mmol), and hydroquinone (0.031 g, 0.286 mmol) at 85 °C. The reaction mixture was allowed to stir at 85 °C for 1 h. The reaction mixture was then washed with saturated aqueous Na_2CO_3 and dried with Na_2SO_4(s). The solvent was removed under reduced pressure, and the crude product was purified by flash chromatography (30% v/v EtOAc in hexanes) to afford compound **3.3** as a white solid (0.742 g, 44%).

^{1}H NMR (500 MHz, $CDCl_3$, δ): 1.34 (s, 12 H), 4.30–4.32 (d, J = 8.76 Hz, 1 H), 4.47–4.50 (d, J = 15.72 Hz, 1H), 5.16 (s, 2H), 6.46 (bs, 1 H), 6.68–6.75 (m, 1 H), 7.35–7.36 (d, J = 7.67 Hz, 2 H), 7.80–7.82 (d, J = 7.77 Hz, 2H); **^{13}C NMR (125 MHz, $CDCl_3$, δ)**: 24.84, 67.02, 83.87, 93.40, 127.24, 129.71, 135.02, 138.83, 153.33; **HRMS** (ESI) calculated for $[C_{16}H_{22}BNO_4]^+$ $(M + NH_4)^+$ requires m/z 320.2016; found m/z 320.2014

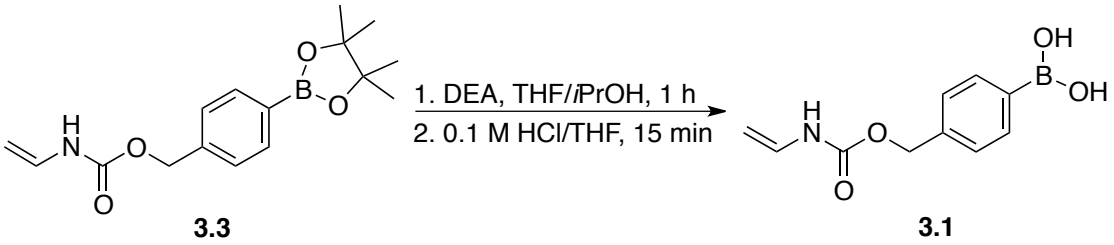

3.3 **3.1**

Boronated carbamate **3.1** was prepared from pinacol-protected boronated carbamate **3.3** by using a procedure modified from the literature.[3] Compound **3.3** (0.050 g, 0.164 mmol) was dissolved in a 4:1 mixture of THF/*i*PrOH (1.60 mL). Diethanolamine (0.019 g, 0.180 mmol) was added dropwise, and the reaction mixture was allowed to stir for 1 h until formation of a white precipitate. The reaction mixture was then filtered, and the precipitate was collected and resuspended in 1.6 mL solution of 1:4 0.1 M HCl/THF. The reaction mixture was stirred for 10 min, and reaction progress was monitored with TLC. (Note: significant product degradation was observed at longer reaction times.) The reaction mixture was then diluted with water, and the organic solvent was removed under reduced pressure until a white precipitate formed. The resulting precipitate was filtered and washed with chloroform to afford compound **3.1** as a white solid (0.026 g, 73%).

^{1}H NMR (500 MHz, CD_3OD, δ): 4.23–4.24 (d, J = 8.87 Hz, 1H), 4.53–5.56 (d, J = 15.88 Hz, 1H), 5.13 (s, 2H), 6.62–6.67 (dd, J = 15.90, 8.92 Hz, 1H), 7.35–7.37 (d, J = 7.65 Hz, 2H), 7.60–7.62 (d, J = 7.60 Hz, 2H); **^{13}C NMR (125 MHz, CD_3OD, δ)**: 67.62, 93.77, 127.96, 131.48, 134.72, 139.20, 156.14; **HRMS** (ESI) calculated for the single methyl boronic ester $[C_{11}H_{14}BNO_4]^+$ $(M + NH_4)^+$ requires m/z 252.1390; found m/z 252.1390

3.7.3 Preparation of ANG, its variants, and their conjugates

ANG and its Q117, K40C, and K40C/Q117G variants were prepared as described previously.[4,5] The B-thiaK40 ANG, P-thiaK40 ANG, B-thiaK40/Q117G ANG, and P-thiaK40/Q117G ANG conjugates were prepared by reaction of K40C ANG or K40C/Q117G ANG (9 mg) with a 50-fold molar excess of compound **3.1** or **3.2**, and a 10-fold molar excess of LAP in 50 mM HEPES–KOH buffer, pH 8.0, containing reduced glutathione (20 mM). Samples were placed in a XL-1500 UV Spectrolinker from Spectronics (Westbury, NY) and irradiated from above with 365-nm light for 30 min. Conjugates were purified by chromatography using a HiTrap SP HP cation-exchange column (GE Healthcare). The molecular mass of each ANG conjugate was confirmed by LC-MS/MS. Protein concentration was determined by using a bicinchoninic acid assay kit from Pierce Chemical (Rockford, IL). This procedure typically afforded 2–3 mg of conjugate.

3.7.4 Unmasking of ANG conjugates *in vitro*

P-thiaK40 ANG, B-thiaK40 ANG, and their Q117G variants (3.0 mg/mL) were incubated with H_2O_2 (1.0 mM) at 37 °C for 3 h, followed by dialysis against PBS to remove excess H_2O_2. The unmasked proteins were then characterized by LC-MS/MS, and further used in *in vitro* enzymatic assay and *in cellulo* cell proliferation assay.

3.7.5 Zymograms

Solutions of wild-type ANG, its variants, and that conjugates (40 ng) were diluted 1:1 with 2× Laemmli buffer from Bio-Rad (Hercules, CA), and the resulting solutions were loaded on to a polyacrylamide gel (15% w/v) containing poly(C). The loaded gel was subjected to

electrophoresis for 1.5 h at 100 V. Subsequent washing, refolding and staining with toluidine blue were performed as described previously.[6]

3.7.6 Assays of ribonucleolytic activity

The ribonucleolytic activity of wild-type ANG, its variants, and their conjugates (100 nM) was determined by measuring the initial velocity of cleavage of 6-FAM–dArUdAdA–6-TAMRA[7] (200 nM) in 100 mM Tris–HCl buffer, pH 7.5, containing NaCl (100 mM). Assays were performed in the wells of a 96-well plate.

3.7.7 Assays of endothelial cell proliferation

HUVEC cells in EGM™-2 were plated at 5,000 cells per well in a 96-well plate. After 24 h, cells were switched to EBM-2 containing ANG or a variant (1 μg/mL). At known times, growth medium was removed and cells were incubated with fluorescent dye CyQUANT® NF (Invitrogen) binding solution. Fluorescence intensity was measured with excitation at 485 nm and emission detection at 530 nm.

3.7.8 Measurement of intracellular ROS levels

The ROS levels within untreated, PMA-treated, and H_2O_2-treated cells were measured by staining with chloromethyl-2′,7′-dichlorofluorescein diacetate (CM-DCFDA). Human astrocytes were counted by using a CyQUANT® NF assay from ThermoFischer. Astrocytes were plated at 10,000 cells per well in a 96-well plate. After 24 h, the astrocytes were treated with variable

concentrations of PMA or H_2O_2 for 1 h before incubating with CM-DCFDA for ROS analysis. Fluorescence intensity was recorded with excitation at 492 nm and emission detection at 520 nm.

3.7.9 Assays of astrocyte survival

Human astrocytes were plated at 10,000 cells per well in a 96-well plate. Wild-type ANG, its variants, their conjugates, and vehicle were added to the cells and incubated for 24 h. Cells were washed with AGM™ medium and treated with variable concentrations of PMA or H_2O_2. After 24 h, the medium was removed, and cells were incubated with CellTiter 96 MTS reagent from Promega (Madison, WI) for 3 h before detection.

3.8 NMR Spectra

^{1}H NMR and ^{13}C NMR Spectra of **LAP** in D_2O

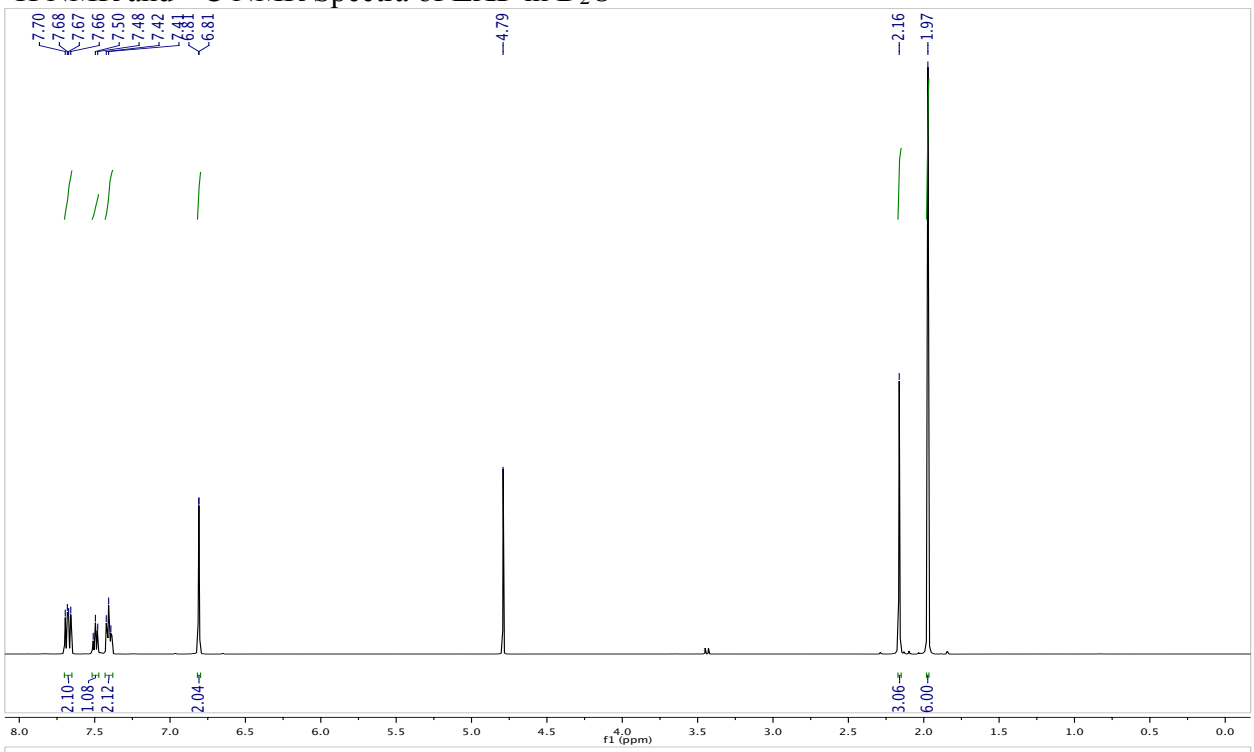

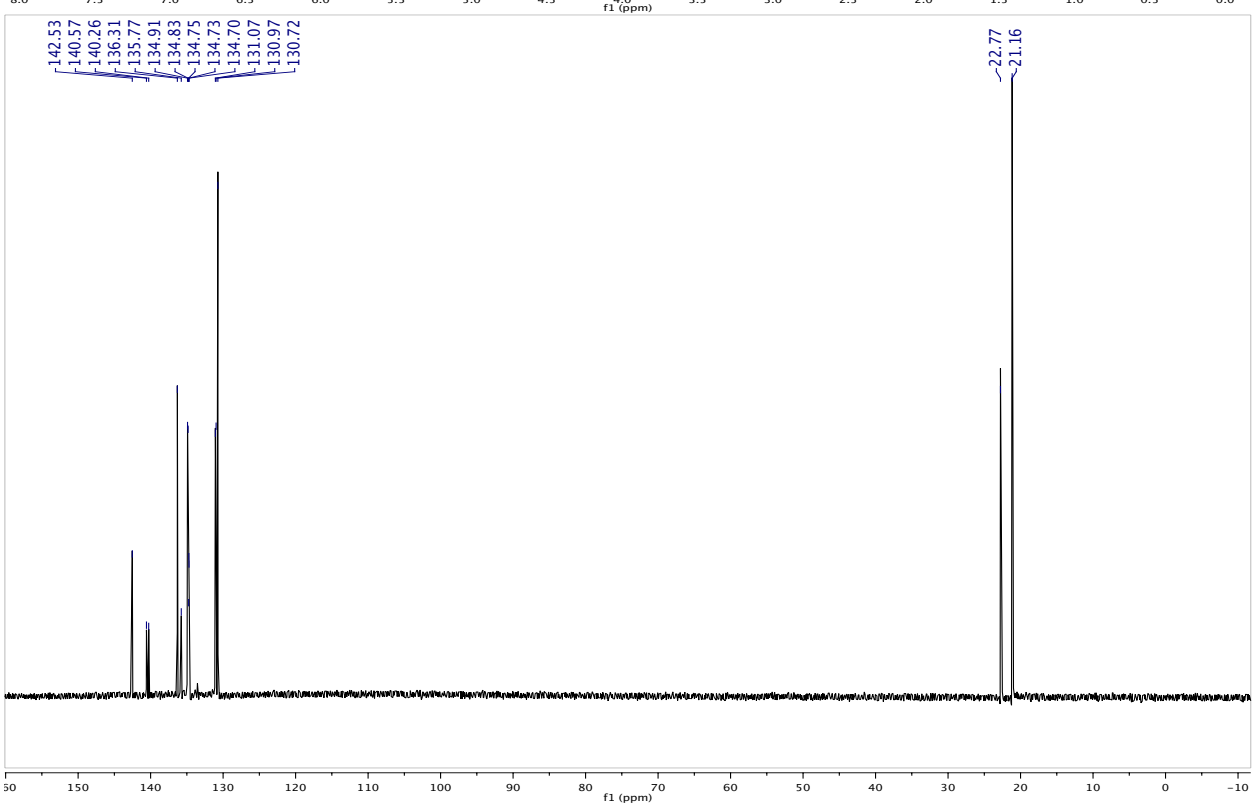

^{1}H NMR and ^{13}C NMR Spectra of Compound **3.2** in $CDCl_3$

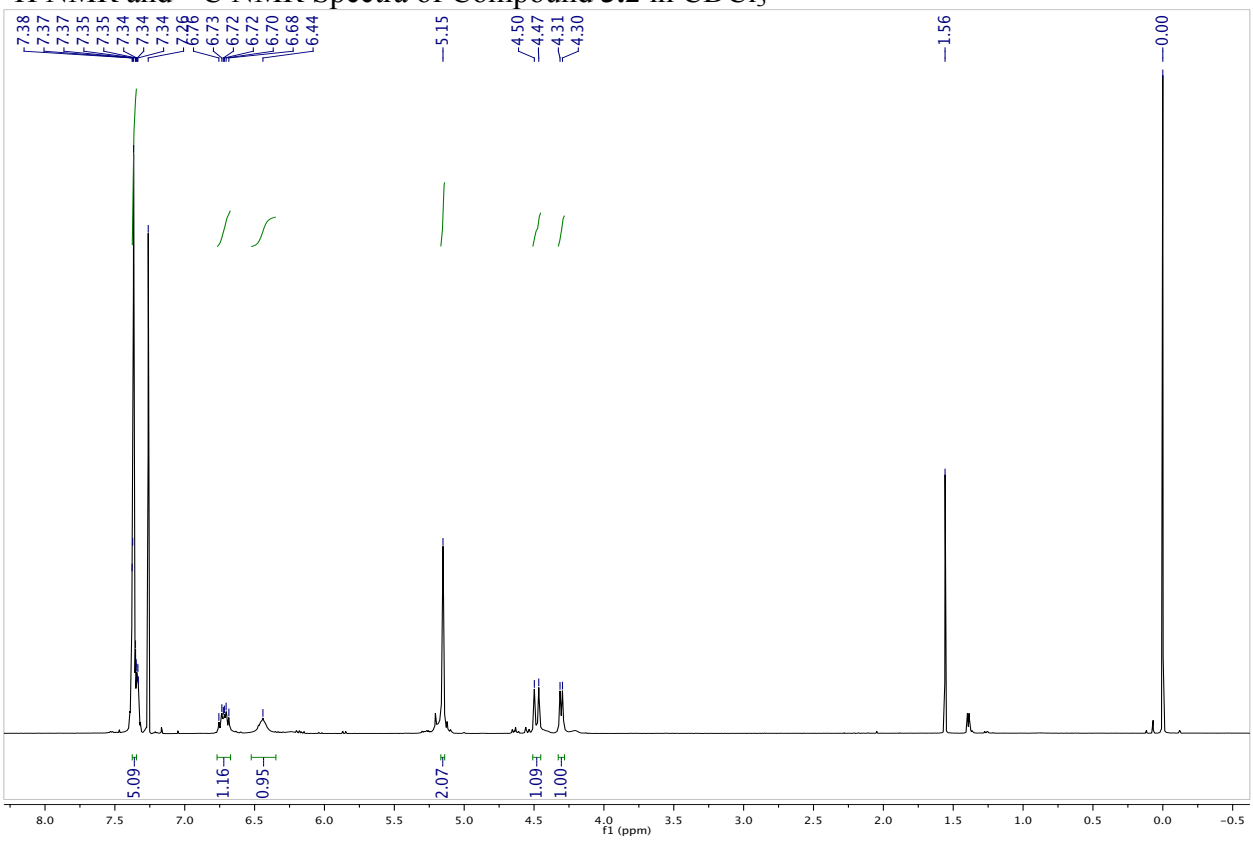

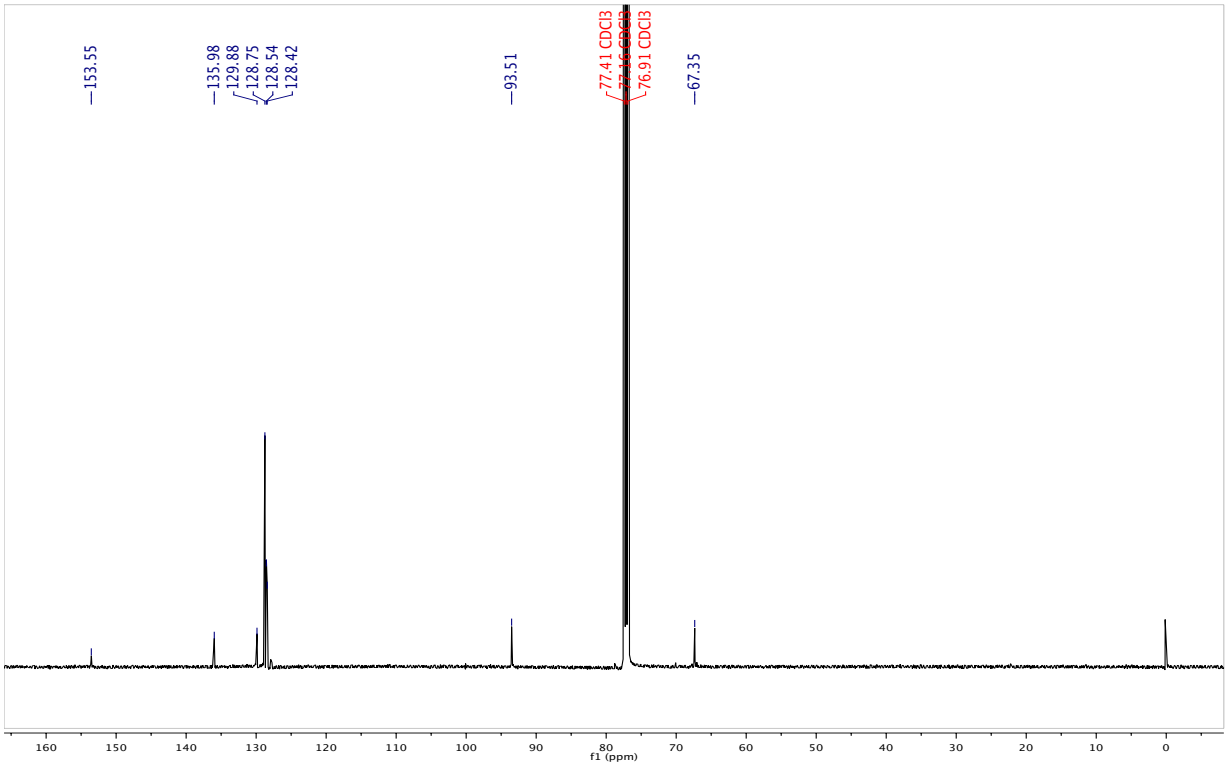

^{1}H NMR and ^{13}C NMR Spectra of Compound **3.3** in $CDCl_3$

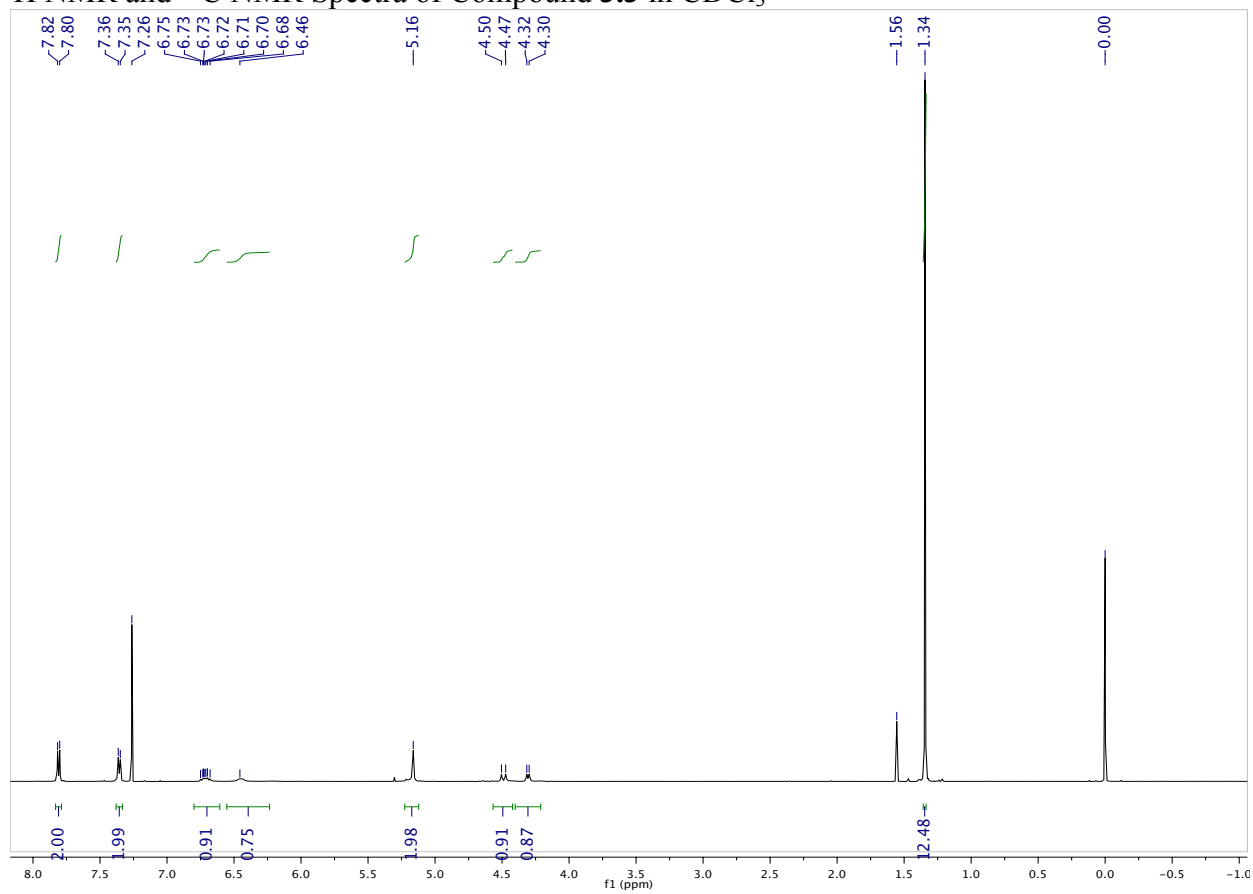

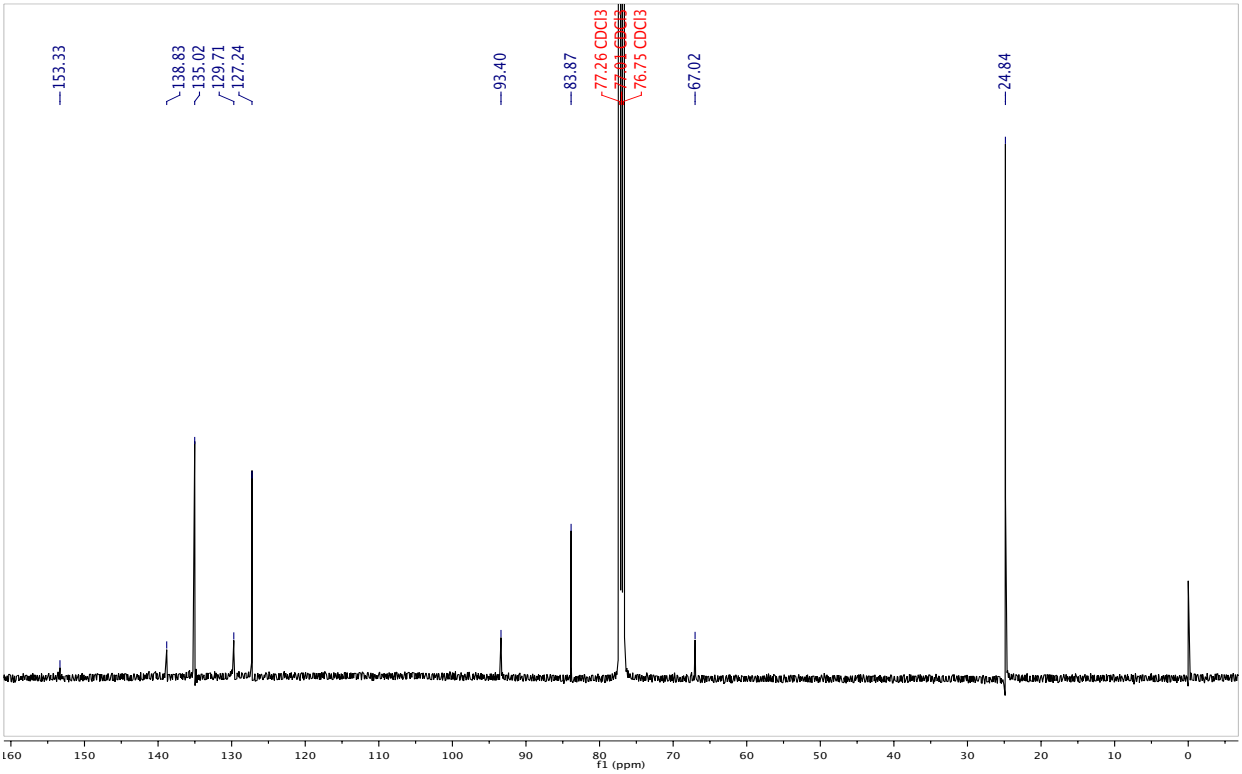

^{1}H NMR and ^{13}C NMR Spectra of Compound **3.1** in CD_3OD

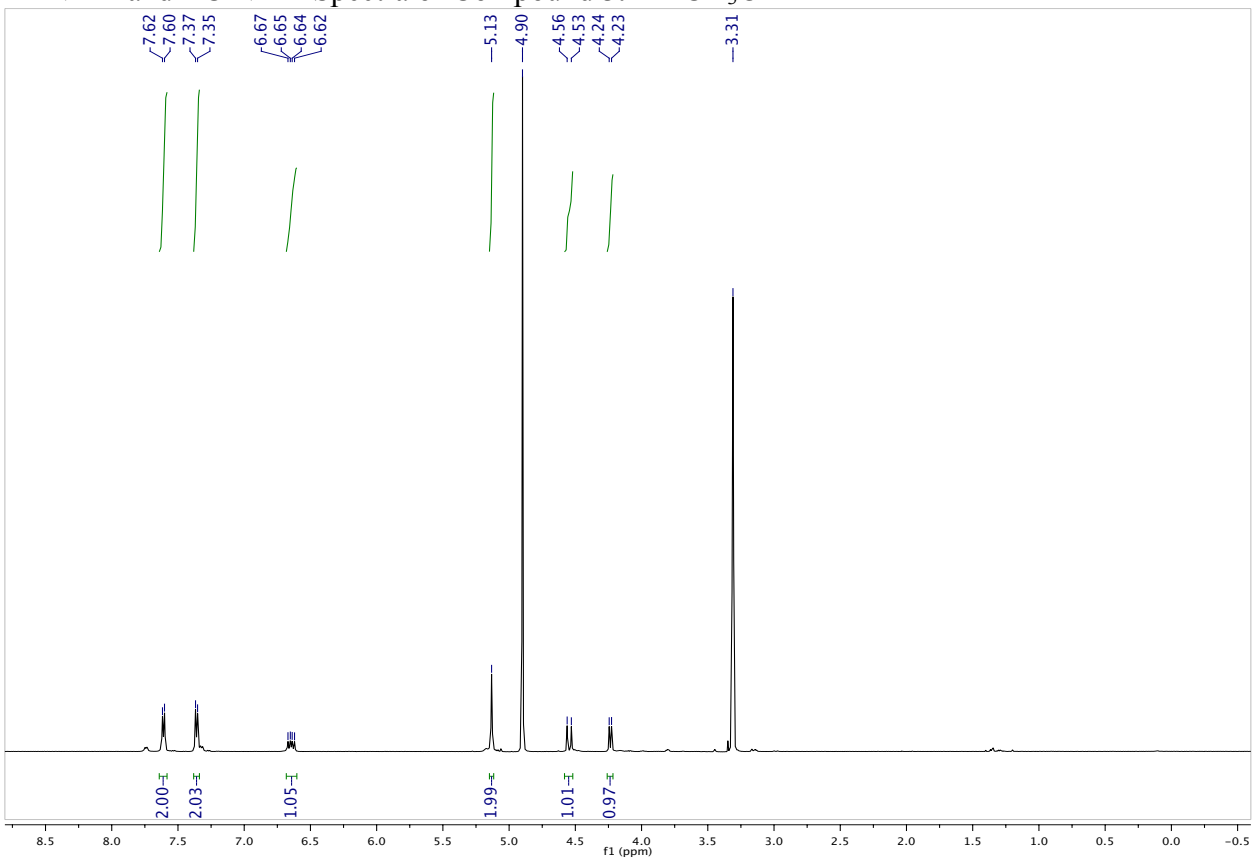

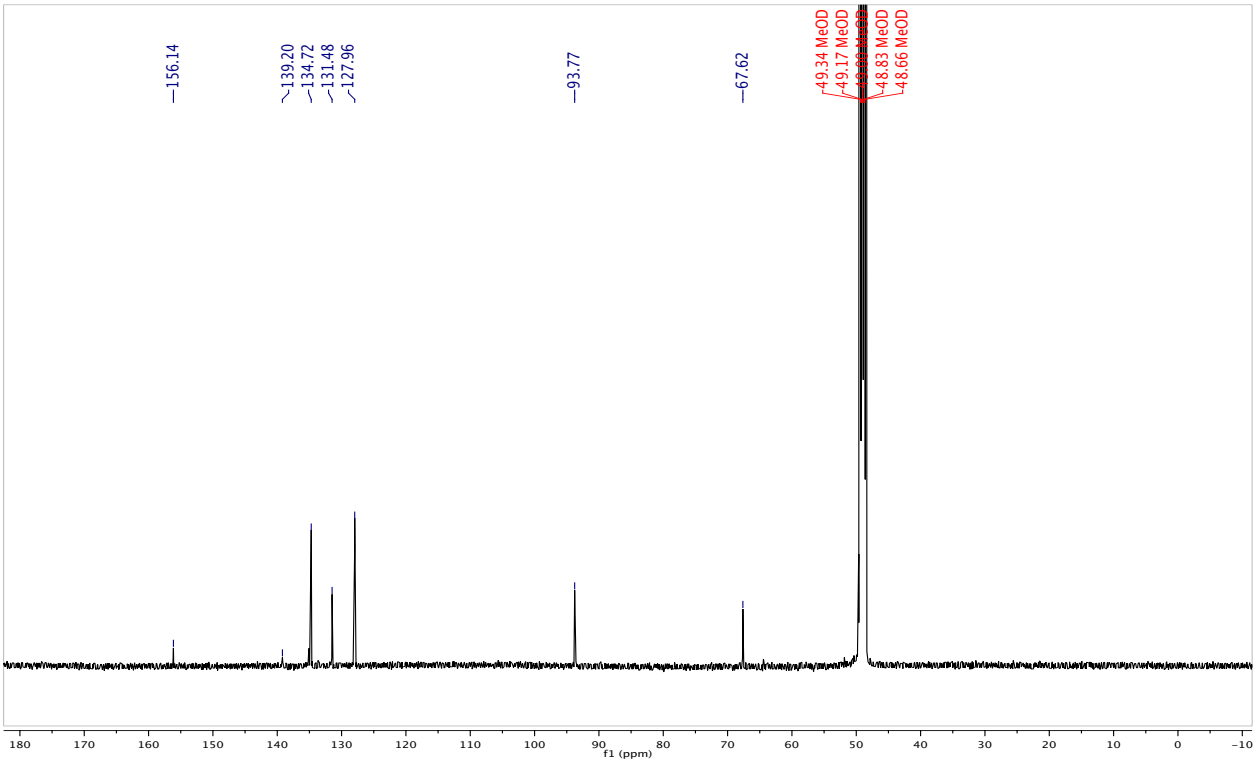

Scheme 3.1

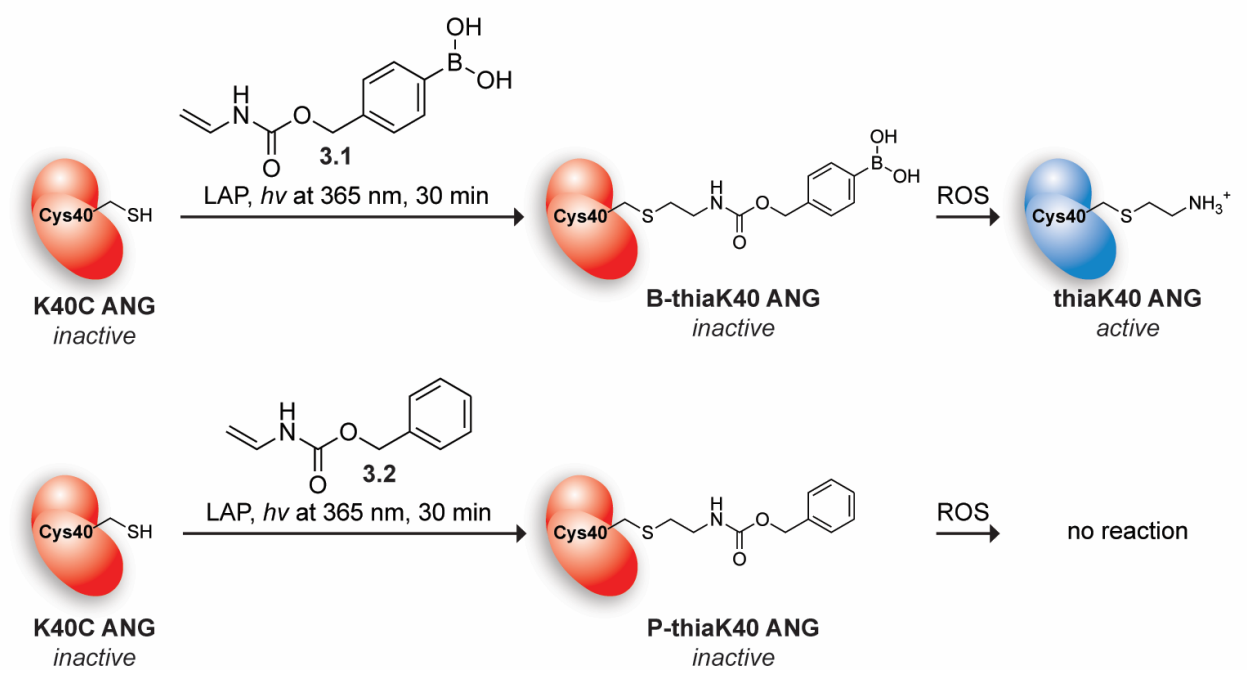
OH
B
OH
H
N
O
O
3.1
Cys40
SH
LAP, hv at 365 nm, 30 min
Cys40
S
ROS
Cys40
S
NH3+
K40C ANG
inactive
B-thiaK40 ANG
inactive
thiaK40 ANG
active
3.2
LAP, hv at 365 nm, 30 min
ROS
no reaction
K40C ANG
inactive
P-thiaK40 ANG
inactive

Scheme 3.1 Synthesis and unmasking of an ROS-responsive conjugate of human ANG. Lys40 is a key residue in the active-site of ANG. The K40C variant, which lacks biological activity, was modified by a thiol-ene reaction with a boronic acid containing a latent amino group (**3.1**). The ensuing B-thiaK40 ANG is also inactive, except in environments with high levels of H_2O_2, which unmask the γ-thialysine residue and restore the biological activity of ANG. P-thiaK40 ANG lacks the boronic acid moiety and is not responsive to H_2O_2.

Scheme 3.2

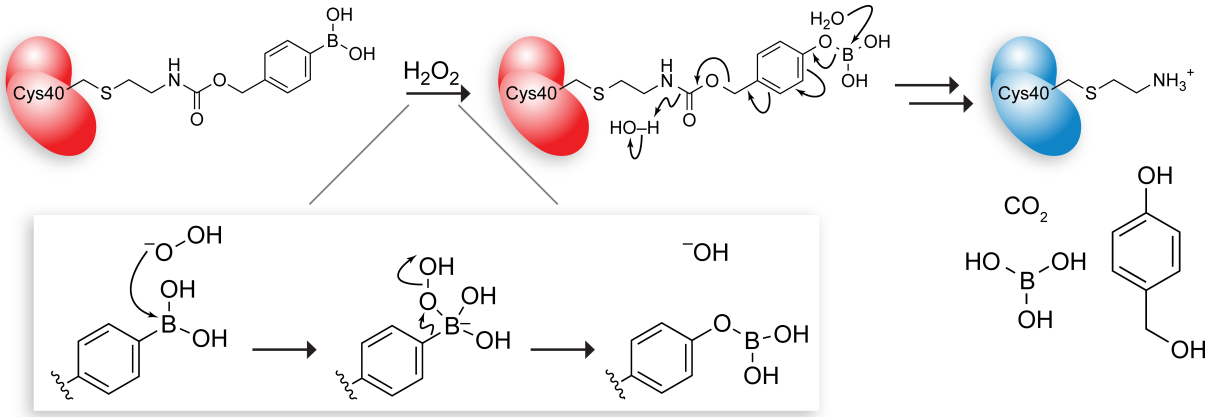

Scheme 3.2 Putative mechanism for the unmasking of B-thiaK40 ANG by an ROS. In the presence of H_2O_2, the boronic acid is oxidized, leading to the formation of carbon dioxide, boric acid, and quinone methide, which is converted to 4-hydroxybenzyl alcohol upon attack by water. Inset: Putative mechanism for the oxidation of a phenylboronic acid moiety by H_2O_2.

Figure 3.1

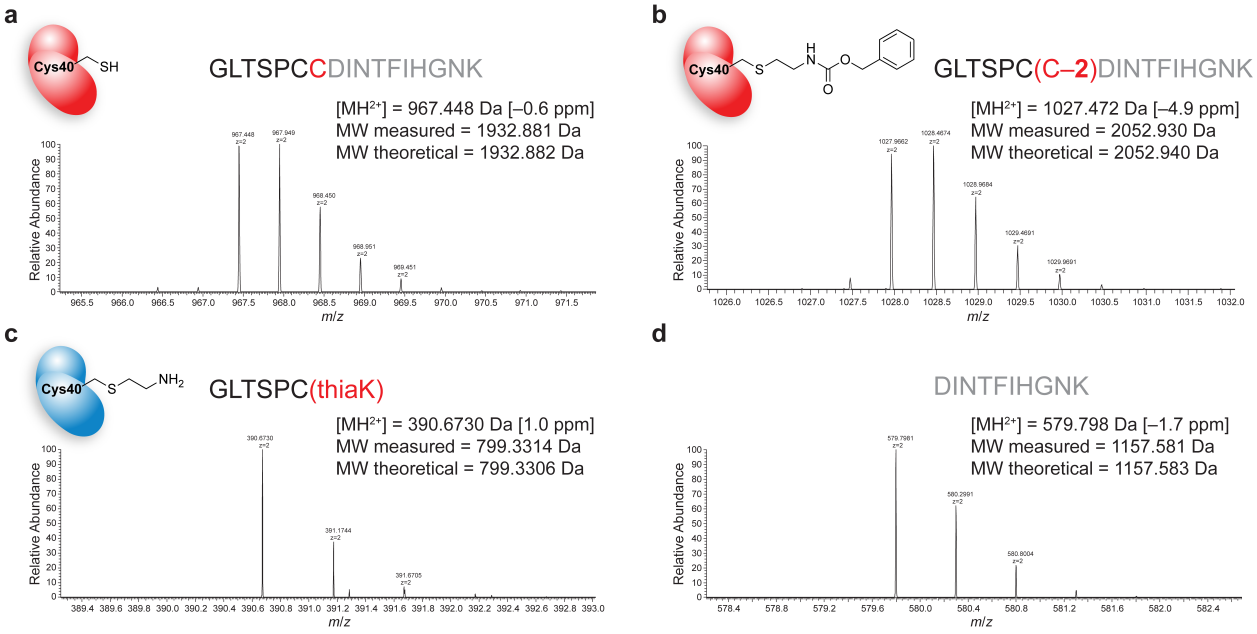
a
Cys40
SH
GLTSPCCDINTFIHGNK
[MH2+] = 967.448 Da [–0.6 ppm]
MW measured = 1932.881 Da
MW theoretical = 1932.882 Da
Relative Abundance
m/z
b
Cys40
S
H
N
O
O
GLTSPC(C–2)DINTFIHGNK
[MH2+] = 1027.472 Da [–4.9 ppm]
MW measured = 2052.930 Da
MW theoretical = 2052.940 Da
Relative Abundance
m/z
c
Cys40
S
NH2
GLTSPC(thiaK)
[MH2+] = 390.6730 Da [1.0 ppm]
MW measured = 799.3314 Da
MW theoretical = 799.3306 Da
Relative Abundance
m/z
d
DINTFIHGNK
[MH2+] = 579.798 Da [–1.7 ppm]
MW measured = 1157.581 Da
MW theoretical = 1157.583 Da
Relative Abundance
m/z

Figure 3.1 MS/MS mass spectra of trypsin digests. (a) K40C ANG, (b) P-thiaK40 ANG variant after treatment with H_2O_2, and (c,d) B-thiaK40 ANG variant after treatment with H_2O_2. The ensuing γ-thialysine residue is cleaved by trypsin, generating two fragments.

Figure 3.2

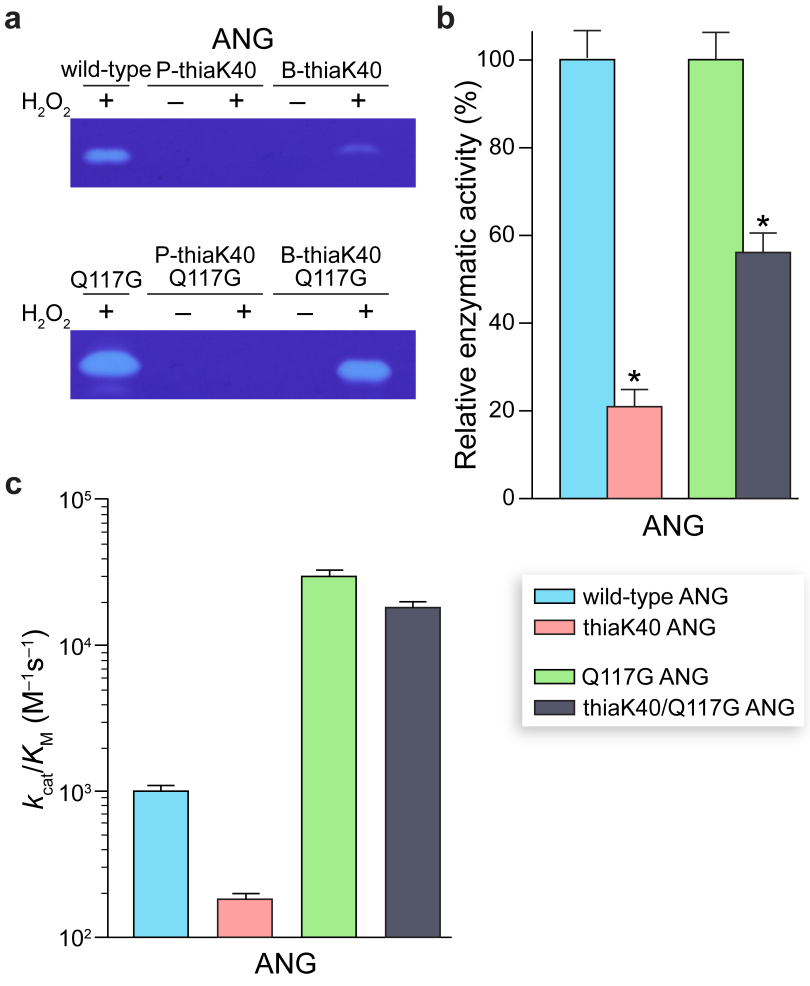
a
ANG
wild-type
P-thiaK40
B-thiaK40
H2O2
+
–
+
–
+
Q117G
P-thiaK40 Q117G
B-thiaK40 Q117G
b
Relative enzymatic activity (%)
100
80
60
40
20
0
*
ANG
c
kcat/KM (M−1s−1)
10⁵
10⁴
10³
10²
ANG
wild-type ANG
thiaK40 ANG
Q117G ANG
thiaK40/Q117G ANG

Figure 3.2 An ROS restores the ribonucleolytic activity of B-thiaK40 ANG and its Q117G variant. (a) Representative zymograms of ANG, Q117G ANG, and their conjugates. Proteins were exposed to H_2O_2 (1.0 mM) at 37 °C for 3 h, and assayed for their ability to cleave poly(C) by negative staining with toluidine blue. (b) Graph of data from all zymograms with ANG, Q117G ANG, and their boronated conjugates (exposed to H_2O_2). Values represent the mean ± SEM (n = 4, technical replicates). *, $p < 0.05$. (c) Graph of ribonucleolytic activity of ANG, Q117G ANG, and their boronated conjugates (exposed to H_2O_2). Values represent the mean ± SEM (n = 3, technical replicates).

Figure 3.3

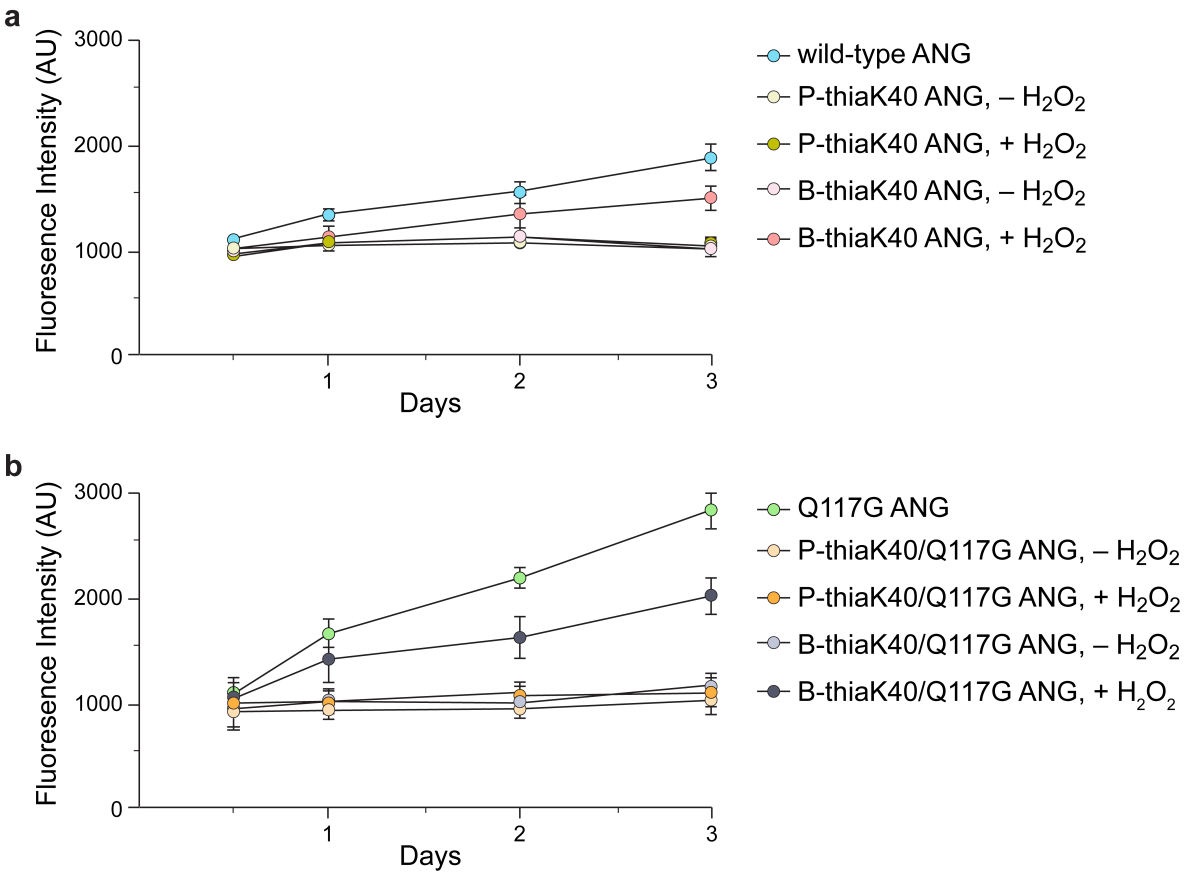
a
Fluoresence Intensity (AU)
3000
2000
1000
0
1
2
3
Days
wild-type ANG
P-thiaK40 ANG, – H2O2
P-thiaK40 ANG, + H2O2
B-thiaK40 ANG, – H2O2
B-thiaK40 ANG, + H2O2
b
Fluoresence Intensity (AU)
3000
2000
1000
0
1
2
3
Days
Q117G ANG
P-thiaK40/Q117G ANG, – H2O2
P-thiaK40/Q117G ANG, + H2O2
B-thiaK40/Q117G ANG, – H2O2
B-thiaK40/Q117G ANG, + H2O2

Figure 3.3 Masked ANG conjugates do not promote the proliferation of human endothelial cells. (a,b) Graphs showing that after pre-exposure of B-thiaK40 ANG and B-thiaK40/Q117G ANG to H_2O_2, the ensuing proteins promote the growth of HUVEC cells. The inactive P-K40 ANG or its P-K40/Q117G variant does not affect growth. Values represent the mean ± SEM (n = 3, biological replicates).

Figure 3.4

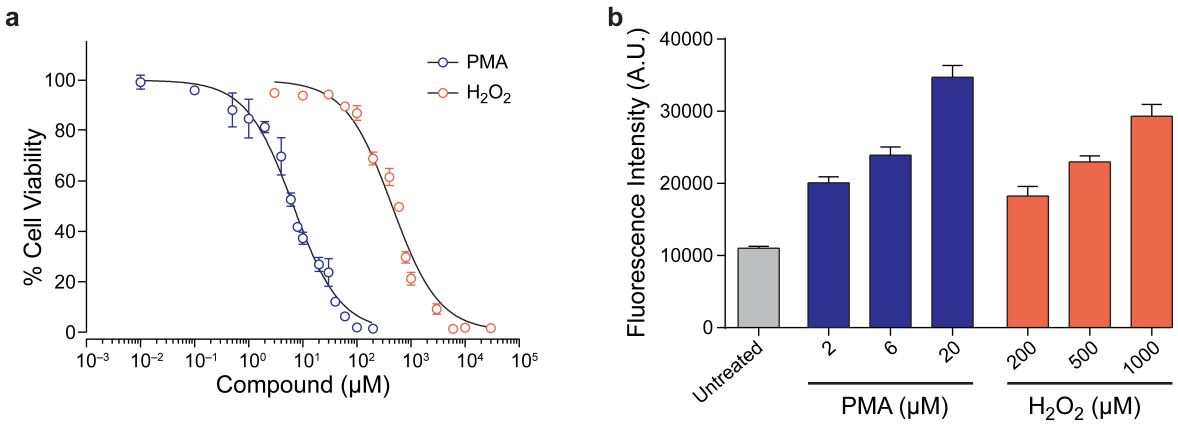
a
% Cell Viability
Compound (μM)
PMA
H2O2
b
Fluorescence Intensity (A.U.)
Untreated
PMA (μM)
H2O2 (μM)

Figure 3.4 H_2O_2 and PMA provoke an increase in intracellular ROS in human astrocytes. (a) Human astrocytes were treated with PMA and H_2O_2 at increasing concentrations for 24 h, after which the cytotoxicity of these agents was evaluated using an MTS assay. (b) Accumulation of intracellular ROS in human astrocytes was dose dependent. Cells were treated with PMA and H_2O_2 at desirable doses for 1 h, after which ROS measurement was performed using a fluorescent dye. Values represent the mean ± SEM (n = 3, technical replicates).

Figure 3.5

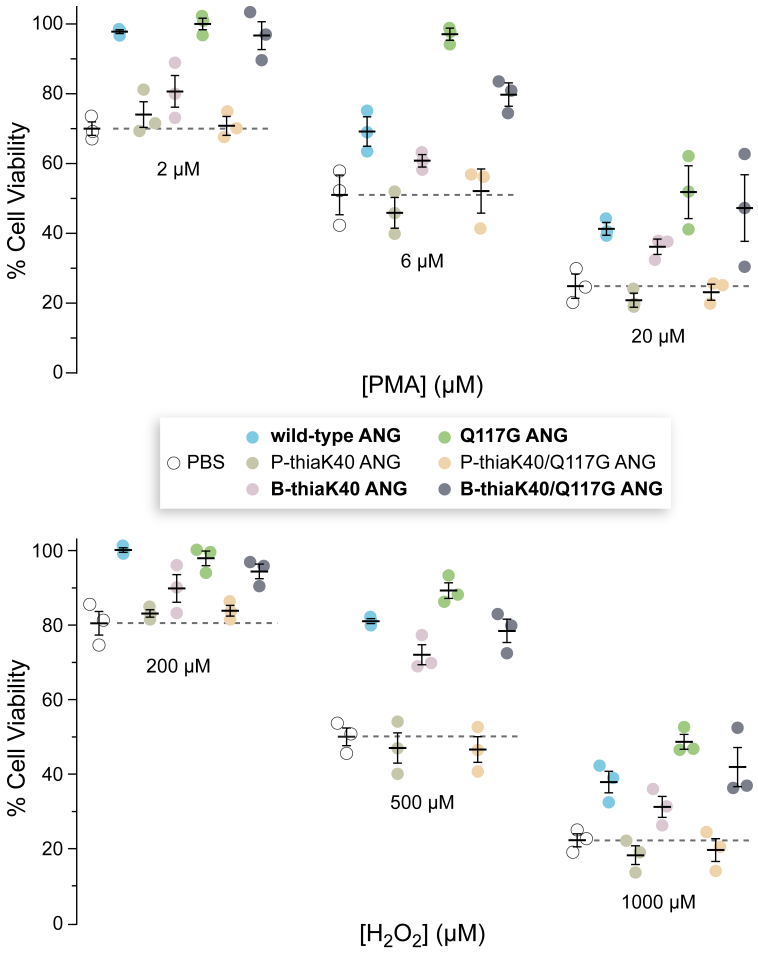
% Cell Viability
100
80
60
40
20
0
2 μM
6 μM
20 μM
[PMA] (μM)
PBS
wild-type ANG
P-thiaK40 ANG
B-thiaK40 ANG
Q117G ANG
P-thiaK40/Q117G ANG
B-thiaK40/Q117G ANG
200 μM
500 μM
1000 μM
[H2O2] (μM)

Figure 3.5 B-thiaK40 ANG and its Q117G variant protect human astrocytes from oxidative stress. Cells were pre-treated for 24 h with ANG, Q117G ANG, or their conjugates (1.0 μg/mL) prior to exposure to PMA or H_2O_2. The cytotoxicity of these agents was assessed 24 h later. Only ANG with a lysine or activatable γ-thialysine residue at position 40 protected cells from oxidative stress. Values represent the mean ± SEM (n = 3, biological replicates).

Figure 3.6

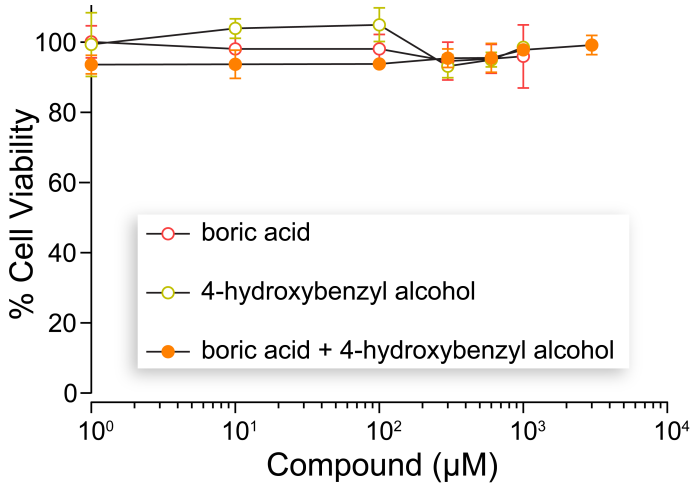
% Cell Viability
100
80
60
40
20
0
boric acid
4-hydroxybenzyl alcohol
boric acid + 4-hydroxybenzyl alcohol
10⁰
10¹
10²
10³
10⁴
Compound (μM)

Figure 3.6 Byproducts of the unmasking of B-thiaK40 ANG and B-thiaK40/Q117G ANG and are not toxic to human astrocytes. Graph of cell viability indicating that treating human astrocytes with boric acid or 4-hydroxybenzyl alcohol (or both) for 48 h results in no cytotoxicity, even at millimolar concentrations. Values represent the mean ± SEM (n = 3, biological replicates).

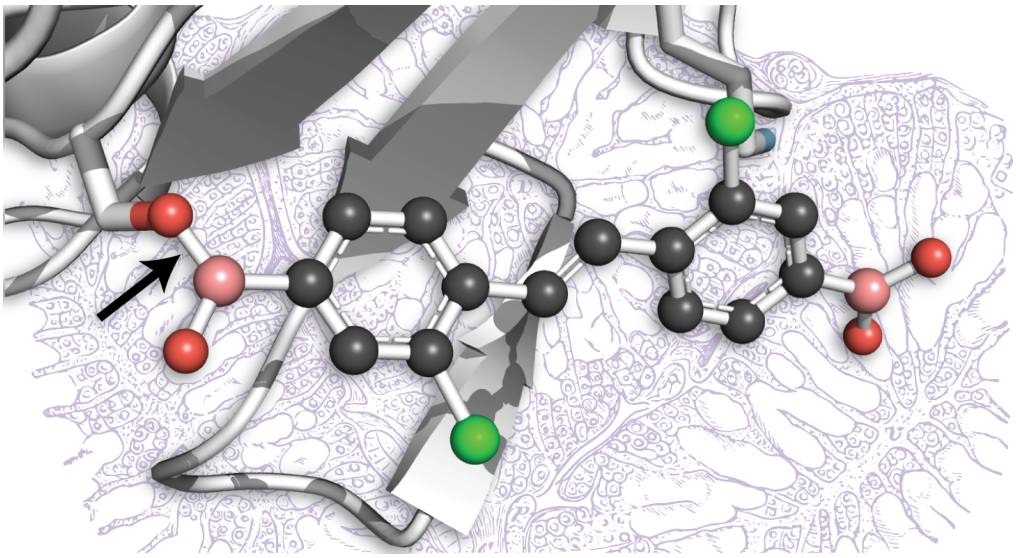

4

Stilbene Boronic Acids Form a Covalent Bond with Human Transthyretin and Antagonize its Aggregation

4.1 Abstract

Transthyretin (TTR) is a homotetrameric protein. Its dissociation into monomers leads to the formation of fibrils that underlie several human amyloidogenic diseases. The binding of small molecules to the pair of thyroxin (T_4) binding sites in TTR stabilizes the homotetramer and attenuates TTR amyloidosis. Herein, we report the design and evaluation of boronic acid-substituted stilbenes that limit TTR amyloidosis *in vitro*. The structure of resveratrol was used as a starting point for rational incorporation of boronic acid groups with the intention of promoting a covalent interaction with a polar residue in the T_4-binding site. Assays of affinity for TTR and inhibition of its tendency to form fibrils were coupled with X-ray crystallographic analysis of nine TTR·ligand complexes. The ensuing structure–function data led to the design and synthesis of a symmetrical diboronic acid that forms a boronic ester with serine 117. This diboronic acid strongly inhibits fibril formation by both wild-type TTR and a common disease-related variant, V30M TTR, compared to its phenolic derivative. Most significantly, the diboronic acid inhibits fibril formation as effectively as does tafamidis, a small-molecule drug in late-stage clinical trials for the treatment of TTR-related amyloidosis. Thus, the strategic deployment of boronic acid moieties within small-molecule ligands can provide a means to modulate protein aggregation.

4.2 Author Contributions

T.P.S., I.W.W., and R.T.R. designed ligands. T.P.S. synthesized and chemically characterized ligands. T.P.S., I.W.W., K.T.F., and R.T.R designed experiments. T.P.S. and I.W.W. performed in vitro assays, grew protein crystals and performed diffraction experiments. I.W.W. and K.T.F. solved structures and prepared models of TTR in complex with ligands. T.P.S., I.W.W., K.T.F., and R.T.R wrote the manuscript.

4.3 Introduction

Amyloidosis is a disease caused by the aggregation of a normally soluble protein.[201,202] Endogenous proteins can be causal for these diseases, which include Alzheimer's, Huntington's, and Parkinson's.[203] One such protein, transthyretin (TTR),[204] is a homotetrameric protein comprised of four identical monomer units, each consisting of 127 amino-acid residues that fold into a β-sandwich (Figure 1).[205,206] The dissociation of the TTR tetramer and aggregation of the ensuing monomers underlies familial amyloid polyneuropathy, familiar cardiomyopathy, and senile systemic amyloidosis.[203,207]

TTR is present in blood (0.25 g/L = 4 μM) and, to a lesser extent, cerebral spinal fluid.[204] A primary role of TTR *in vivo* is to transport thyroxin (T_4) and retinol, a hydrophobic hormone and fat-soluble vitamin A_1, respectively. Due to the abundance of other lipid-binding proteins (*e.g.*, thyroid-binding globulin and albumin), most of the T_4-binding sites of TTR are empty in blood. In cerebral spinal fluid, TTR also binds to β-amyloid, worsening the neurotoxicity that underlies Alzheimer's disease.[208-210]

The binding of a ligand can stabilize the folded state of a protein.[211,212] Evidence for the coupling of binding and stability appeared in 1890, when O'Sullivan and Thompson demonstrated that cane sugar increases markedly the thermostability of invertase, which is an enzyme that catalyzes the hydrolysis of sucrose.[213] Since then, ligands have been used to enhance the conformational stability of countless proteins, including TTR. Many small molecules have been synthesized and tested as putative TTR ligands, and several have demonstrated efficacy in attenuating amyloidosis.[214,215] Most efforts have focused on ligands that bind to the two identical T_4-binding sites at a dimer–dimer interface (Figure 4.1), as such ligands discourage dissociation to the monomeric state.[216] A few of these compounds have become viable treatment options,

including difluenisal, which is an FDA-approved non-steroid anti-inflammatory drug that has had limited adoption due to long-term gastrointestinal side-effects associated with cyclooxygenase inhibition,[217,218] and tafamidis, which is in late-stage clinical trials.[219-221]

An attractive approach to increase the potency and pharmacokinetics of a ligand is to evoke the formation of a covalent bond.[222,223] This strategy is well suited for TTR amyloidosis, not only because with an optimized dosage there might be no appreciable competition in serum with the natural ligand, T_4, but also because sustained stabilization of the TTR tetramer deters the accumulation of monomers that leads to a cascade of aggregation.[224] Previous work by Kelly and coworkers has shown that small molecules can modify TTR chemoselectively by targeting the ε amino group of Lys15/Lys15′ at the entry to the T_4-binding binding site. This work employed irreversible reactions, including conjugate addition with activated esters and thioesters[225,226] and vinyl sulfonamides,[227] and sulfation with aryl fluorosulfates.[228,229] Such ligands can, however, react irreversibly with other plasma proteins,[227] leading to potential immunogenic responses to the protein–ligand adduct[222] and the generation of potential toxic byproducts.[225]

To accrue the benefits of covalent binding without the liabilities, we sought ligands for TTR that bind in a *covalent but reversible* manner. Boronic acids interact with Lewis bases in aqueous media.[2,5] Boronic acids (including the FDA-approved drug Bortezomib[121]) are well known as serine/threonine protease inhibitors,[25,230-232] anti-microbial and anti-cancer agents,[27,28] and delivery vehicles.[21,91,93,233] Boronic acid-based fluorogenic probes have been developed for sensing both saccharides[234] and reactive oxygen species (ROS),[106,235] as well as for molecular recognition.[15] These applications arise from the ability of boronic acids to form a covalent bond with a Lewis base that is reversible under physiological conditions.[13,236] Notably, boronic acids

are benign, as their metabolic byproduct, boric acid, is present in a normal diet.[237]

Here, we report on the development of boronic acid-based ligands for the T_4-binding site of the TTR tetramer. An iterative strategy involving chemical synthesis and structure–function analysis led us to potent, covalent inhibitors of TTR aggregation. This strategy serves as a model for a new class of amyloidosis antagonists.

4.4 Results and Discussion

We chose stilbene as a scaffold for the design of an initial series of boronic acid-containing TTR ligands (Scheme 4.1). This scaffold is present in the natural product resveratrol (**4.1**), and has been employed in other TTR ligands.[205,215,226,238-240] Moreover, stilbenes are readily accessible by a convergent synthetic route, as the two rings can be functionalized separately and then joined with a Wittig reaction.

Resveratrol occupies the T_4-binding site with moderate affinity (Table 4.1 and Figure 4.1).[205] We began by replacing the phenolic hydroxyl group, which is known to form a hydrogen bond with Ser117/117′, with a boronic acid group to generate stilbene **4.2** (Scheme 4.1). Halogen substitution is known to provide additional van der Waals interactions within the inner pocket of the T_4-binding site, enhancing the affinity of TTR ligands.[241] Accordingly, we added a chloro group *meta* to the boronic acid moiety to generate stilbenes **4.3** and **4.4**.

We performed competitive binding assays to compare affinities among the diphenol series of ligands (Table 4.1 and Figure 4.5A). We observed no change in values of $K_{d,2}$ between stilbene **4.1** and **4.2**. Interestingly, chlorinated stilbene **4.3** showed a higher value of $K_{d,2}$ relative to its non-halogenated counterpart, stilbene **4.1**. This decrease in affinity contrasts with stilbene **4.4**, which exhibited increased affinity as a result of chlorination and showed the strongest

affinity for TTR of stilbenes **4.1**–**4.4**, having a $K_{d,2}$ value of 441 nM.

Next, we assessed the ability of these molecules to inhibit fibril formation by both wild-type TTR and the common V30M variant, which is associated with familial amyloid polyneuropathy (Table 4.1 and Figure 4.6A). We found that all of the stilbenes in this series inhibited aggregation at 7.2 μM and at a molar ratio of 2 ligand:1 protein. Stilbenes **4.1** and **4.2** showed 25% and 23% fibril formation for V30M TTR, whereas stilbenes **4.3** and **4.4** showed 14% and 11%, respectively. These differences are not significant. Herein, we consider compounds that limit aggregation to ≤10% over 96 h as potent inhibitors, and stilbenes **4.1**–**4.4** did not achieve this threshold.

Next, we solved co-crystal structures of TTR and resveratrol analogs **4.2**–**4.4** to discern if the boronated stilbenes formed a covalent bond with TTR. To our surprise, each phenylboronic acid moiety was observed in the "reverse" binding mode (Figures 4.2A and 4.2B) relative to its parent phenol, resveratrol (Figures 4.1 and 4.3A). In other words, the boronic acid group resided in the outer pocket of the T_4-binding site No indication of boronic ester formation with amino acid residues was apparent (Figures 4.7 and 4.9).

To attempt to reconfigure this unexpected orientation, we designed a second series of stilbenes in which a carboxylic acid group was installed at the *meta* position of the ring not modified in the first series (Scheme 4.2). Previous work had shown that incorporating an anionic substituent into ligands could introduce advantageous electrostatic interactions with Lys15/15′ of TTR.[205,220,242] We hypothesized that this interaction would orient the boronic acid to the inner pocket of the T_4-binding site, and perhaps promote boronate-ester formation.

The first pair, stilbenes **4.5** and **4.6**, exhibited $K_{d,2}$ values in the low micromolar range, 3- and 2-fold higher than those of stilbenes **4.1** and **4.2**, respectively (Table 4.2 and Figure 4.5B).

The installation of a chloro group in stilbenes **4.7** and **4.8** restored values of $K_{d,2}$ to the high nanomolar range. Consistent with the higher values of $K_{d,2}$, the non-halogenated stilbenes **4.5** and **4.6** also showed poor ability to prevent fibril formation under acidic fibril-forming conditions (Table 4.2 and Figure 4.6B). Incubation of wild-type TTR with phenol **4.5** showed 77% fibril formation and actually seemed to facilitate fibril formation of the V30M variant (112% at 7.2 μM). Boronic acid **4.6** performed significantly better as an inhibitor than did phenol **4.5** for both wild-type TTR and the V30M variant (11% and 28%, respectively). The chlorinated pair **4.7** and **4.8** showed potent fibril inhibition (<10%) for both TTRs. These differences were, however, within experimental error. Again, co-crystallography revealed that boronic acids **4.6** and **4.8** were bound in the reverse mode, relative to their paired phenols. In other words, the carboxylic acid group was in the inner pocket, near Ser117/117′, and the boronic acid group was in the outer pocket, near Lys15/15′ (Table 4.14; Figures 4.2C and 4.2D). As with boronic acids **4.2** and **4.4**, boronic acids **4.6** and **4.8** did not exhibit covalent interactions with binding-pocket residues.

The final series of stilbenes contained a boronic acid moiety on each ring (Scheme 4.3). We synthesized C_2 symmetrical diboronic acid **4.10**, which has two *meta*-chloro and *para*-boronic acid groups (relative to the stilbene olefin), as well as the analogous C_2 symmetrical diphenol **4.9**. Additionally, we synthesized stilbene **4.11**, which has one boronic acid group *meta* to the linker, to investigate whether this position of the boronic acid enhances interactions with Lys15/15′ in the outer pocket. We also included tafamidis (**4.12**) in this series as a benchmark for our assays.

In the competitive binding assay, diphenol **4.9** had a $K_{d,2}$ value of 819 nM (Figure 4.5C and Table 4.3). The analogous diboronic acid, **4.10**, had a $K_{d,2}$ value of 469 nM, which was the

largest decrease in $K_{d,2}$ value that we observed between a boronic acid and its paired phenol. These two stilbenes comprise the only pair that can be compared directly, as their C_2 symmetry precludes alternative binding orientations. The difference in affinity for TTR was amplified in the fibril formation assay, where diboronic acid **4.10** showed much more potent inhibition of fibril formation than did diphenol **4.9**, both for wild-type TTR (3% versus 12% at 7.2 μM) and for the V30M variant (8% versus 27% at 7.2 μM) (Table 4.3 and Figure 4.6C). Asymmetric diboronic acid **4.11** had a value of $K_{d,2}$ similar to that of diphenol **4.9** (864 nM) as well as similar fibril formation inhibition, suggesting that the location of the boronic acid plays a role in optimizing interactions within the binding pocket. Gratifyingly, co-crystallographic data of diboronic acids **4.10** and **4.11** showed the formation of a boronic ester with Ser117/117′ (Figures 4.2E and 4.2F).

We sought a new class of small-molecule ligands for TTR, which is a validated target for pharmacological intervention.[207,219-221] Towards that goal, we investigated the effects of incorporating a boronic acid substituent on the well-known stilbene scaffold, embodied in resveratrol (**4.1**). The results enabled us to reach several conclusions. First, a boronic acid group can enhance the potency of a TTR ligand. Second, boronic acids prefer to bind in the T_4-binding site such that the boronic acid group is exposed to solvent. Finally, a boronic ester can form with an amino-acid residue.

The installation of a boronic acid group tends to increase the affinity of a stilbene for TTR. The value of $K_{d,2}$ for each boronic acid ligand for TTR is lower than (or equivalent to) that of its analogous phenol (Tables 4.1–4.3). Moreover, a boronic acid group enhances the ability of a stilbene to deter the formation of TTR fibrils (Tables 4.1–4.3). Nonetheless, our structural studies revealed that in each complex between TTR and a stilbene containing a single boronic

acid group, that group was in the outer pocket of the T_4-binding site, exposed to solvent (Figures 4.2A–4.2D, 4.7, 4.9, 4.11, and 4.13).

The modest increase in affinity incurred by adding a single boronic acid group could be due to a weak noncovalent interaction between the *ε*-amino group of Lys15/15′ and the vacant *p*-orbital of the boron. Kelly and coworkers demonstrated that this amino group, which likely has a low pK_a, can act as a nucleophile.[225] In our complexes, the relevant B···N distances are 3.3–3.5 Å for stilbenes **4.2**, **4.4**, **4.6**, **4.8**, and **4.10** (Table 4.14). We did not, however, observe electron-densities or atomic geometries consistent with the formation of a dative N→B bond between these two functionalities, nor were any additional hydrogen bonds apparent between TTR residues and the boronic acid group (Figures 4.2A–4.2D, 4.7, 4.9, 4.11, and 4.13). Additional hydrogen bonds did, however, arise elsewhere in the complexes with a single boronic acid. For example, the two *meta* hydroxyl groups in stilbenes **4.2** and **4.4** (but not **4.1** and **4.3**) interact closely (2.0–2.3 Å) with Ser117/117′ (Table 4.14).

Stilbenes and similar compounds bind to TTR in one of two modes.[217,224,229,243-246] Although a consensus explanation is not apparent, the polarity of pendant functional groups can play a role in ligand orientation.[240,247] In our stilbenes, however, the relevant log*P* values of phenol (1.46), benzoic acid (1.87), and phenylboronic acid (1.59) are similar,[248] suggesting that hydrophilicity alone contributes little to their orientation in the T_4-binding site. The installation of a chloro group on one ring, as in stilbenes **4.4** and **4.8**, led to increased affinity and enhanced efficacy (Tables 4.1 and 4.2), but did not affect binding orientation (Figures 4.2B and 4.2D).

To negate binding orientation as a factor, we designed a class of molecules containing a boronic acid substituent on *each* stilbene ring. If such a ligand were to bind to TTR, then a boronic acid group would necessarily be in the inner pocket of the T_4-binding site. We were

gratified that this strategy was successful, as both stilbenes **4.10** and **4.11** did bind to TTR with high affinity (Table 4.3). Moreover, the boronic acid group in the inner pocket formed an ester with Ser117/117′. Boronic esters have demonstrable utility as mimics of the high-energy tetrahedral intermediate in reactions catalyzed by serine/threonine proteases.[25,230-232] In those covalent complexes, an active-site serine or threonine residue forms a tetrahedral, sp^3-hybridized boronate ester with a boronic acid group.[249]

Despite the hydration of boronic acid groups in aqueous solution[5] and in marked contrast to other known boronate esters with proteins, we observe planar, sp^2-hybridized boronate esters with Ser117/117′ of TTR (Figures 4.2E and 4.2F). We are aware of only one other structure in which a planar boronate ester is formed with a hydroxyl residue of a protein (PDB entry 1p06).[250] That other structure is, however, distinct because a lone pair of electrons from a proximal histidine residue appears to participate in a dative bond with the vacant *p*-orbital of the boron. The presence of a planar ester could indicate that formation of a tetrahedral adduct is hindered sterically, unlike in the active site of a serine/threonine protease. Hence, our results could demarcate the lower limit of affinity enhancement upon introducing boronic acid-based inhibitors in this particular context.

Finally, we note the variable role of chloro groups on the affinity of stilbenes for TTR. A chloro group can fill unoccupied cavities, which would otherwise compromise affinity and efficacy.[251,252] Second, the position of the chloro group in both of the ester-forming boronates enables the formation of a halogen bond.[253] The relevant O···Cl distance is close to the sum of the van der Waals radii ($r_O + r_{Cl}$ = 3.27 Å; Figure 4.4).[241] The geometries observed in the TTR complexes with stilbenes **4.10** and **4.11** (Table 4.15) suggest a halogen-bond energy of 0.7–0.9 kcal/mol.[254] Still, the consequences of installing a chloro group on the stilbene scaffold are

unlike those of installing a boronic acid group, which consistently increases affinity for TTR (*vide supra*). For example, the addition of a chloro group to stilbene **4.1** to form stilbene **4.3** decreases affinity, whereas the addition of a chloro group to stilbene **4.5** to form stilbene **4.7**, increases affinity. Notably, the phenolic ring of stilbene **4.5** was found to occupy two conformations in the inner pocket of the T_4-binding site, which could explain, in part, the lower affinity of stilbene **4.5** relative to stilbene **4.7** (Figures 4.3B, 4.10, and 4.12). The judicious use of halogen substituents in stilbene scaffolds merits additional investigation.

4.5 Conclusions

A series of paired stilbenes was designed, synthesized, and tested as ligands for TTR. These ligands contained either a phenolic hydroxyl group or a phenylboronic acid group. We find that a pendant boronic acid group can serve as the basis for potent small-molecule inhibitors of TTR amyloidosis. The formation of a covalent bond with a serine residue anchors them in the T_4-binding site in the dimer–dimer interface, enhancing efficacy compared to analogous noncovalent ligands. These stilbene boronic acids strongly inhibit the TTR fibril-formation that leads to amyloidosis, and their efficacy extends to V30M TTR, which is a common disease-related variant.

4.6 Acknowledgements

We are grateful to Dr. C. L. Jenkins for contributive discussions. I.W.W. was supported by Biotechnology Training Grant T32 GM008349 (NIH) and a Genentech Predoctoral Fellowship. This work was supported by Grants R01 GM044783 (NIH) and MCB 1518160 (NSF).

4.7 Materials and Methods

4.7.1 General Information

Tafamidis (2-(3,5-dichlorophenyl)-6-benzoxazolecarboxylic acid) was from Carbosynth Limited (Berkshire, UK). Resveratrol (**4.1**), 8-anilino-1-naphthalenesulfonic acid (ANS), and other reagents for biochemical assays were from Sigma–Aldrich (St Louis, MO). All other chemicals were from Sigma–Aldrich (Milwaukee, WI) and were used without further purification. All glassware was flame-dried, and all reactions were performed under an atmosphere of N_2(g). Reagent-grade solvents: dichloromethane (DCM), tetrahydrofuran (THF), triethylamine (TEA), and dimethylformamide (DMF) were dried over a column of alumina and were removed from a dry still under an inert atmosphere.

Flash column chromatography was performed with Silicycle 40–63 Å silica (230–400 mesh), and thin-layer chromatography (TLC) was performed with EMD 250-μm silica gel 60-F_{254} plates. All procedures were performed in air at ambient temperature (~22 °C) and pressure (1.0 atm) unless indicated otherwise. The phrase "concentrated under reduced pressure" refers to the removal of solvents and other volatile materials using a rotary evaporator at water aspirator pressure (<20 torr) while maintaining a water bath below 40 °C. Residual solvent was removed from samples at high vacuum (<0.1 torr).

^{1}H and ^{13}C NMR spectra were acquired with a Bruker Avance III 500i spectrometer at the National Magnetic Resonance Facility at Madison (NMRFAM). Chemical shift data are reported in units of δ (ppm) relative to residual solvent. Mass spectra were acquired with an LCT instrument (Waters) at the Mass Spectrometry Facility in the Department of Chemistry at the University of Wisconsin–Madison.

4.7.2 Chemical Synthesis

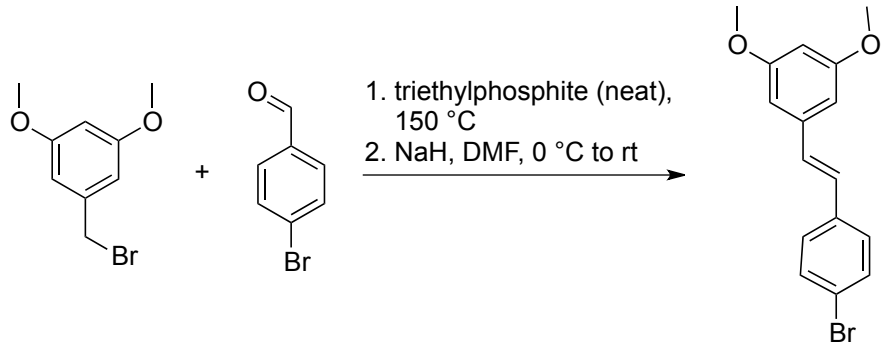

4.2a

3,5-Dimethoxybenzyl bromide (1.2 g, 5.5 mmol) was dissolved in neat triethylphosphite (1.2 mL, 6.6 mmol) and heated to 150 °C for 4 h. The reaction mixture was cooled to 0 °C and diluted with DMF (40 mL). NaH (60% w/v in mineral oil, 0.28 g, 7.12 mmol) was added to the resulting solution, and the reaction mixture was stirred at 0 °C for 20 min. A solution of 4-bromo-benzaldehyde (1.0 g, 5.5 mmol) in DMF (15 mL) was then added dropwise. The reaction mixture was allowed to warm to room temperature and stirred overnight. The reaction mixture was then diluted in EtOAc (20 mL), washed with 10% w/v citric acid (30 mL), followed by brine (30 mL). The organic layer was separated, dried with Na_2SO_4(s), and filtered. The solvent was removed under reduced pressure, and the crude product was purified by flash column chromatography (10% v/v EtOAc in hexanes) to afford compound **4.2a** as a white solid (1.56 g, 89%).

^{1}H NMR (500 MHz, $CDCl_3$, δ): 3.83 (s, 6H), 6.41 (s, 1H), 6.65 (s, 2H), 6.98–7.01 (d, J = 16.28 Hz, 1H), 7.01–7.04 (d, J = 16.34 Hz, 1H), 7.35–7.37 (d, J = 8.48 Hz, 2H), 7.46–7.48 (d, J = 8.51 Hz, 2H); **^{13}C NMR (100 MHz, $CDCl_3$, δ)**: 55.42, 100.31, 104.74, 121.57, 128.03, 128.16,

129.50, 131.92, 136.19, 139.07, 161.12; **ASAP–MS (*m*/*z*)**: $[M + H]^+$ calcd for $C_{16}H_{15}BrO_2$, 319.0329; found, 319.0331.

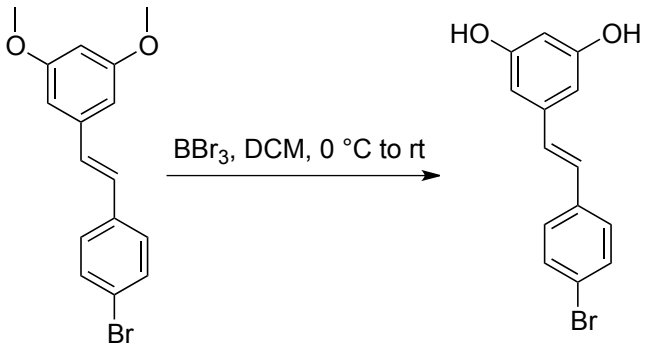

4.2a **4.2b**

Compound **4.2a** (0.5 g, 1.6 mmol) was dissolved in DCM (7 mL), and the resulting solution was cooled to 0 °C. A solution of 1.0 M BBr_3 in DCM (7.8 mL) was added dropwise at 0 °C. The reaction mixture was allowed to warm to room temperature and stirred for 4 h. The reaction mixture was then poured carefully into a separation funnel containing ice water (~15 mL). The mixture was extracted with DCM (3 × 15 mL). The organic layers were combined and washed with brine (15 mL), dried with Na_2SO_4(s), and filtered. The solvent was removed under reduced pressure, and the crude product was suspended in ice-cold DCM. The resulting precipitate was isolated by filtration to afford compound **4.2b** as a white solid (0.326 g, 70%).

^{1}H NMR (500 MHz, CD_3OD, *δ*): 6.22 (s, 1H), 6.51 (s, 2H), 7.00–7.03 (d, *J* = 16.33 Hz, 1H), 7.04–7.07 (d, *J* = 16.33 Hz, 1H), 7.45–7.47 (d, *J* = 8.5 Hz, 2H), 7.50–7.51 (d, *J* = 8.5 Hz, 2H); **^{13}C NMR (125 MHz, CD_3OD, *δ*)**: 103.43, 106.15, 121.97, 128.05, 129.17, 130.97, 132.78, 138.04, 140.42, 159.80; **HRMS–ESI (*m*/*z*)**: $[M - H]^-$ calcd for $C_{14}H_{11}BrO_2$, 288.9870; found, 288.9869.

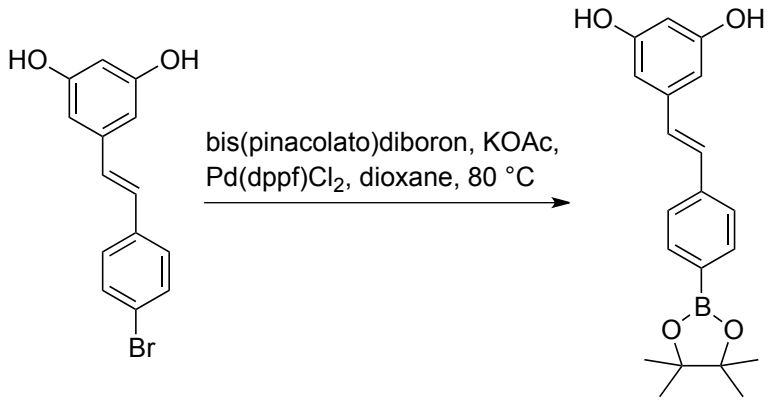

4.2b **4.2c**

Compound **4.2b** (0.250 g, 0.858 mmol), KOAc (0.245 g, 2.57 mmol), bis(pinacolato)diboron (0.652 g, 2.57 mmol), and Pd(dppf)Cl_2 (0.062 g, 0.0858 mmol) were added to a Schlenk flask, which was then evacuated and backfilled with N_2(g). Dioxane (8.5 mL) was deoxygenated by sonication under high vacuum and backfilled with N_2(g). The deoxygenated dioxane was then added by cannula into the reaction flask, and the reaction mixture was heated to 80 °C and stirred overnight. The reaction mixture was then filtered, and the solvent was removed under reduced pressure. The crude product was purified by flash column chromatography (20% v/v EtOAc in hexanes) to afford compound **4.2c** as a white solid (0.245 g, 84%).

^{1}H NMR (500 MHz, CD_3OD, δ): 1.34 (s, 12H), 6.22 (s, 1H), 6.51 (s, 2H), 7.02–7.06 (d, J = 16.27 Hz, 1H), 7.06–7.10 (d, J = 16.36 Hz, 1H), 7.50–7.52 (d, J = 7.93 Hz, 2H), 7.71–7.72 (d, J = 7.79 Hz, 2H); **^{13}C NMR (125 MHz, CD_3OD, δ)**: 25.19, 85.04, 103.42, 160.21, 126.77, 129.23, 131.16, 136.08, 140.54, 141.63, 159.75; **HRMS–ESI (m/z)**: $[M - H]^+$ calcd for $C_{20}H_{23}BO_4$, 336.1653; found, 336.1653.

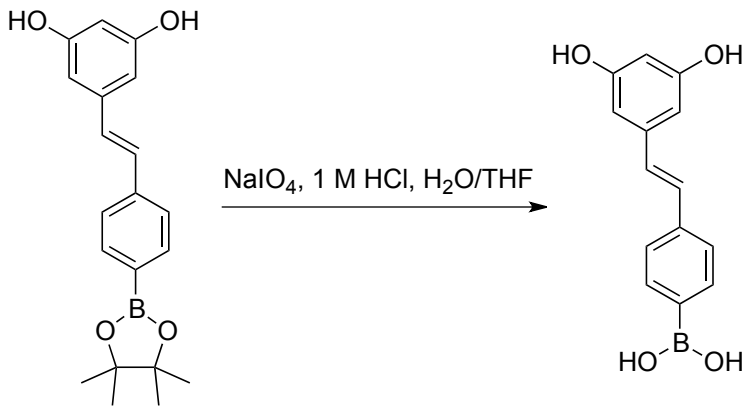

4.2c **4.2**

Compound **4.2c** (0.050 g, 0.147 mmol) was dissolved in 4:1 THF/H_2O (1.5 mL). $NaIO_4$ (0.157 g, 0.739 mmol) was added to the resulting solution, followed by 1.0 M HCl (36 µL, 0.036 mmol). The reaction mixture was allowed to stir overnight. The reaction mixture was then diluted with H_2O (2 mL) and extracted with EtOAc (3 × 4 mL). The organic layers were combined and washed with brine (10 mL), dried with Na_2SO_4(s), and filtered. The solvent was removed under reduced pressure, and the crude product was purified by flash column chromatography (3% v/v CH_3OH in DCM) to afford compound **4.2** as a white crystalline solid (0.027 g, 67%).

^{1}H NMR (500 MHz, CD_3OD, δ): 6.20 (s, 1H), 6.50 (s, 2H), 7.95 (bs, 2H), 7.51–7.52 (d, J = 8.17 Hz, 2H), 7.60–7.62 (d, J = 8.13 Hz, 2H); **^{13}C NMR (125 MHz, CD_3OD, δ)**: 103.32, 106.13, 126.69, 129.26, 130.67, 135.09, 140.06, 140.64, 159.78; **HRMS–ESI (m/z)**: $[M - H]^-$ calcd for the single methyl boronic ester $C_{15}H_{15}BO_4$, 268.1027; found, 268.1027.

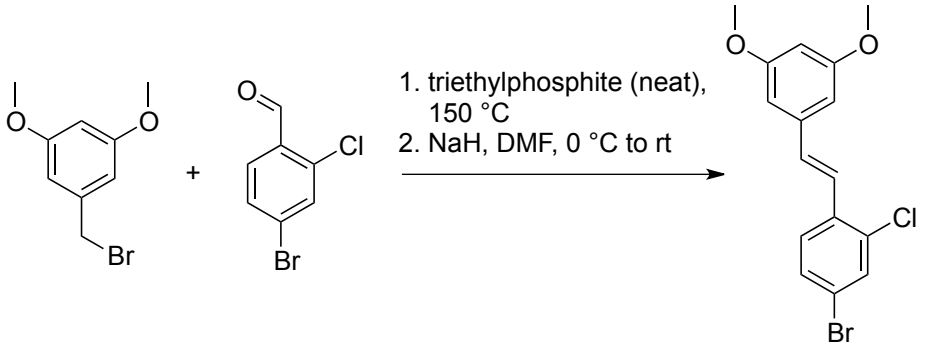

4.4a

3,5-Dimethoxybenzyl bromide (0.74 g, 3.4 mmol) was dissolved in neat triethylphosphite (0.7 mL, 4.0 mmol), and the resulting solution was heated to 150 °C for 4 h. The reaction mixture was cooled to 0 °C and added to DMF (20 mL). NaH (60% w/v in mineral oil, 0.17 g, 4.36 mmol) was added to the resulting solution, and the reaction mixture was stirred at 0 °C for 20 min. A solution of 4-bromo-2-chloro benzaldehyde (0.74 g, 3.36 mmol) in DMF (10 mL) was then added dropwise. The reaction mixture was allowed to warm to room temperature and stirred overnight. The reaction mixture was then diluted with EtOAc (15 mL), washed with 10% w/v citric acid (20 mL), followed by brine (20 mL). The organic layer was separated, dried with Na_2SO_4(s), and filtered. The solvent was removed under reduced pressure, and the crude product was purified by flash column chromatography (5% v/v EtOAc in hexanes) to afford compound **4.4a** as a white solid (1.10 g, 91%).

^{1}H NMR (400 MHz, $CDCl_3$, δ): 3.84 (s, 6H), 6.44 (s, 1H), 6.69 (s, 2H), 6.97–7.01 (d, J = 16.24 Hz, 1H), 7.36–7.40 (m, 2H), 7.50–7.52 (d, J = 8.42 Hz, 1H), 7.55 (s, 1H); **^{13}C NMR (100 MHz, $CDCl_3$, δ)**: 55.51, 100.60, 105.11, 121.37, 124.27, 127.60, 130.27, 131.89, 132.43, 134.20, 134.41, 138.81, 161.12; **ASAP–MS (*m*/*z*)**: $[M + H]^+$ calcd for $C_{16}H_{14}BrClO_2$, 352.9939; found, 352.9939.

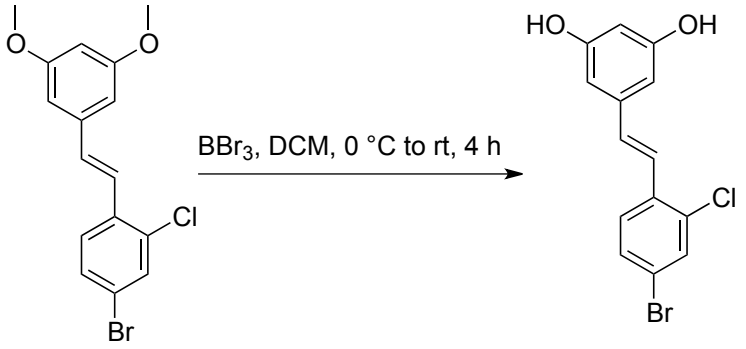

4.4a **4.4b**

Compound **4.4a** (0.500 g, 1.42 mmol) was dissolved in DCM (14 mL), and the reaction mixture was cooled to 0 °C. A solution of 1.0 M BBr_3 (7.10 mmol) in DCM (7.1 mL) was then added dropwise at 0 °C. The reaction mixture was allowed to warm to room temperature and stirred for 4 h. The reaction mixture was then poured carefully into a separation funnel containing ice water (~10 mL) and extracted with DCM (3 × 10 mL). The organic layers were combined and washed with brine (15 mL), dried with Na_2SO_4(s), and filtered. The solvent was removed under reduced pressure, and the crude product was suspended in cold DCM (5 mL). The resulting precipitate was filtered to afford compound **4.4b** as a white solid (0.335 g, 72%).

^{1}H NMR (500 MHz, CD_3OD, δ): 6.23, (s, 1H), 6.51 (s, 2H), 7.03–7.07 (d, J = 16.23 Hz, 1H), 7.31–7.35 (d, J = 16.23 Hz, 1H), 7.45–7.47 (d, J = 8.31 Hz, 1H), 7.60 (s, 1H), 7.67–7.69 (d, J = 8.47 Hz, 1H); **^{13}C NMR (125 MHz, CD_3OD, δ)**: 103.79, 106.34, 124.89, 126.71, 133.26, 133.34, 133.90, 135.91, 137.59, 140.29, 159.89; **HRMS–ESI (m/z)**: $[M - H]^-$ calcd for $C_{14}H_{10}BrClO_2$, 322.9480; found, 322.9480.

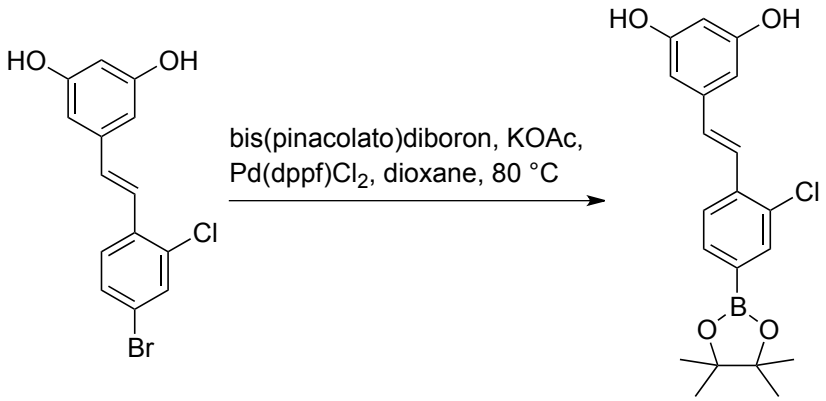

4.4b **4.4c**

Compound **4.4b** (0.100 g, 0.308 mmol), KOAc (0.088 g, 0.926 mmol), bis(pinacolato)diboron (0.235 g, 0.926 mmol), and Pd(dppf)Cl_2 (0.0225 g, 0.0308 mmol) were added to a flame-dried Schlenk flask, which was then evacuated and backfilled with N_2(g). Dioxane (3.5 mL) was deoxygenated by sonication under high vacuum and backfilled with N_2(g). The deoxygenated dioxane was then added by cannula into the reaction flask, and the reaction mixture was heated to 80 °C and stirred overnight. The reaction mixture was filtered and the solvent was removed under reduced pressure. The crude product was purified by flash column chromatography (2% v/v CH_3OH in DCM) to afford compound **4.4c** as a white solid (0.080 g, 69%).

^{1}H NMR (500 MHz, CD_3OD, δ): 1.33 (s, 12H), 6.23 (s, 1H), 6.53 (s, 2H), 7.05–7.09 (d, J = 16.29 Hz, 1H), 7.40–7.44 (d, J = 16.28 Hz, 1H), 7.60–7.62 (d, J = 7.98 Hz, 1H), 7.70 (s, 1H), 7.72–7.74 (d, J = 7.83 Hz, 1H); **^{13}C NMR (125 MHz, CD_3OD, δ)**: 25.18, 75.82, 85.42, 103.90, 106.42, 124.82, 126.88, 133.83, 133.90, 134.11, 136.74, 139.11, 140.17, 159.84; **HRMS–ESI (*m*/*z*)**: $[M - H]^-$ calcd for $C_{20}H_{22}BClO_4$, 370.1263; found, 370.1263.

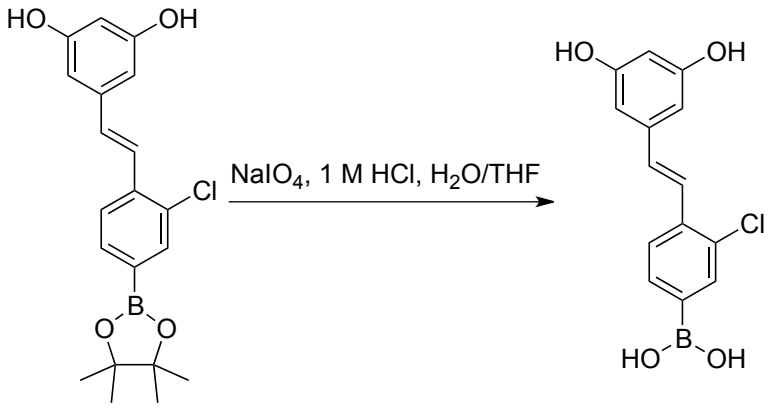

4.4c **4.4**

Compound **4.4c** (0.050 g, 0.134 mmol) was dissolved in 4:1 THF/H_2O (1.3 mL). $NaIO_4$ (0.143 g, 0.670 mmol) was added to the resulting solution, followed by 1.0 M HCl (33 µL, 0.033 mmol). The reaction mixture was then stirred overnight. The reaction mixture was diluted with H_2O (1.0 mL) and extracted with EtOAc (3 × 2 mL). The organic layers were combined and washed with brine (6 mL), dried with Na_2SO_4(s), and filtered. The solvent was removed under reduced pressure, and the crude mixture was purified by flash column chromatography (4% v/v CH_3OH in DCM) to afford compound **4.4** as a white crystalline solid (0.022 g, 88%).

^{1}H NMR (500 MHz, CD_3OD, δ): 6.23 (s, 1H), 6.52 (s, 2H), 7.05–7.09 (d, J = 16.20 Hz, 1H), 7.41–7.45 (d, J = 16.23 Hz, 1H), 7.54–7.56 (d, J = 7.85 Hz, 1H), 7.63 (s, 1H), 7.75–7.76 (d, J = 7.81 Hz, 1H); **^{13}C NMR (125 MHz, CD_3OD, δ)**: 103.77, 106.32, 124.88, 126.71, 133.26, 133.34, 133.90, 135.91, 137.59, 140.29, 159.89; **HRMS–ESI (*m*/*z*)**: $[M - H]^-$ calcd for $C_{14}H_{12}BClO_4$, 288.0481; found, 288.0482.

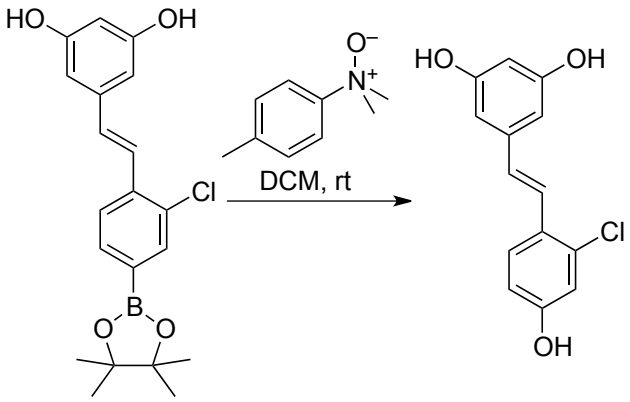

4.4c **4.3**

Compound **4.3** was derived from the oxidation of compound **4.4c** with an aryl *N*-oxide in one step as described previously.[255] Here, compound **4.4c** (0.020 g, 0.053 mmol) was dissolved in DCM (0.6 mL). *N*,*N*-Dimethyl-*p*-toluidine-*N*-oxide (0.012 g, 0.081 mmol) was added to the resulting solution, and the reaction mixture was stirred for 1 h. The solvent was removed under reduced pressure, and the crude product was purified by flash column chromatography (15% v/v EtOAc in hexanes) to afford compound **3** as a pale yellow solid (0.010 g, 70%).

^{1}H NMR (500 MHz, CD_3OD, δ): 6.18–6.19 (t, J = 2.15 Hz, 1H), 6.47 (s, 2H), 6.74–6.76 (d, J = 8.66 Hz, 1H), 6.82 (s, 1H), 6.82–6.85 (d, J = 14.57 Hz, 1H), 7.31–7.34 (d, J = 16.16 Hz, 1H), 7.58–7.59 (d, J = 8.64 Hz, 1H); **^{13}C NMR (125 MHz, CD_3OD, δ)**: 103.10, 105.96, 115.92, 117.03, 124.95, 127.75, 128.32, 129.78, 134.77, 140.91, 159.08, 159.77; **HRMS–ESI (*m*/*z*)**: $[M - H]^-$ calcd for $C_{14}H_{11}ClO_3$, 261.0324; found, 261.0325.

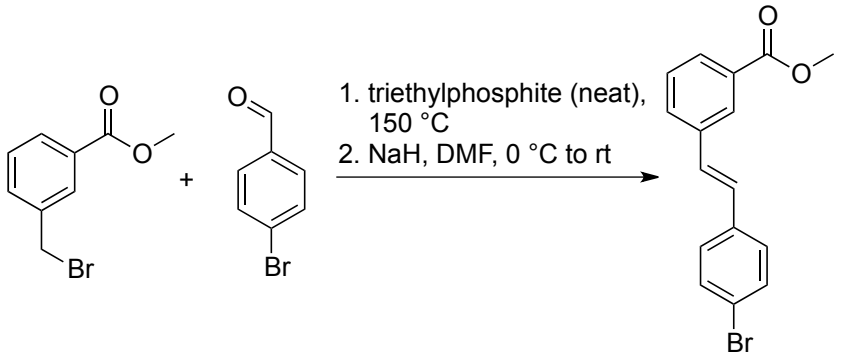

4.6a

Ethyl 3-(bromomethyl)benzoate (2.0 g, 8.7 mmol) was dissolved in neat triethylphosphite (1.78 mL, 10.4 mmol) and heated to 150 °C for 4 h. The reaction mixture was cooled to 0 °C and diluted with DMF (87 mL). NaH (60% w/v in mineral oil, 0.69 g, 17.46 mmol) was added to the resulting solution, and the reaction mixture stirred at 0 °C for 20 min. A solution of 4-bromobenzaldehyde (1.62 g, 8.73 mmol) in DMF (87 mL) was then added dropwise. The reaction mixture was allowed to warm to room temperature and stirred overnight. The reaction mixture was then diluted in EtOAc (50 mL), washed with 10% w/v citric acid (20 mL), followed by brine (20 mL). The organic layer was separated, dried with Na_2SO_4(s), and filtered. The solvent was removed under reduced pressure, and the crude product was purified by flash column chromatography (10 % v/v EtOAc in hexanes) to afford the **4.6a** as a white solid (1.75 g, 63%).

^{1}H NMR (500 MHz, CD_3OD, δ): 3.84 (s, 3H), 6.94–6.96 (d, J = 8.70 Hz, 2H), 7.09–7.12 (d, J = 16.28, 1H), 7.20–7.25 (d, J = 16.41 Hz, 1H), 7.45–7.48 (t, J = 7.67, 1H), 7.53–7.55 (d, J = 8.62 Hz, 2H), 7.76–7.78 (d, J = 7.85 Hz, 1H), 7.88–7.90 (d, J = 7.72, 1H), 8.18 (s, 1H); **^{13}C NMR (125 MHz, CD_3OD, δ)**: 54.31, 113.73, 124.97, 126.93, 127.58, 127.80, 128.40, 129.13, 130.01,

138.21, 159.72, 168.62; **HRMS–ESI (*m*/*z*)**: $M^{+\bullet}$ calcd for $C_{16}H_{13}BrO_2$, 316.0094; found, 316.0081.

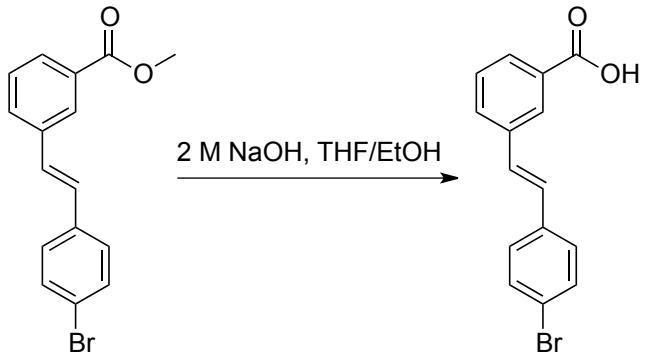

4.6a **4.6b**

Compound **4.6a** (1.5 g, 4.7 mmol) was dissolved in 3:1 THF/EtOH (47 mL). A solution of 2 M NaOH (4.7 mL, 9.4 mmol) was added to the resulting solution, and the reaction mixture was stirred overnight. The reaction mixture was then diluted with EtOAc (20 mL), washed with 10% w/v citric acid (20 mL), followed by brine (20 mL). The organic layer was separated, dried with Na_2SO_4(s), and filtered. The solvent was removed under reduced pressure, and the crude product was purified by flash column chromatography (20% v/v EtOAc in hexanes) to afford compound **4.6b** as a white solid (1.36 g, 96%).

^{1}H NMR (500 MHz, DMSO, *δ*): 7.33–7.36 (d, *J* = 16.52 Hz, 1H), 7.40–7.43 (d, *J* = 16.44 Hz, 1H), 7.50–7.54 (t, *J* = 7.68 Hz, 1H), 7.58–7.60 (d, *J* = 8.64 Hz, 2H), 7.63–7.61 (d, *J* = 8.66 Hz, 2H), 7.84–7.88 (t, *J* = 8.63 Hz, 2H), 8.16 (s, 1H), 13.10 (s, 1H); **^{13}C NMR (125 MHz, DMSO, *δ*)**: 121.27, 127.81, 128.68, 128.92, 129.00, 129.10, 129.51, 131.04, 132.09, 136.61, 137.66, 167.69; **HRMS–ESI (*m*/*z*)**: $M^{+\bullet}$ calcd for $C_{15}H_{11}BrO_2$, 301.9937; found, 301.9944.

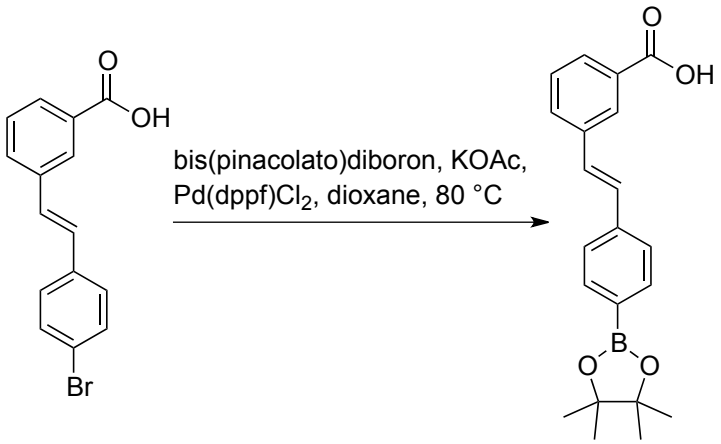

4.6b **4.6c**

Compound **4.6b** (1.0 g, 3.3 mmol), KOAc (0.971 g, 9.9 mmol), bis(pinacolato)diboron (2.5 g, 9.9 mmol), and Pd(dppf)Cl_2 (0.24 g, 0.33 mmol) were added to a flame-dried Schlenk flask, which was then evacuated and backfilled with N_2(g). Dioxane (33 mL) was deoxygenated by sonication under high vacuum and backfilled with N_2(g). The deoxygenated dioxane was then added by cannula into the reaction flask, and the reaction mixture was stirred overnight at 80 °C. The reaction mixture was filtered, and the solvent was removed under reduced pressure. The crude product was purified by flash column chromatography (20% v/v EtOAc in hexanes) to afford compound **4.6c** as a white solid (0.850 g, 73%).

^{1}H NMR (500 MHz, $CDCl_3$, δ): 1.36, (s, 12H), 7.22 (s, 2H), 7.46–7.50 (t, J = 7.44 Hz, 1H), 7.54–7.55 (d, J = 7.72 Hz, 1H), 7.76–7.77 (d, J = 8.12 Hz, 2H), 7.81–7.83 (d, J = 8.10 Hz, 2H), 8.00–8.01 (d, J = 8.11 Hz, 1H), 8.27–8.28 (d, J = 7.72 Hz, 1H), 8.28 (s, 1H); **^{13}C NMR (125 MHz, $CDCl_3$, δ)**: 24.90, 83.87, 125.97, 128.19, 128.32, 128.94, 129.28, 129.70, 130.06, 131.67, 135.23, 137.70, 139.50; **HRMS–ESI (m/z)**: $[M + NH_4]^+$ calcd for $C_{21}H_{23}BO_4$, 367.2064; found, 367.2062.

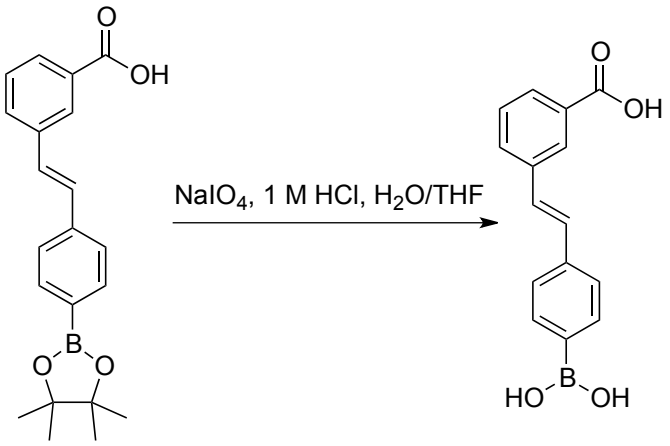

4.6c **4.6**

Compound **6c** (0.5 g, 1.48 mmol) was dissolved in 4:1 THF/H_2O (15 mL). $NaIO_4$ (0.405 g, 1.89 mmol) was added to the resulting solution, followed by 1.0 M HCl (0.15 mL, 0.158 mmol). The reaction mixture was then stirred overnight. The reaction mixture was diluted with H_2O (10 mL) and extracted with EtOAc (3 × 15 mL). The organic layers were combined and washed with brine (20 mL), dried with Na_2SO_4(s), and filtered. The solvent was removed under reduced pressure, and the crude product was purified by flash column chromatography (10% v/v CH_3OH in DCM) to afford compound **4.6** as a white crystalline solid (0.345 g, 90%).

^{1}H NMR (500 MHz, $CDCl_3$, δ): 7.24–7.27 (d, J = 16.43 Hz, 1H), 7.28–7.32 (d, J = 16.45 Hz, 1H), 7.49–7.76 (t, J = 7.70 Hz, 1H), 7.58–7.59 (d, J = 7.94 Hz, 2H), 7.62–7.64 (d, J = 7.92 Hz, 2H), 7.80–7.82 (d, J = 7.87 Hz, 1H), 7.90–7.92 (d, J = 7.81 Hz, 1H), 8.21 (s, 1H); **^{13}C NMR (125 MHz, $CDCl_3$, δ)**: 125.51, 127.32, 127.86, 128.37, 128.51, 129.41, 130.43, 131.07, 133.70, 137.77, 138.27, 168.32; **HRMS–ESI (m/z)**: $[M - H]^-$ calcd for single methyl boronic acid $C_{16}H_{15}BO_4$, 280.1026; found, 280.1033.

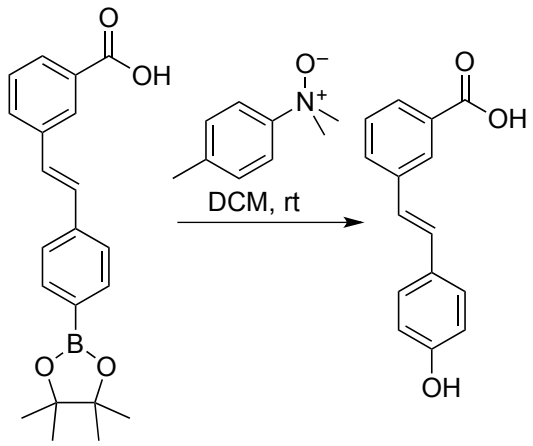

6c **5**

Compound **6c** (0.050 g, 0.142 mmol) was dissolved in DCM (1.4 mL). *N*,*N*-Dimethyl-*p*-toluidine-*N*-oxide (0.032 g, 0.213 mmol) was added to the resulting solution, and the reaction mixture was allowed to stir for 1 h. The reaction mixture was filtered, and the solvent was removed under reduced pressure. The crude product was purified by flash column chromatography (2% v/v MeOH in DCM) to afford compound **5** as a white solid (0.030 g, 88%).

^{1}H NMR (500 MHz, CD_3OD, δ): 6.78–6.80 (d, J = 8.61 Hz, 2H), 7.02–7.05 (d, J = 16.32 Hz, 1H), 7.15–7.19 (d, J = 16.34 Hz, 1H), 7.42–7.44 (d, J = 8.26 Hz, 2H), 7.42–7.45 (t, J = 7.28 Hz, 1H), 7.73–7.75 (d, J = 7.82 Hz, 1H), 7.85–7.87 (d, J = 7.79 Hz, 1H), 8.15 (s, 1H); **^{13}C NMR** (125 MHz, CD_3OD, δ): 116.52, 125.56, 128.25, 129.04, 129.10, 129.80, 130.04, 130.90, 131.42, 132.30, 139.80; **HRMS–ESI** (m/z): $[M - H]^-$ calcd for $C_{15}H_{12}O_3$, 239.0714; found, 239.0716.

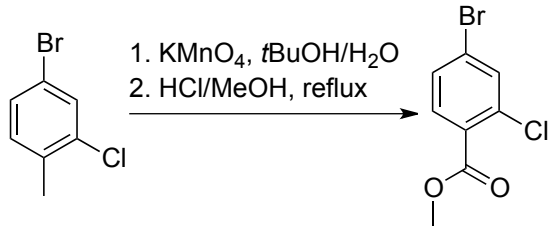

4.8a

2-Chloro-4-bromo toluene (1 g, 4.8 mmol) was dissolved in 1:1 water/*tert*-butanol (20 mL). $KMnO_4$ (1.53 g, 9.7 mmol) was added to the resulting solution, and the reaction mixture was heated to 70 °C with a reflux condenser for 2 h. The reaction mixture was then allowed to cool to room temperature, and more $KMnO_4$ (1.53 g, 9.7 mmol) was added. The reaction mixture was then reheated to 70 °C in a flask with a reflux condenser and stirred overnight at 70 °C. The warm reaction mixture was filtered, and the resulting $KMnO_4$ cake was rinsed with water (~10 mL). The filtrate was acidified to pH 3 with concentrated HCl and extracted with EtOAc (3 × 20 mL). The organic layers were combined, dried with $NaSO_4$(s), and filtered. The solvent was removed under reduced pressure to afford the carboxylic acid precursor as a white solid. This precursor was dissolved in 3 M HCl in MeOH (15 mL) and heated to reflux for 12 h. The reaction mixture was allowed to cool to room temperature, and N_2(g) was bubbled through the solution for 20 min to remove excess HCl(g). The solvent was removed under reduced pressure, and the crude product was purified by flash column chromatography (20% v/v EtOAc in hexanes) to afford compound **4.8a** as a colorless oil (1.15 g, 96% yield over 2 steps).

^{1}H NMR (500 MHz, CD_3OD, δ): 3.93 (s, 3H), 7.59–7.61 (d, J = 8.47 Hz, 1H), 7.76–7.77 (m, 2H); **^{13}C NMR** (125 MHz, CD_3OD, δ): 53.07, 127.34, 130.51, 131.41, 133.71, 134.63, 135.53, 166.72; **HRMS–ESI** (m/z): $M^{+\bullet}$ calcd for $C_8H_6BrClO_2$, 247.9235; found, 247.9237.

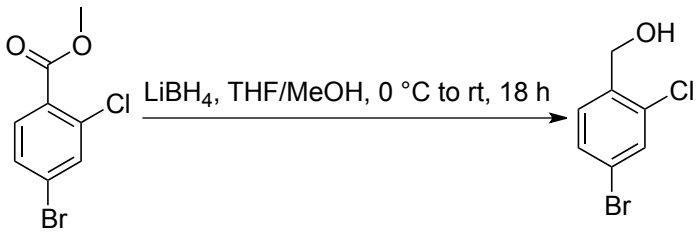

4.8a **4.8b**

Compound **4.8a** (1.00 g, 4.01 mmol) was dissolved in THF (47 mL), and the resulting solution was cooled to 0 °C. 2 M $LiBH_4$ in THF (12 mL, 23.5 mmol) was then added dropwise, followed by methanol (4 mL). The reaction mixture was allowed to warm to room temperature and stirred overnight. The reaction mixture was quenched by adding EtOAc (20 mL) dropwise, followed by water (15 mL), and then acidification to pH 5 with 1.0 M HCl. The resulting lithium salts were removed by filtration, and the filtrate was extracted with EtOAc (3 × 15 mL). The organic layers were combined, dried with $NaSO_4$(s), and filtered. The solvent was removed under reduced pressure, and the crude product was purified by flash column chromatography (20% v/v EtOAc in hexanes) to afford compound **4.8b** as a white solid (0.843 g, 95%).

^{1}H NMR (500 MHz, $CDCl_3$, δ): 1.91 (bs, 1H), 4.74 (s, 2H), 7.38–7.39 (d, J = 8.22 Hz, 1H), 7.42–7.44 (d, J = 8.23, 1H) 7.53 (s, 1H); **^{13}C NMR** (500 MHz, $CDCl_3$, δ): 62.48, 121.68, 129.93, 130.42, 132.05, 133.54, 137.43; **HRMS–ESI** (m/z): $M^{+\bullet}$ calcd for C_7H_6OBrCl, 219.9286; found, 219.9282.

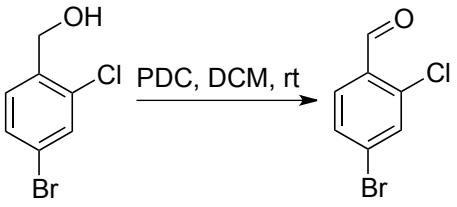

4.8b **4.8c**

Compound **4.8b** (0.5 g, 2.28 mmol) was dissolved in DCM (22 mL). Pyridinium dichromate (PDC, 2.57 g, 6.84 mmol) was added to the resulting solution, and the reaction mixture was allowed to stir overnight. The reaction mixture was then filtered through a pad of Celite®, and the solvent was removed under reduced pressure. The crude product was purified by flash column chromatography (10% v/v EtOAc in hexanes) to afford compound **4.8c** as a white solid (0.440 g, 88%).

^{1}H NMR (500MHz, $CDCl_3$, δ): 7.54–7.55 (d, J = 8.25 Hz, 1H), 7.66 (s, 1H), 7.78–7.80 (d, J = 8.32 Hz, 1H), 10.42 (s, 1H); **^{13}C NMR (125 MHz, $CDCl_3$, δ)**: 129.78, 130.55, 131.09, 131.45, 133.49, 138.71, 188.95; **ASAP–MS (*m*/*z*)**: $[M+H]^+$ calcd for C_7H_4BrClO, 218.9207; found, 218.9216.

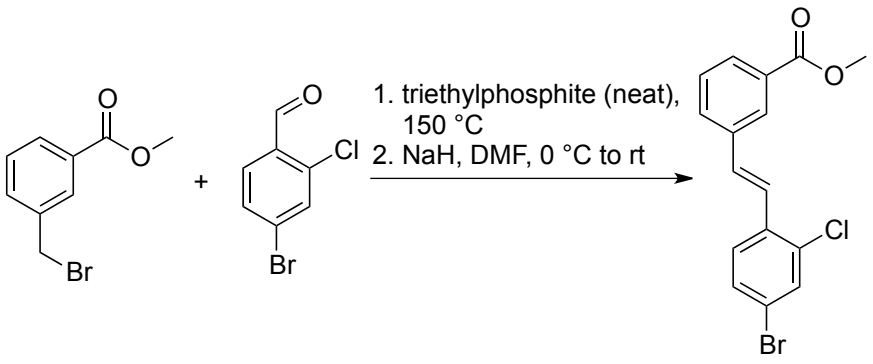

4.8c **4.8d**

Ethyl 3-(bromomethyl)benzoate (1.04 g, 4.55 mmol) was dissolved in neat triethylphosphite (0.9 mL, 5.46 mmol), and the resulting solution was heated to 150 °C for 4 h. The reaction mixture was cooled to 0 °C and diluted with DMF (40 mL). NaH (60% w/v in mineral oil, 0.23 g, 5.91 mmol) was added to the resulting solution, and the reaction mixture was stirred at 0 °C for 20 min. A solution of 4-bromo-2-chlorobenzaldehyde (**4.8c**; 1.0 g, 4.6 mmol) in DMF (5 mL) was added dropwise. The reaction mixture was then allowed to warm to room temperature and stirred overnight. The reaction mixture was diluted in EtOAc (5 mL), washed with 10% w/v citric acid (5 mL), followed by brine (5 mL). The organic layer was separated, dried with Na_2SO_4(s), and filtered. The solvent was removed under reduced pressure, and the crude product was purified by flash column chromatography (10% v/v EtOAc in hexanes) to afford compound **4.8d** as a white solid (1.3 g, 83%).

^{1}H NMR (500MHz, $CDCl_3$, δ): 3.95 (s, 3H), 7.08–7.11 (d, J = 16.31 Hz, 1H), 7.39–7.41 (d, J = 8.53 Hz, 1H), 7.44–7.47 (t, J = 8.02 Hz, 1H), 7.45–7.49 (d, J = 16.56 Hz, 1H), 7.53–7.55 (d, J = 8.45 Hz, 1H), 7.56 (s, 1H), 7.71–7.73 (d, J = 7.73 Hz, 1H), 7.96–7.97 (d, J = 7.70 Hz, 1H), 8.19 (s, 1H); **^{13}C NMR (125 MHz, $CDCl_3$, δ)**: 52.43, 121.70, 125.02, 127.66, 128.15, 129.02, 129.35,

130.39, 130.88, 131.12, 132.55, 134.26, 134.35, 137.19, 167.02; **HRMS–ESI (*m*/*z*)**: $[M + NH_4]^+$ calcd for $C_{16}H_{12}BrClO_2$, 368.0048; found, 368.0053.

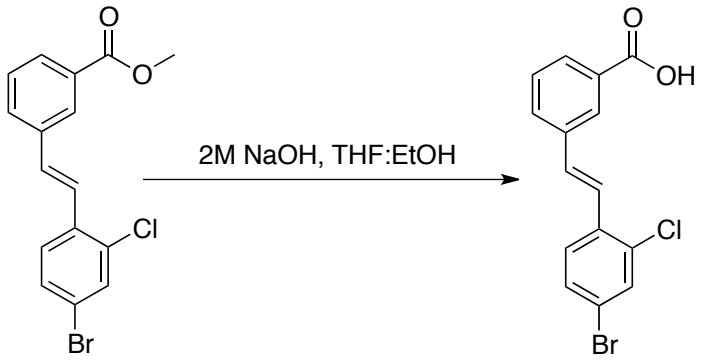

4.8d **4.8e**

Compound **4.8d** (1.34 g, 3.83 mmol) was dissolved in 3:1 THF/EtOH (40 mL). 2.0 M NaOH (3.3 mL, 7.7 mmol) was added to the resulting solution, and the reaction mixture was stirred overnight. The reaction mixture was diluted with EtOAc (20 mL), washed with 10% w/v citric acid (30 mL), followed by brine (30 mL). The organic layer was separated, dried with $Na_2SO_4(s)$, and filtered. The solvent was removed under reduced pressure, and the crude product was purified by flash column chromatography (20% v/v EtOAc in hexanes) to afford compound **4.8e** as a white solid (1.22 g, 95%).

^{1}H NMR (500 MHz, DMSO, δ): 7.42–7.45 (d, J = 16.39 Hz, 1H), 7.47–7.50 (d, J = 16.41 Hz, 1H), 7.53–7.56 (t, J = 7.71 Hz, 1H), 7.60–7.62 (d, J = 8.54, 1H), 7.79 (s, 1H), 7.86–7.88 (d, J = 8.63 Hz, 1H), 7.88–7.92 (t, J = 7.86, 2H), 8.15 (s, 1H), 13.01 (bs, 1H); **^{13}C NMR (125 MHz, DMSO, δ)**: 121.99, 124.85, 128.89, 129.10, 129.94, 130.17, 131.41, 131.73, 132.08, 132.38, 132.87, 134.61, 135.22, 138.07, 167.31; **HRMS–ESI (m/z)**: $[M - H]^-$ calcd for $C_{15}H_{10}BrClO_2$, 334.9479; found, 334.9476.

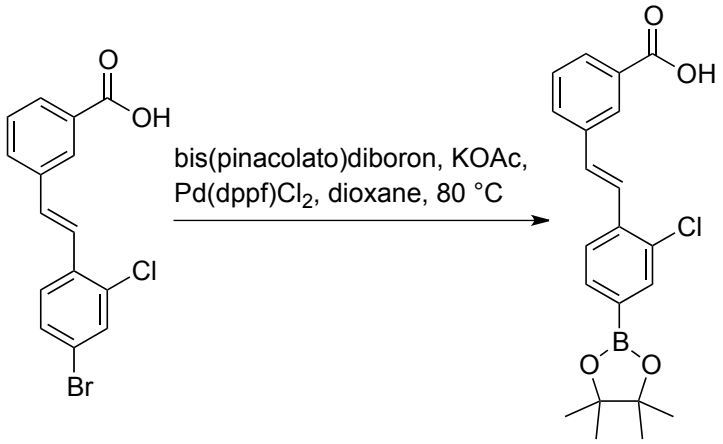

4.8e **4.8f**

Compound **4.8e** (0.200 g, 0.580 mmol), KOAc (0.171 g, 1.791 mmol), bis(pinacolato)diboron (0.45 g, 1.79 mmol), and $Pd(dppf)Cl_2$ (0.043 g, 0.059 mmol) were added to a flame-dried Schlenk flask, which was then evacuated and backfilled with N_2(g). Dioxane (6 mL) was deoxygenated by sonication under high vacuum and backfilled with N_2(g). The deoxygenated dioxane was then added by cannula into the reaction flask, and the reaction mixture was stirred overnight at 80 °C. The reaction mixture was filtered, and the solvent was removed under reduced pressure. The crude product was purified by flash column chromatography (1% v/v CH_3OH in DCM) to afford compound **4.8f** as a white solid (0.183 g, 82%).

^{1}H NMR (500 MHz, CD_3OD, δ): 1.36 (s, 12H), 7.33–7.36 (d, J = 16.30 Hz, 1H), 7.49–7.52 (t, J = 8.41 Hz, 1H), 7.61–7.64 (d, J = 16.47 Hz, 1H), 7.66–7.67 (d, J = 7.46, 1H), 7.73 (s, 1H), 7.83–7.85 (d, J = 7.75 Hz, 2H), 7.95–7.97 (d, J = 7.73, 1H), 8.24 (s, 1H); **^{13}C NMR (125 MHz, CD_3OD, δ)**: 25.19, 85.51, 126.33, 127.18, 129.00, 130.07, 130.41, 132.16, 132.61, 134.18, 136.79, 138.74, 138.86, 169.56; **HRMS–ESI (*m*/*z*)**: $[M + NH_4]^+$ calcd for $C_{21}H_{22}BClO_4$, 401.1675; found, 401.1666.

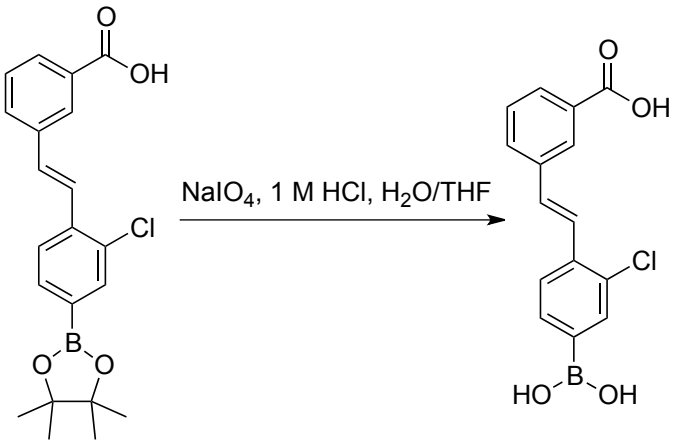

4.8f **4.8**

Compound **4.8f** (0.100 g, 0.260 mmol) was dissolved in 4:1 THF/H_2O (2.6 mL). $NaIO_4$ (0.28 g, 1.30 mmol) was added to the resulting solution, followed by 0.02 mL of 1.0 M HCl (0.02 mmol). The reaction mixture was then stirred overnight. The reaction mixture was diluted with H_2O (2 mL) and extracted with EtOAc (3 × 3 mL). The organic layers were combined and washed with brine (5 mL), dried with Na_2SO_4(s), and filtered. The solvent was removed under reduced pressure, and the crude product was purified by flash column chromatography (1–3% v/v CH_3OH in DCM) to afford compound **4.8** as a white crystalline solid (0.058 g, 75%).

^{1}H NMR (500 MHz, CD_3OD, δ): 7.32–7.35 (d, J = 16.37 Hz, 1H), 7.51–7.54 (t, J = 7.73 Hz, 1H), 7.51–7.67 (m, 3H), 7.84–7.85 (d, J = 7.29 Hz, 2H), 7.97–7.98 (d, J = 7.76 Hz, 1H), 8.25 (s, 1H); **^{13}C NMR (125 MHz, CD_3OD, δ)**: 126.41, 126.94, 128.93, 130.04, 130.29, 132.07, 132.63, 133.31, 134.12, 135.95, 137.29, 138.82, 169.61; **HRMS–ESI (m/z)**: $[M - H]^-$ calcd for the single methyl boronic ester $C_{16}H_{14}BClO_4$, 314.0637; found, 314.0635.

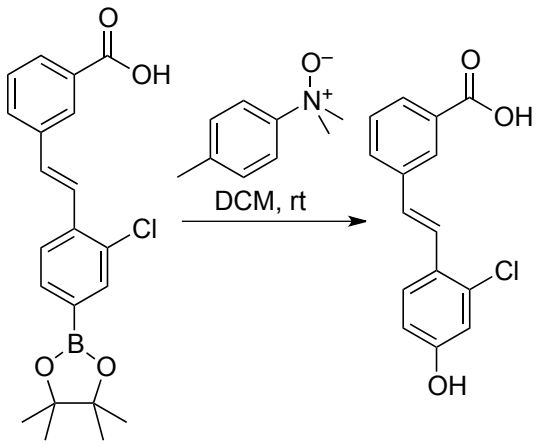

4.8f **4.7**

Compound **8f** (0.100 g, 0.259 mmol) was dissolved in DCM (2.6 mL). *N*,*N*-Dimethyl-*p*-toluidine-*N*-oxide (0.060 g, 0.389 mmol) was added to the resulting solution, and the reaction mixture was then stirred overnight. The solvent was removed under reduced pressure, and the crude product was purified by flash column chromatography (2% v/v MeOH in DCM) to afford compound **7** as a white solid (0.051 g, 72%).

^{1}H NMR (500 MHz, CD_3OD, δ): 6.77–6.68 (d, J = 8.63 Hz, 1H), 6.84 (s, 1H), 7.06–7.10 (d, J = 16.34 Hz, 1H), 7.45–7.48 (t, J = 7.72 Hz, 1H), 7.49–7.52 (d, J = 16.31 Hz, 1H), 7.65–7.67 (d, J = 8.63 Hz, 1H), 7.75–7.77 (d, J = 7.91 Hz, 1H), 7.89–7.91 (d, J = 7.78 Hz, 1H), 8.17 (s, 1H); **^{13}C NMR (125 MHz, CD_3OD, δ)**: 115.98, 117.09, 126.42, 127.43, 128.47, 128.48, 128.58, 129.60, 129.92, 131.70, 132.43, 135.06, 139.41, 159.45, 169.74; **HRMS–ESI (*m*/*z*)**: $[M - H]^-$ calcd for $C_{15}H_{11}ClO_3$, 273.0324; found, 273.0327.

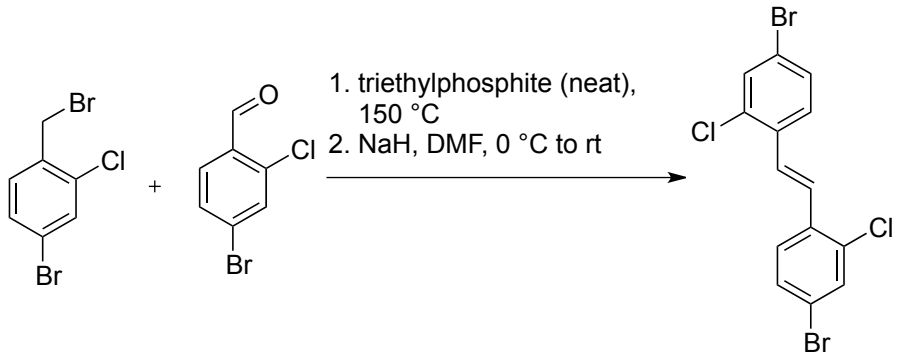

4.8c **4.10a**

4-Bromo-1-(bromomethyl)-2-chloro-benzene (0.300 g, 1.05 mmol) was dissolved in neat triethylphosphite (0.217 mL, 1.26 mmol) and heated to 150 °C for 4 h. The reaction mixture was then cooled to 0 °C and diluted with DMF (8 mL). NaH (60% w/v in mineral oil, 0.054 g, 1.36 mmol) was added to the resulting solution, and the reaction mixture was stirred at 0 °C for 20 min. A solution of 4-bromo-2-chloro-benzaldehyde (**4.8c**; 0.230 g, 1.05 mmol) in DMF (2.5 mL) was then added dropwise. The reaction mixture was allowed to warm to room temperature and stirred overnight. The reaction mixture was diluted with EtOAc (8 mL), washed with 10% w/v citric acid (10 mL), followed by brine (10 mL). The organic layer was then separated, dried with Na_2SO_4 (s), and filtered. The solvent was removed under reduced pressure, and the crude product was suspended in cold DCM (10 mL). The resulting precipitate was collected by filtration to afford compound **4.10a** as a white solid (0.306 g, 72% yield).

^{1}H NMR (500 MHz, $CDCl_3$, δ): 7.39 (s, 2H), 7.41–7.43 (d, J = 8.42 Hz, 2H), 7.58 (s, 2H), 7.58–7.59 (d, J = 7.12 Hz, 2H); **^{13}C NMR** (125 MHz, $CDCl_3$, δ): 121.99, 126.70, 127.83, 130.35, 132.45, 133.89, 134.30; **ASAP–MS** (m/z): $M^{+\bullet}$ calcd for $C_{14}H_8Br_2Cl_2$, 403.8365; found, 403.8367.

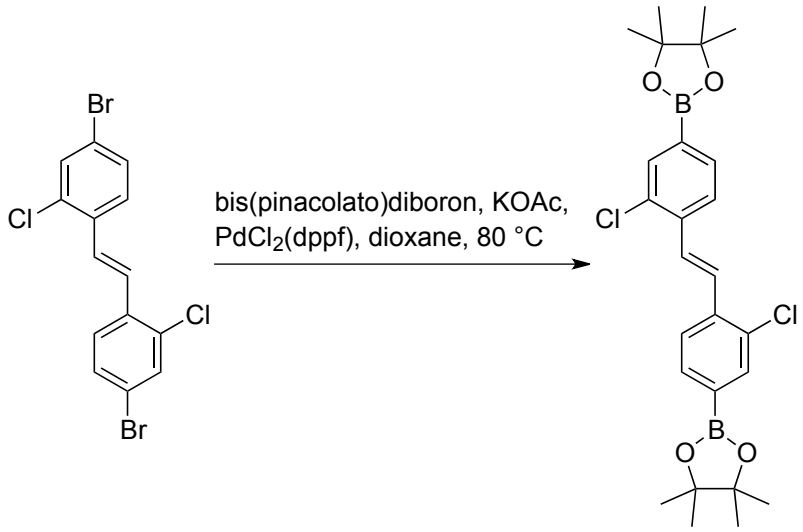

4.10a **4.10b**

Compound **4.10a** (0.050 g, 0.123 mmol), KOAc (0.071 g, 0.742 mmol), bis(pinacolato)diboron (0.187 g, 0.742 mmol), and $Pd(dppf)Cl_2$ (9 mg, 0.012 mmol) were added to a flame-dried Schlenk flask, which was then evacuated and backfilled with N_2(g). Dioxane (2 mL) was deoxygenated by sonication under high vacuum and backfilled with N_2(g). The deoxygenated dioxane was then added by cannula into the reaction flask, and the reaction mixture was heated to 80 °C and stirred overnight (Note: higher yields of the diboronated product were found at more dilute reaction concentrations). The reaction mixture was filtered, and the solvent was removed under reduced pressure. The crude product was purified by flash column chromatography (50% v/v DCM in hexanes) to afford **4.10b** as a white solid (0.056 g, 92%).

^{1}H NMR (500 MHz, $CDCl_3$, δ): 1.35 (s, 24H), 7.56 (s, 2H), 7.67–7.69 (d, J = 7.76 Hz, 2H), 7.73–7.75 (d, J = 7.85 Hz, 2H), 7.83 (s, 2H); **^{13}C NMR (125 MHz, $CDCl_3$, δ)**: 24.88, 84.18, 126.17, 127.94, 133.02, 133.45, 136.06, 137.45; **ASAP–MS (*m*/*z*)**: $[M + H]^+$ calcd for $C_{26}H_{32}B_2Cl_2O_4$, 499.2009; found, 499.2001.

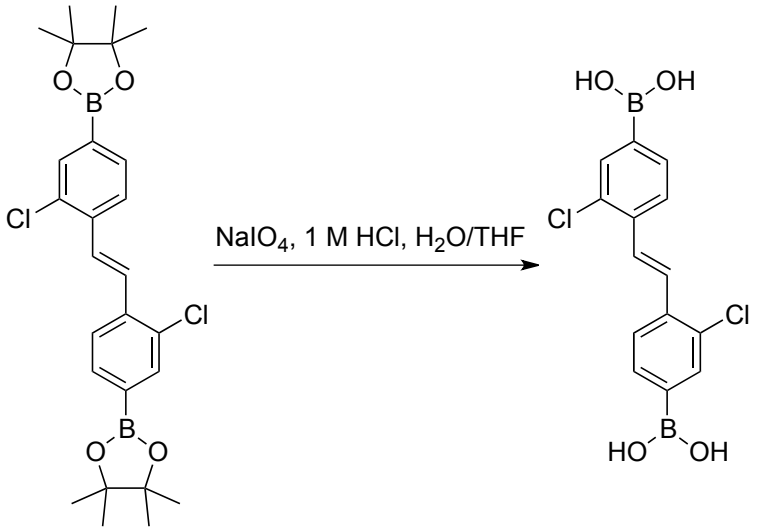

4.10b **4.10**

Compound **4.10b** (0.020 g, 0.040 mmol) was dissolved in 4:1 THF/H_2O (0.6 mL). $NaIO_4$ (0.042 g, 0.200 mmol) was added to the resulting solution, followed by a few drops of 1.0 M HCl. The reaction mixture was then stirred overnight. The reaction mixture was then diluted with H_2O (1 mL) and extracted with EtOAc (3 × 2 mL). The organic layers were combined and washed with saturated brine (3 mL), dried with Na_2SO_4(s), and filtered. The solvent was removed under reduced pressure, and the crude product was purified by flash column chromatography (3% v/v CH_3OH in DCM) to afford compound **4.10** as a white crystalline solid (0.010 g, 74%).

^{1}H NMR (500 MHz, CD_3OD, δ): 7.59 (s, 1H), 7.59–7.60 (d, J = 8.42 Hz, 2H), 7.66 (s, 1H), 7.78–7.80 (d, J = 7.78 Hz, 2H); **^{13}C NMR** (125 MHz, CD_3OD, δ): 127.14, 128.69, 133.38, 134.25, 135.98; **MALDI–MS** (m/z): $M^{+\bullet}$ calcd for $C_{14}H_{12}B_2Cl_2O_4$, 336.03; found, 336.00.

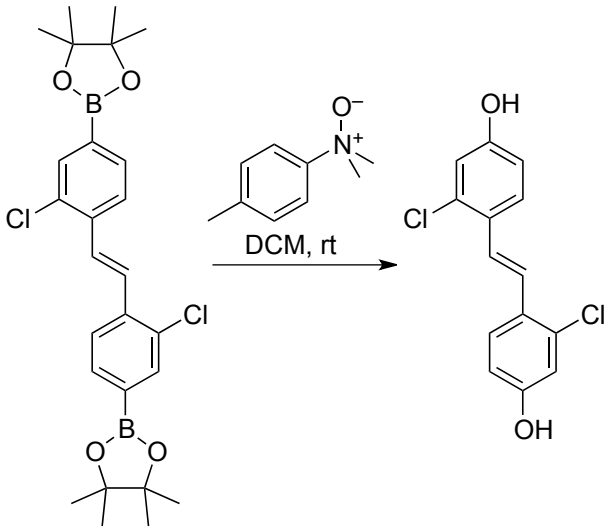

4.10b **4.9**

Compound **4.10b** (0.020 g, 0.040 mmol) was dissolved in DCM (0.5 mL). *N*,*N*-Dimethyl-*p*-toluidine-*N*-oxide (0.018 g, 0.120 mmol) was added to the resulting solution, and the reaction mixture was stirred for 1 h. The solvent was removed under reduced pressure, and the crude product was purified by flash column chromatography (2% v/v MeOH in DCM) to afford compound **4.9** as a white solid (9 mg, 80%).

^{1}H NMR (500 MHz, CD_3OD, δ): 6.75–6.77 (d, J = 8.61 Hz, 2H), 6.83 (s, 2H), 7.24 (s, 2H), 7.55–7.57 (d, J = 8.59 Hz, 2H); **^{13}C NMR (125 MHz, CD_3OD, δ)**: 115.93, 117.07, 125.22, 128.00, 128.36, 134.73, 159.09; **HRMS–ESI (*m*/*z*)**: $[M - H]^-$ calcd for $C_{14}H_{10}Cl_2O_2$, 278.9985; found, 278.9985.

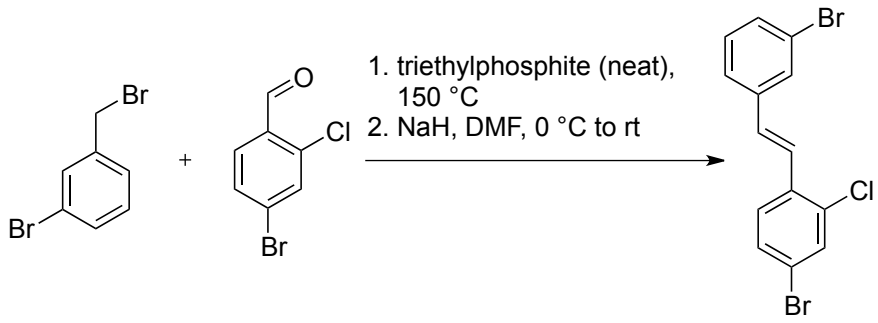

4.8c **4.11a**

3-Bromobenzyl bromide (0.500 g, 2.00 mmol) was dissolved in neat triethylphosphite (0.411 mL, 2.4 mmol), and the resulting solution was heated to 150 °C for 4 h. The reaction mixture was cooled to 0 °C and then diluted with DMF (10 mL). NaH (60% w/v in mineral oil, 0.096 g, 2.4 mmol) was added to the resulting solution, and the reaction mixture stirred at 0 °C for 20 min. A solution of 4-bromo-2-chloro-benzaldehyde (**4.8c**; 0.447 g, 2.04 mmol) in DMF (10 mL) was then added drop-wise. The reaction mixture was allowed to warm to room temperature and stirred overnight. The reaction mixture was diluted in EtOAc (20 mL), washed with 10% w/v citric acid (30 mL), followed by brine (30 mL). The organic layer was separated, dried with Na_2SO_4(s), and filtered. The solvent was removed under reduced pressure, and the crude product was suspended in ice-cold DCM (5 mL). The resulting precipitate was collected by filtration to afford compound **4.11a** as a white solid (0.514 g, 69%).

^{1}H NMR (500 MHz, CD_3OD, δ): 7.09–7.13 (d, J = 16.3 Hz, 1H), 7.26–7.29 (d, J = 12.53 Hz, 2H), 7.35–7.39 (t, J = 7.61 Hz, 1H), 7.53 (s, 3H), 7.61–7.63 (d, J = 7.74 Hz, 1H), 7.79 (s, 1H); **^{13}C NMR (125 MHz, CD_3OD, δ)**: 124.42, 125.32, 126.40, 127.54, 127.67, 131.61, 131.80, 131.80, 132.97, 134.94, 135.71, 141.09; **ASAP–MS (m/z)**: $M^{+\bullet}$ calcd for $C_{14}H_9Br_2Cl$, 369.8754; found, 369.8740.

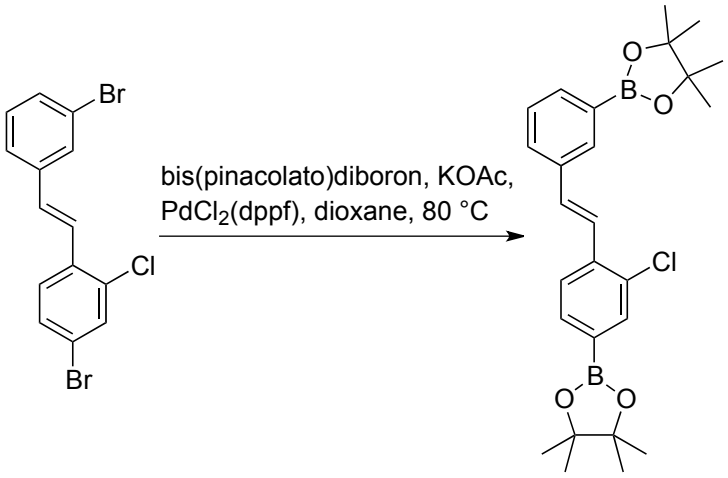

4.11a **4.11b**

Compound **4.11a** (0.100 g, 0.270 mmol), KOAc (0.152 g, 1.62 mmol), bis(pinacolato)diboron (0.410 g, 1.62 mmol), and $Pd(dppf)Cl_2$ (0.0270 g, 0.020 mmol) were added to a flame-dried Schlenk flask, which was then evacuated and backfilled with N_2(g). Dioxane (3.6 mL) was deoxygenated by sonication under high vacuum and backfilled with N_2(g). The deoxygenated dioxane was then added by cannula into the reaction flask, and the reaction mixture was heated to 80 °C and stirred overnight. The reaction mixture was filtered, and the solvent was removed under reduced pressure. The crude product was purified by flash column chromatography (2% v/v DCM in hexanes) to afford **4.11b** as a white solid (0.111 g, 87%).

^{1}H NMR (500 MHz, CD_3OD, δ): 1.36 (s, 12H), 1.38 (s, 12H), 7.27–7.30 (d, J = 16.29 Hz, 1H), 7.38–7.41 (t, J = 7.47 Hz, 1H), 7.55–7.58 (d, J = 16.30 Hz, 1H), 7.64–7.66 (d, J = 7.73 Hz, 1H), 7.67–7.70 (t, J = 7.88 Hz, 2H), 7.72 (s, 1H), 7.81–7.82 (d, J = 7.75 Hz, 1H), 7.96 (s, 1H); **^{13}C NMR (125 MHz, CD_3OD, δ)**: 26.45, 26.48, 50.43, 50.60, 86.55, 86.74, 126.43, 128.29, 130.59, 132.18, 134.79, 135.29, 135.31, 135.40, 136.90, 138.03, 138.91, 140.44; **HRMS–ESI (m/z)**: $[M + NH_4]^+$ calcd for $C_{26}H_{33}B_2ClO_4$, 484.2607; found, 484.2600.

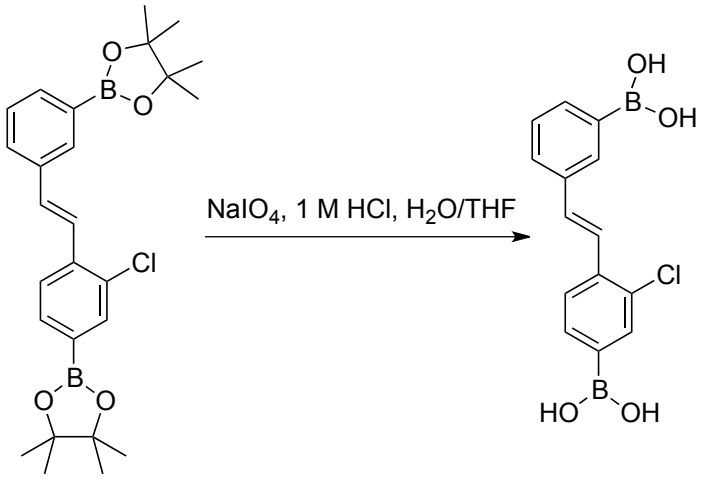

4.11b **4.11**

Compound **4.11b** (0.100 g, 0.214 mmol) was dissolved in 4:1 THF/H_2O (2.1 mL). $NaIO_4$ (0.227 g, 1.07 mmol) was added to the resulting solution, followed by a few drops of 1.0 M HCl. The reaction mixture was then stirred overnight. The reaction mixture was diluted with H_2O (2 mL) and extracted with EtOAc (3 × 2 mL). The organic layers were combined and washed with brine (4 mL), dried with Na_2SO_4(s), and filtered. The solvent was removed under reduced pressure, and the crude product was purified by flash column chromatography (2% v/v CH_3OH in DCM) to afford compound **4.11** as a white crystalline solid (0.040 g, 63%).

^{1}H NMR (500 MHz, CD_3OD, δ): 7.24–7.27 (d, J = 16.3 Hz, 1H), 7.37–7.40 (t, J = 7.57 Hz, 1H), 7.52–7.57 (m, 3H), 7.63–7.64 (d, J = 4.84 Hz, 2H), 7.79 (s, 2H); **^{13}C NMR (125 MHz, CD_3OD, δ)**: 125.12, 126.78, 128.85, 129.02, 129.16, 129.80, 133.24, 133.95, 134.31, 135.93, 137.64; **HRMS–ESI (m/z)**: $[M - H]^-$ calcd for the single methyl boronate ester $C_{15}H_{14}B_2ClO_4$, 315.0772; found, 315.0772.

4.7.3 Protein Expression and Purification

Plasmids that direct the expression of wild-type TTR and its V30M variant were prepared in the pET32b vector from Merck KGaA (Darmstadt, Germany) by standard methods.[256] To create the plasmid encoding V30M TTR, two double-stranded DNA fragments were prepared by PCR using complementary primers containing V30M-generating substitutions and gene-specific primers targeting opposite termini for assembly with the plasmid fragment. Wild-type TTR and its V30M variant were produced in *Escherichia coli* strain BL-21 from Merck KGaA cultured in Luria–Bertani medium containing ampicillin (200 μM) at 37 °C. Gene expression was induced when $OD_{600\ nm}$ reached ~2.0, and cells were then grown for an additional 4 h at 37 °C. Cell pellets were resuspended in 20 mM Tris–HCl buffer, pH 7.4, containing EDTA (1.0 mM) and lysed with a high-pressure cell disruptor from Constant Systems (Kennesaw, GA). The soluble fraction was isolated by centrifugation for 10 min at 10,500*g* and for 1 h at 30,000*g*.

Wild-type TTR and its V30M variant were purified as described previously,[257] with minor modifications. The lysate was fractionated with aqueous ammonium sulfate at 60–85% saturation. The precipitate was dissolved in 20 mM Tris–HCl buffer, pH 7.8, containing EDTA (1.0 mM) and dialyzed overnight against this same buffer. The isolate was clarified at 30,000*g* for 30 min, filtered, and applied to a Hitrap Q HP column from GE Healthcare Life Sciences (Pittsburgh, PA) that had been equilibrated with the dialysis buffer. TTR was eluted with the same buffer containing NaCl (1.0 M) and was subjected to gel-filtration chromatography on a Superdex 75 column from GE Healthcare Life Sciences (Pittsburgh, PA) that had been pre-equilibrated with 10 mM sodium phosphate buffer, pH 7.6, containing KCl (100 mM). Pure tetrameric TTR eluted at ~0.6 column volumes. The concentration of wild-type TTR and its V30M variant was determined from the $A_{280\ nm}$ by using $\varepsilon = 18.5 \times 10^3\ M^{-1}cm^{-1}$ and confirmed

with a bicinchoninic acid (BCA) assay using a kit from Pierce Biotechnology (Rockford, IL).

4.7.4 Competitive Fluorescence Assay

Fluorescence measurements were performed with a Photon Technology International Quantamaster spectrofluorometer (Edison, NJ). Wild-type TTR was found to form a complex with ANS that has a K_d value of 3.2 μM (data not shown).[258] To determine the affinity for ligands, wild-type TTR was incubated in 2.00 mL of 10 mM sodium phosphate buffer, pH 7.6, containing KCl (100 mM) and ANS (0.50 or 5.0 μM) until the fluorescence signal (excitation: 410 nm; emission: 460 nm) was stable (~30 min). A ligand (1 nM–10 μM) was then added in aliquots (5 μL) from a stock solution in dimethyl formamide (DMF). The fluorescence intensity at each ligand concentration was recorded before adding the next dose. Average intensities were adjusted for the dilution incurred upon adding ligand and were expressed as a percent change from the initial measurement.

The data did not fit well to the one- or two-site competitive binding models used previously to describe other systems.[258] The asymmetric behavior is likely a consequence of two distinct binding events. The steepest inflection point at higher ligand concentrations can be attributed to the half-maximal concentration required to compete ANS from the second binding site. The Prusoff–Cheng relation was used to account for this competition, resulting in a logistic equation:[259]

$$\%\Delta I = \%I_o + \frac{\%I_f - \%I_o}{\left(1 + 10^{n\left(\log\left(K_{d,2}\left(1 + \frac{[ANS]}{K_{d,ANS}}\right)\right) - [ligand]\right)}\right)^S} \quad (1)$$

where $K_{d,2}$ is the equilibrium dissociation constant of the second site, n is the Hill coefficient, and S is the symmetry parameter. Values of $K_{d,2}$ were determined with Prism 6 software from Graphpad (La Jolla, CA) by holding constant the ligand concentration, ANS concentration, and $K_{d,ANS}$ = 3.2 μM and varying other parameters to maximize the value of R^2, which was >0.99 for all datasets. The value of $K_{d,2}$ = (373 ± 10) nM for the TTR·tafamidis complex determined with this method is similar to the value of K_d = 278 nM determined with isothermal titration calorimetry.[220] Values of $K_{d,1}$ were not obtainable by this method due to the small change in fluorescence intensity upon binding to the first site, though modest inflection points were observed in the low nanomolar range (Figure 4.5).

4.7.5 Fibril Formation Assay

Light-scattering at 400 nm was used to assess the formation of fibrils under acidic conditions, as described previously.[260] Ligands were incubated with TTR (7.2 or 14.4 μM) for 30 min prior to twofold dilution with 50 mM sodium acetate buffer, pH 4.4, containing KCl (100 mM). Absorbance at 400 nm was measured ten times with four replicates in clear, flat-bottomed, 96-well plates at 0 and 96 h using an M1000 plate reader from Tecan (Maennedorf, Switzerland). Percent fibril formation was calculated from the difference in the light scattering that accumulated after 96 h in ligand-containing wells versus wells containing only vehicle (DMF), using the equation:

$$\%\ \text{fibril formation} = \frac{A_{400\ \text{nm,ligand,96 h}} - A_{400\ \text{nm,ligand,0 h}}}{A_{400\ \text{nm,DMF,96 h}} - A_{400\ \text{nm,DMF,0 h}}} \times 100\% \qquad (2)$$

Standard deviations from the four replicates were propagated through this calculation.

4.7.6 Protein Crystallization and X-ray Structure Determination

Crystals were grown using vapor diffusion of wild-type TTR (~6.0 mg/mL in 10 mM sodium phosphate buffer, pH 7.6, containing 100 mM KCl) and stilbenes **4.2–4.8**, **4.10**, or **4.11** (7.2 mM, added from a stock solution in DMF). Hanging drops (2 μL protein·ligand solution + 2 μL mother liquor) above a reservoir of 1.0–1.3 M sodium citrate buffer, pH 5.5, containing glycerol (1–3% v/v)[205] yielded crystals after 1–3 days. TTR precipitated in the presence of stilbene **4.9** (7.2 mM). Crystals were cryoprotected by brief transfer into a solution of 1.5 M sodium citrate buffer, pH 5.5, containing glycerol (10% v/v). Diffraction data were collected at Sector 21 of the Life Sciences Collaborative Access Team (LS-CAT) at the Advanced Photon Source of Argonne National Laboratory (Argonne, IL). Data were reduced using HKL2000 (Tables 4.5–4.13).[261] Boronate ester restraints were obtained by measuring the bond lengths and angles from ten CSD small-molecule structures (Table 4.4). Initial phases were obtained by molecular replacement using the protein atoms of Protein Data Bank (PDB) entry 2qgb as a model.[247] Refinement and model building were conducted with the programs Phenix and Coot (Tables 4.5–4.13 and Figures 4.7–4.15).[262,263] Ligand models in idealized geometries were prepared with the program WebMO, and restraints were prepared in Phenix with the program eLBOW. Restraints generated by eLBOW were modified to impose planarity on the four carbon atoms in the olefin of the stilbene and on the carbon, boron, and two oxygen atoms in a boronic acid group. Short interatomic distances in TTR·ligand complexes are listed in Table 4.14. Atomic coordinates and structure factors for all nine TTR·ligand complexes have been deposited in the PDB.

4.8 NMR Spectra

^{1}H NMR ($CDCl_3$) and ^{13}C NMR ($CDCl_3$) of Compound **4.2a**

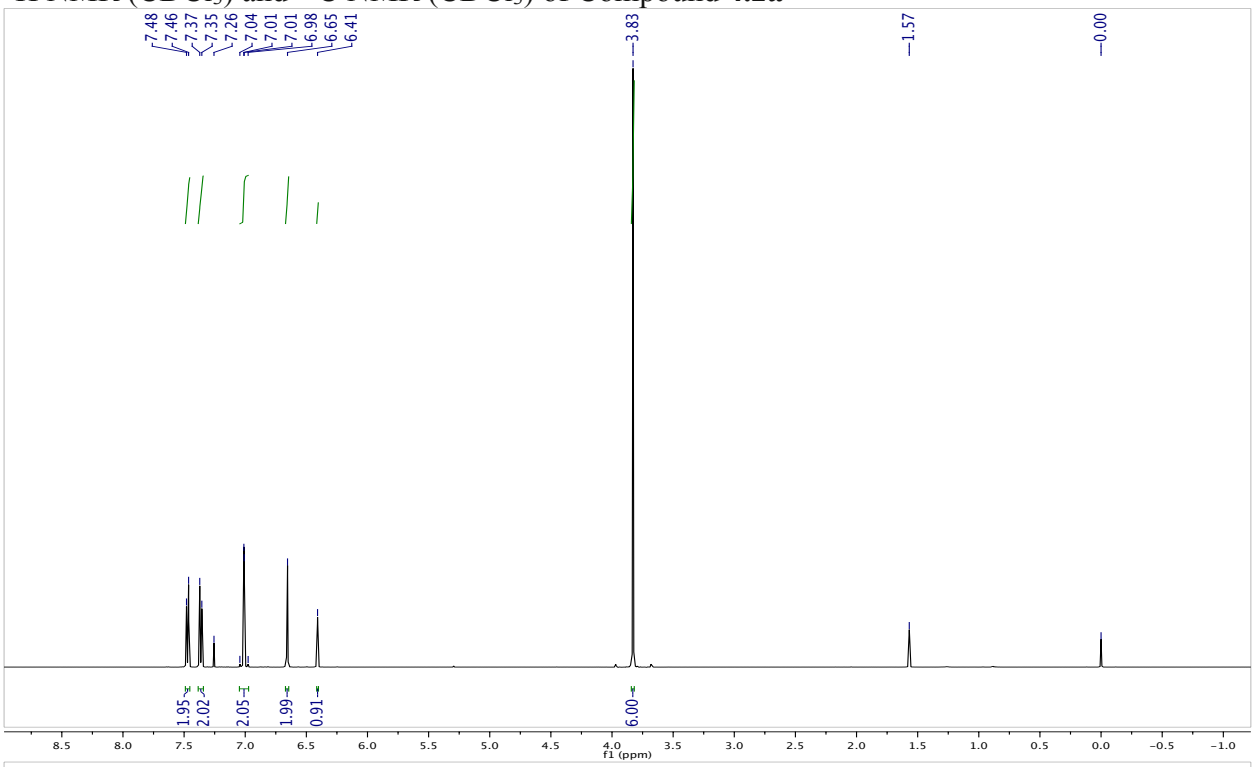

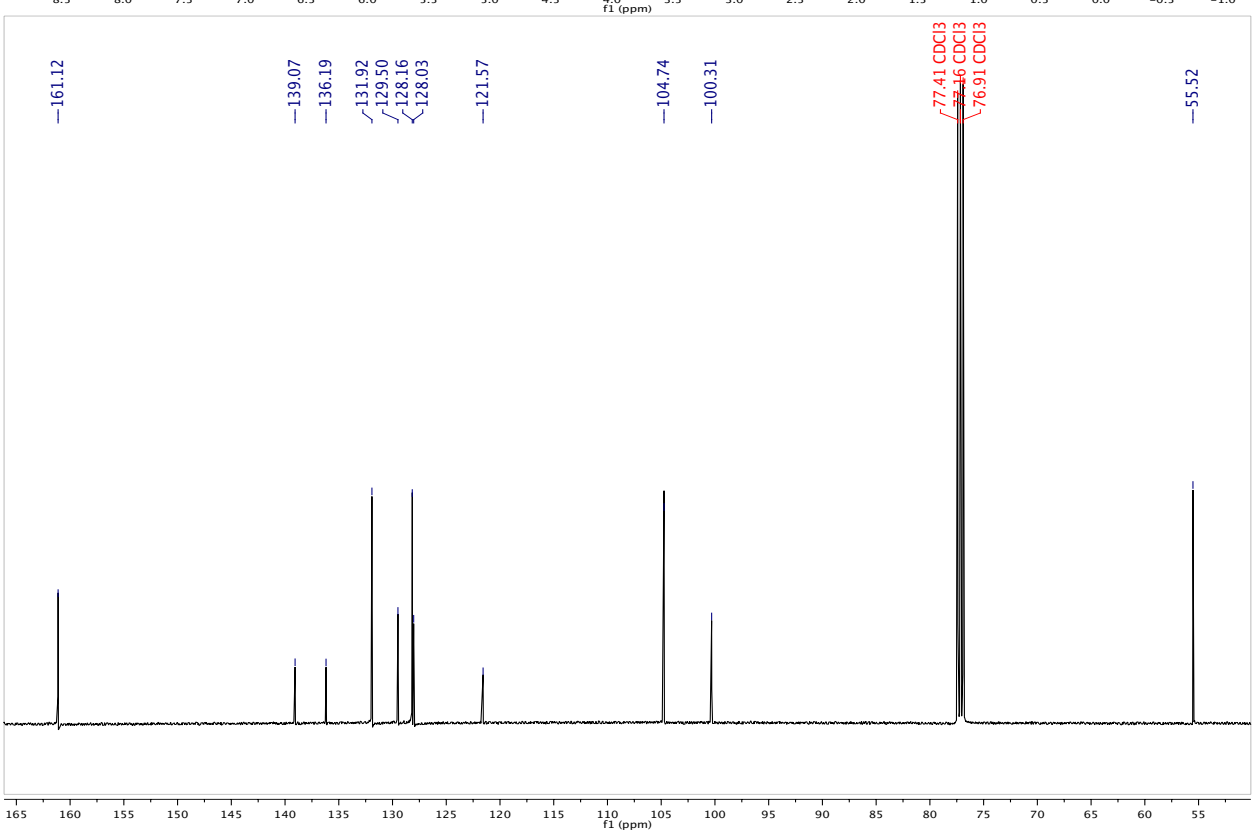

^{1}H NMR (CD_3OD) and ^{13}C NMR (CD_3OD) of Compound **4.2b**

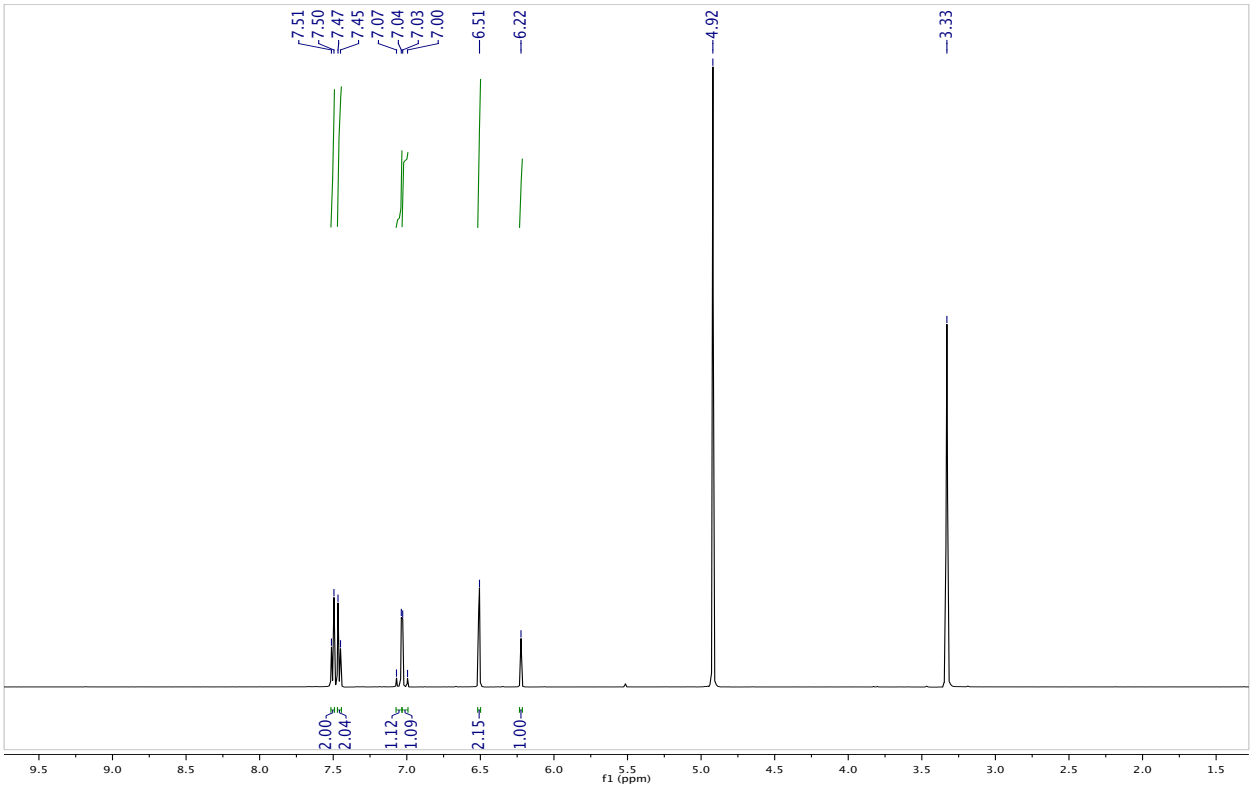

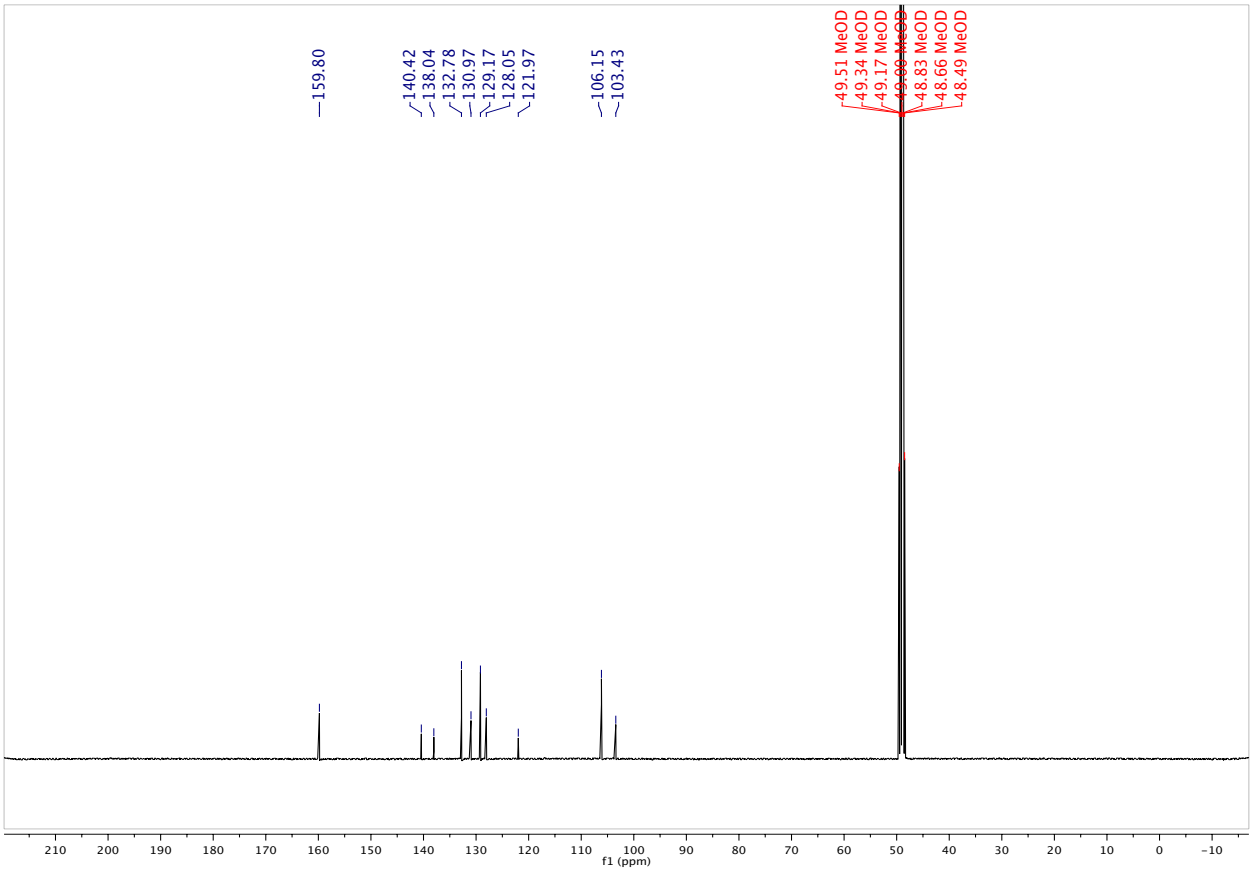

^{1}H NMR (CD_3OD) and ^{13}C NMR (CD_3OD) of Compound **4.2c**

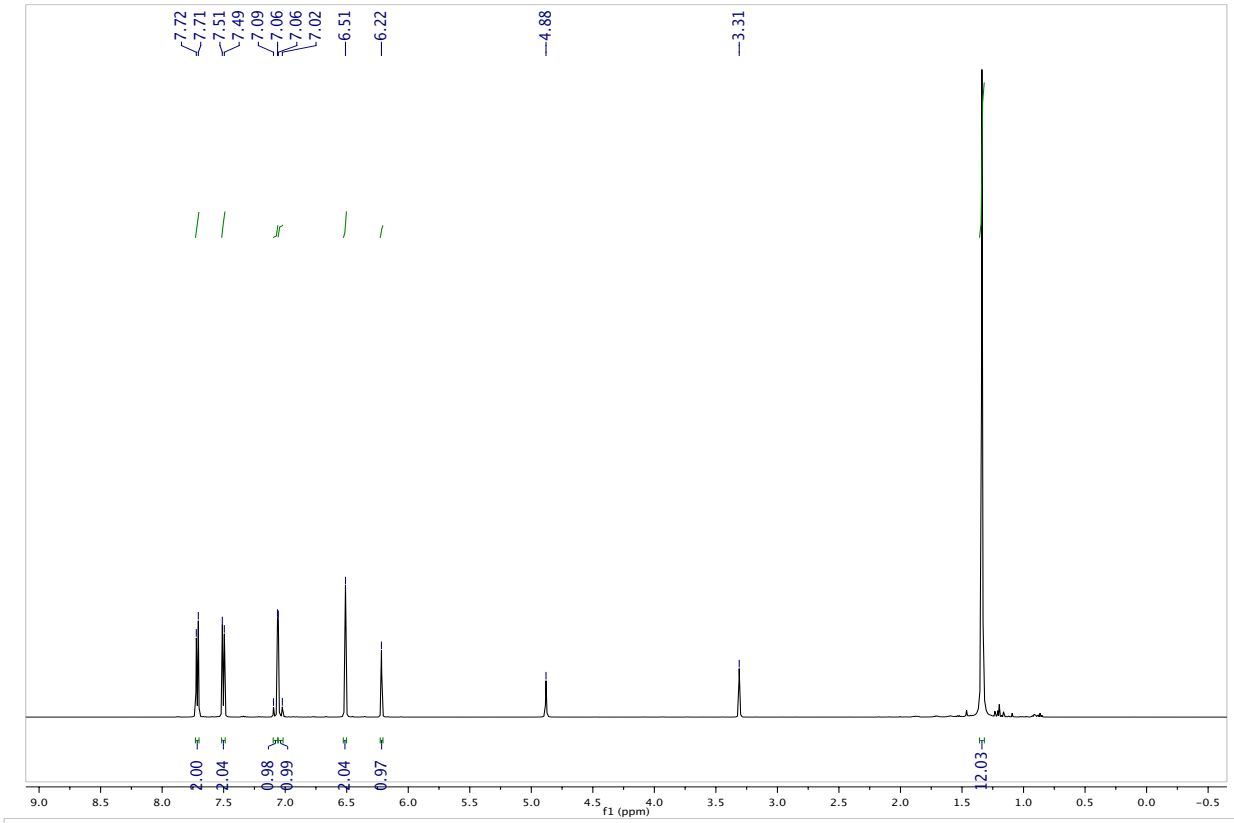

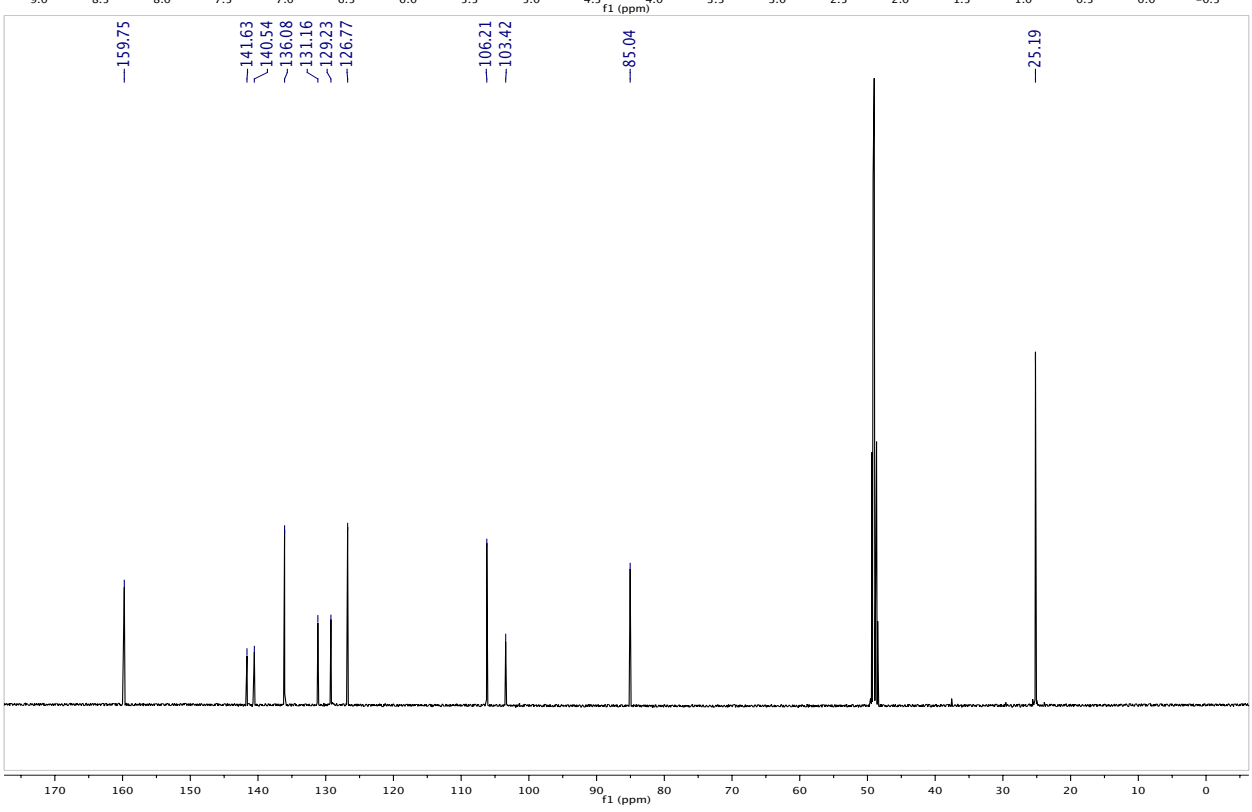

^{1}H NMR (CD_3OD) and ^{13}C NMR (CD_3OD) of Compound **4.2**

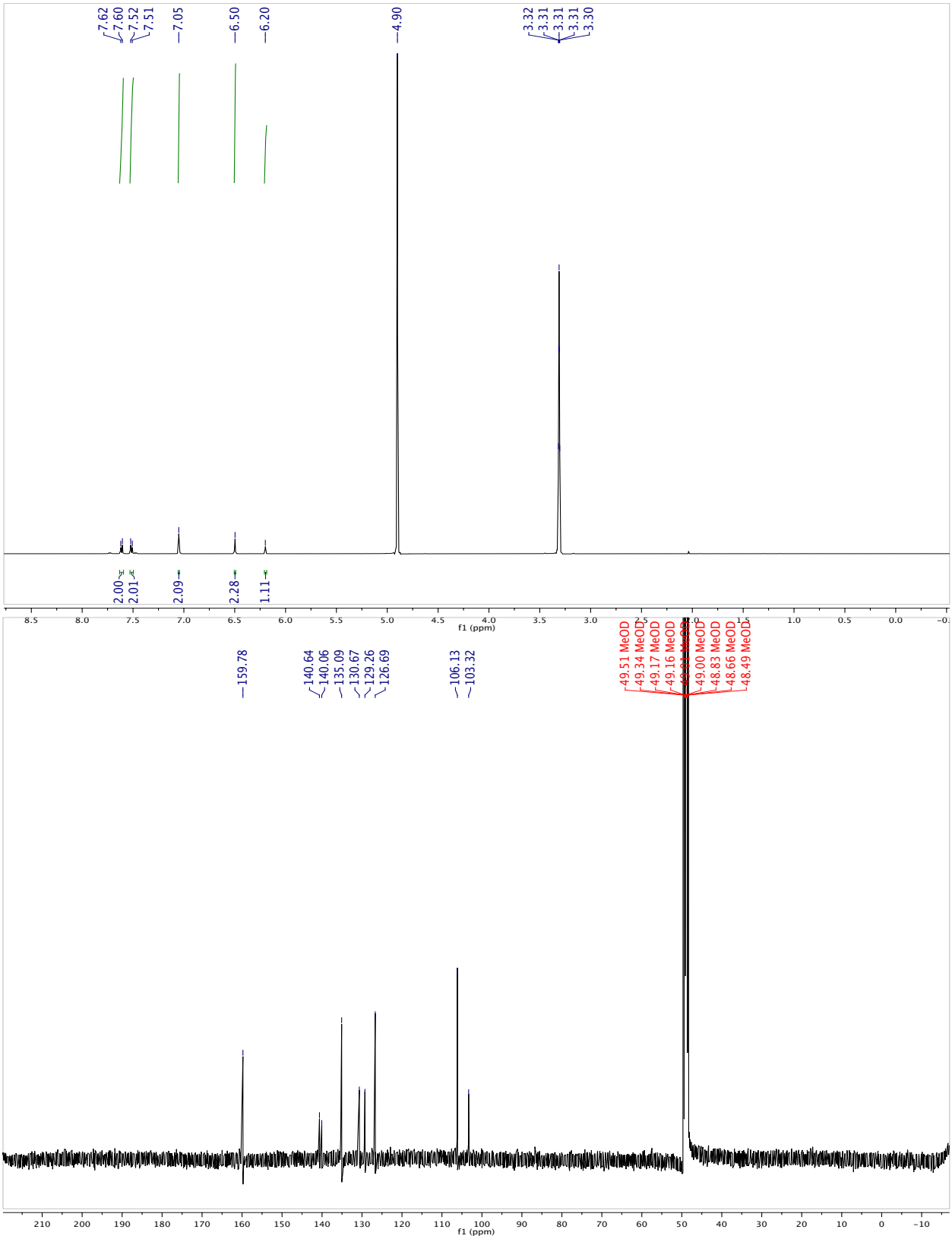

^{1}H NMR ($CDCl_3$) and ^{13}C NMR ($CDCl_3$) of Compound **4.4a**

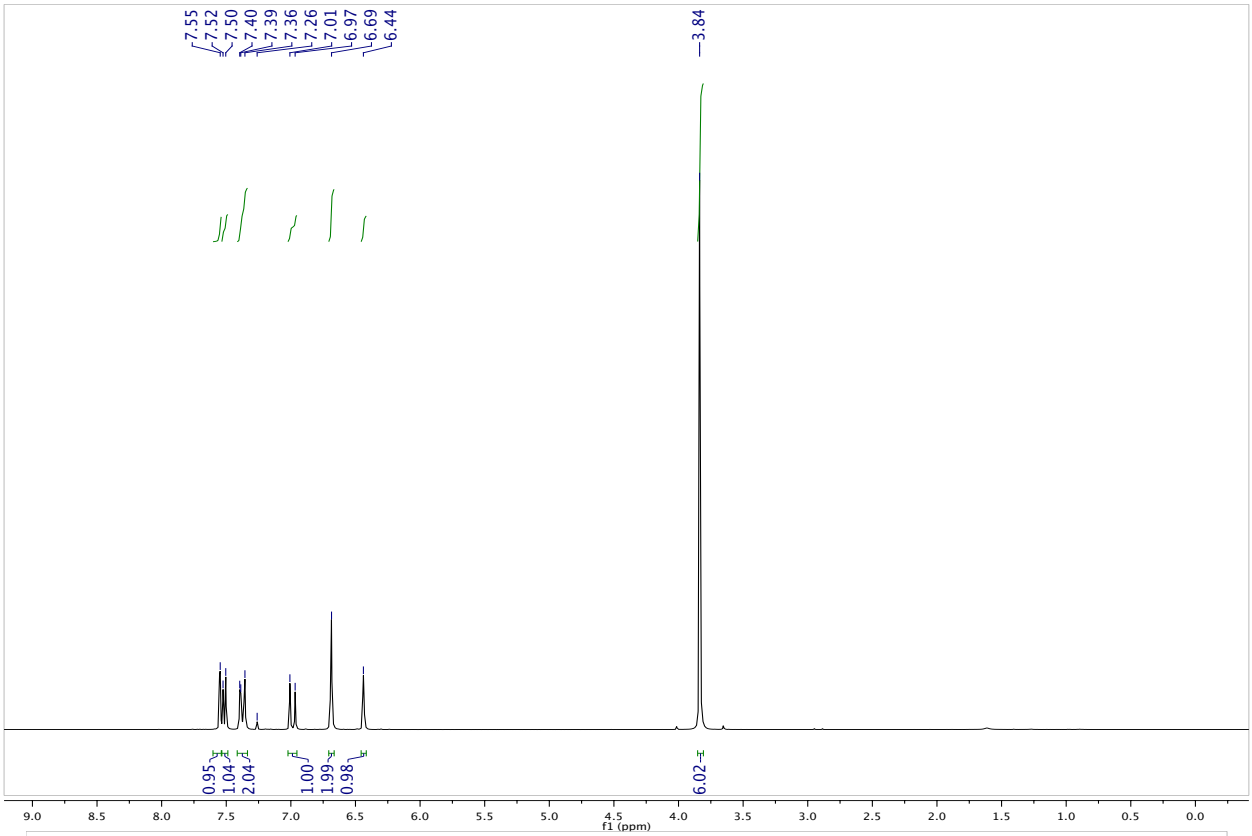

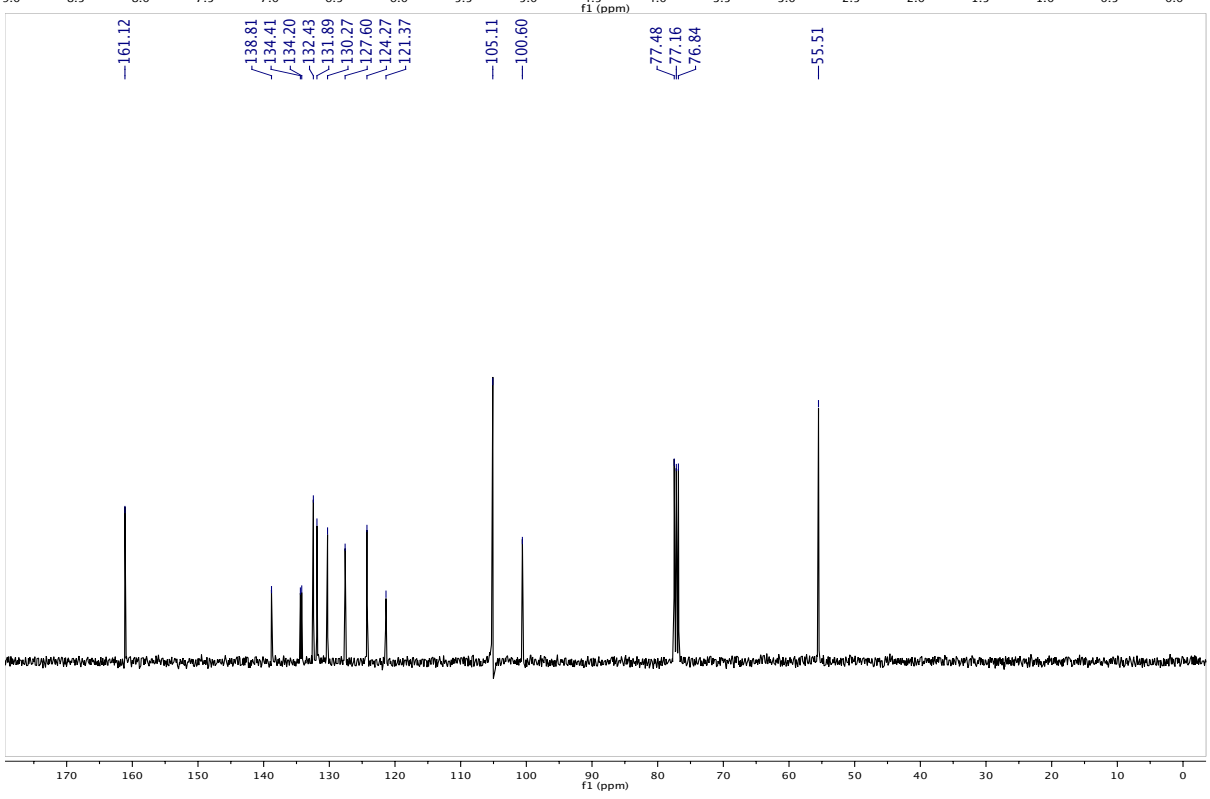

^{1}H NMR (CD_3OD) and ^{13}C NMR (CD_3OD) of Compound **4.4b**

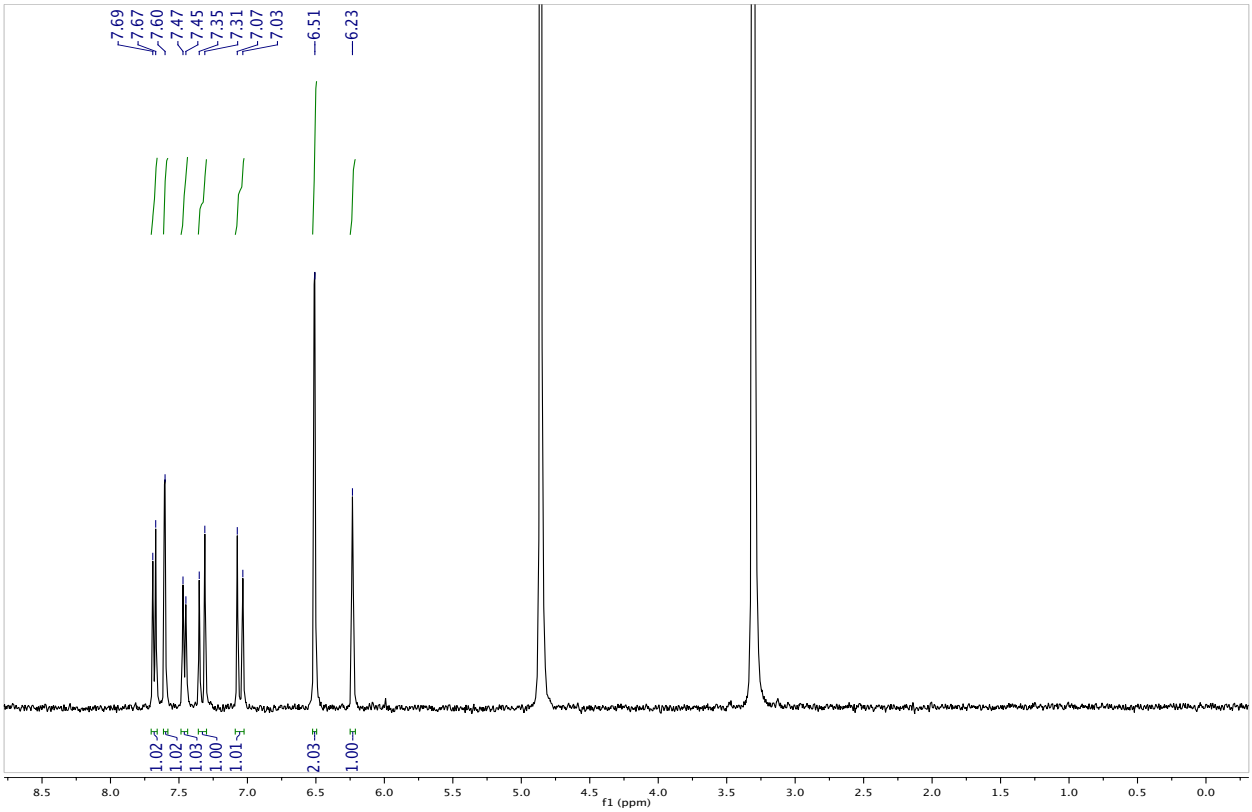

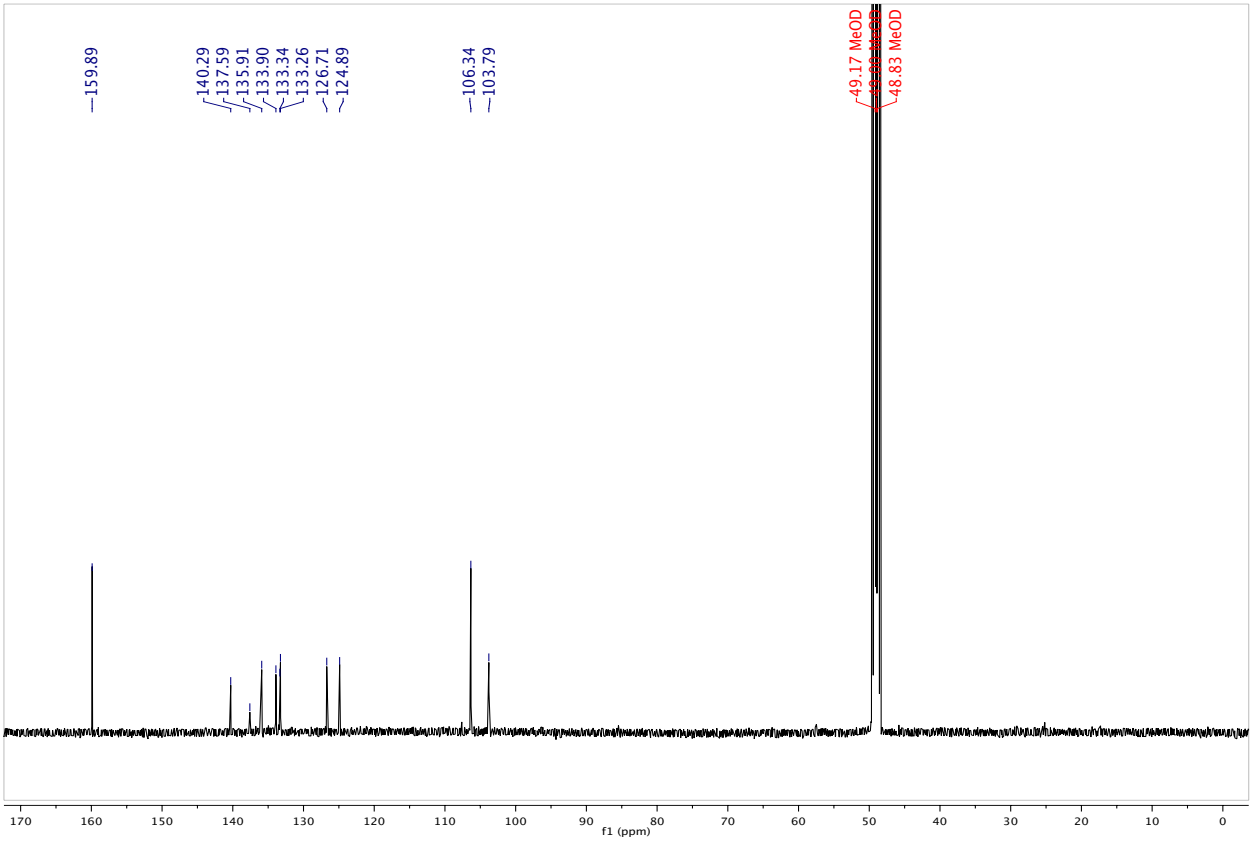

^{1}H NMR (CD_3OD) and ^{13}C NMR (CD_3OD) of Compound **4.4c**

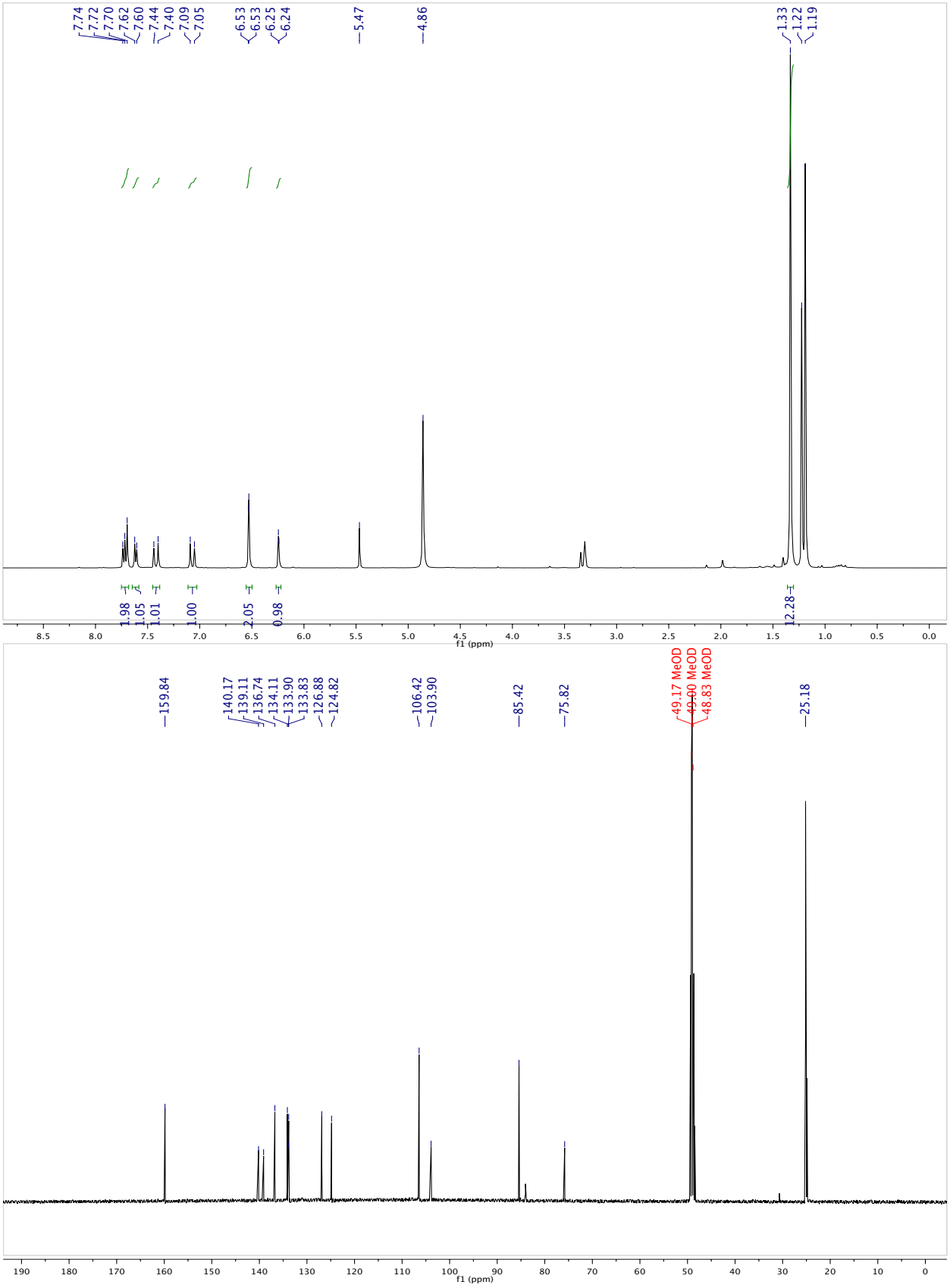

^{1}H NMR (CD_3OD) and ^{13}C NMR (CD_3OD) of Compound **4.4**

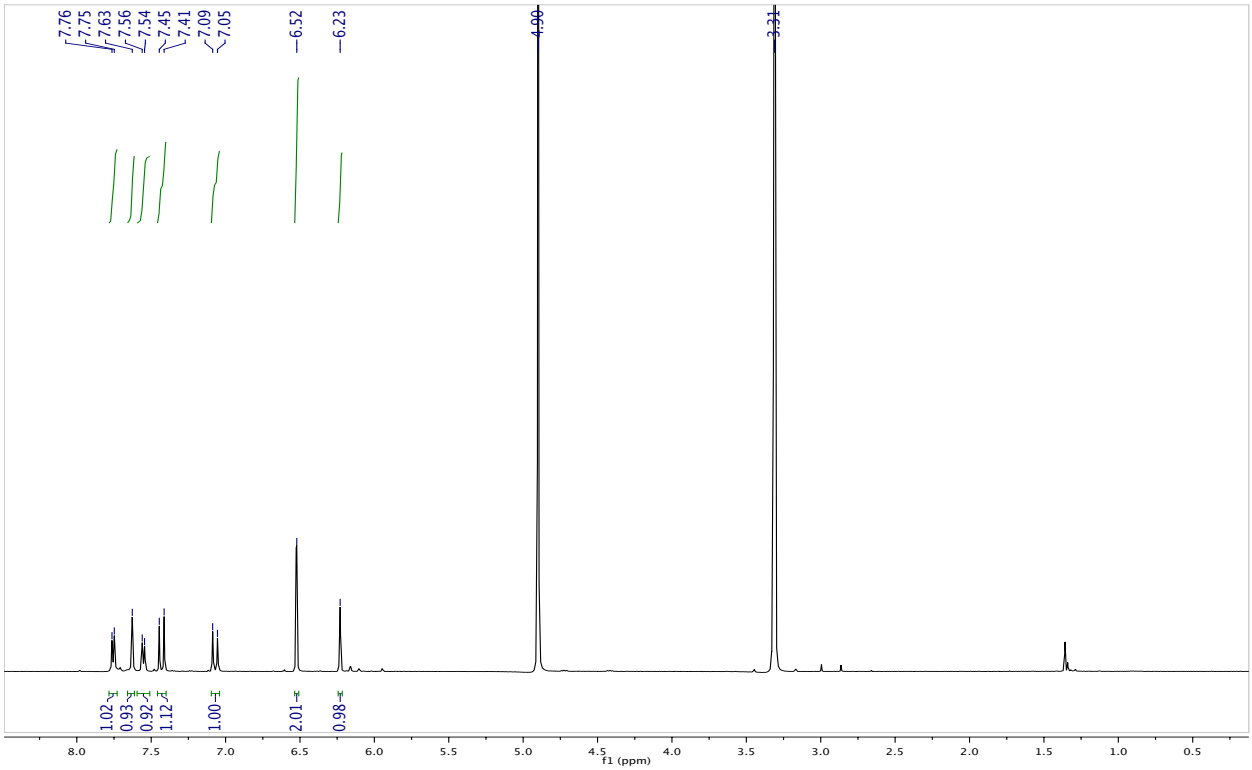

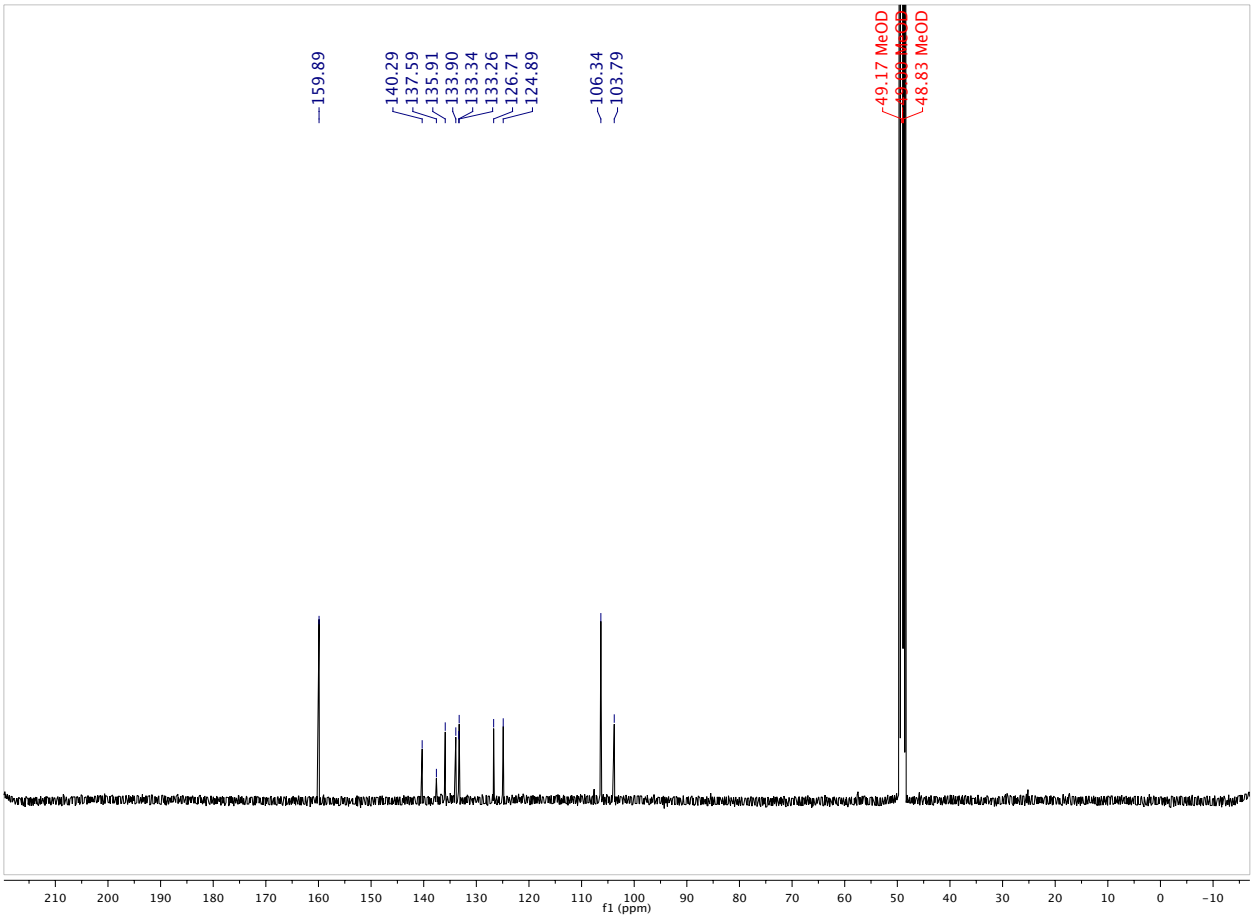

^{1}H NMR (CD_3OD) and ^{13}C NMR (CD_3OD) of Compound **4.3**

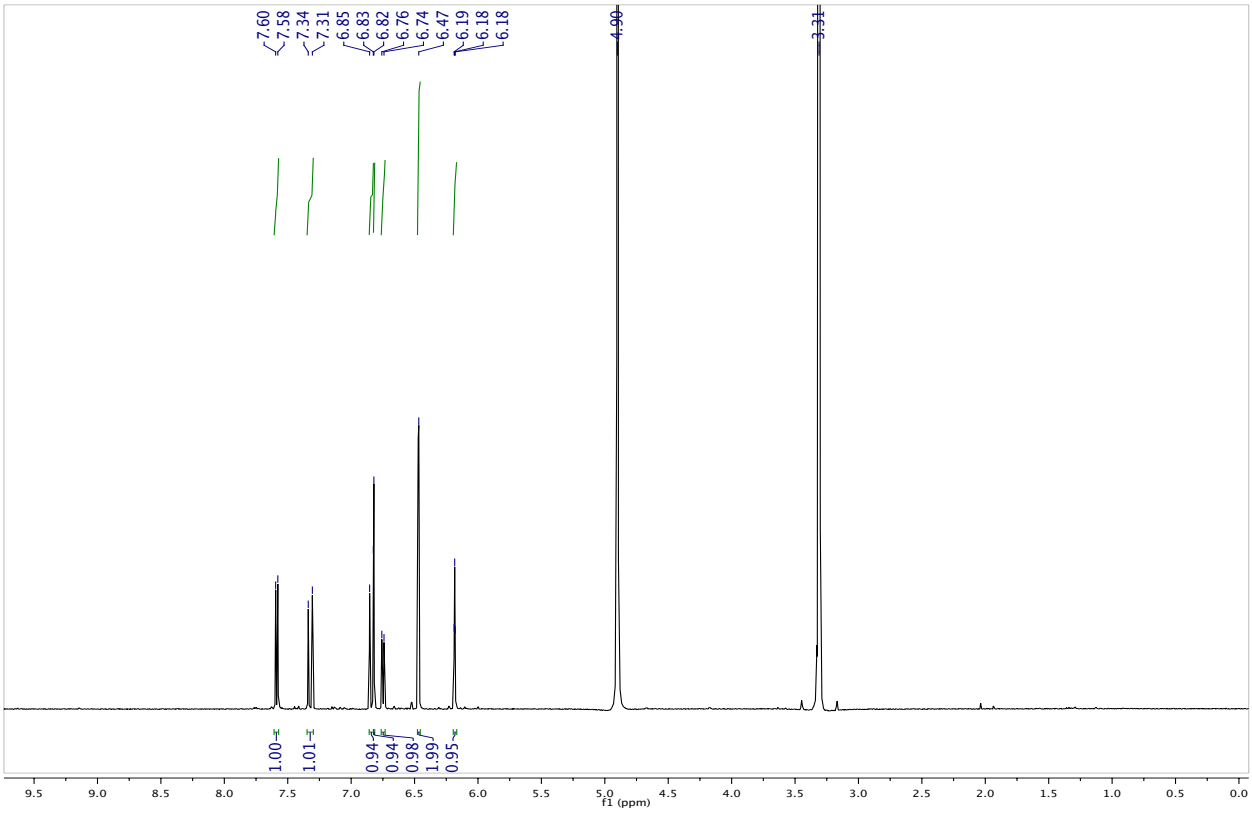

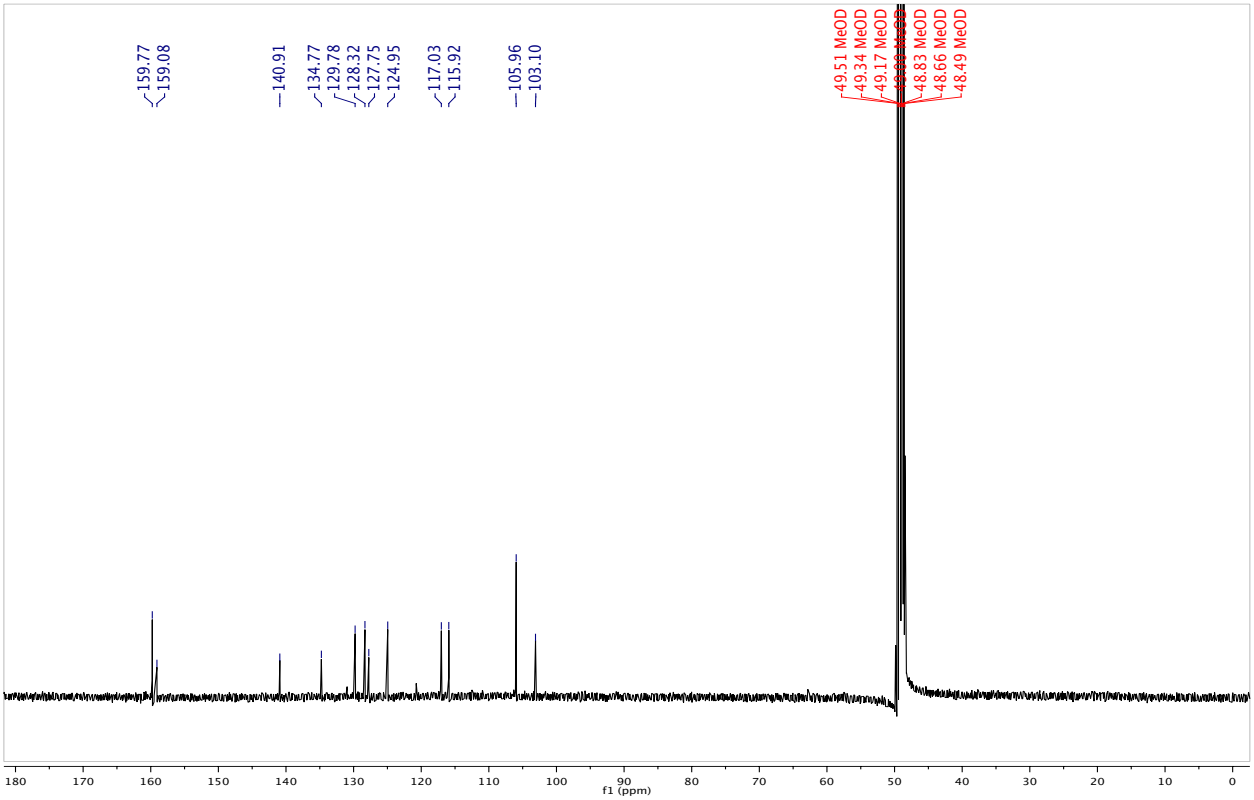

^{1}H NMR (CD_3OD) and ^{13}C NMR (CD_3OD) of Compound **4.6a**

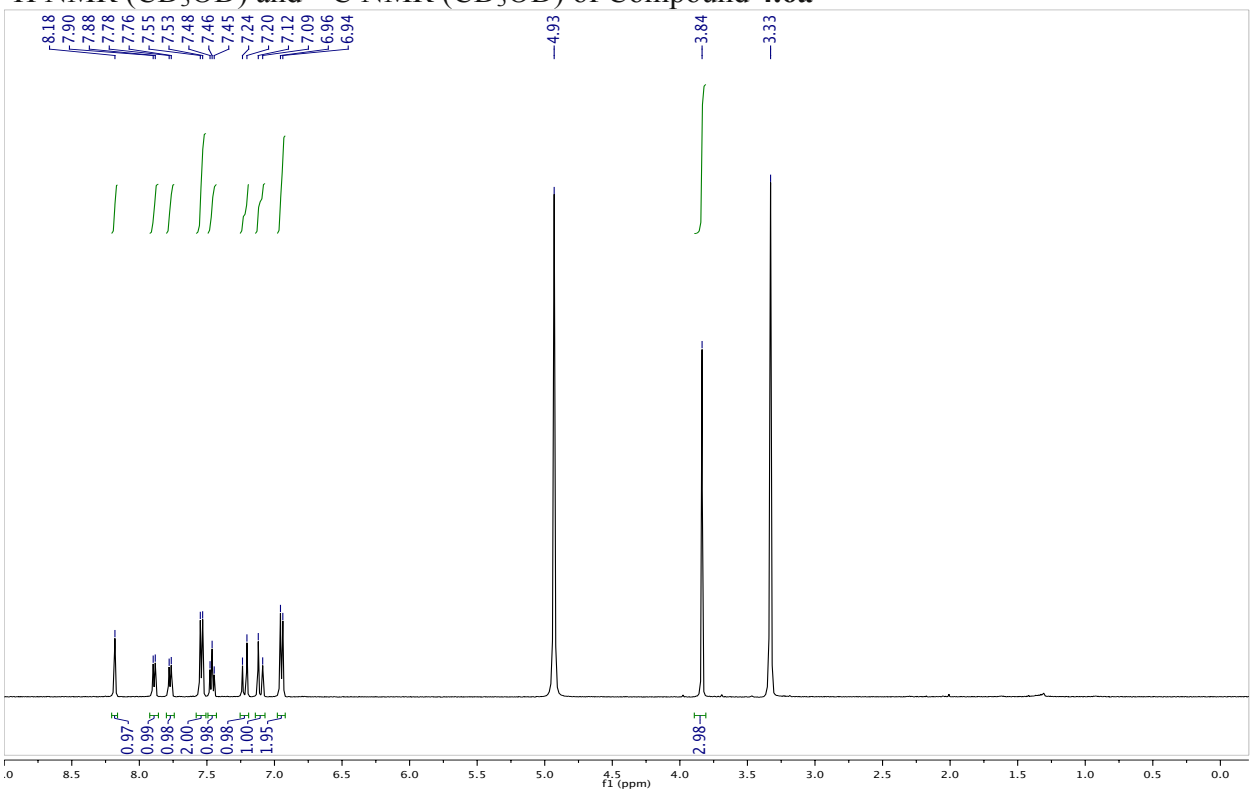

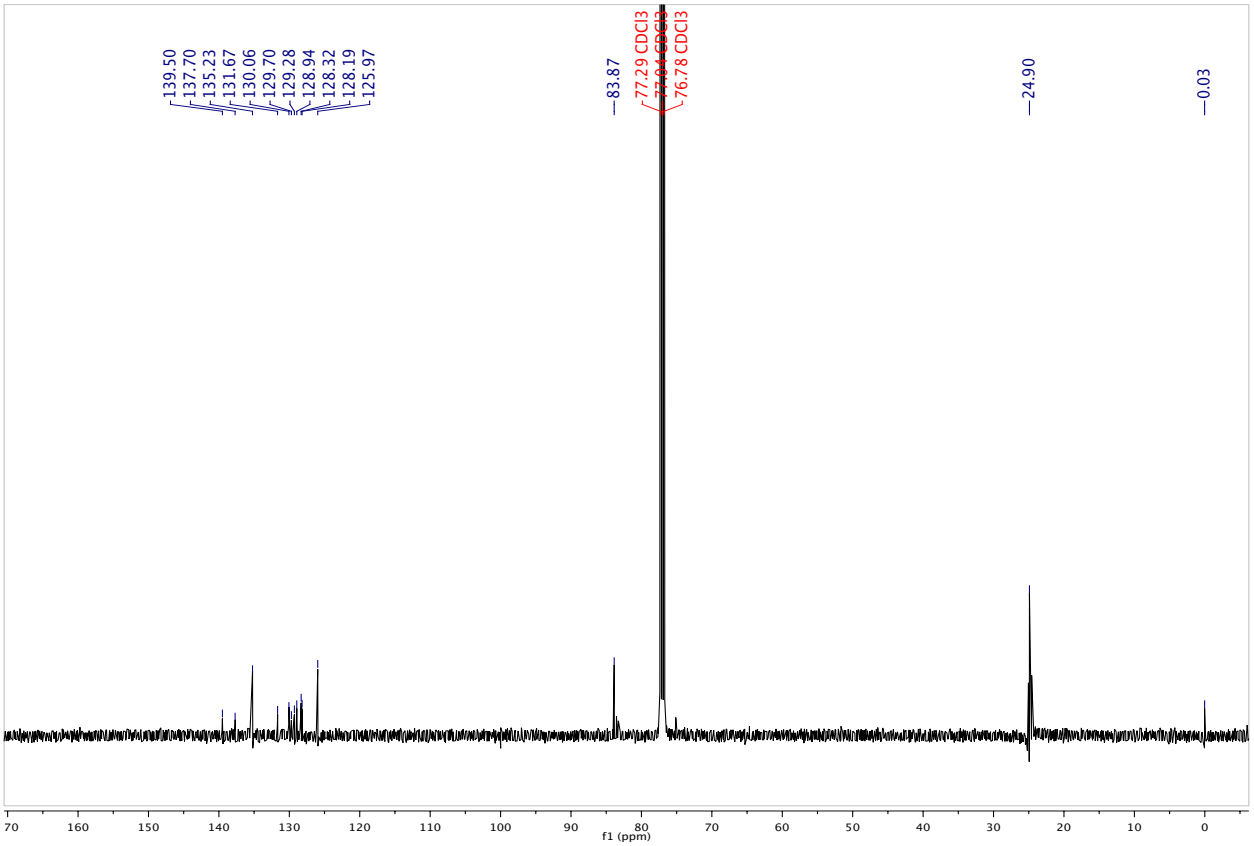

^{1}H NMR (DMSO) and ^{13}C NMR (DMSO) of Compound **4.6b**

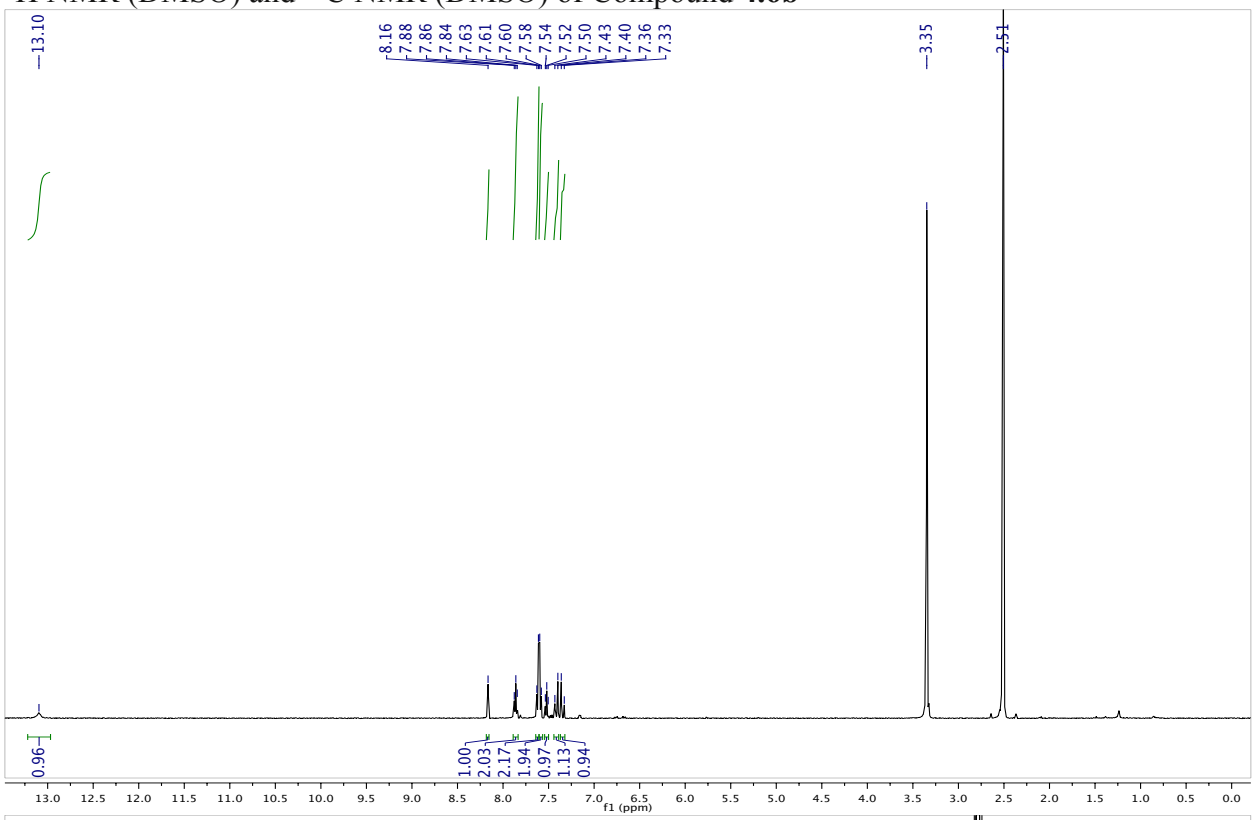

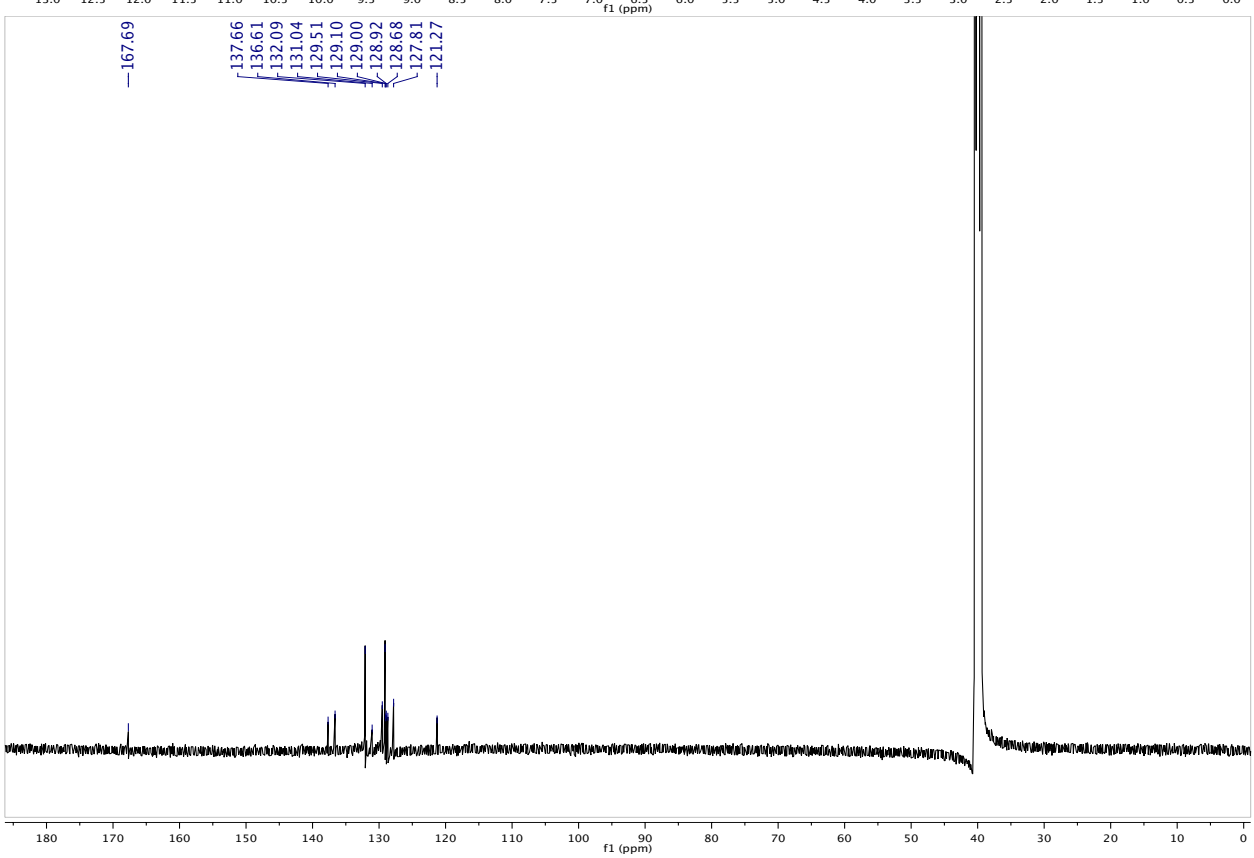

^{1}H NMR ($CDCl_3$) and ^{13}C NMR ($CDCl_3$) of Compound **4.6c**

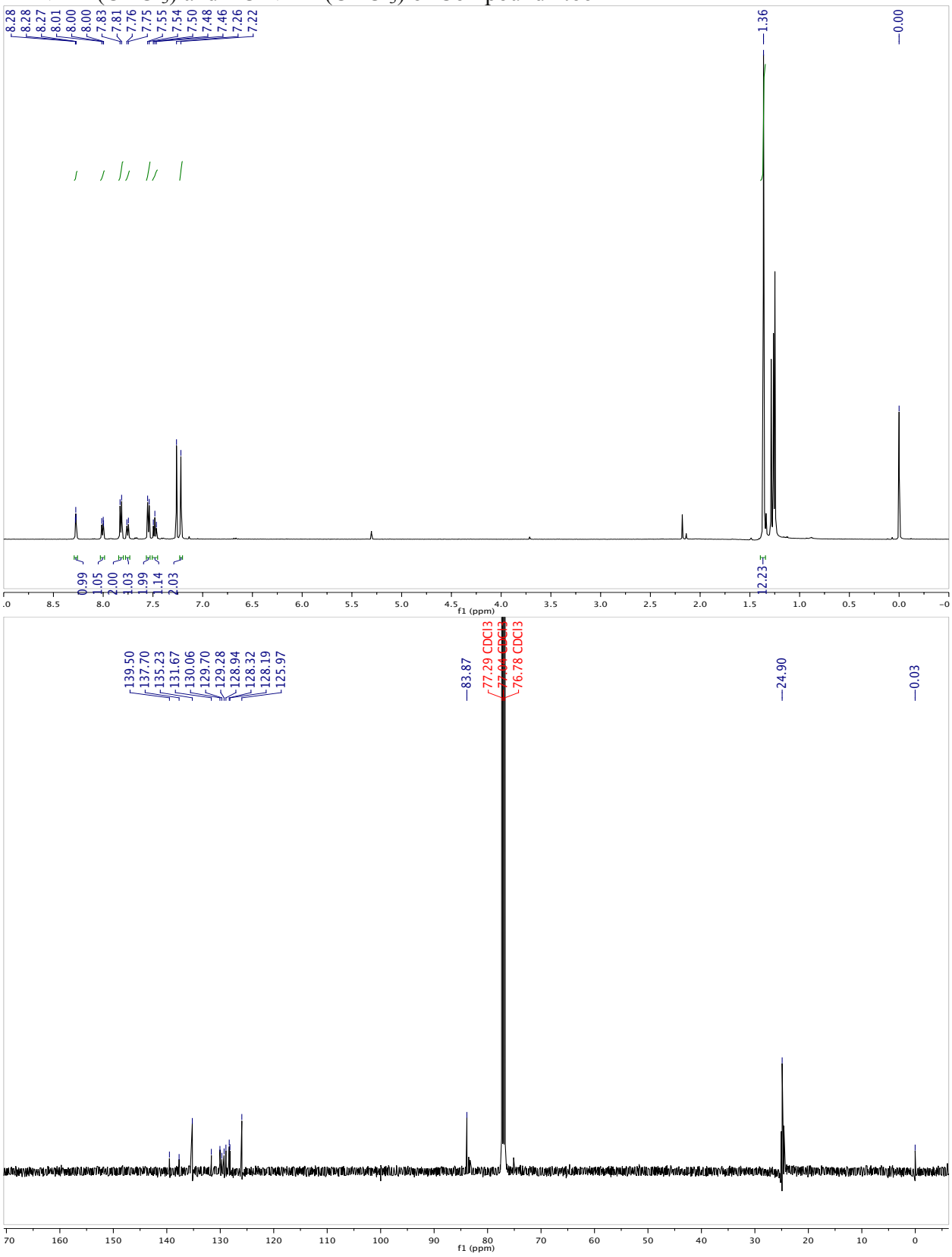

^{1}H NMR (CD_3OD) and ^{13}C NMR (CD_3OD) of Compound **4.6**

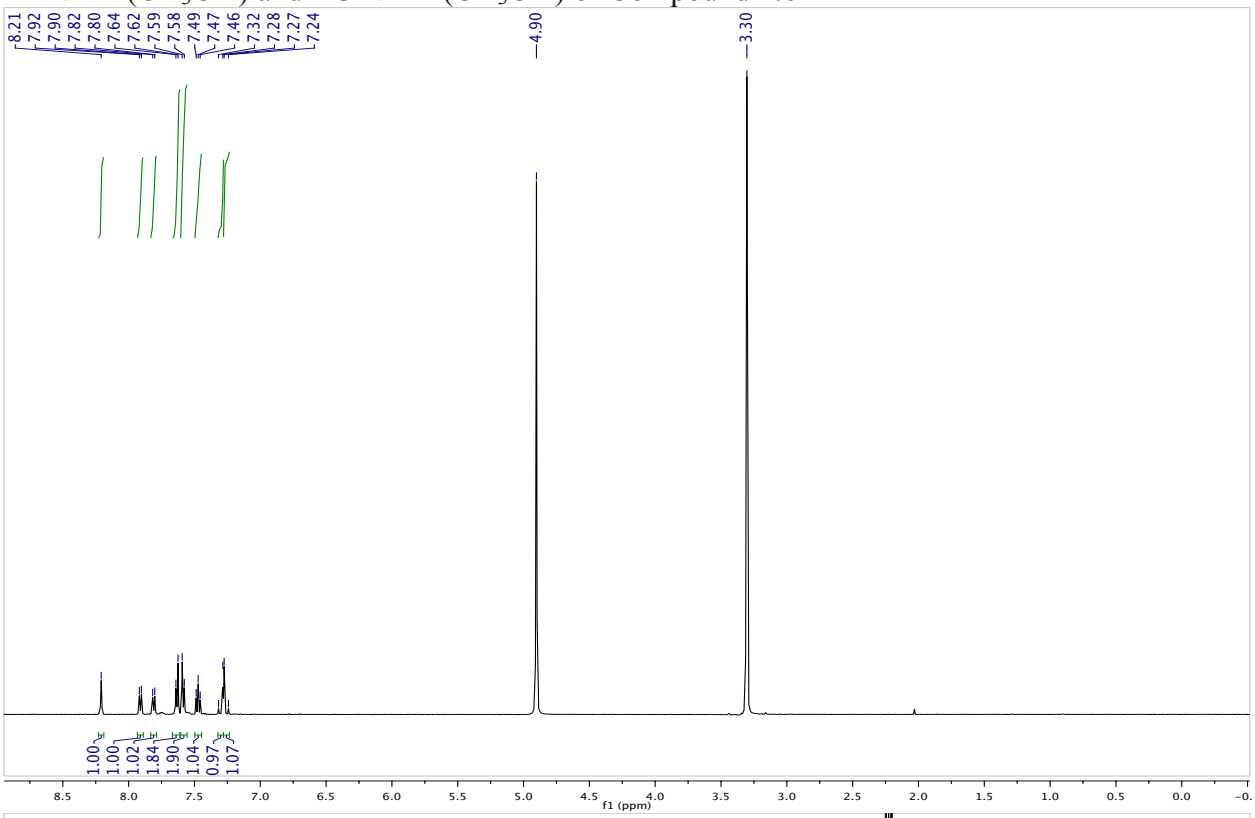

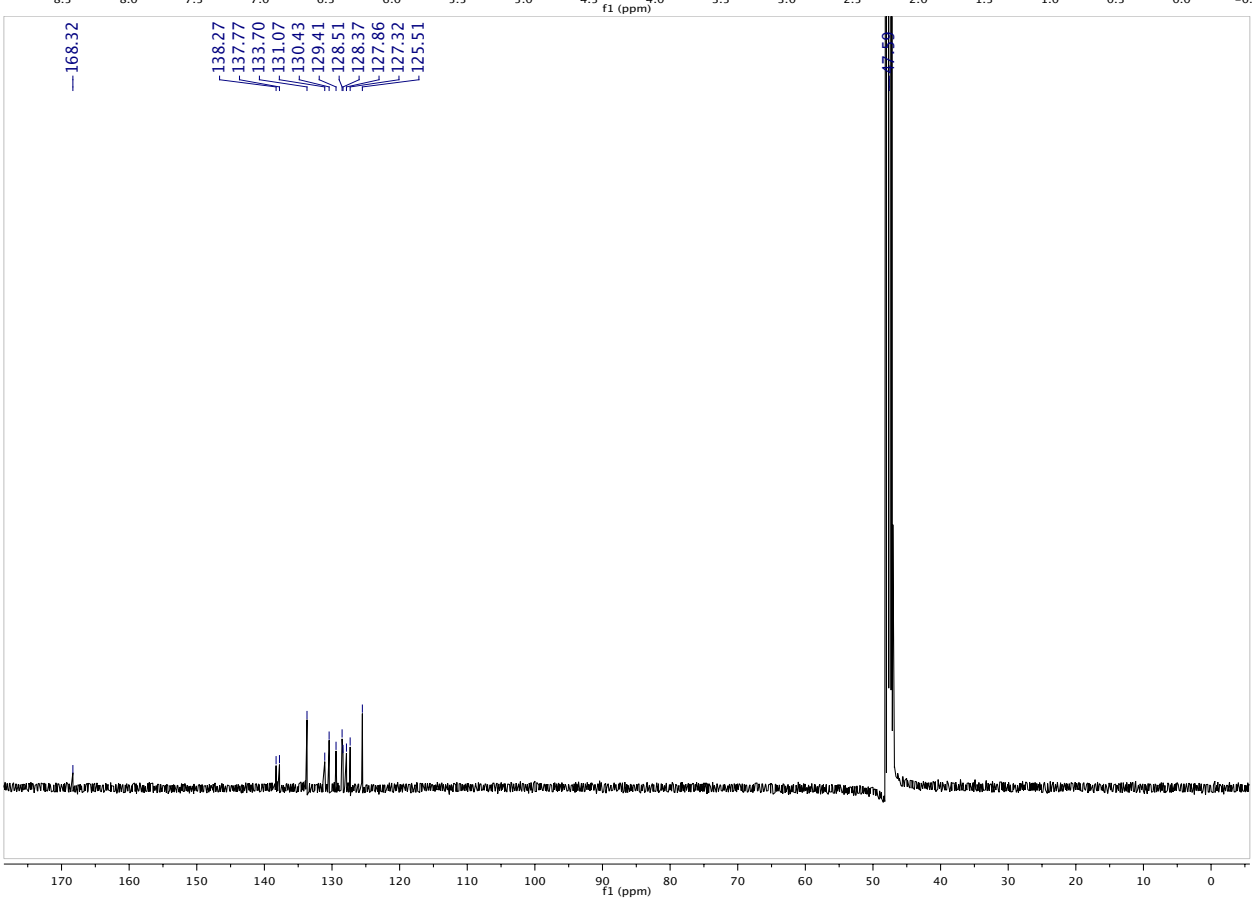

^{1}H NMR (CD_3OD) and ^{13}C NMR (CD_3OD) of Compound **4.5**

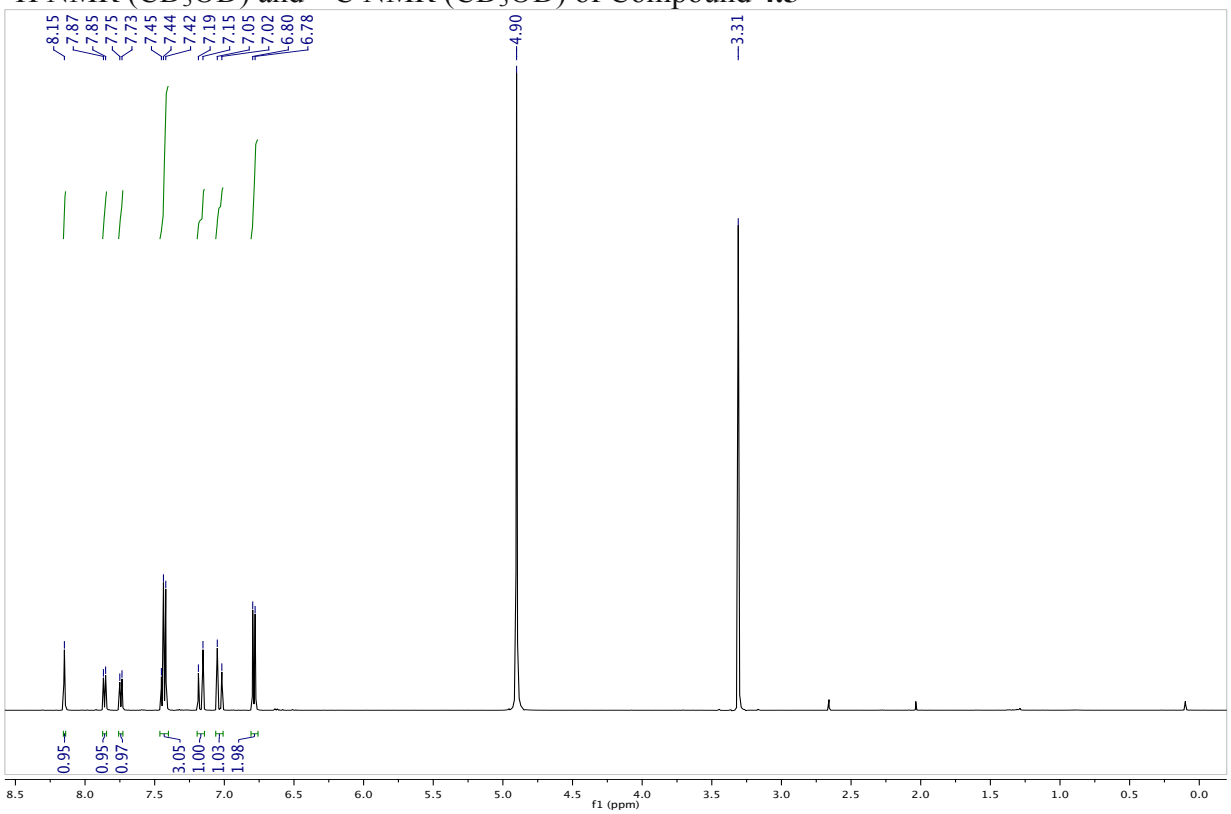

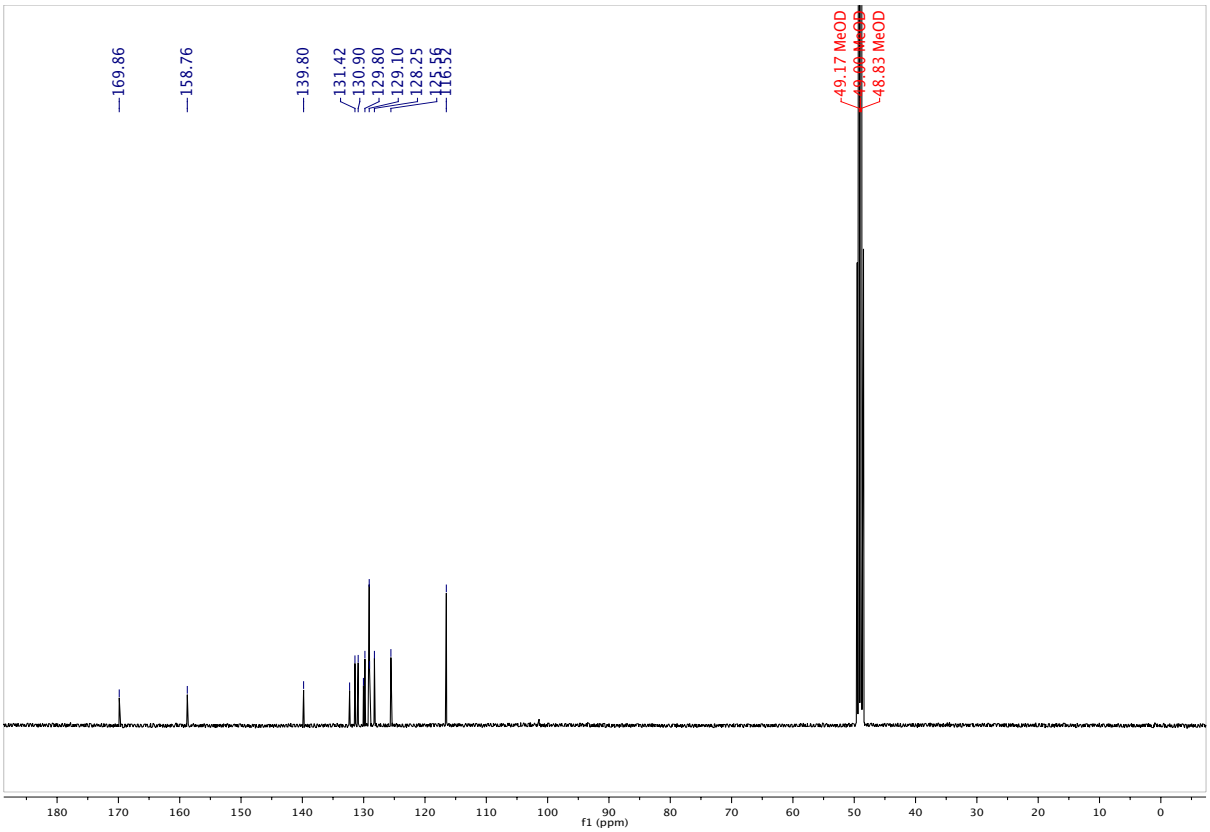

^{1}H NMR (CD_3OD) and ^{13}C NMR (CD_3OD) of Compound **4.8a**

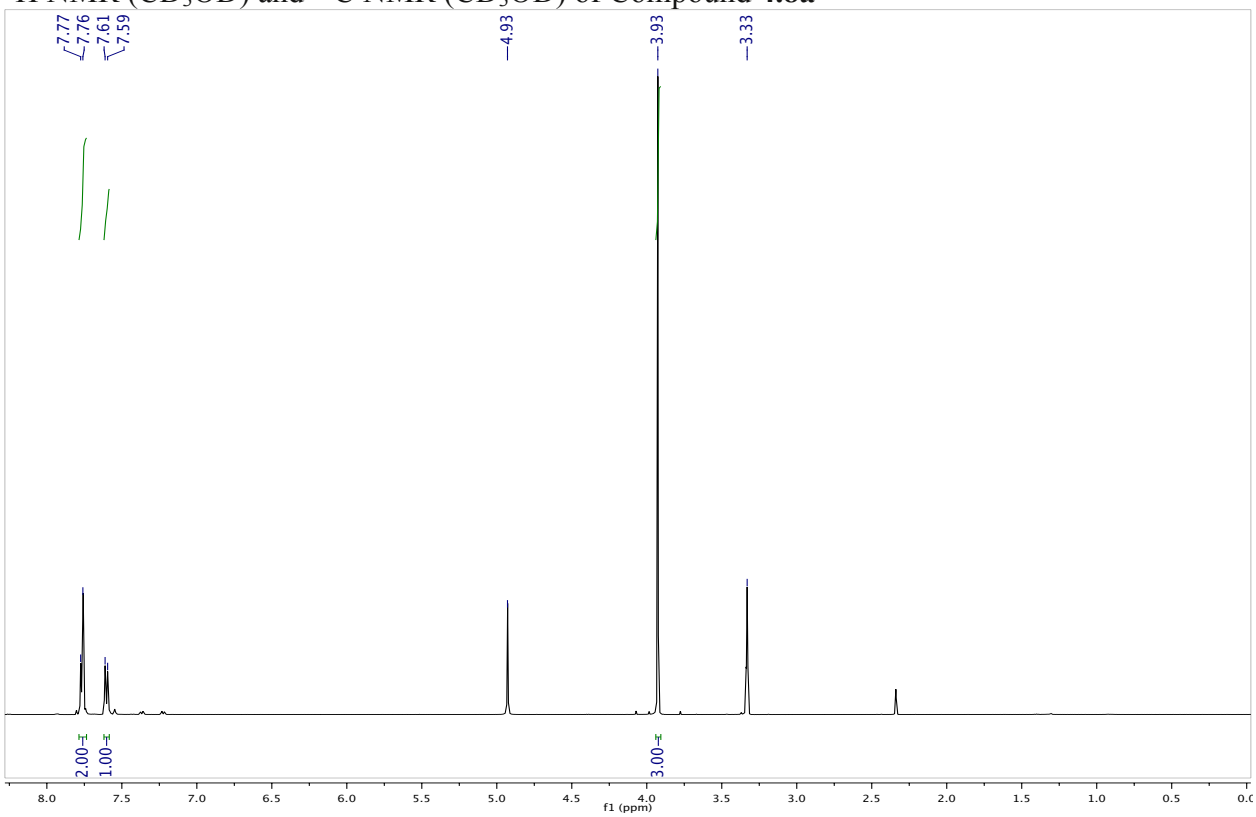

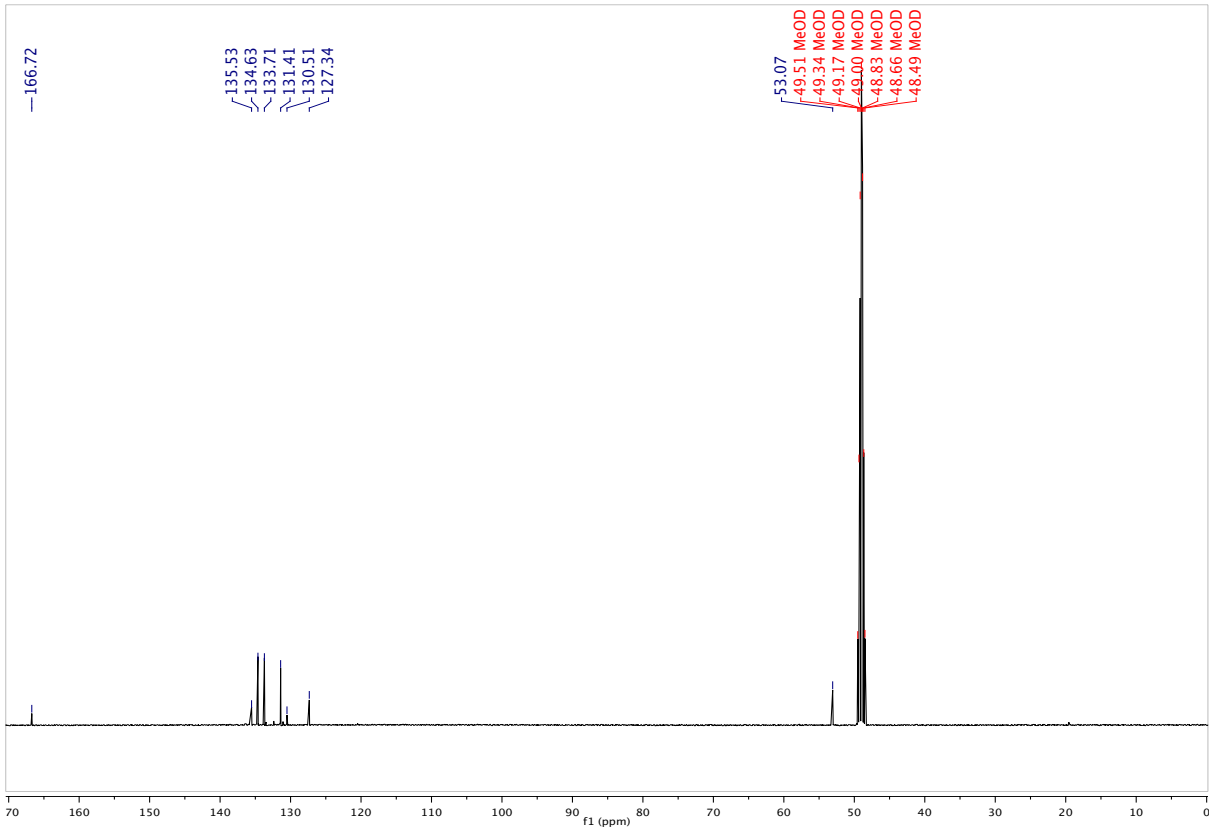

^{1}HNMR ($CDCl_3$) and ^{13}CNMR ($CDCl_3$) of Compound **4.8b**

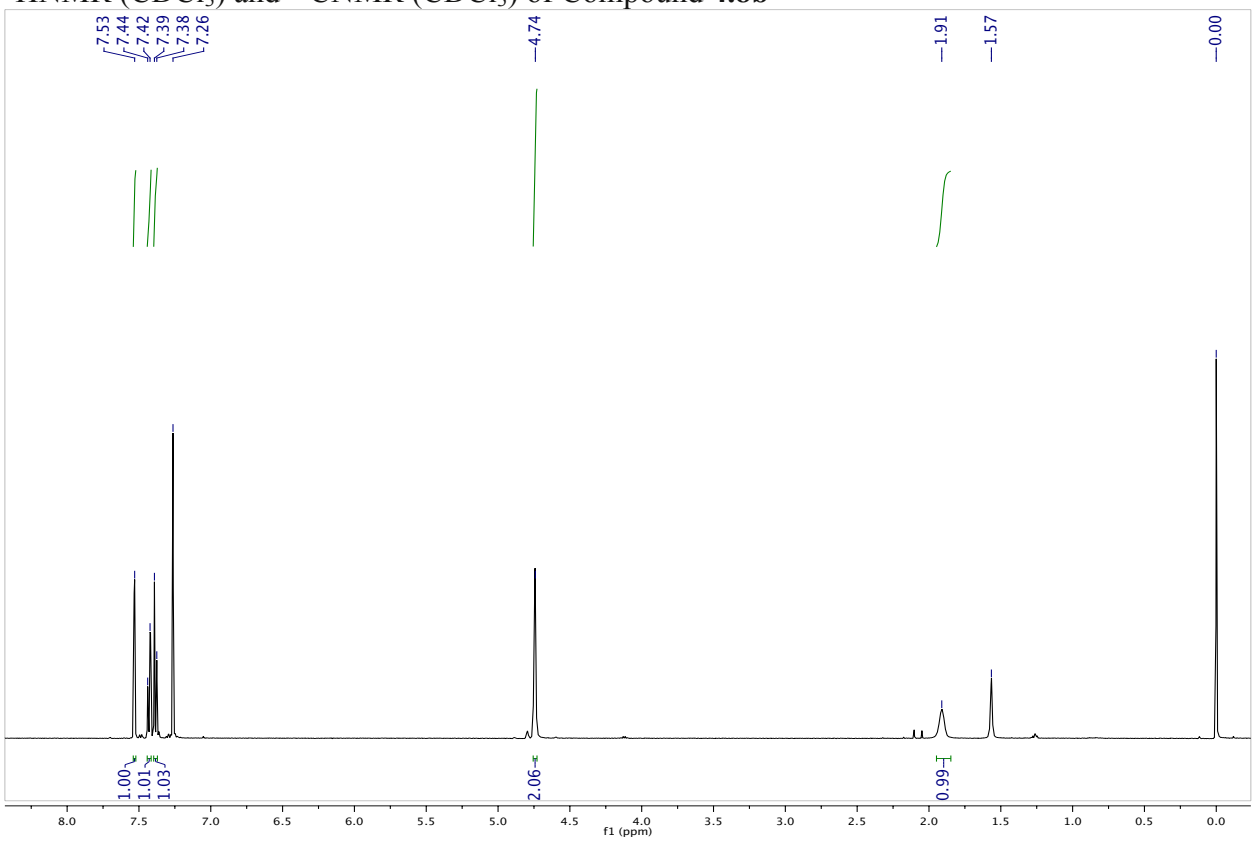

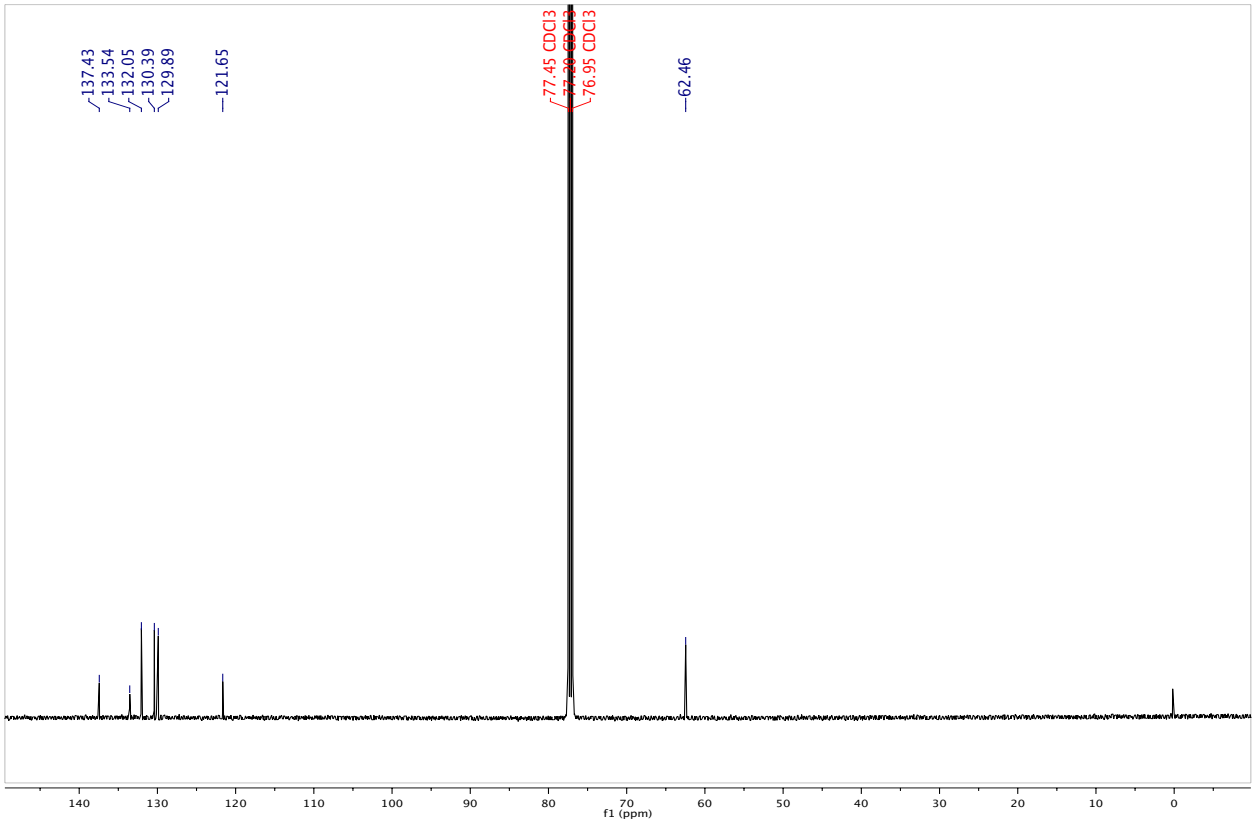

^{1}H NMR ($CDCl_3$) and ^{13}C NMR ($CDCl_3$) of Compound **4.8c**

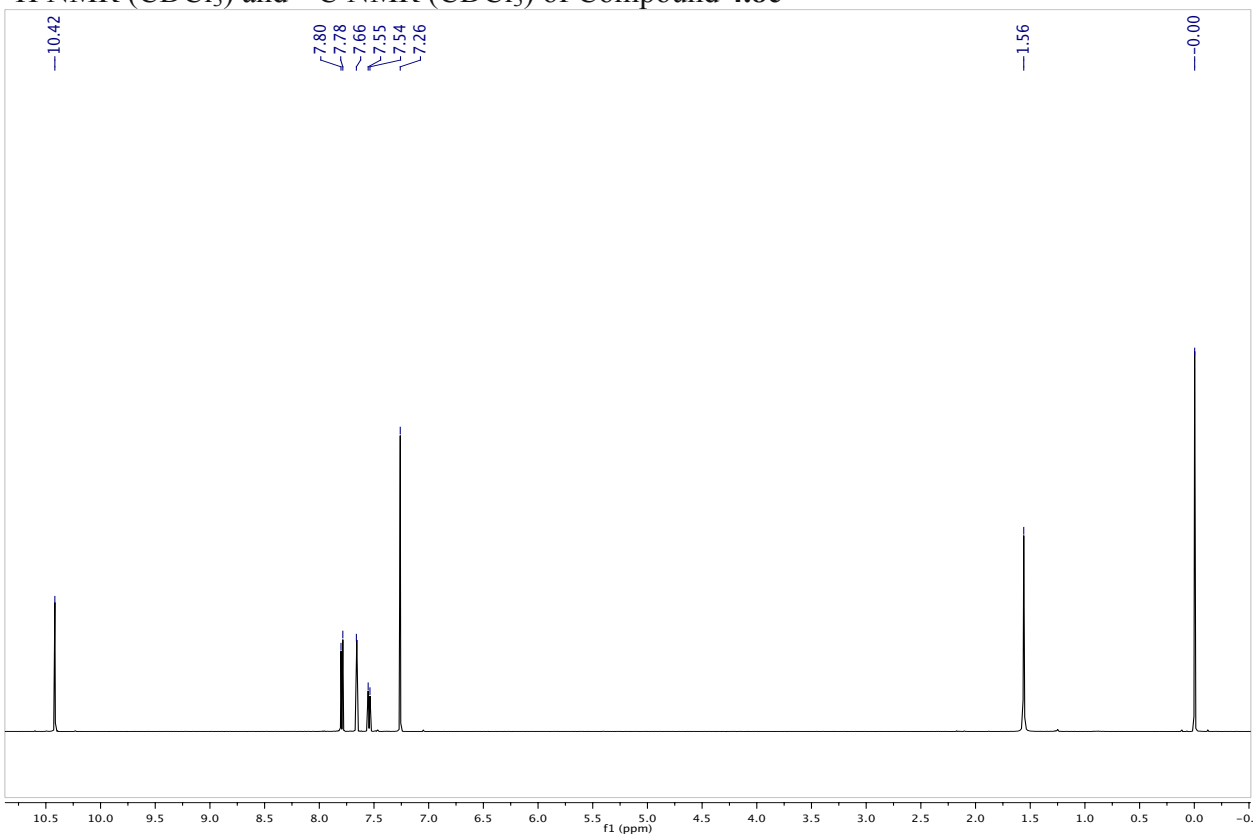

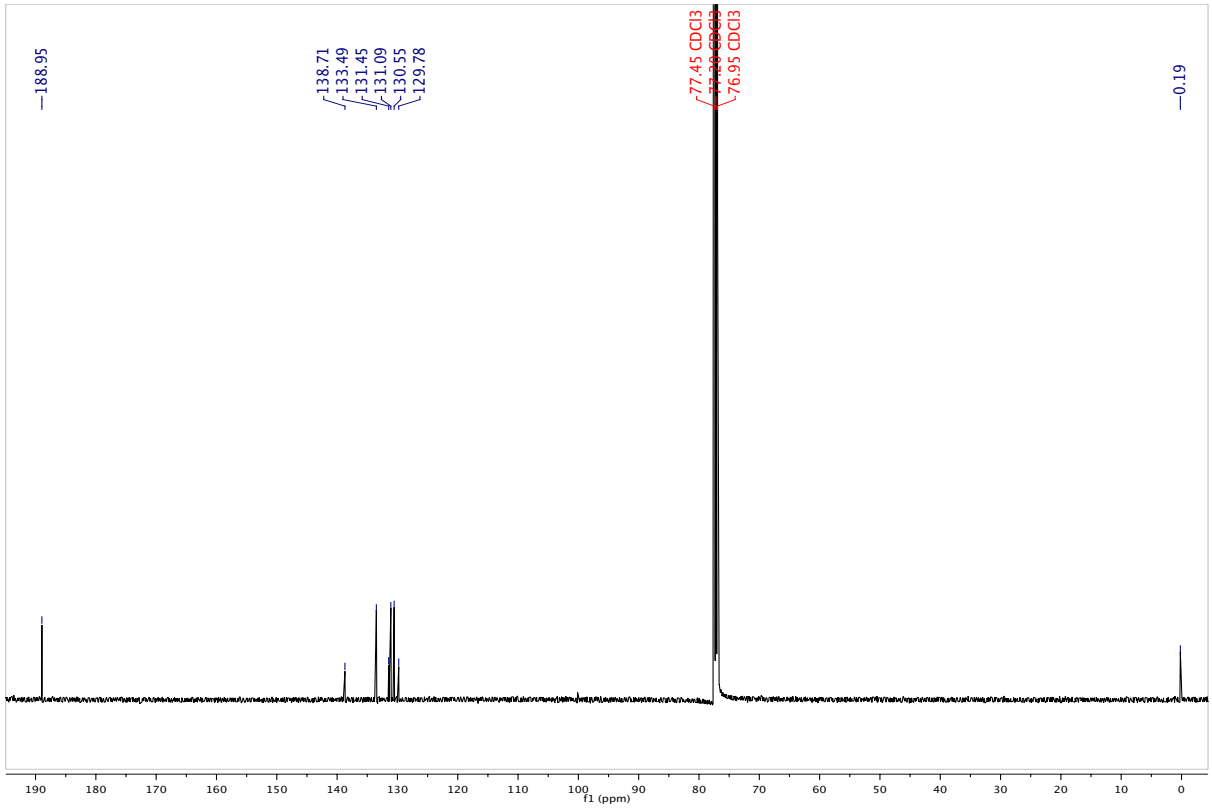

^{1}H NMR ($CDCl_3$) and ^{13}C NMR ($CDCl_3$) of Compound **4.8d**

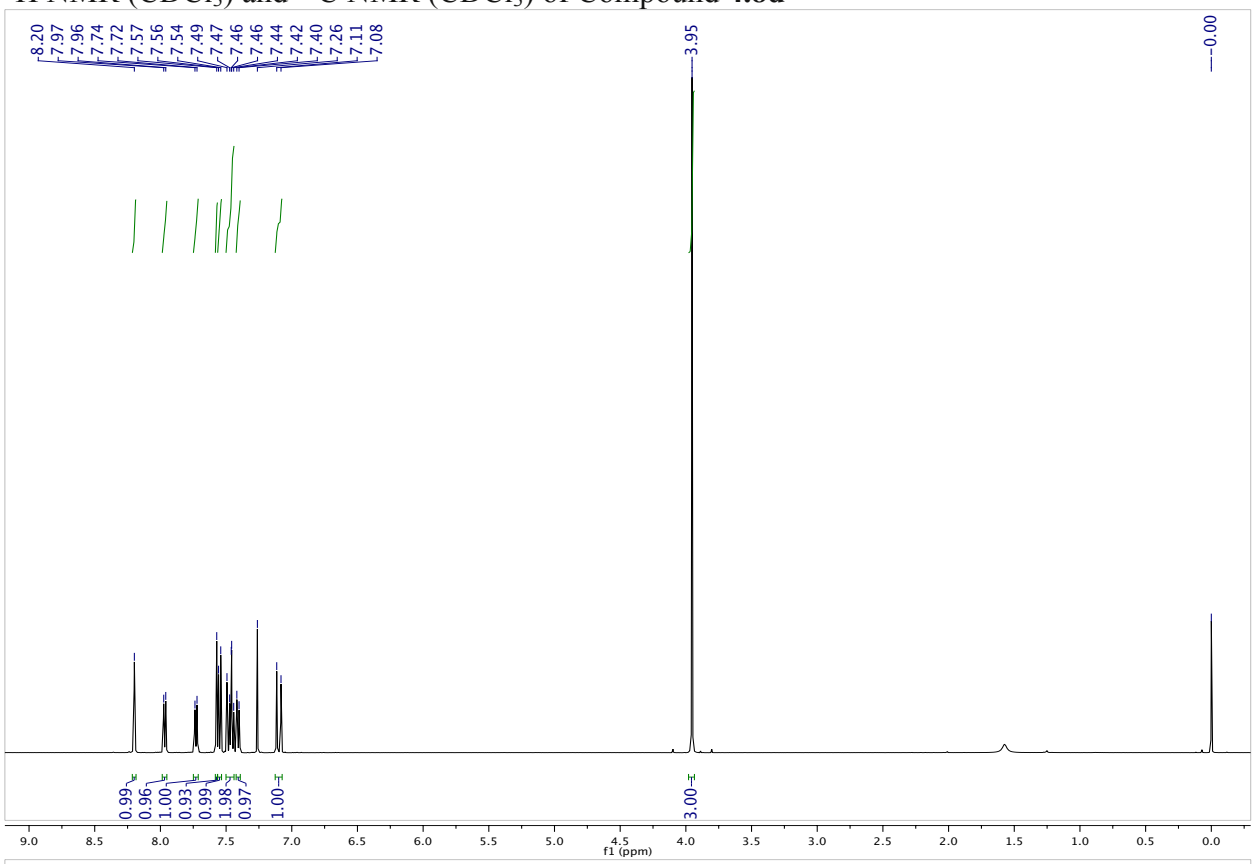

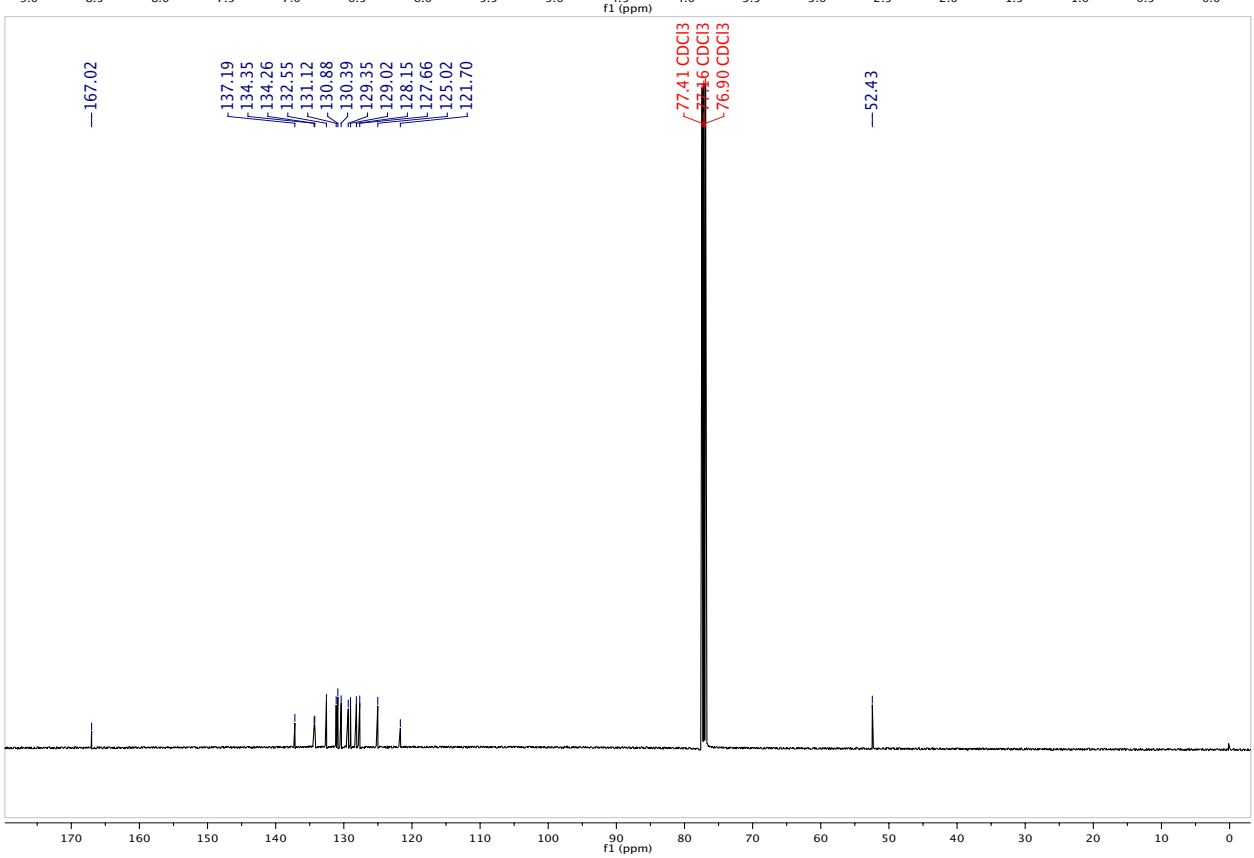

^{1}H NMR (DMSO) and ^{13}C NMR (DMSO) of Compound **4.8e**

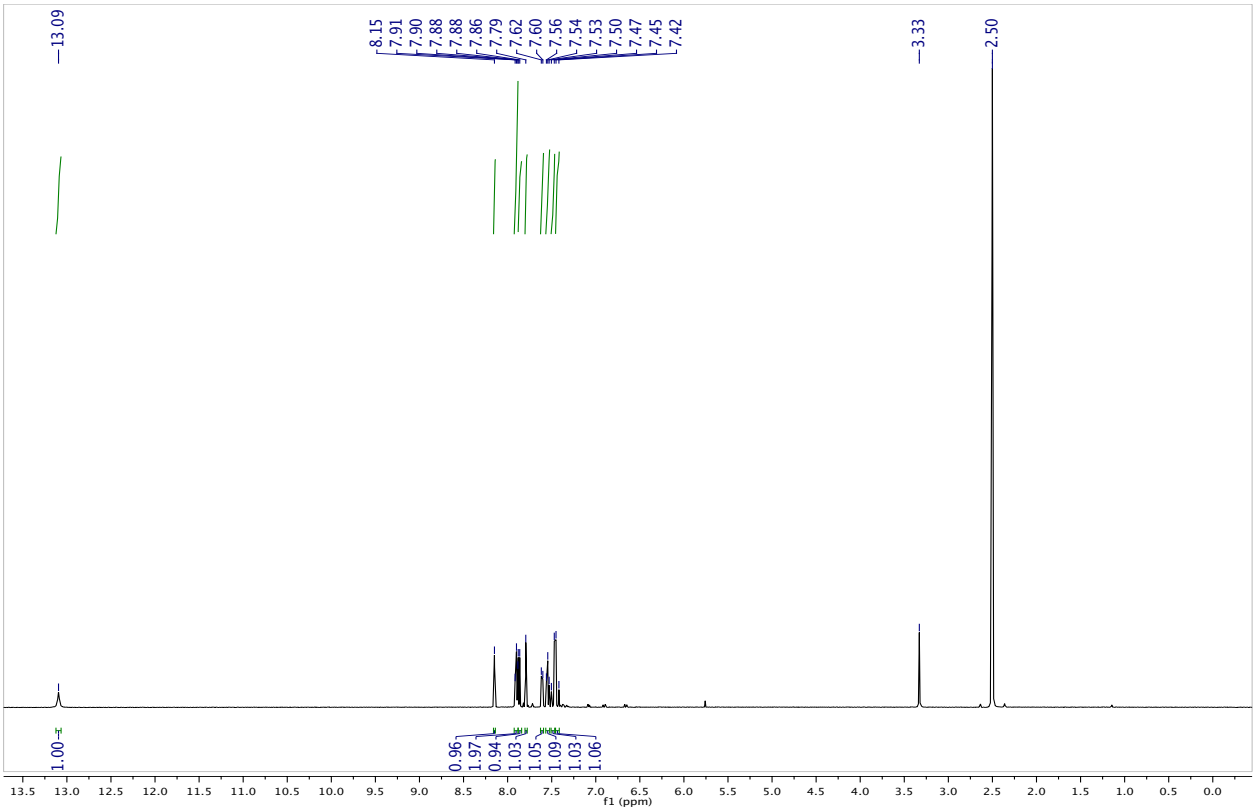

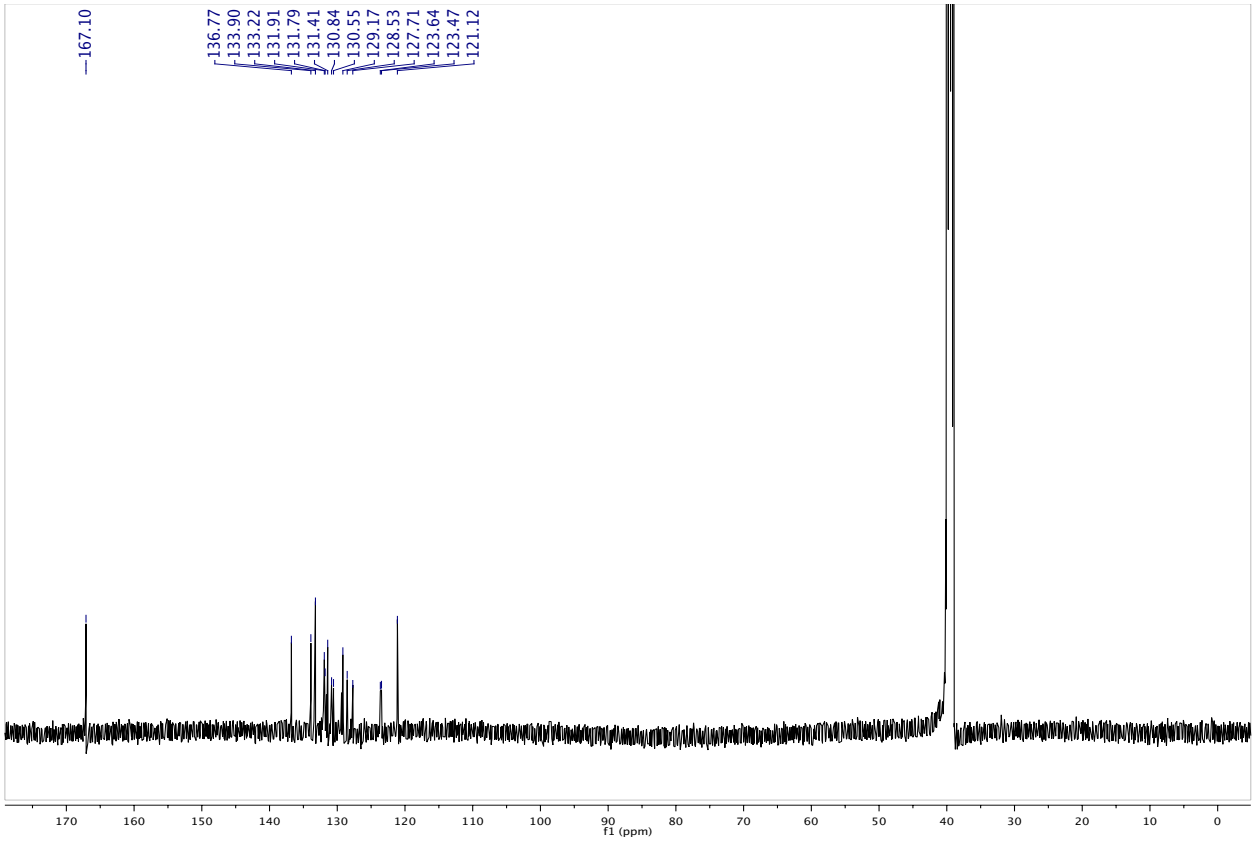

^{1}H NMR (CD_3OD) and ^{13}C NMR (CD_3OD) of Compound **4.8f**

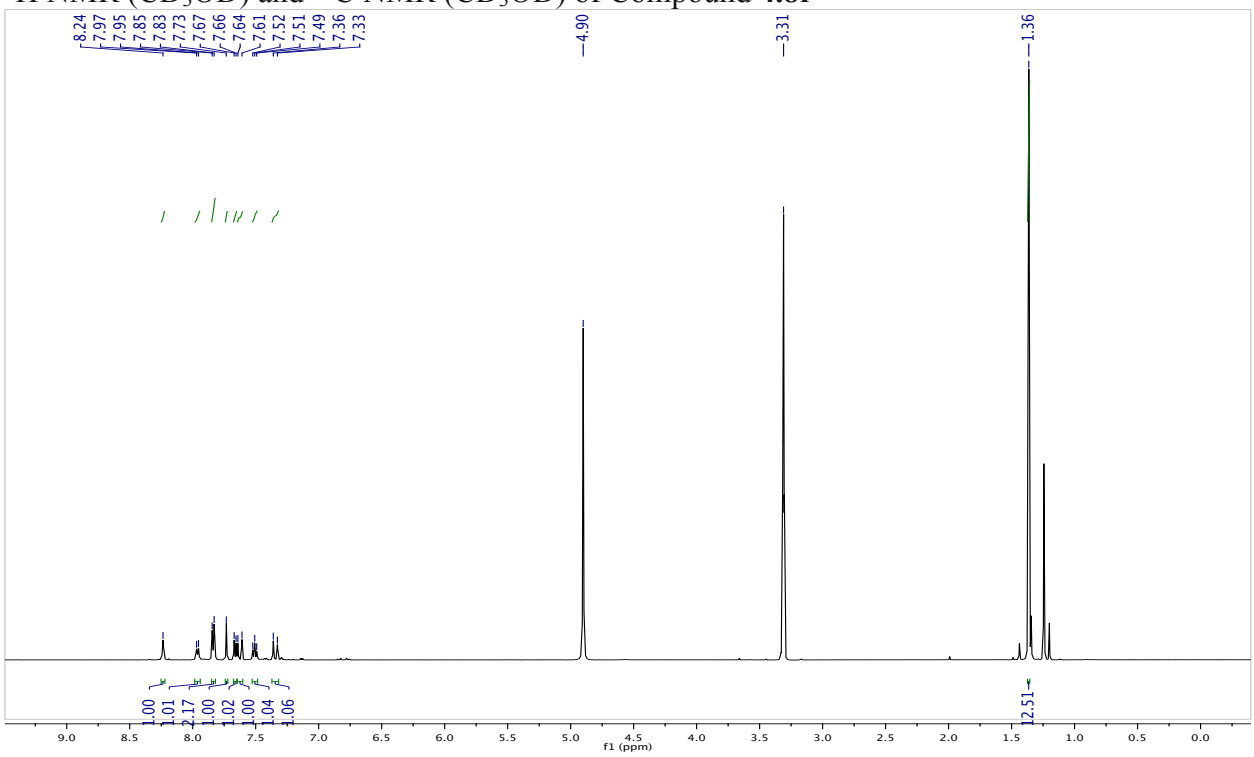

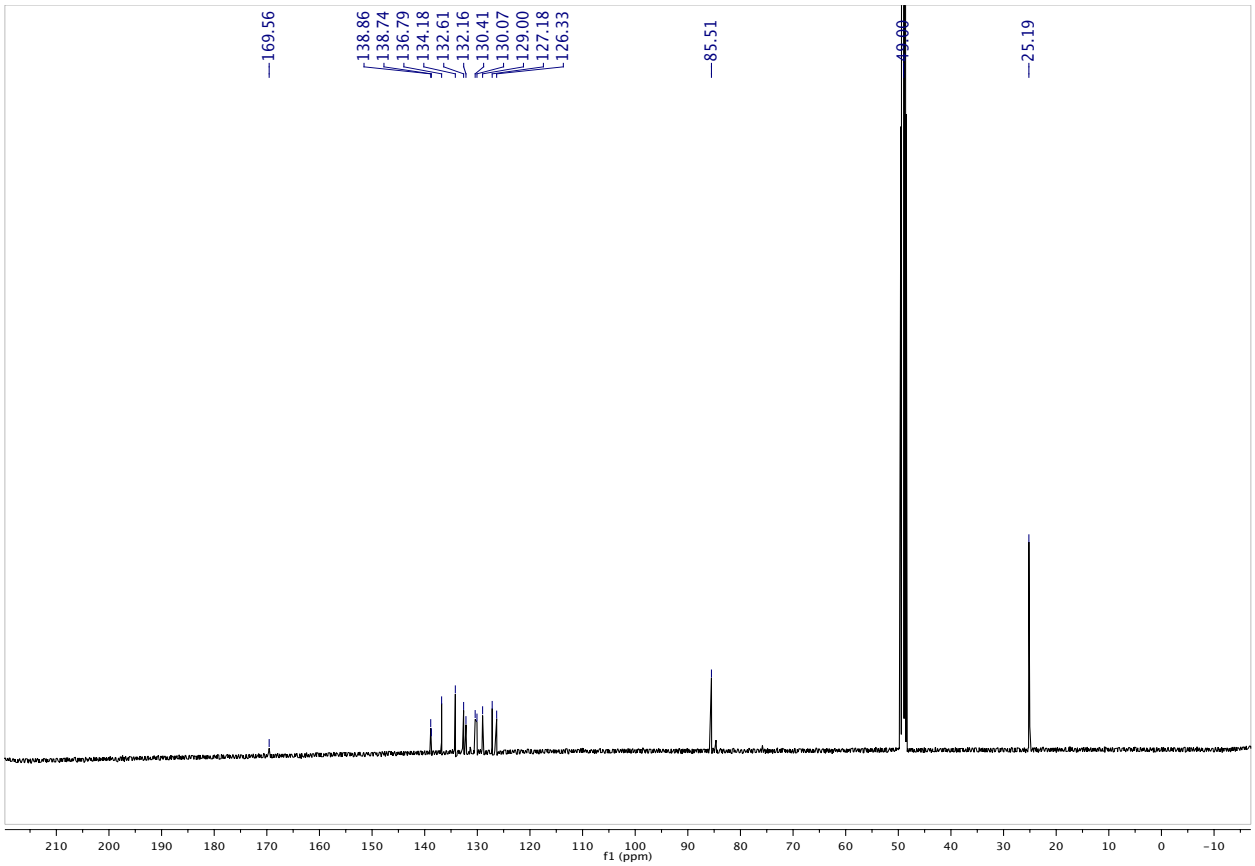

^{1}H NMR (CD_3OD) and ^{13}C NMR (CD_3OD) of Compound **4.8**

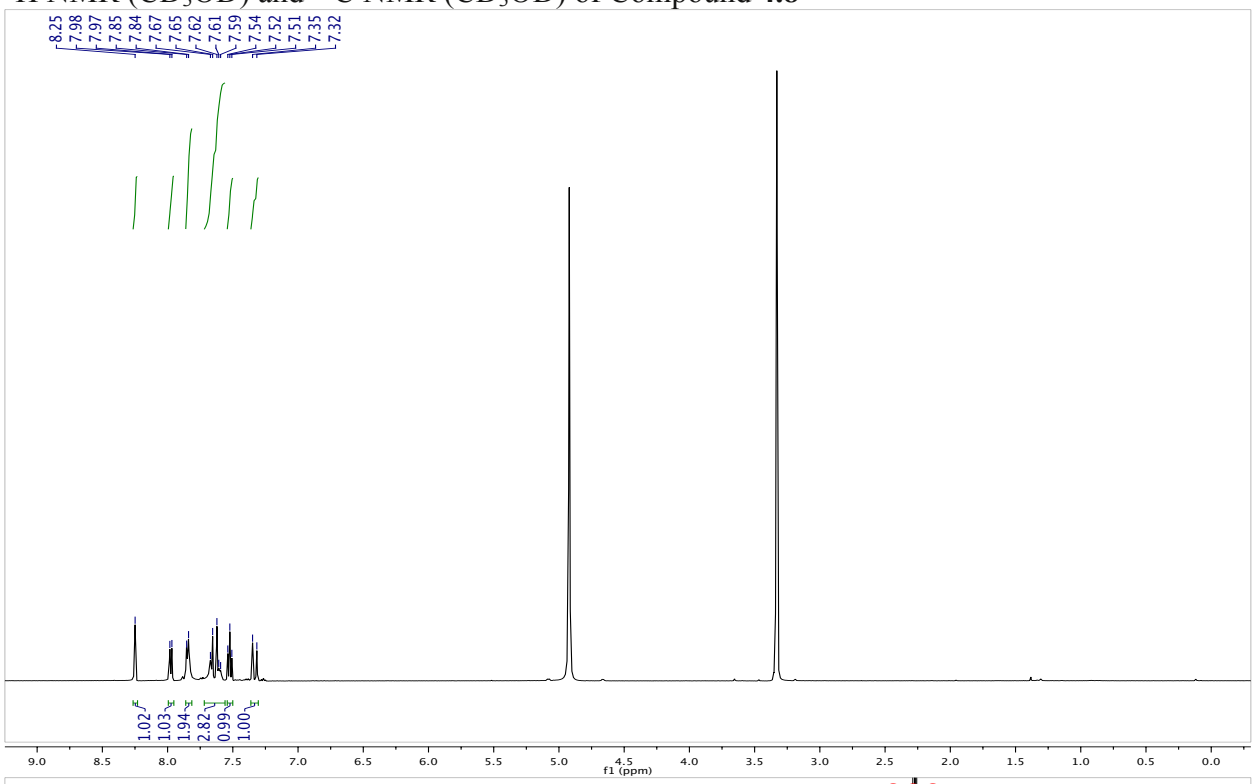

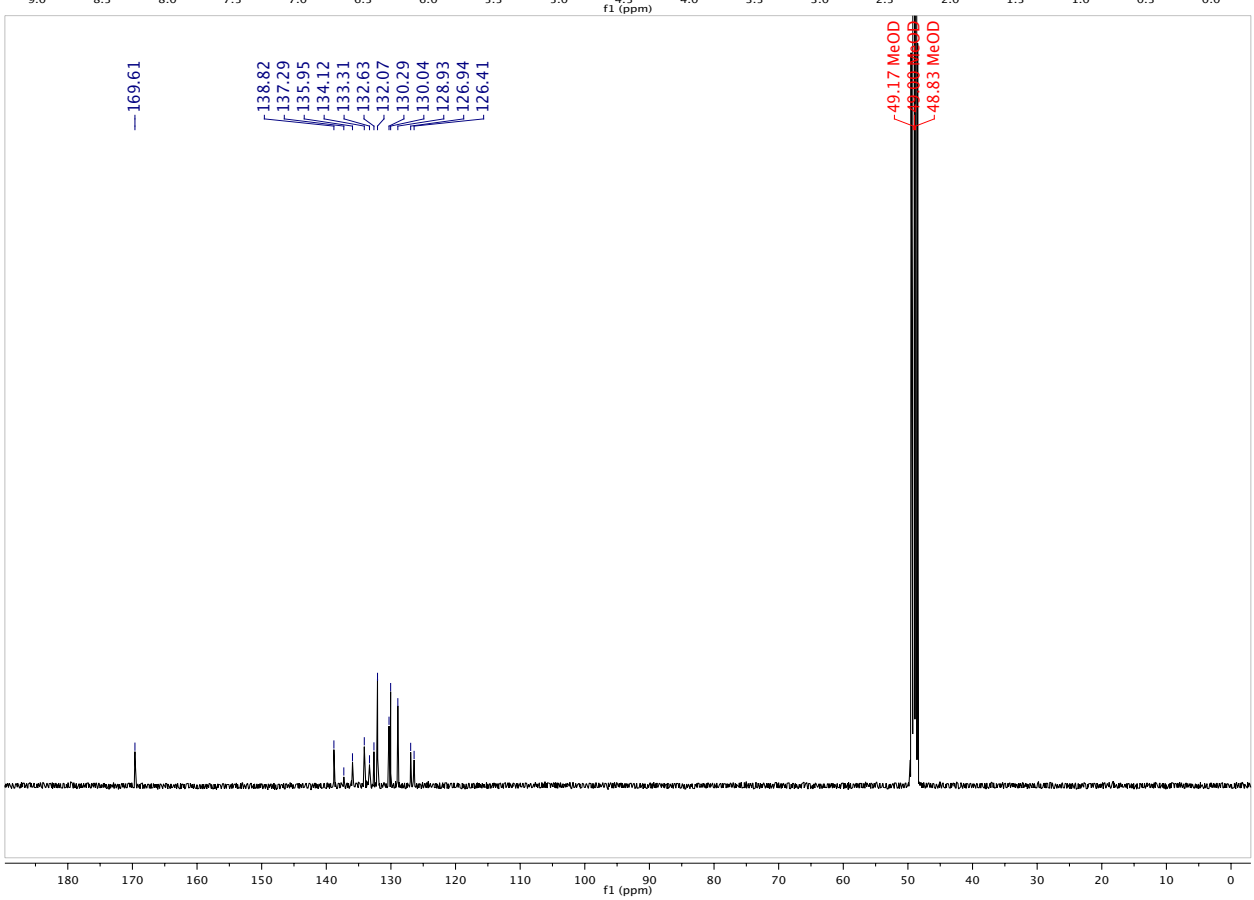

^{1}H NMR (CD_3OD) and ^{13}C NMR (CD_3OD) of Compound **4.7**

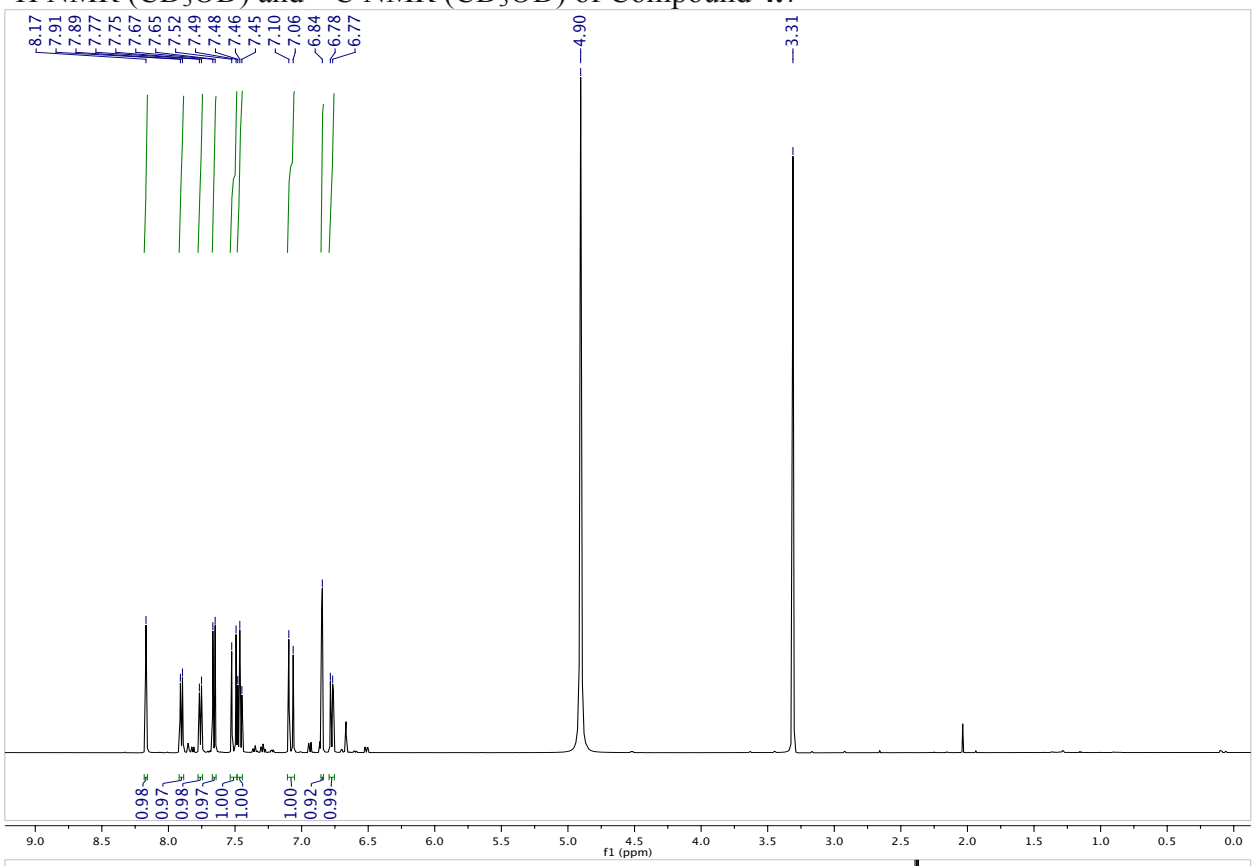

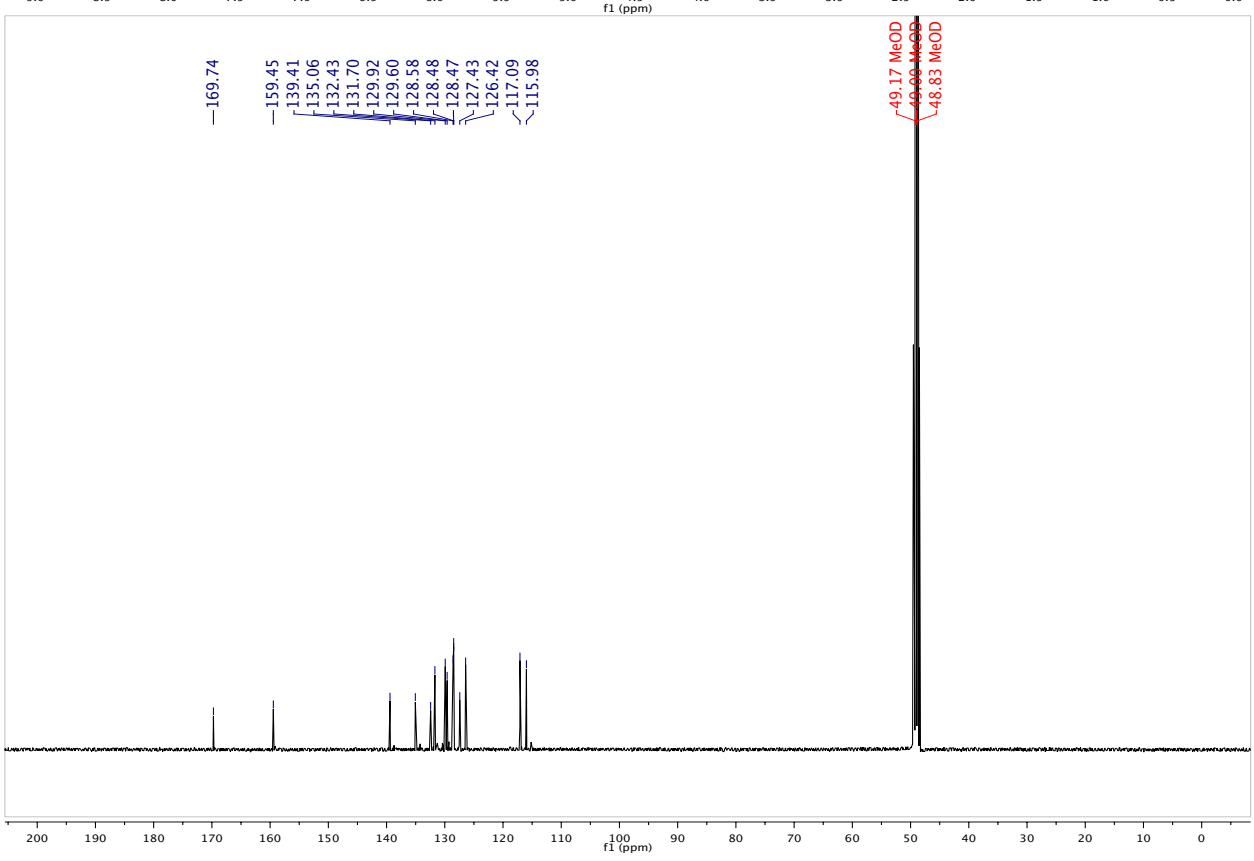

^{1}H NMR ($CDCl_3$) and ^{13}C NMR ($CDCl_3$) of Compound **4.10a**

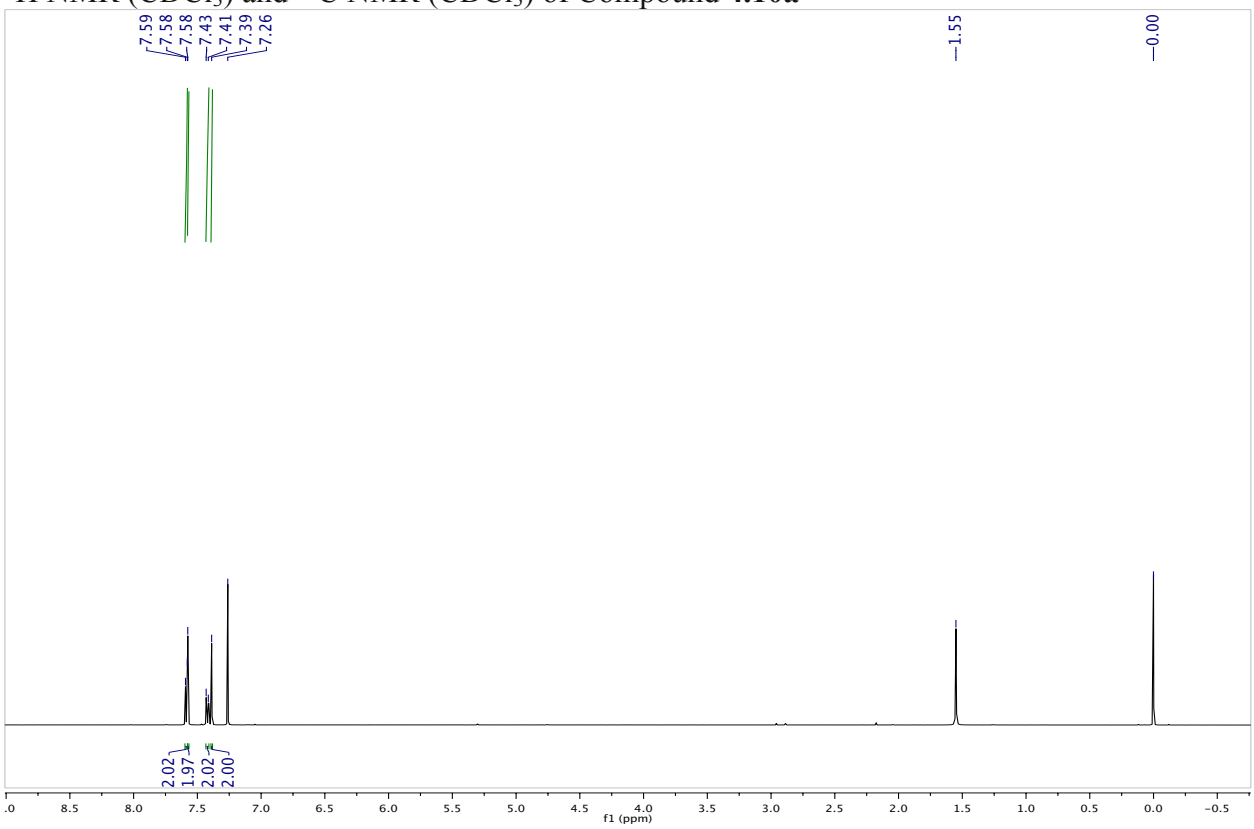

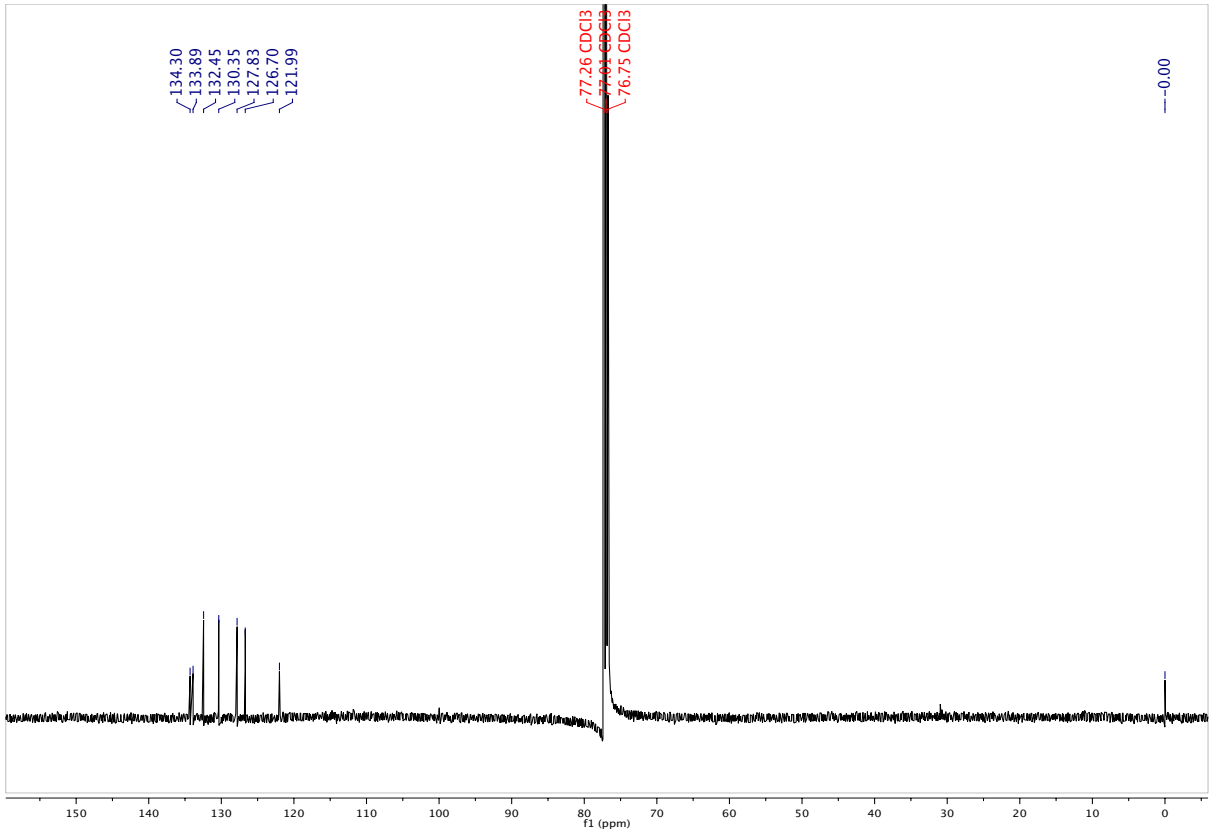

^{1}H NMR ($CDCl_3$) and ^{13}C NMR ($CDCl_3$) of Compound **4.10b**

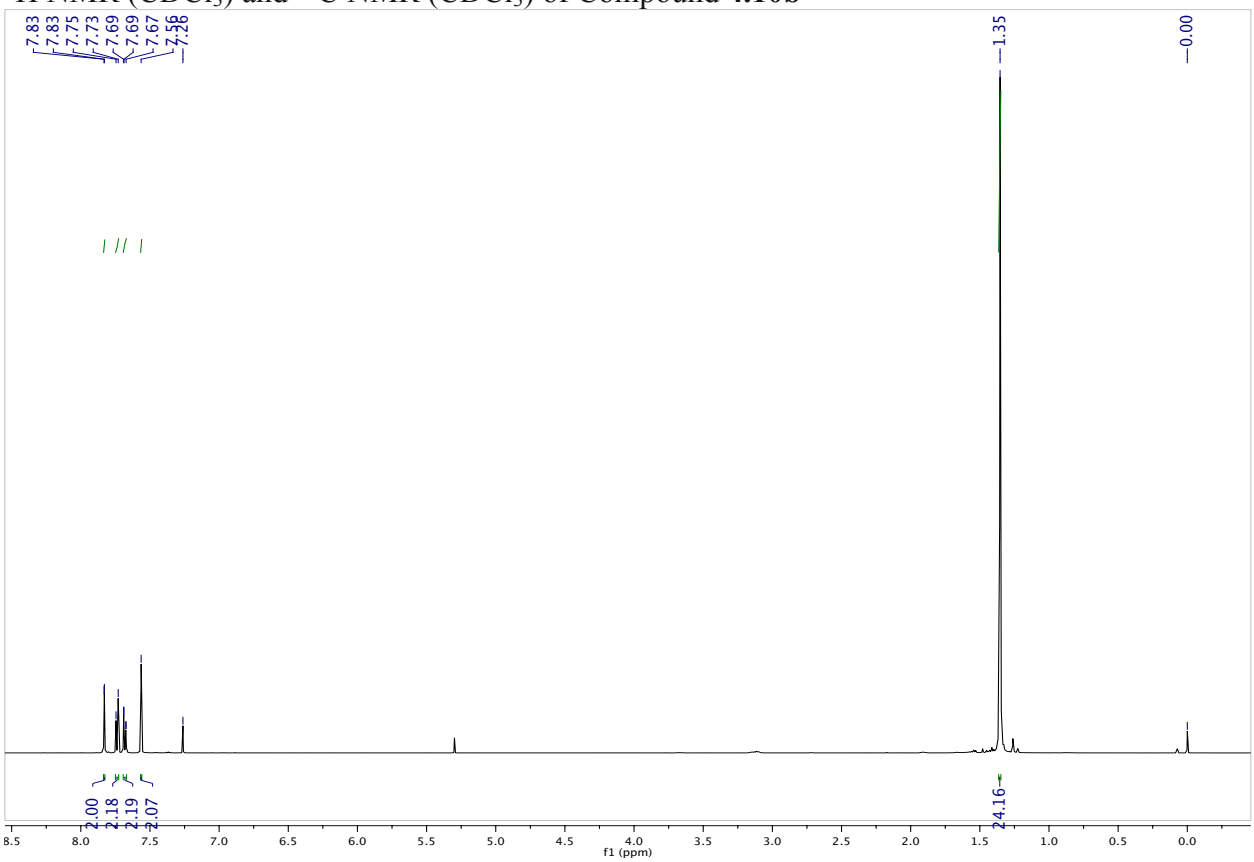

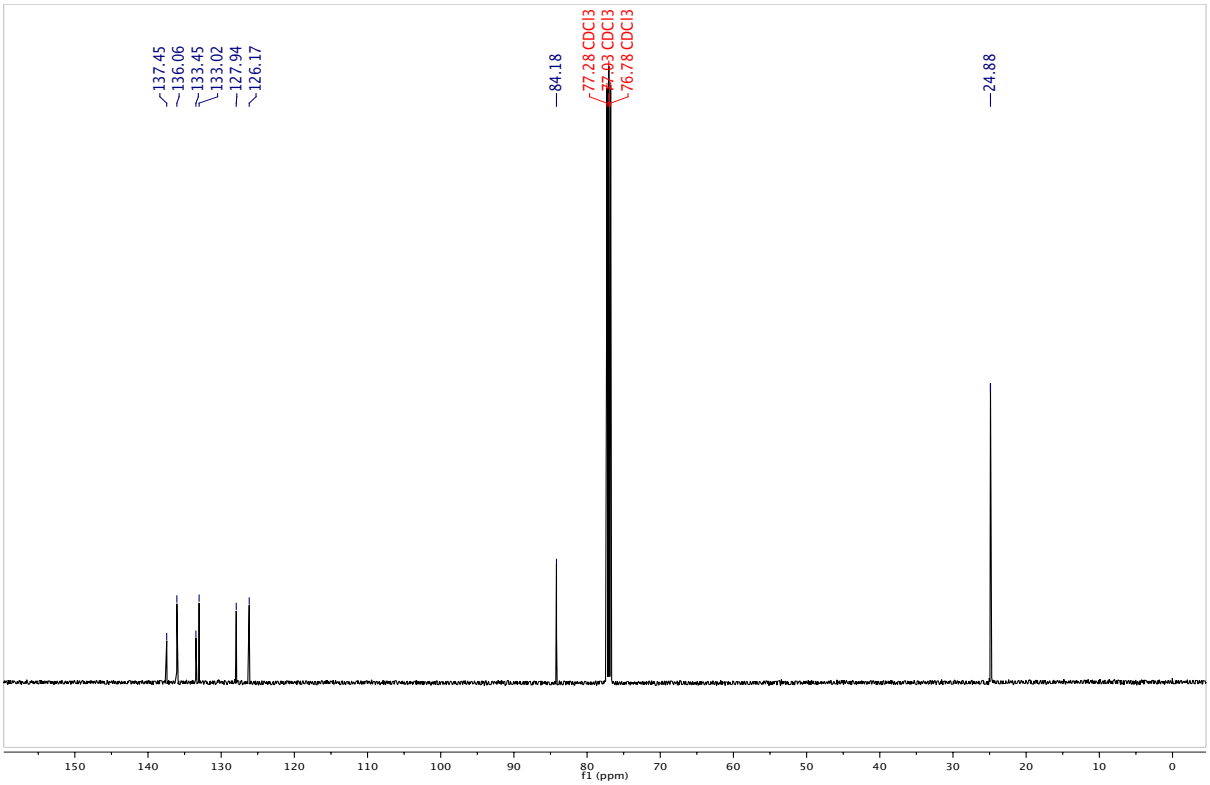

^{1}H NMR (CD_3OD) and ^{13}C NMR (CD_3OD) of Compound **4.10**

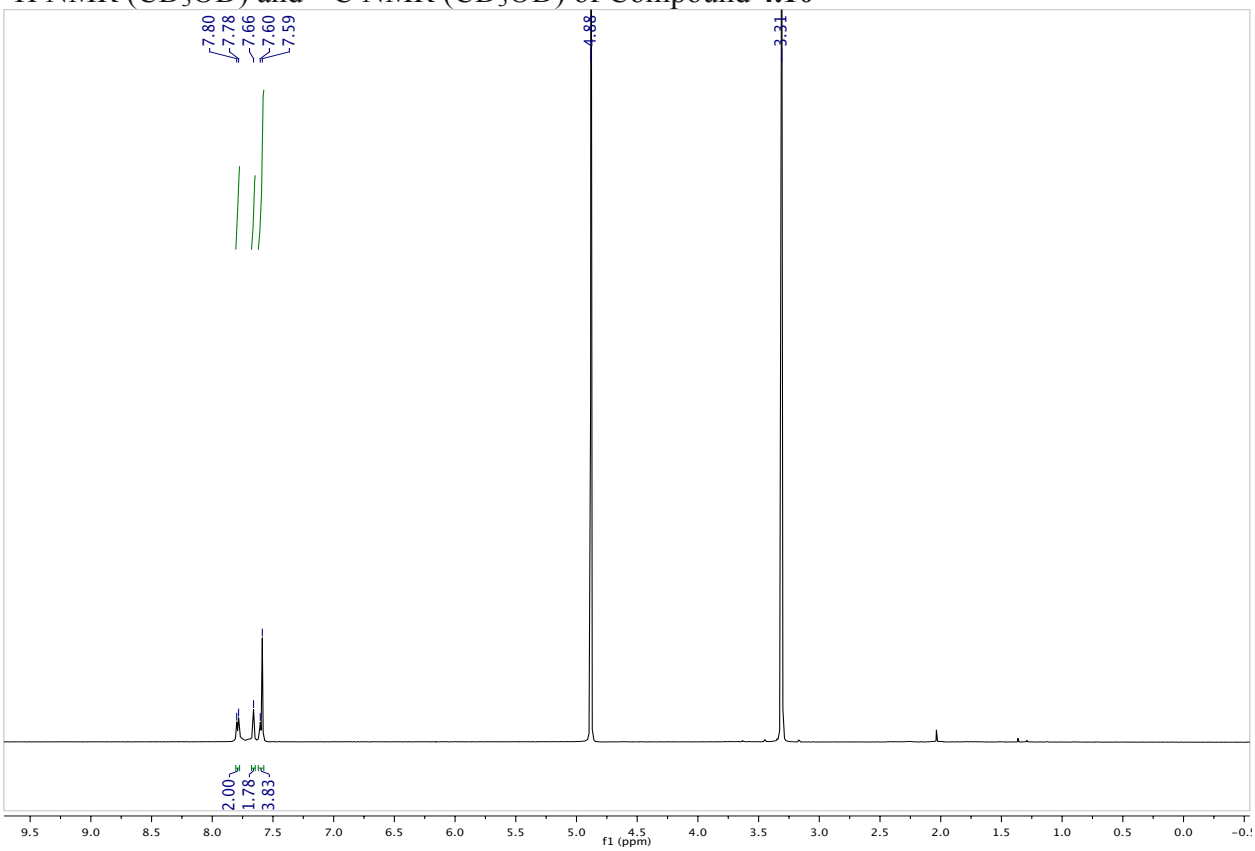

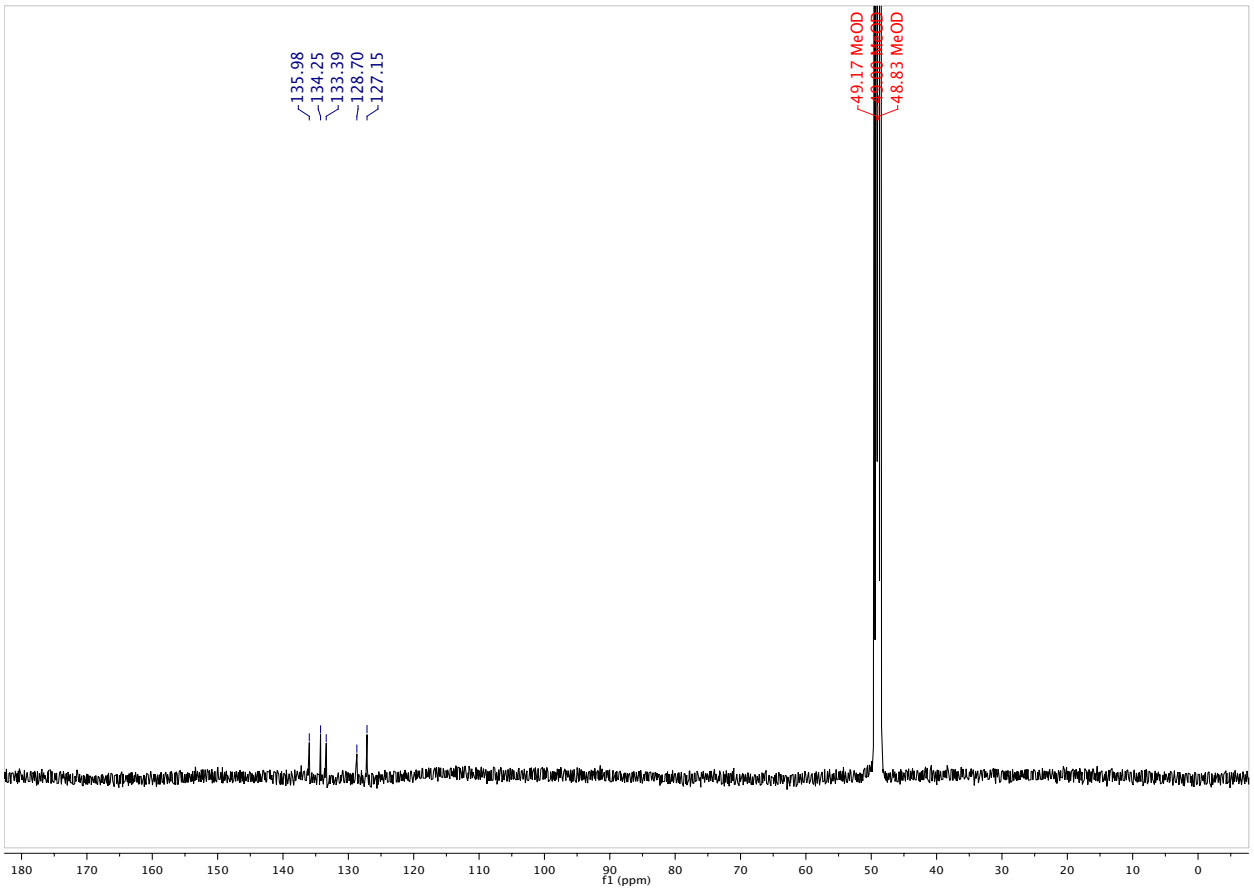

^{1}H NMR (CD_3OD) and ^{13}C NMR (CD_3OD) of Compound **4.9**

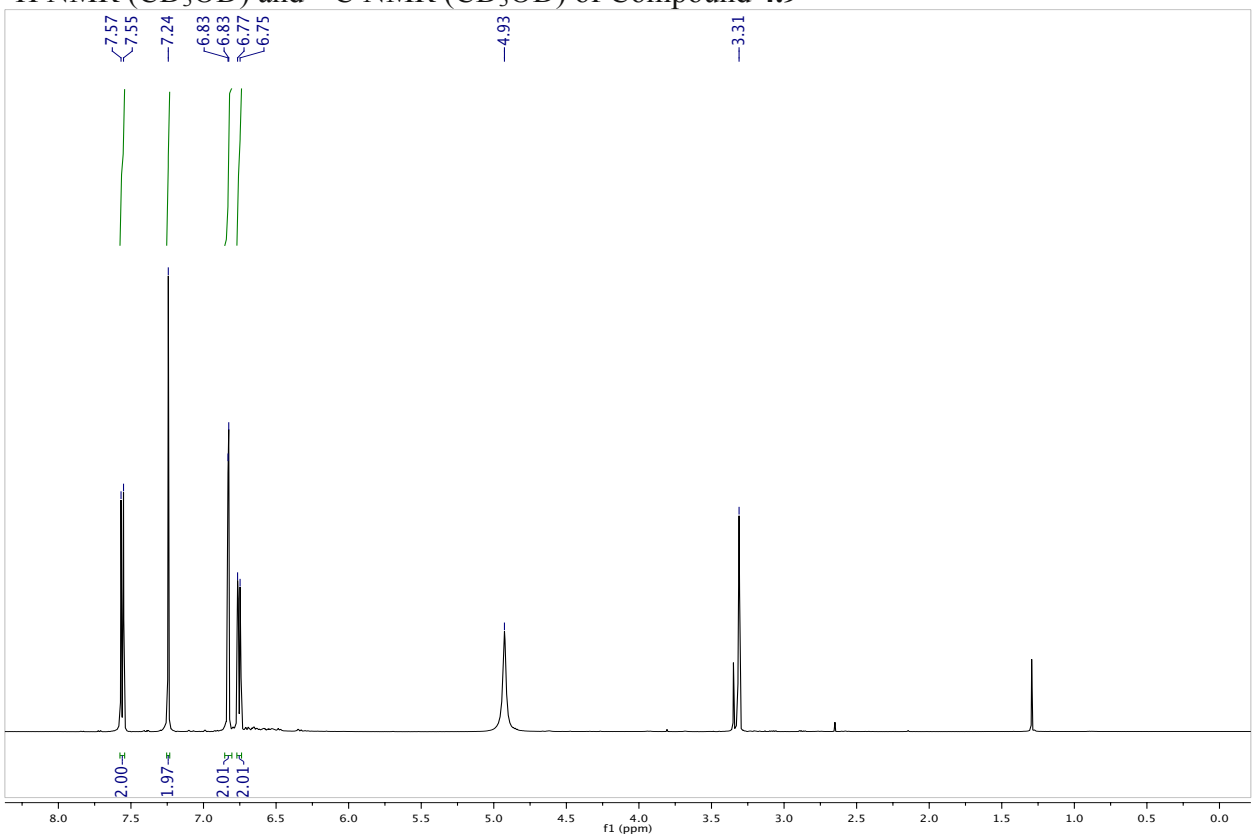

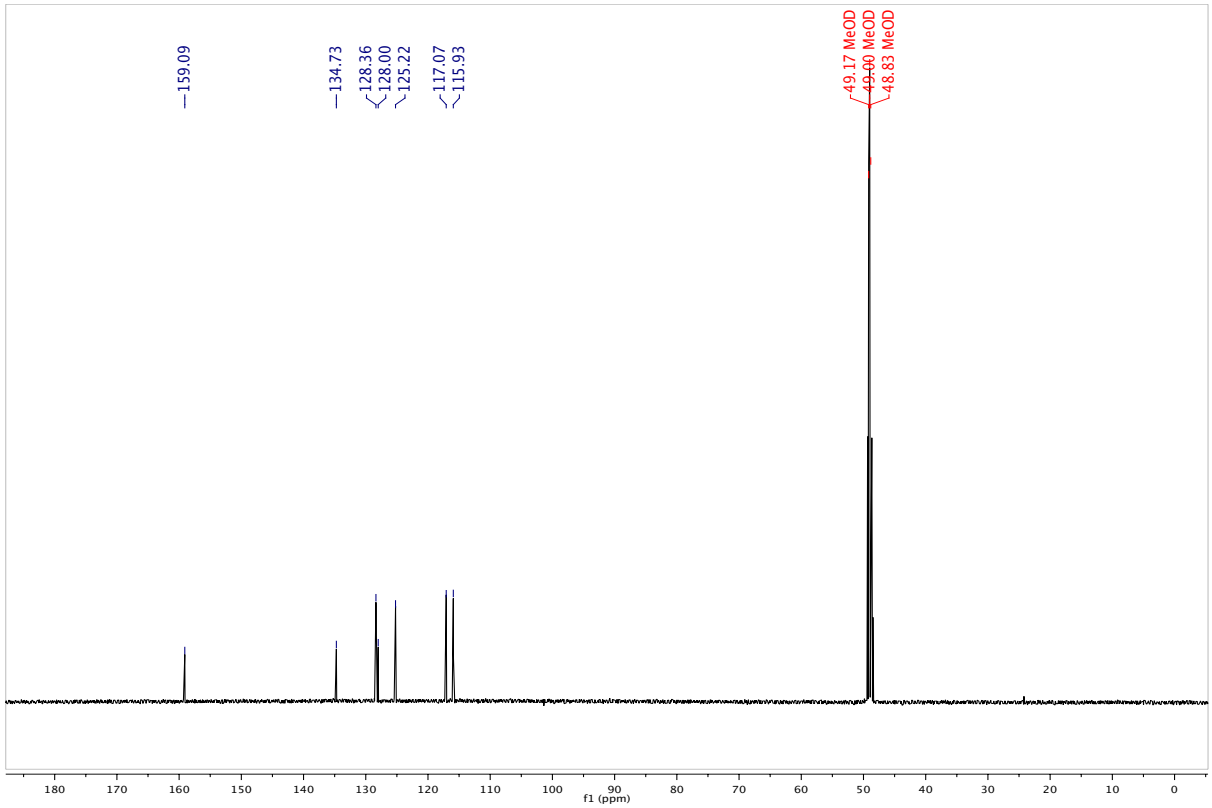

^{1}H NMR (CD_3OD) and ^{13}C NMR (CD_3OD) of Compound **4.11a**

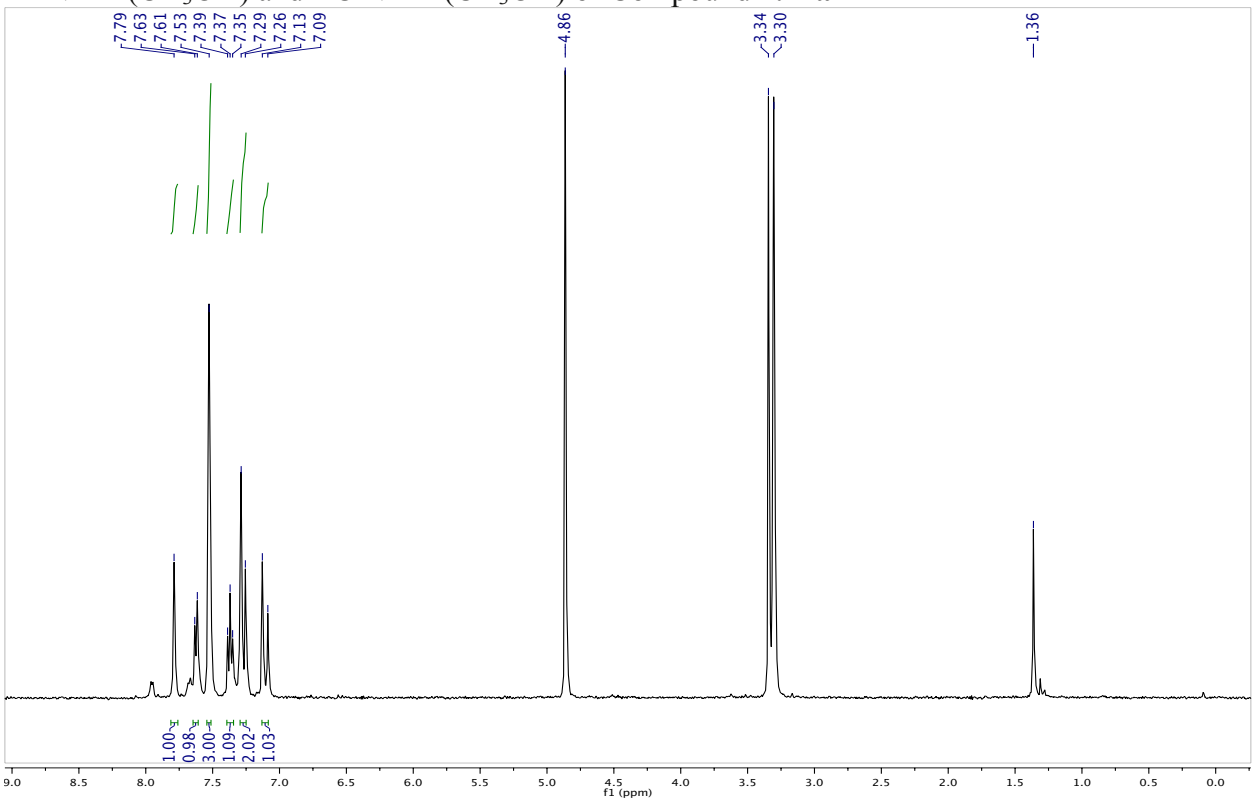

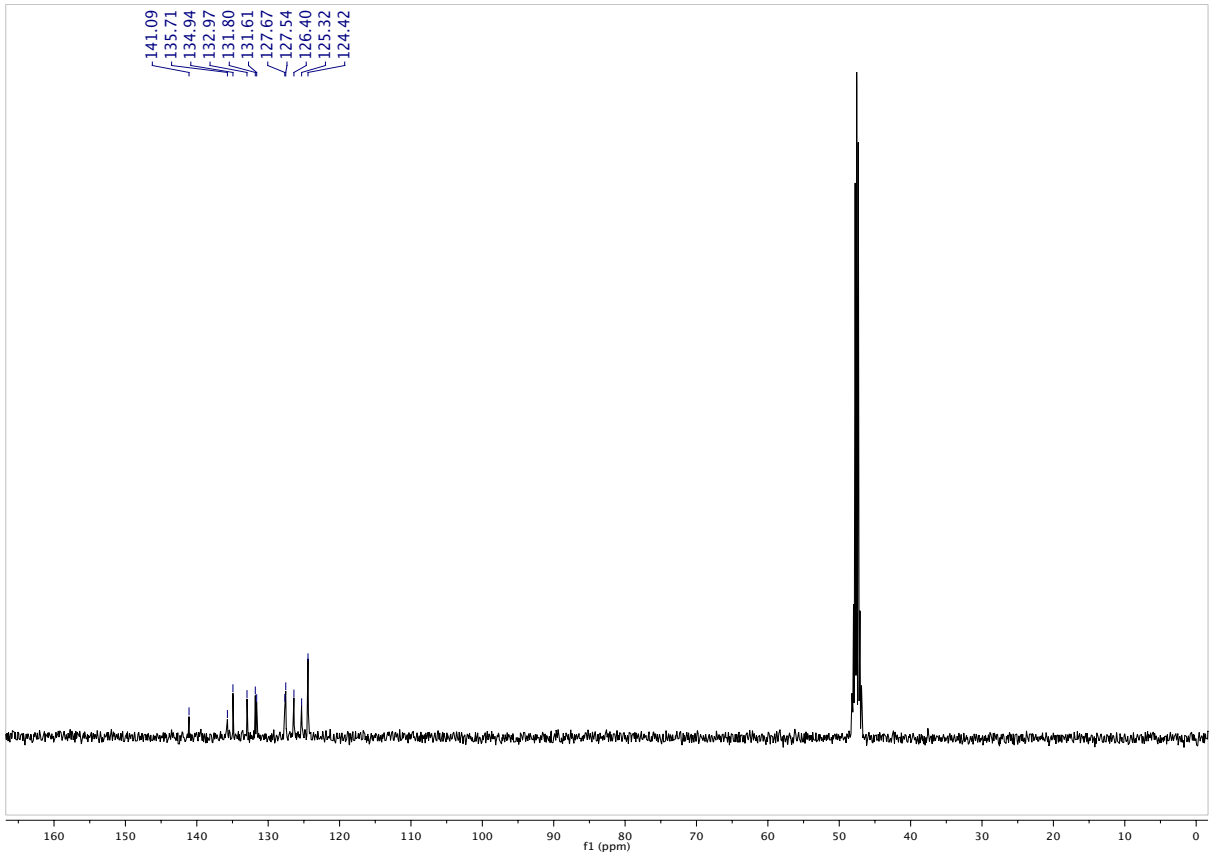

^{1}H NMR (CD_3OD) and ^{13}C NMR (CD_3OD) of Compound **4.11b**

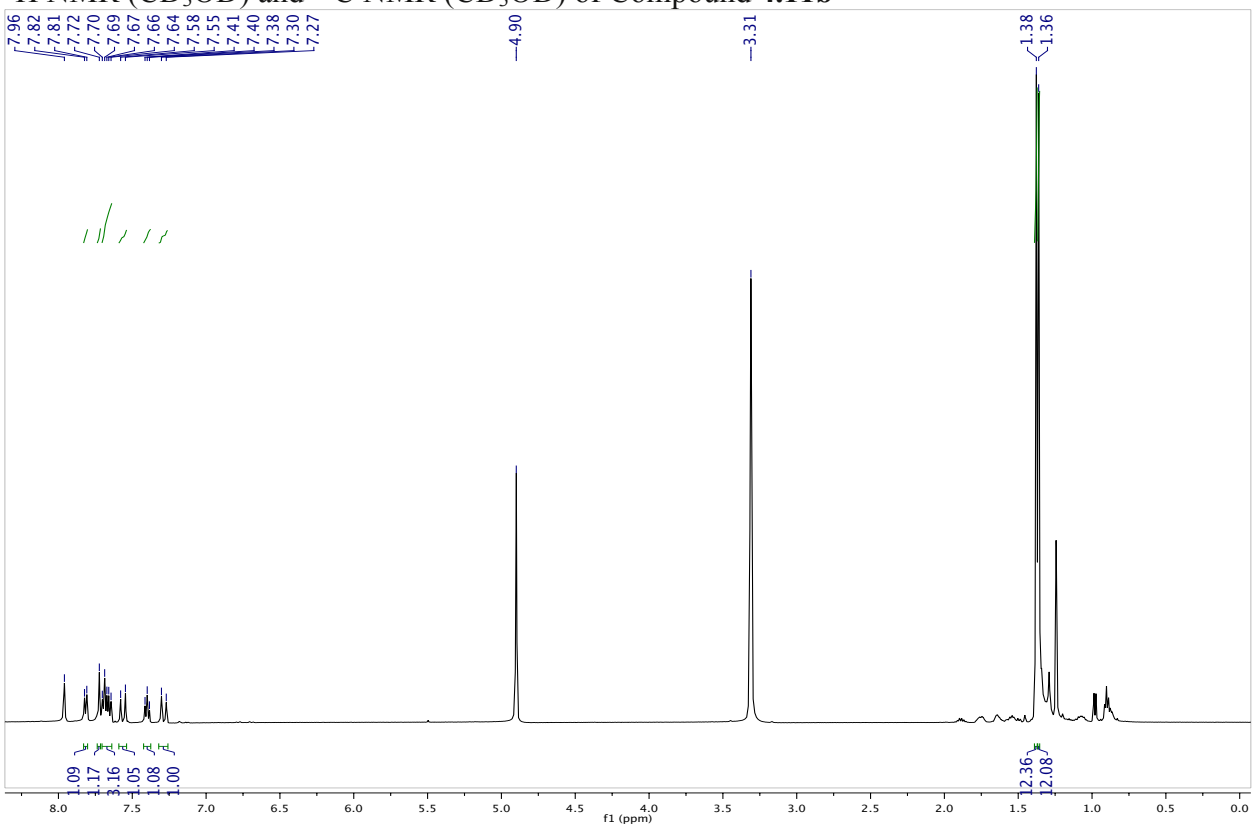

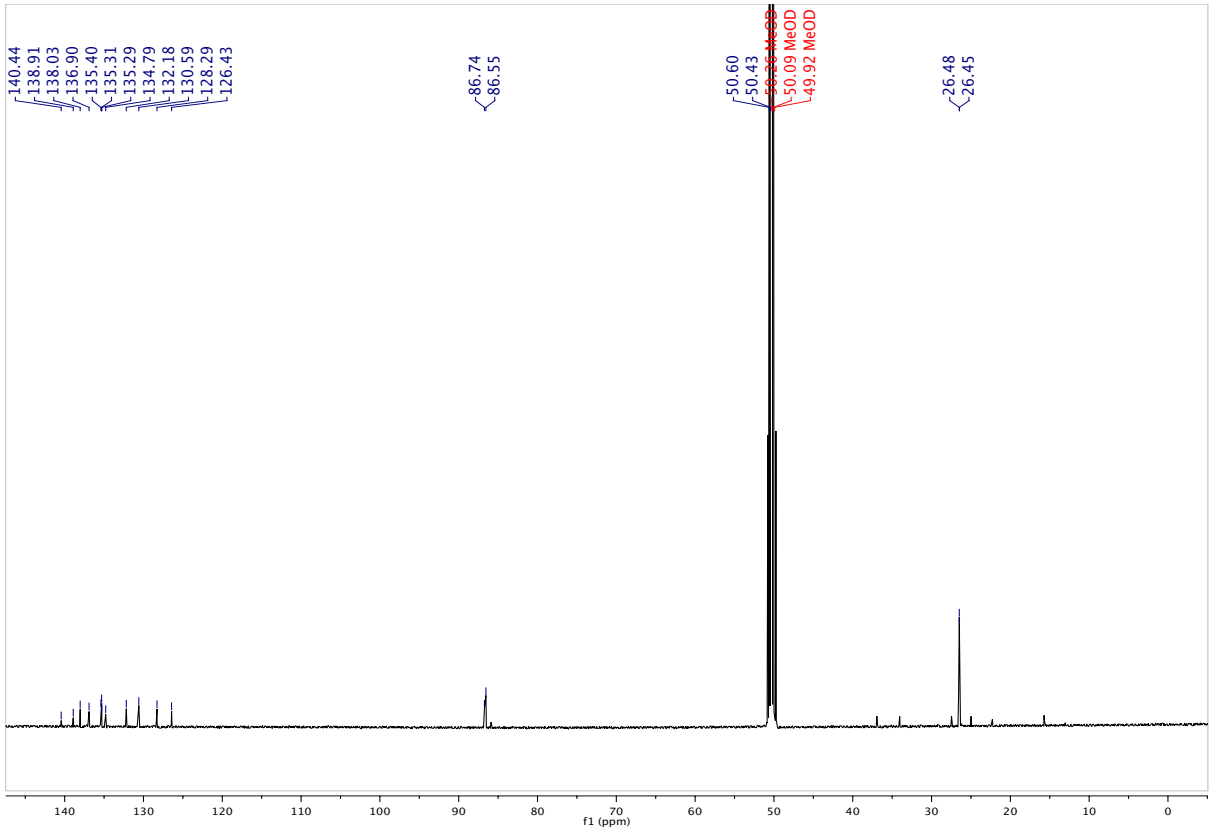

^{1}H NMR (CD_3OD) and ^{13}C NMR (CD_3OD) of Compound **4.11**

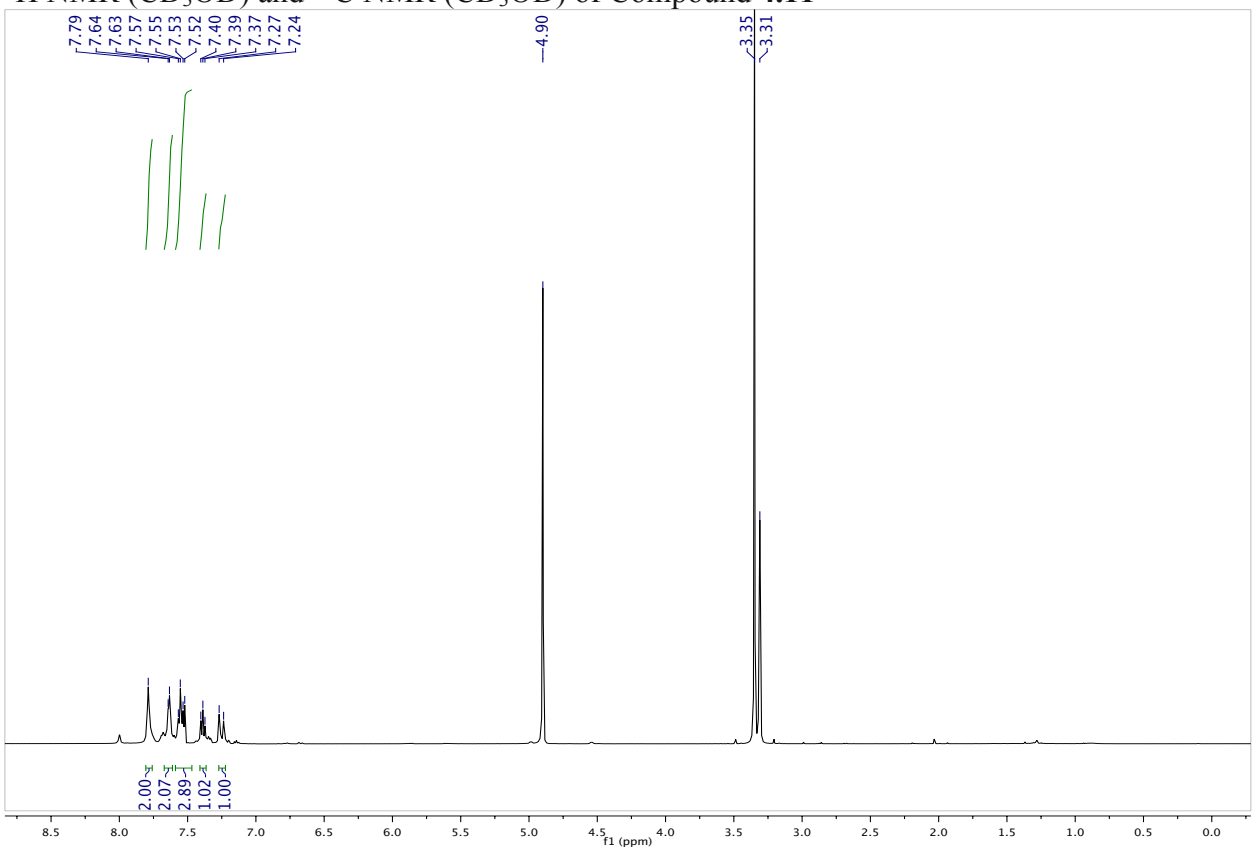

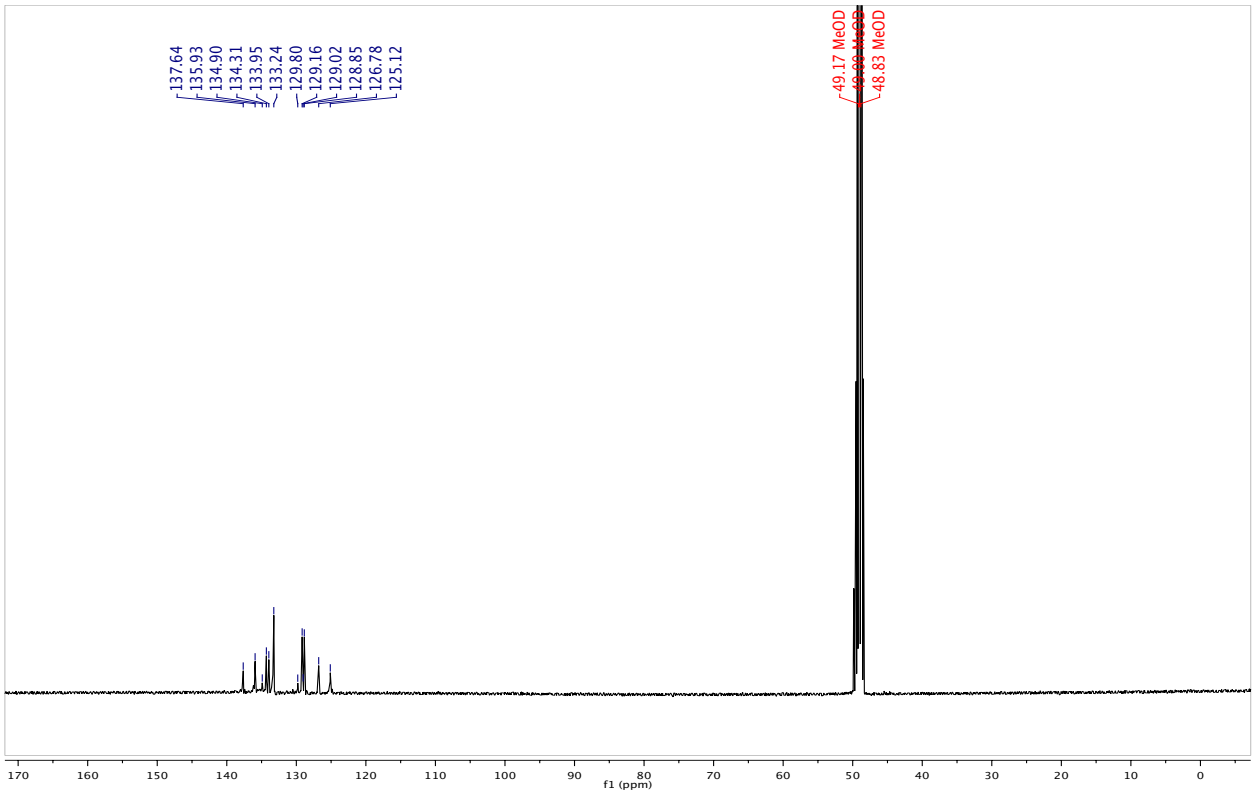

Table 4.2 Interaction of Diphenols **4.1–4.4** with Wild-type TTR and its V30M Variant

		wild-type TTR		V30M TTR		
compound	$K_{d,2}$ (nM)	%FF 1:1[a]	%FF 2:1[a]	%FF 1:1[a]	%FF 2:1[a]	binding mode[b]
4.1 (resveratrol)	472 ± 29	28 ± 8	9 ± 2	53 ± 12	26 ± 4	forward
4.2	473 ± 16	21 ± 4	9 ± 2	48 ± 11	23 ± 6	reverse
4.3	728 ± 22	22 ± 4	7 ± 3	44 ± 10	14 ± 4	forward
4.4	441 ± 5	19 ± 4	4 ± 2	36 ± 8	12 ± 3	reverse

[a]%FF, percent fibril formation. [b]"forward": upper phenyl ring depicted in Scheme 4.1 lies in the outer pocket of the T_4-binding site, according to X-ray diffraction analysis (Figures 4.2 and 4.3); "reverse": upper ring lies in the inner pocket.[216]

Table 4.2 Interactions of Carboxylic Acids **4.5–4.8** with Wild-type TTR and its V30M Variant

		wild-type TTR		V30M TTR		
compound	$K_{d,2}$ (nM)	%FF 1:1[a]	%FF 2:1[a]	%FF 1:1[a]	%FF 2:1[a]	binding mode[b]
4.5	1763 ± 140	75 ± 24	77 ± 14	112 ± 25	120 ± 32	forward
4.6	986 ± 15	21 ± 4	11 ± 2	48 ± 12	28 ± 8	reverse
4.7	469 ± 10	21 ± 4	3 ± 1	41 ± 10	9 ± 2	forward
4.8	451 ± 9	16 ± 4	4 ± 1	32 ± 9	10 ± 2	reverse

[a]%FF, percent fibril formation. [b]"forward": upper phenyl ring depicted in Scheme 4.2 lies in the outer pocket of the T_4-binding site, according to X-ray diffraction analysis (Figures 4.2 and 4.3); "reverse": upper ring lies in the inner pocket.[216]

Table 4.3 Interactions of Compounds **4.9–4.12** with Wild-type TTR and its V30M Variant

		wild-type TTR		V30M TTR		
compound	$K_{d,2}$ (nM)	%FF 1:1[a]	%FF 2:1[a]	%FF 1:1[a]	%FF 2:1[a]	binding mode[b]
4.9	819 ± 12	30 ± 6	12 ± 2	62 ± 16	27 ± 10	ND[c]
4.10	469 ± 27	20 ± 3	3 ± 3	32 ± 9	8 ± 3	symmetric/covalent
4.11	794 ± 33	26 ± 4	10 ± 3	54 ± 16	16 ± 5	forward/covalent
4.12(tafamidis)	373 ± 11	22 ± 5	0 ± 6	5 ± 13	8 ± 7	forward[d]

[a]%FF, percent fibril formation. [b]"forward": upper phenyl ring depicted in Scheme 4.3 lies in the outer pocket of the T_4-binding site, according to X-ray diffraction analysis (Figure 4.2); "reverse": upper ring lies in the inner pocket.[216] [c]ND, not determined. [d]Ref. [220].

Scheme 4.1 Diphenol Ligands

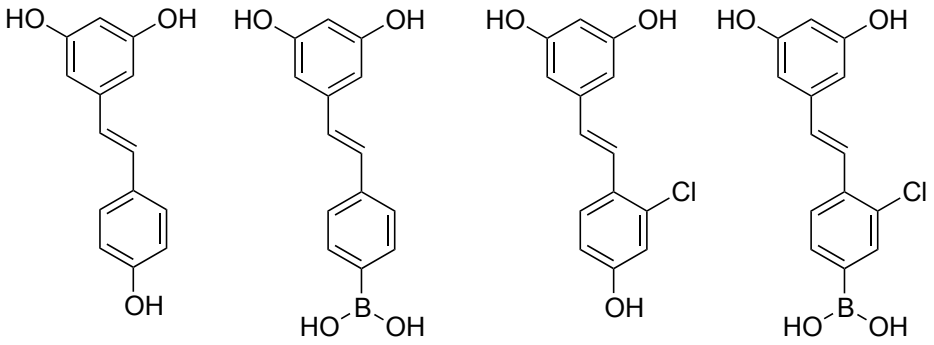

4.1 Resveratrol **4.2** **4.3** **4.4**

Scheme 4.2 Carboxylic Acid Ligands

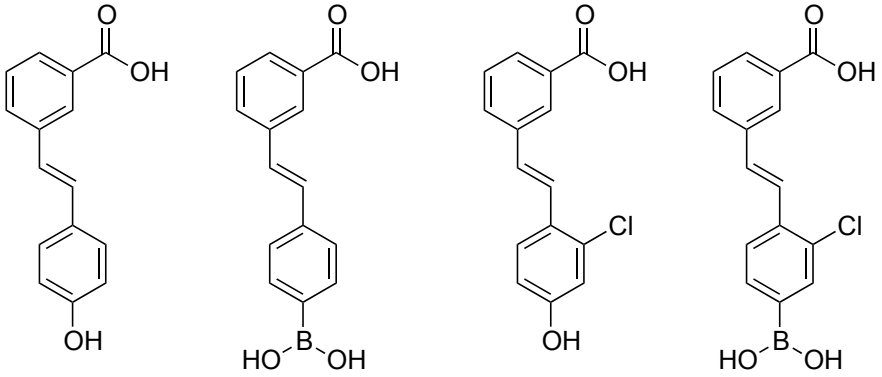

4.5 **4.6** **4.7** **4.8**

Scheme 4.3 Diboronic Acid and Related Ligands

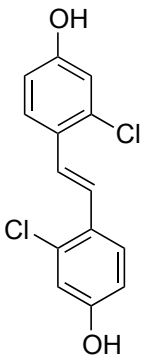

4.9

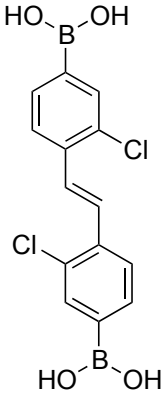

4.10

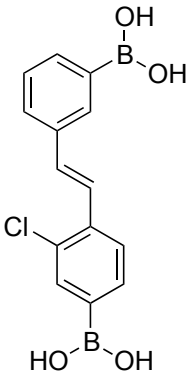

4.11

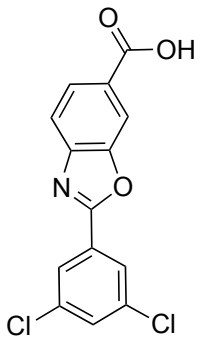

4.12 Tafamidis

Figure 4.1

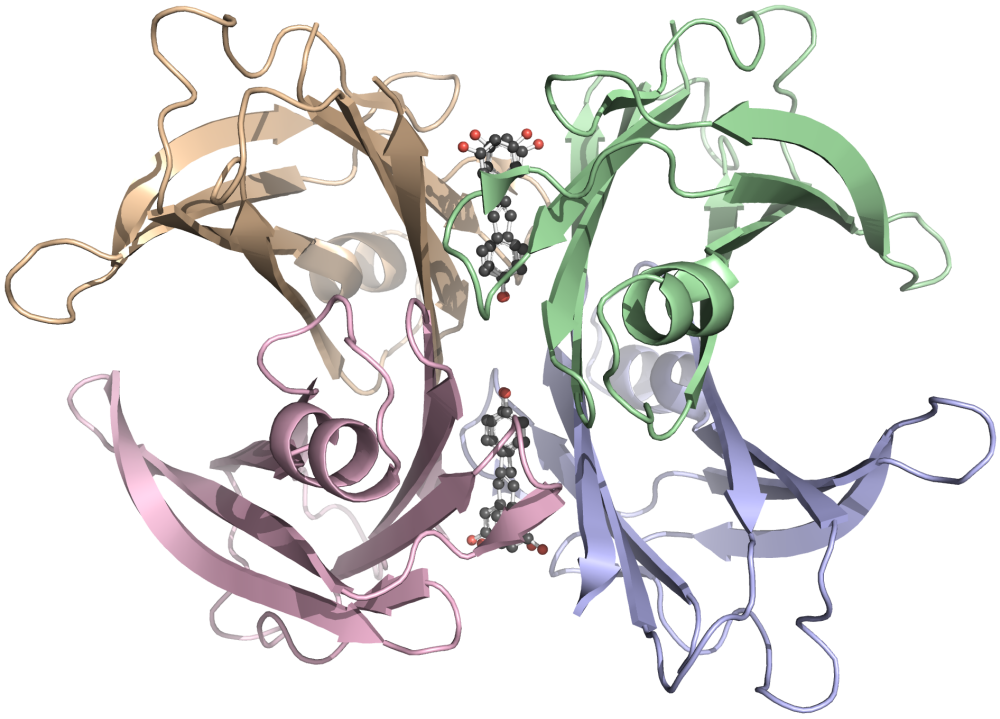

Figure 4.1 Three-dimensional structure of the TTR·resveratrol complex. TTR monomers (tan, red, green, and purple ribbons) have a β-sandwich fold and assemble into a tetramer, which binds to two molecules of resveratrol (ball-and-stick). The rings of resveratrol (**4.1**) occupy inner and outer pockets of the two T_4-binding sites at the dimer–dimer interfaces. The image was created with the program PyMOL and PDB entry 1dvs.[205]

Figure 4.2

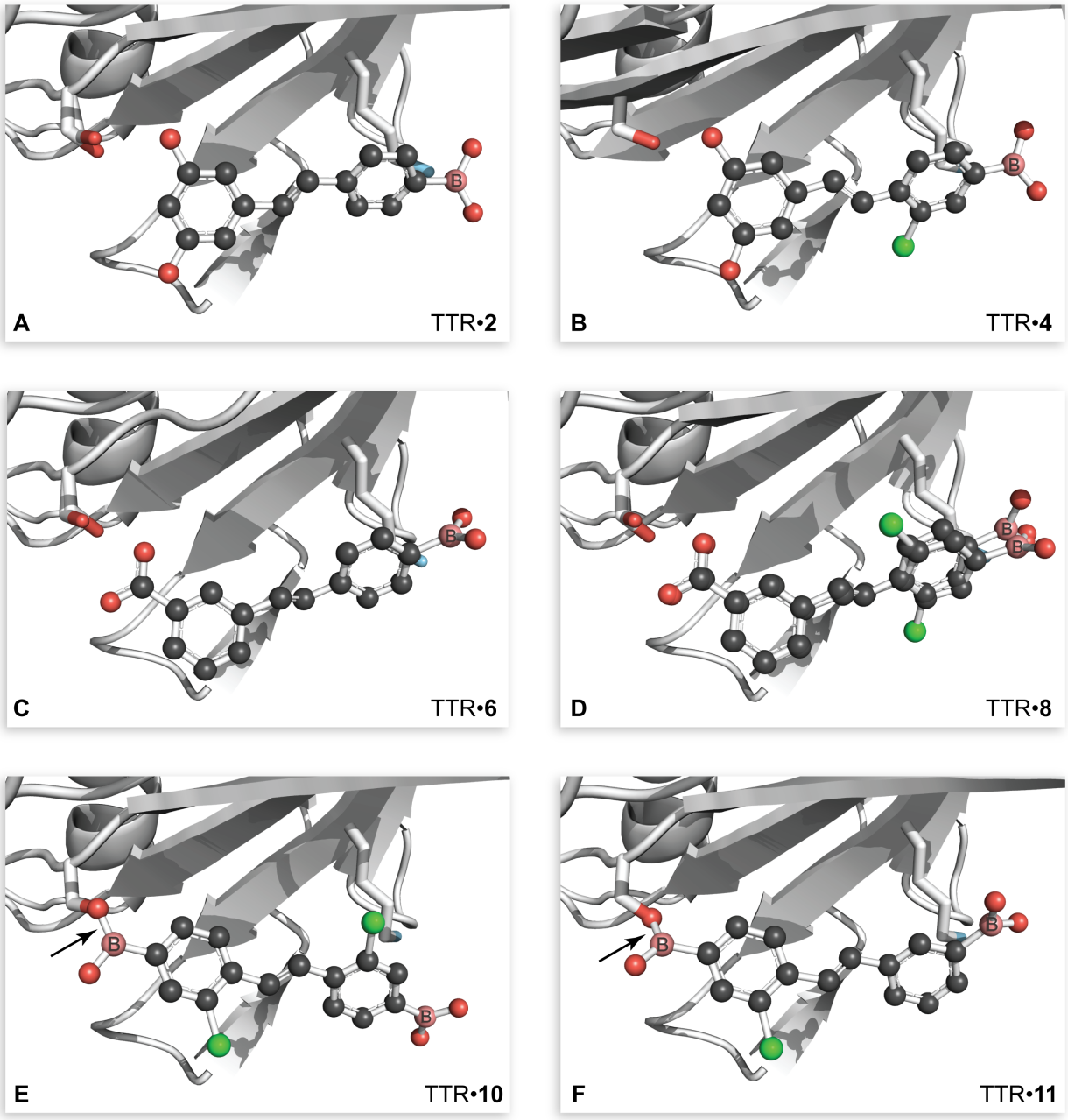

Figure 4.2 Three-dimensional structures of TTR·ligand complexes that contain a boronic acid group. One monomer (chain B) of the TTR tetramer is shown, and is in the same orientation in each panel. The main chain of TTR is rendered as a ribbon, and the side chains of Lys15 and Ser117 are shown explicitly. Ligands are depicted in a ball-and-stick rendition with CPK coloring and boron atoms labeled explicitly. Alternative conformations of Ser117 or the ligand are shown in some panels. Arrows indicate the $O_{117}{}^{\gamma}$–B bond in the TTR·**4.10** and TTR·**4.11** complexes. Images were created with the program PyMOL. (A) TTR·**4.2** (PDB entry 5u48). (B) TTR·**4.4** (5u4a). (C) TTR·**4.6** (5u4c). (D) TTR·**4.8** (5u4e). (E) TTR·**4.10** (5u4f). (F) TTR·**4.11** (5u4g).

Figure 4.3

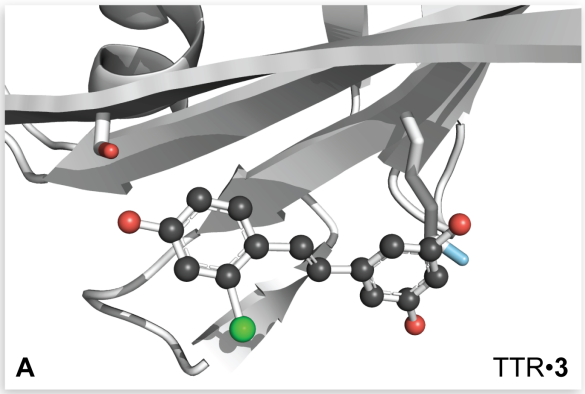

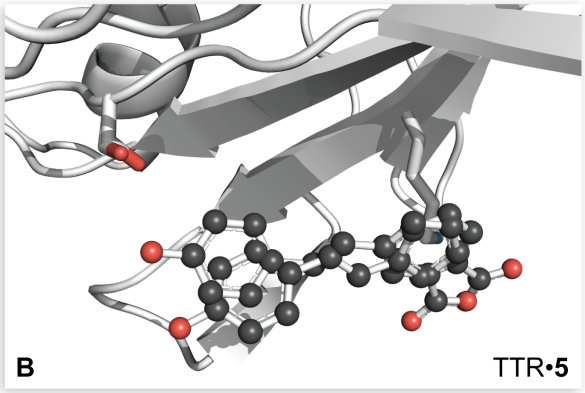

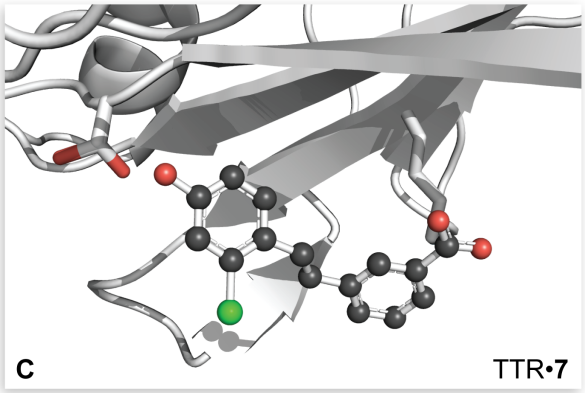

Figure 4.3 Three-dimensional structures of TTR·ligand complexes that do not contain a boronic acid group. One monomer of the TTR tetramer is shown, and is in the same orientation in each panel. The main chain of TTR is rendered as a ribbon, and the side chains of Lys15 and Ser117 are shown explicitly. Ligands are depicted in a ball-and-stick rendition with CPK coloring. Alternative conformations of Ser117 or the ligand are shown in panels B and C. Images were created with the program PyMOL. (A) TTR·**4.3** (PDB entry 5u49, chain A). (B) TTR·**4.5** (5u4b, chain B). (C) TTR·**4.7** (5u4d, chain B).

Figure 4.4

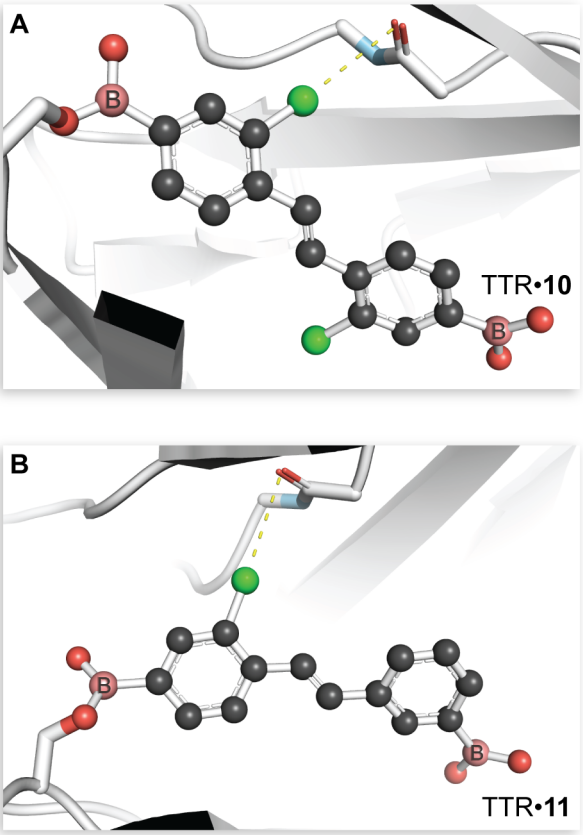

Figure 4.4 Halogen-bonding interactions in the TTR·**4.10** and TTR·**4.11** complexes. One monomer (chain B) of the TTR tetramer is shown. Chloro groups in the two ester-forming boronates exhibit C–Cl···O_{108}′ angles that are nearly linear and Cl··· O_{108}′ distances (dashed yellow lines) that are 3.6–3.8 Å (Table S12). Images were created with the program PyMOL. (A) TTR·**4.10** (PDB entry 5u4f). (B) TTR·**4.11** (5u4g).

Figure 4.5

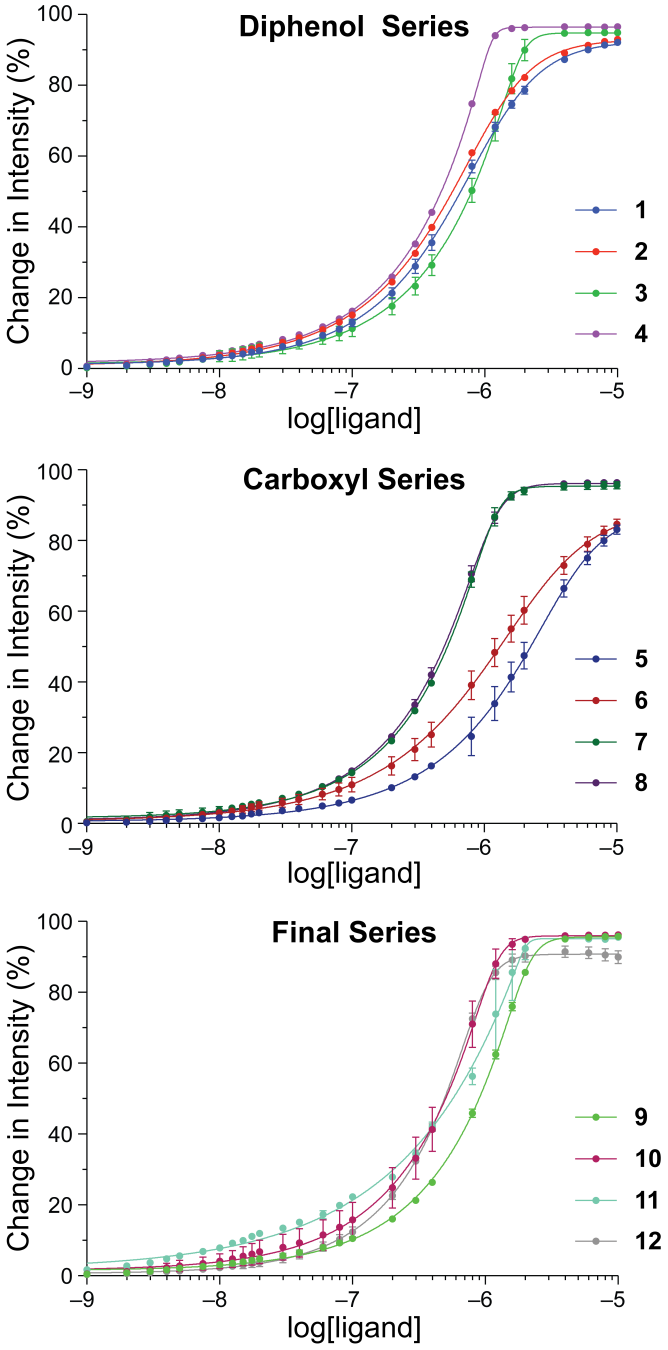
Diphenol Series
Change in Intensity (%)
log[ligand]
1
2
3
4
Carboxyl Series
Change in Intensity (%)
log[ligand]
5
6
7
8
Final Series
Change in Intensity (%)
log[ligand]
9
10
11
12

Figure 4.5 Graphs showing the results of ANS competition assays. (A) Compounds **4.1–4.4**. (B) Compounds **4.5–4.8**. (C) Compounds **4.9–4.12**. Data were fitted to eq 1 to derive values of $K_{d,2}$ (Table 1); $R^2 > 0.99$ for each dataset.

Figure 4.6

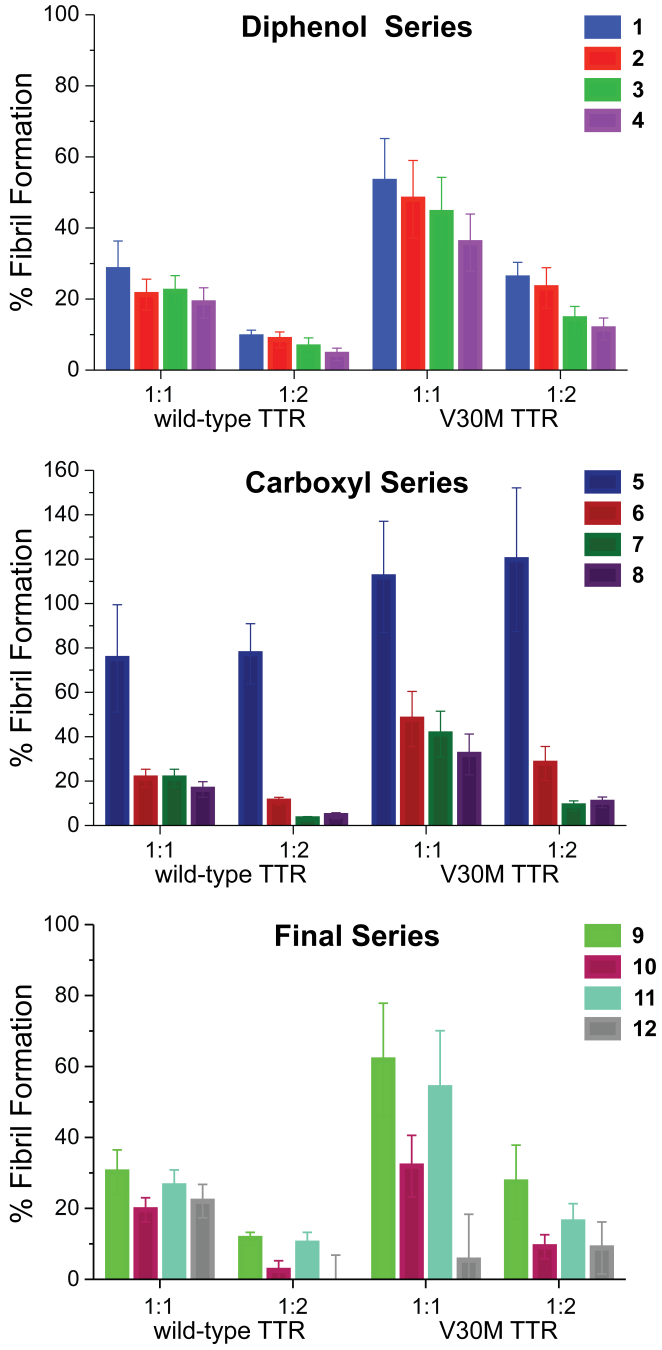
Diphenol Series
1
2
3
4
% Fibril Formation
100
80
60
40
20
0
1:1
1:2
1:1
1:2
wild-type TTR
V30M TTR
Carboxyl Series
5
6
7
8
% Fibril Formation
160
140
120
100
80
60
40
20
0
1:1
1:2
1:1
1:2
wild-type TTR
V30M TTR
Final Series
9
10
11
12
% Fibril Formation
100
80
60
40
20
0
1:1
1:2
1:1
1:2
wild-type TTR
V30M TTR

Figure 4.6 Graphs showing the results of 96-h fibril-formation assays at two different TTR:compound ratios. (A) Compounds **4.1–4.4**. (B) Compounds **4.5–4.8**. (C) Compounds **4.9–4.12**. Error bars represent the standard deviation of 16 measurements propagated through eq 2.

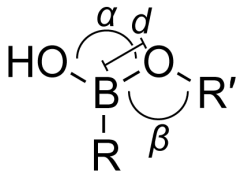

CSD entry	*α* (°)	*β* (°)	*d* (Å)	*n*
DOFLIU	124	123	1.37	2
DOFLOA	125	124	1.37	2
DOFLUG	122	123	1.38	4
HOXPOA	120	120	1.37	2
LUKWUK	118	120	1.36	1
NEYVIX	119	121	1.36	1
QEHMAT	119	120	1.35	1
REZYEA	119	122	1.36	4
TOMKAJ	118	112	1.39	2
WUMCAK	118	109	1.37	1
Mean ± SD	120 ± 3	119 ± 5	1.37 ± 0.02	

Ligand	Chain	*α* (°)	*β* (°)	*d* (Å)
4.10	A	116	109	1.44
4.10	B	116	108	1.37
4.11	A	121	116	1.42
4.11	B	124	109	1.43

Table 4.4 Bond angles and bond lengths of planar boronic esters in small-molecule crystal structures in the Cambridge Structural Database (CSD) and in protein co-crystal structures reported in this work. The parameter *n* refers to the number of B–OR′ bonds in the structure. The means values of the bond angles α and β, and the bond length $r_{B–OR'}$ from these small-molecule structures were used in the refinement of X-ray diffraction data from the TTR·4.10 and TTR·4.11 complexes with the program phenix refine.

Table 4.5 Crystallographic data collection and refinement statistics for TTR in complex with **4.2.**

Complex	**4.2**
PDB Code	5u48
Data Collection	
X-Ray Source	LS-CAT 21-ID-G
Detector	MAR 300 CCD
Wavelength (Å)	0.97857
Resolution, last shell (Å)	35.5-1.50 (1.55-1.50)
Space group	$P\,2_1\,2_1\,2_1$
Unit cell, *a*, *b*, *c* (Å)	$a = 43.228$, $b = 84.947$ $c = 64.606$
Unit cell, α, β, γ (°)	$\alpha = \beta = \gamma = 90$
No. of Reflections	284040
No. of Unique Reflections	39026 (1904)
Redundancy (last shell)	7.3 (7.3)
Mean I/σ (last shell)	28.6 (2.6)
Completeness (last shell)	99.9 (100.0)
R-meas (last shell)	0.056 (0.738)
R-pim (last shell)	0.021 (0.272)
Wilson *B*-factor	18.16
Average Mosaicity (°)	0.2
Refinement	
Working Set (last shell)	35141 (3422)
Test Set (last shell)	3843 (376)
R_{work} (last shell)	0.178 (0.233)
R_{free} (last shell)	0.205 (0.260)
RMSD of Bond Lengths (Å)	0.007
RMSD of Bond Angles (°)	1.05
Total Number of Atoms	1985
Protein Residues	231
Protein	1826
Ligand	38
Water	121
Average *B*-factor	23.9
Protein	23.4
Ligand	22.4
Water	31.9
Ramachandran Favored, Allowed, Outliers (%) from MolProbity	98.7, 1.3, 0

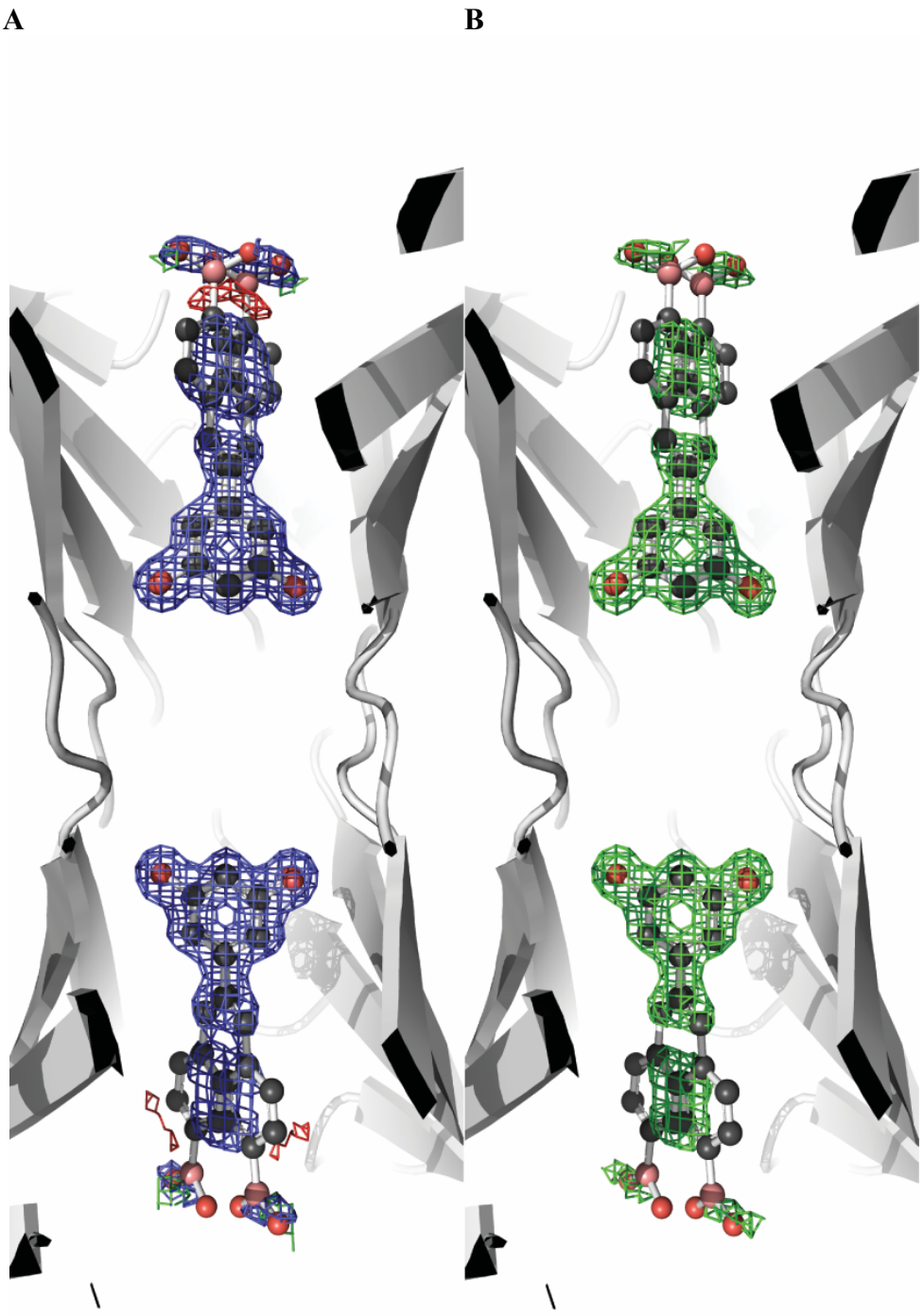

Figure 4.7 Electron density in the TTR·**4.2** complex. (A) Final structure. Blue: $2F_o - F_c$ contoured at 1.0σ; red and green: $F_o - F_c$ contoured at -3.0σ and 3.0σ, respectively. (B) Final structure after ligand removal and refinement by simulated annealing. Green: $F_o - F_c$ contoured at 3.0σ.

Table 4.6 Crystallographic data collection and refinement statistics for TTR in complex with **4.3**

Complex	**4.3**
PDB Code	5u49
Data Collection	
X-Ray Source	LS-CAT 21-ID-D
Detector	Detris Eiger 9M
Wavelength (Å)	1.239801
Resolution, last shell (Å)	33.0-2.22 (2.30-2.22)
Space group	*I* 2 2 2
Unit cell, *a*, *b*, *c* (Å)	$a = 44.517$, $b = 65.895$ $c = 84.594$
Unit cell, α, β, γ (°)	$\alpha = \beta = \gamma = 90$
No. of Reflections	39109
No. of Unique Reflections	5956 (300)
Redundancy (last shell)	6.6 (4.4)
Mean I/σ (last shell)	19.2 (2.3)
Completeness (last shell)	98.7 (98.0)
R-meas (last shell)	0.395 (1.722)
R-pim (last shell)	0.151 (0.757)
Wilson *B*-factor	38.3
Average Mosaicity (°)	1.3
Refinement	
Working Set (last shell)	5598 (1311)
Test Set (last shell)	621 (146)
R_{work} (last shell)	0.202 (0.249)
R_{free} (last shell)	0.275 (0.318)
RMSD of Bond Lengths (Å)	0.008
RMSD of Bond Angles (°)	1.04
Total Number of Atoms	925
Protein Residues	116
Protein	896
Ligand	18
Water	11
Average *B*-factor	41.2
Protein	41.3
Ligand	39.5
Water	38.5
Ramachandran Favored, Allowed, Outliers (%) from MolProbity	96.5, 3.5, 0

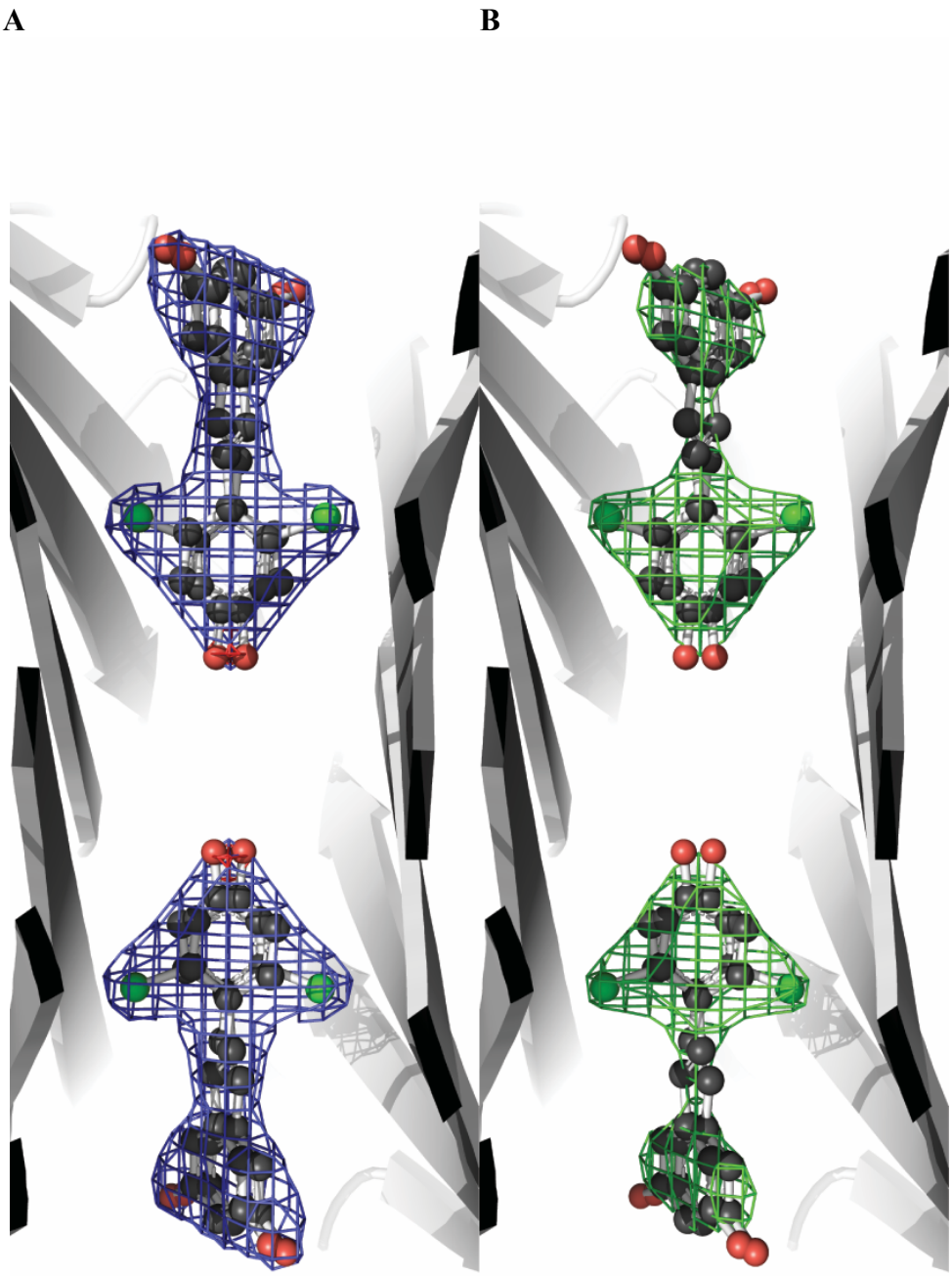

Figure 4.8 Electron density in the TTR·**4.3** complex. (A) Final structure. Blue: $2F_o - F_c$ contoured at 1.0σ; red and green: $F_o - F_c$ contoured at -3.0σ and 3.0σ, respectively. (B) Final structure after ligand removal and refinement by simulated annealing. Green: $F_o - F_c$ contoured at 3.0σ.

Table 4.7 Crystallographic data collection and refinement statistics for TTR in complex with **4.4**.

Complex	**4.4**
PDB Code	5u4a
Data Collection	
X-Ray Source	LS-CAT 21-ID-G
Detector	MAR 300 CCD
Wavelength (Å)	0.97857
Resolution, last shell (Å)	35.5-1.90 (1.96-1.90)
Space group	$P\ 2_1\ 2_1\ 2_1$
Unit cell, *a*, *b*, *c* (Å)	$a = 42.822$, $b = 84.928$ $c = 64.19$
Unit cell, α, β, γ (°)	$\alpha = \beta = \gamma = 90$
No. of Reflections	137456
No. of Unique Reflections	19212 (936)
Redundancy (last shell)	7.2 (7.2)
Mean I/σ (last shell)	19.4 (2.3)
Completeness (last shell)	99.8 (100.0)
R-meas (last shell)	0.097 (0.787)
R-pim (last shell)	0.037 (0.289)
Wilson *B*-factor	33.6
Average Mosaicity (°)	1.4
Refinement	
Working Set (last shell)	17310 (1291)
Test Set (last shell)	1859 (143)
R_{work} (last shell)	0.223 (0.247)
R_{free} (last shell)	0.276 (0.279)
RMSD of Bond Lengths (Å)	0.007
RMSD of Bond Angles (°)	1.03
Total Number of Atoms	1907
Protein Residues	232
Protein	1792
Ligand	40
Water	75
Average *B*-factor	39
Protein	38.9
Ligand	32.4
Water	44.6
Ramachandran Favored, Allowed, Outliers (%) from MolProbity	97.4, 2.2, 0.4

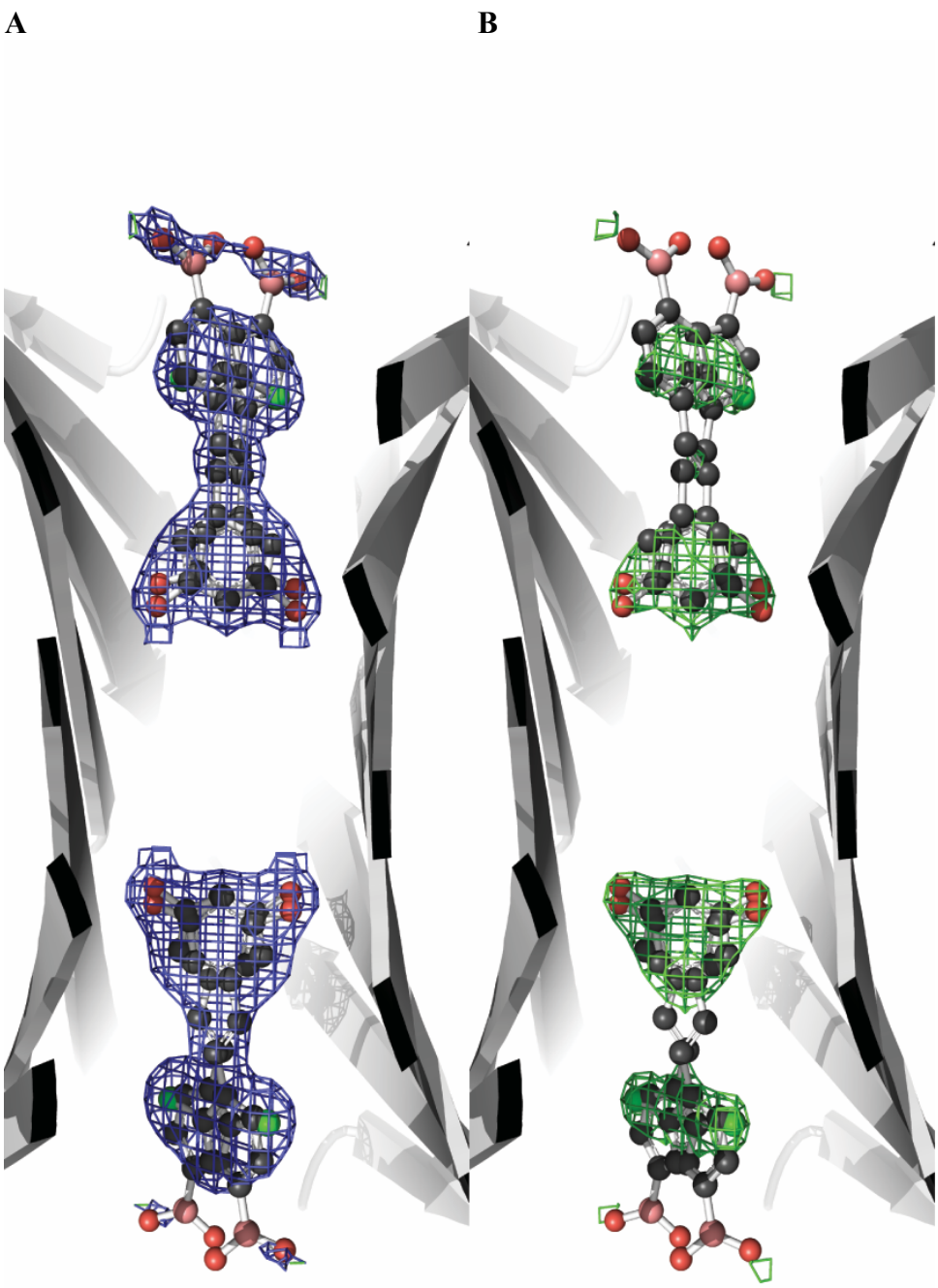

Figure 4.9 Electron density in the TTR·**4.4** complex. (A) Final structure. Blue: $2F_o - F_c$ contoured at 1.0σ; red and green: $F_o - F_c$ contoured at -3.0σ and 3.0σ, respectively. (B) Final structure after ligand removal and refinement by simulated annealing. Green: $F_o - F_c$ contoured at 3.0σ.

Table 4.8 Crystallographic data collection and refinement statistics for TTR in complex with **4.5**.

Complex	**4.5**
PDB Code	5u4b
Data Collection	
X-Ray Source	LS-CAT 21-ID-G
Detector	MAR 300 CCD
Wavelength (Å)	0.97857
Resolution, last shell (Å)	38.5-1.45 (1.5-1.45)
Space group	$P\,2_1\,2_1\,2_1$
Unit cell, *a*, *b*, *c* (Å)	$a = 43.052$, $b = 85.446$ $c = 64.107$
Unit cell, α, β, γ (°)	$\alpha = \beta = \gamma = 90$
No. of Reflections	311252
No. of Unique Reflections	42801 (2112)
Redundancy (last shell)	7.3 (7.2)
Mean I/σ (last shell)	25.4 (2.7)
Completeness (last shell)	99.9 (100.0)
R-meas (last shell)	0.065 (0.582)
R-pim (last shell)	0.024 (0.214)
Wilson *B*-factor	15.4
Average Mosaicity (°)	0.2
Refinement	
Working Set (last shell)	38552 (3756)
Test Set (last shell)	4230 (405)
R_{work} (last shell)	0.185 (0.252)
R_{free} (last shell	0.207 (0.295)
RMSD of Bond Lengths (Å)	0.007
RMSD of Bond Angles (°)	1.035
Total Number of Atoms	2088
Protein Residues	231
Protein	1858
Ligand	72
Water	158
Average *B*-factor	19.6
Protein	18.8
Ligand	26.8
Water	27.3
Ramachandran Favored, Allowed, Outliers (%) from MolProbity	99.2, 0.8, 0

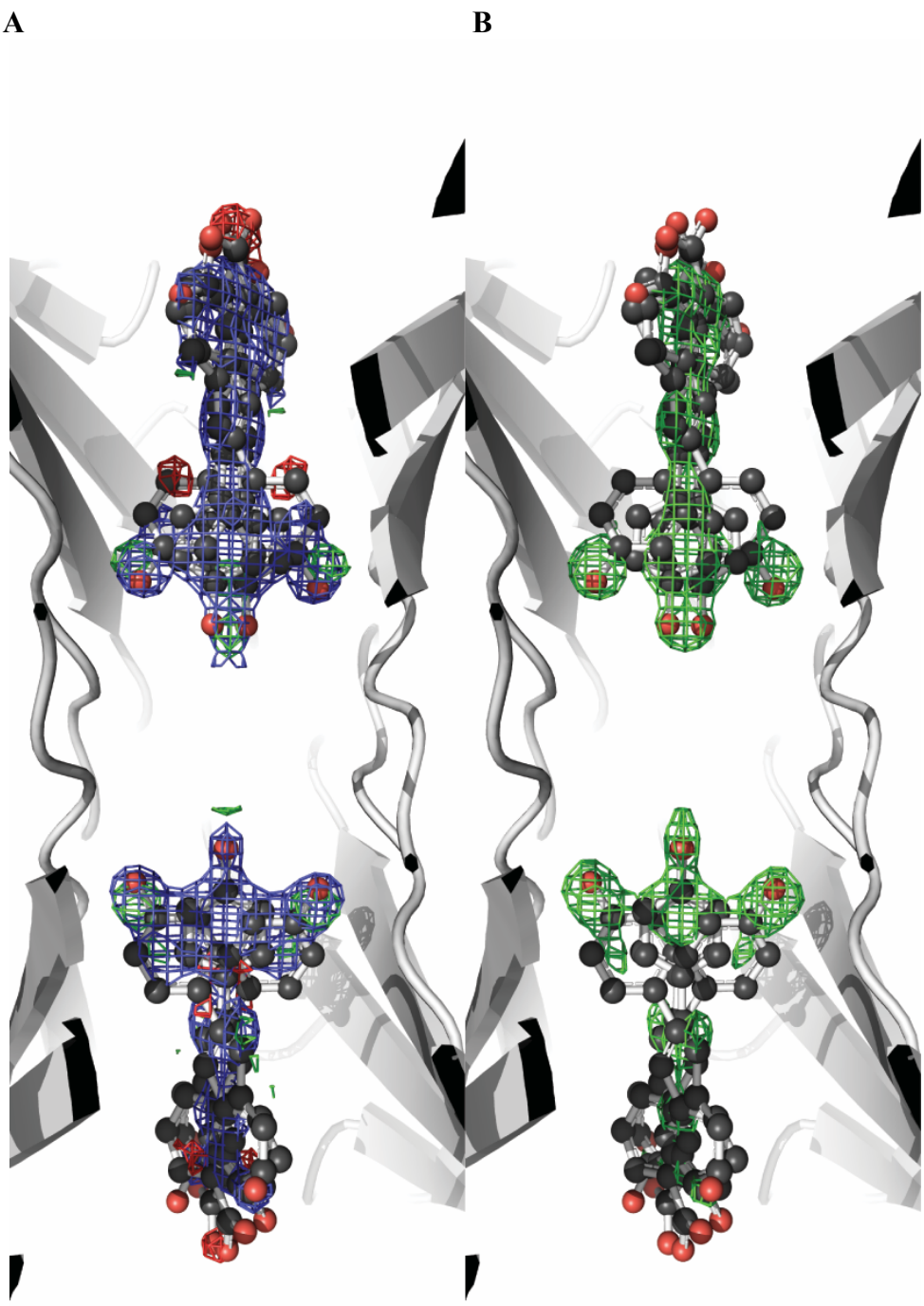

Figure 4.10 Electron density in the TTR·**4.5** complex. (A) Final structure. Blue: $2F_o - F_c$ contoured at 1.0σ; red and green: $F_o - F_c$ contoured at -3.0σ and 3.0σ, respectively. (B) Final structure after ligand removal and refinement by simulated annealing. Green: $F_o - F_c$ contoured at 3.0σ.

Table 4.9 Crystallographic data collection and refinement statistics for TTR in complex with **4.6**.

Complex	**4.6**
PDB Code	5u4c
Data Collection	
X-Ray Source	LS-CAT 21-ID-G
Detector	MAR 300 CCD
Wavelength (Å)	0.97857
Resolution, last shell (Å)	36.0-1.7 (1.76-1.70)
Space group	$P\,2_1\,2_1\,2_1$
Unit cell, *a*, *b*, *c* (Å)	$a = 42.924$, $b = 85.580$ $c = 63.762$
Unit cell, α, β, γ (°)	$\alpha = \beta = \gamma = 90$
No. of Reflections	191623
No. of Unique Reflections	26541 (1303)
Redundancy (last shell)	7.2 (7.1)
Mean I/σ (last shell)	23.9 (2.0)
Completeness (last shell)	99.6 (99.1)
R-meas (last shell)	0.065 (0.818)
R-pim (last shell)	0.024 (0.301)
Wilson *B*-factor	19.4
Average Mosaicity (°)	0.6
Refinement	
Working Set (last shell)	23900 (2334)
Test Set (last shell)	2593 (224)
R_{work} (last shell)	0.176 (0.225)
R_{free} (last shell)	0.204 (0.271)
RMSD of Bond Lengths (Å)	0.007
RMSD of Bond Angles (°)	1.061
Total Number of Atoms	2043
Protein Residues	231
Protein	1869
Ligand	40
Water	134
Average *B*-factor	23.8
Protein	23.7
Ligand	30.8
Water	30.1
Ramachandran Favored, Allowed, Outliers (%) from MolProbity	97.9, 1.7, 0.4

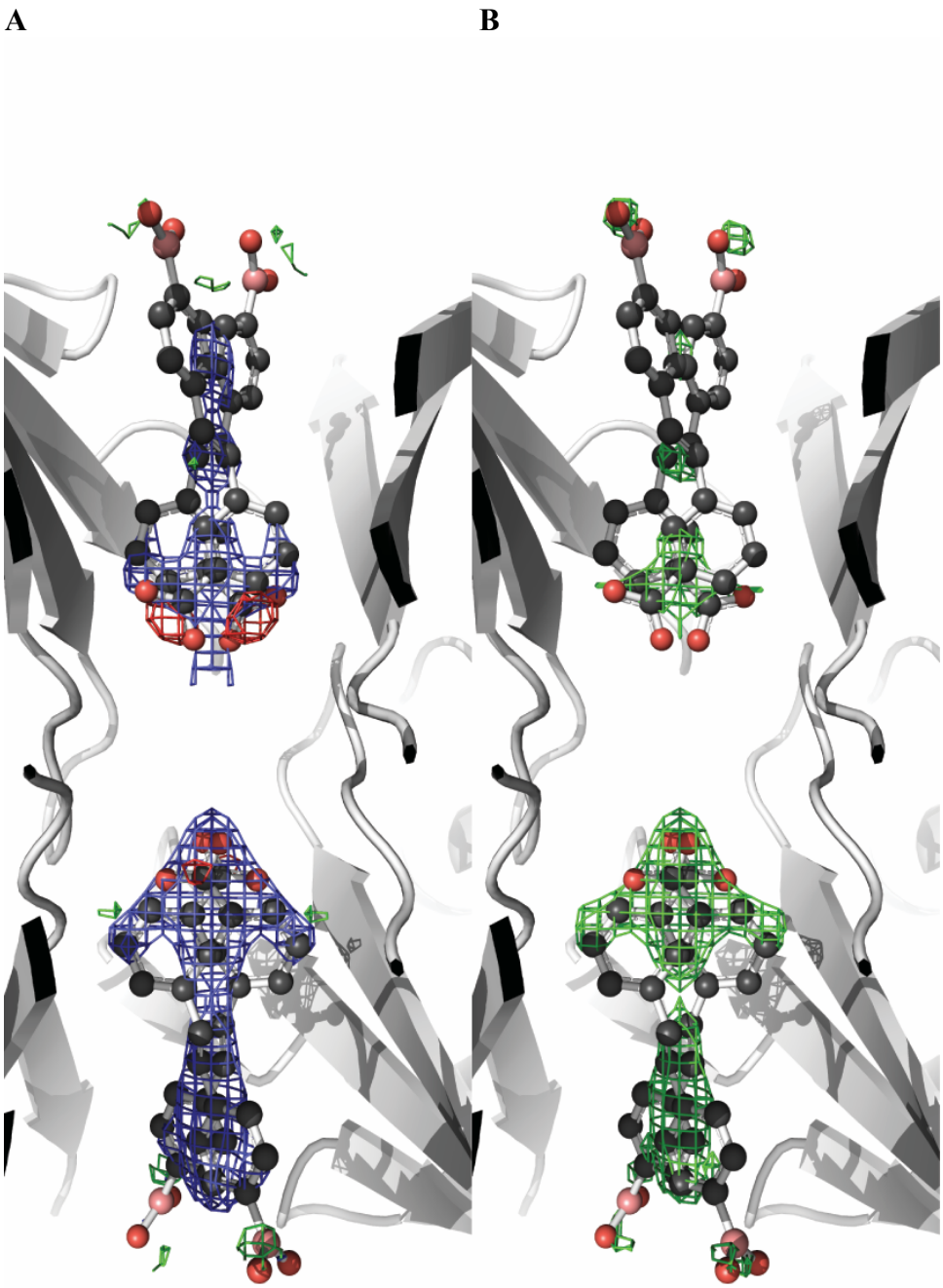

Figure 4.11 Electron density in the TTR·**4.6** complex. (A) Final structure. Blue: $2F_o - F_c$ contoured at 1.0σ; red and green: $F_o - F_c$ contoured at -3.0σ and 3.0σ, respectively. (B) Final structure after ligand removal and refinement by simulated annealing. Green: $F_o - F_c$ contoured at 3.0σ.

Table 4.10 Crystallographic data collection and refinement statistics for TTR in complex with **4.7**.

Complex	**4.7**
PDB Code	5u4d
Data Collection	
X-Ray Source	LS-CAT 21-ID-F
Detector	MAR 225 CCD
Wavelength (Å)	0.97872
Resolution, last shell (Å)	38.5-1.55 (1.60-1.55)
Space group	$P\,2_1\,2_1\,2_1$
Unit cell, *a*, *b*, *c* (Å)	$a = 43.207$, $b = 84.814$ $c = 64.618$
Unit cell, α, β, γ (°)	$\alpha = \beta = \gamma = 90$
No. of Reflections	216074
No. of Unique Reflections	35258 (1735)
Redundancy (last shell)	6.1 (5.2)
Mean I/σ (last shell)	23.7 (2.1)
Completeness (last shell)	99.8 (99.5)
R-meas (last shell)	0.072 (0.675)
R-pim (last shell)	0.028 (0.291)
Wilson *B*-factor	19.2
Average Mosaicity (°)	0.2
Refinement	
Working Set (last shell)	31740 (3067)
Test Set (last shell)	3474 (364)
R_{work} (last shell)	0.206 (0.303)
R_{free} (last shell)	0.243 (0.356)
RMSD of Bond Lengths (Å)	0.007
RMSD of Bond Angles (°)	1.038
Total Number of Atoms	1989
Protein Residues	231
Protein	1821
Ligand	38
Water	130
Average *B*-factor	26.4
Protein	25.8
Ligand	26.6
Water	34.1
Ramachandran Favored, Allowed, Outliers (%) from MolProbity	97.5, 2.5, 0

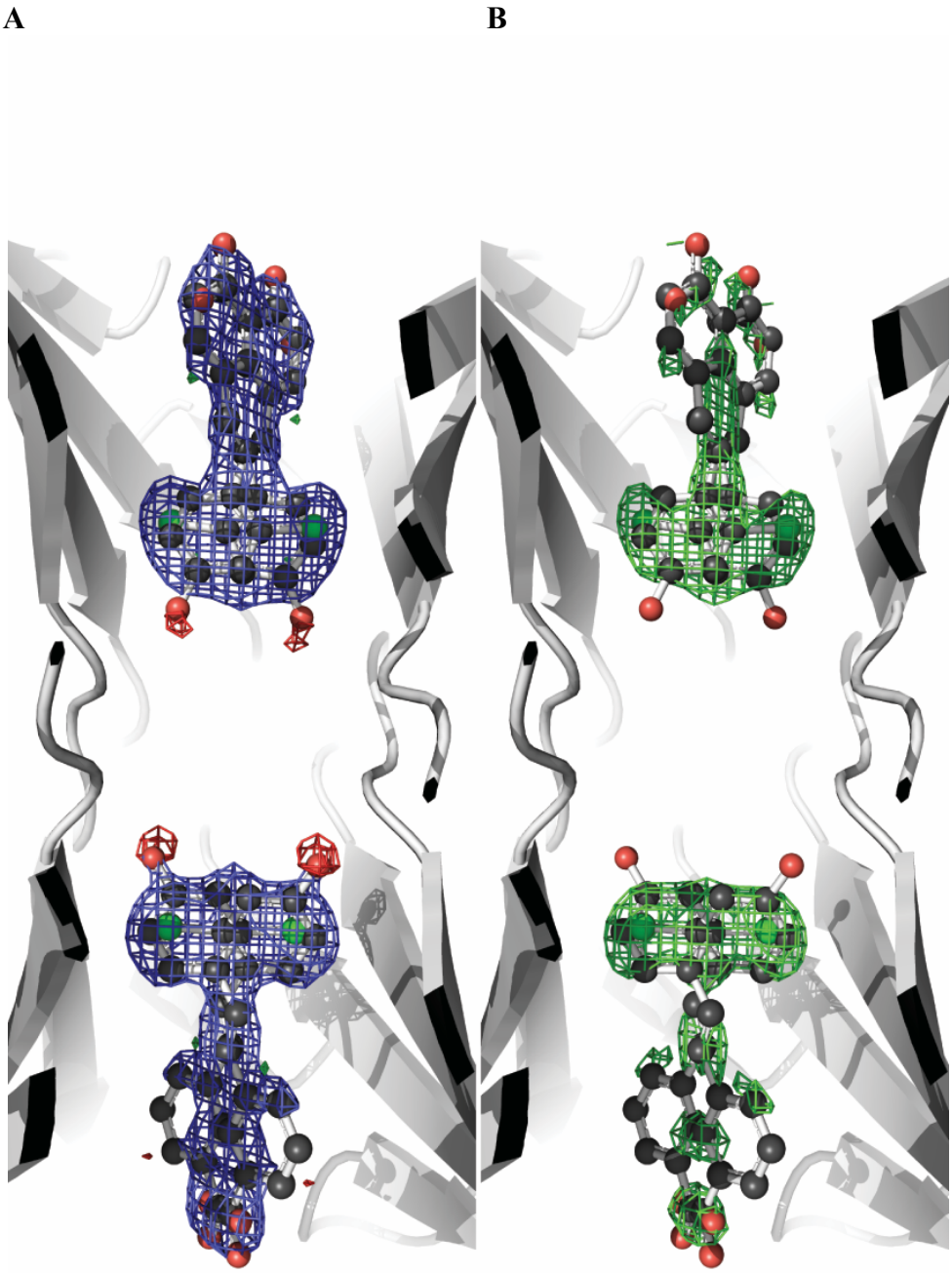

Figure 4.12 Electron density in the TTR·**4.7** complex. (A) Final structure. Blue: $2F_o - F_c$ contoured at 1.0σ; red and green: $F_o - F_c$ contoured at -3.0σ and 3.0σ, respectively. (B) Final structure after ligand removal and refinement by simulated annealing. Green: $F_o - F_c$ contoured at 3.0σ.

Table 4.11 Crystallographic data collection and refinement statistics for TTR in complex with **4.8**.

Complex	**4.8**
PDB Code	5u4e
Data Collection	
X-Ray Source	LS-CAT 21-ID-G
Detector	MAR 300 CCD
Wavelength (Å)	0.97857
Resolution, last shell (Å)	26.0-1.45 (1.50-1.45)
Space group	$P\,2_1\,2_1\,2_1$
Unit cell, a, b, c (Å)	a = 43.029, b = 85.861 c = 63.831
Unit cell, α, β, γ (°)	$\alpha = \beta = \gamma = 90$
No. of Reflections	309849
No. of Unique Reflections	42788 (2094)
Redundancy (last shell)	7.2 (7.1)
Mean I/σ (last shell)	30.2 (2.5)
Completeness (last shell)	100.0 (99.9)
R-meas (last shell)	0.055 (0.659)
R-pim (last shell)	0.20 (0.243)
Wilson B-factor	15.4
Average Mosaicity (°)	0.4
Refinement	
Working Set (last shell)	38504 (3747)
Test Set (last shell)	4229 (405)
R_{work} (last shell)	0.18 (0.259)
R_{free} (last shell)	0.198 (0.290)
RMSD of Bond Lengths (Å)	0.007
RMSD of Bond Angles (°)	1.163
Total Number of Atoms	2154
Protein Residues	231
Protein	1901
Ligand	84
Water	169
Average B-factor	19.8
Protein	19.2
Ligand	20.1
Water	28.6
Ramachandran Favored, Allowed, Outliers (%) from MolProbity	98.4, 1.2, 0.4

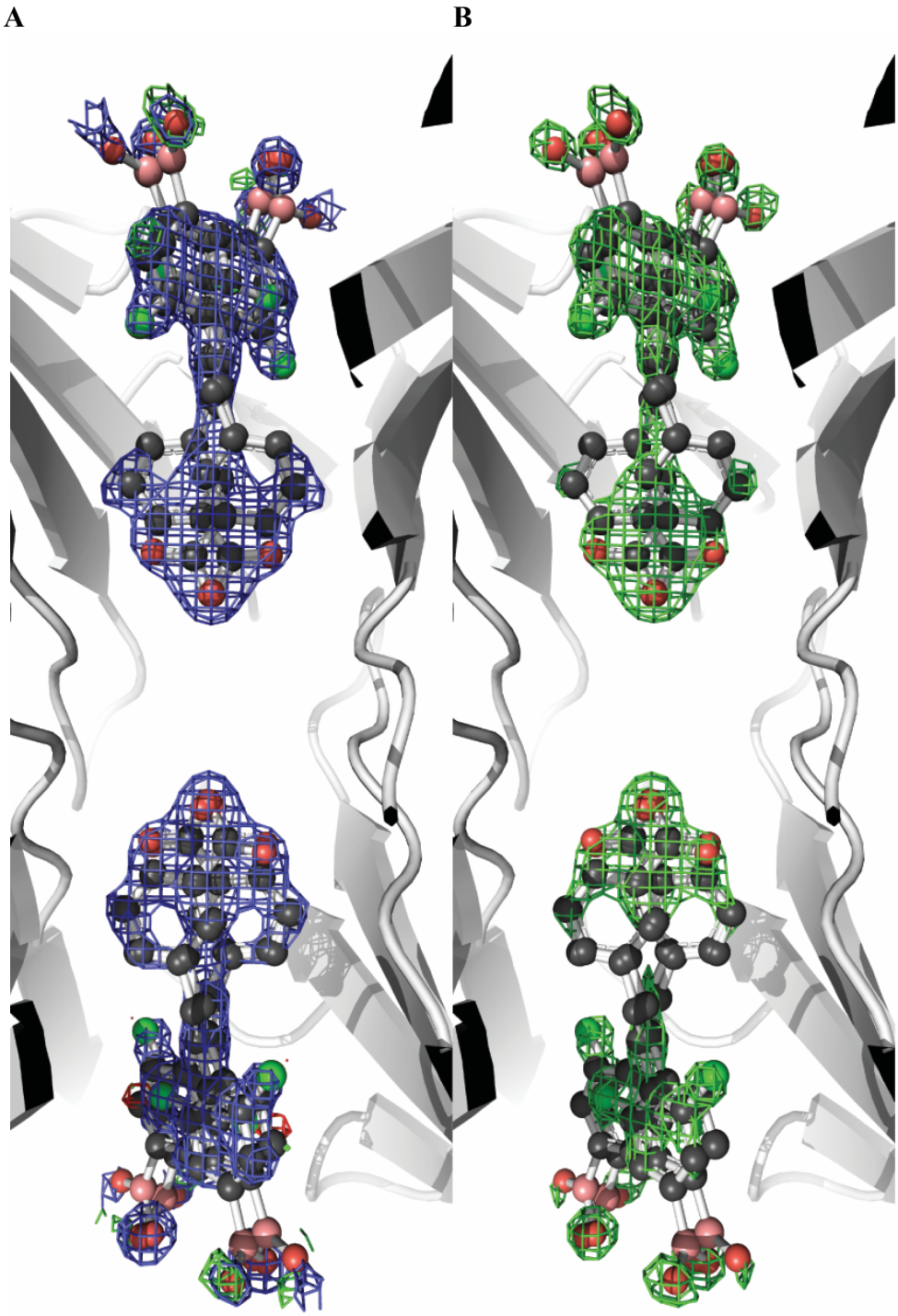

Figure 4.13 Electron density in the TTR·**4.8** complex. (A) Final structure. Blue: $2F_o - F_c$ contoured at 1.0σ; red and green: $F_o - F_c$ contoured at -3.0σ and 3.0σ, respectively. (B) Final structure after ligand removal and refinement by simulated annealing. Green: $F_o - F_c$ contoured at 3.0σ.

Table 4.12 Crystallographic data collection and refinement statistics for TTR in complex with **4.10**.

Complex	**4.10**
PDB Code	5u4f
Data Collection	
X-Ray Source	LS-CAT 21-ID-F
Detector	MAR 225 CCD
Wavelength (Å)	0.97872
Resolution, last shell (Å)	38.5-1.8 (1.86-1.80)
Space group	$P\ 2_1\ 2_1\ 2_1$
Unit cell, *a*, *b*, *c* (Å)	$a = 43.019$, $b = 85.118$ $c = 64.023$
Unit cell, α, β, γ (°)	$\alpha = \beta = \gamma = 90$
No. of Reflections	163190
No. of Unique Reflections	22450 (1087)
Redundancy (last shell)	7.3 (7.3)
Mean I/σ (last shell)	29.4 (3.1)
Completeness (last shell)	99.7 (99.4)
R-meas (last shell)	0.057 (0.513)
R-pim (last shell)	0.021 (0.187)
Wilson *B*-factor	22.8
Average Mosaicity (°)	0.6
Refinement	
Working Set (last shell)	20232 (1898)
Test Set (last shell)	2189 (199)
R_{work} (last shell)	0.188 (0.246)
R_{free} (last shell	0.223 (0.281)
RMSD of Bond Lengths (Å)	0.009
RMSD of Bond Angles (°)	1.207
Total Number of Atoms	1947
Protein Residues	231
Protein	1799
Ligand	40
Water	108
Average *B*-factor	27.6
Protein	27.3
Ligand	30.5
Water	32.6
Ramachandran Favored, Allowed, Outliers (%) from MolProbity	97.9, 1.7, 0.4

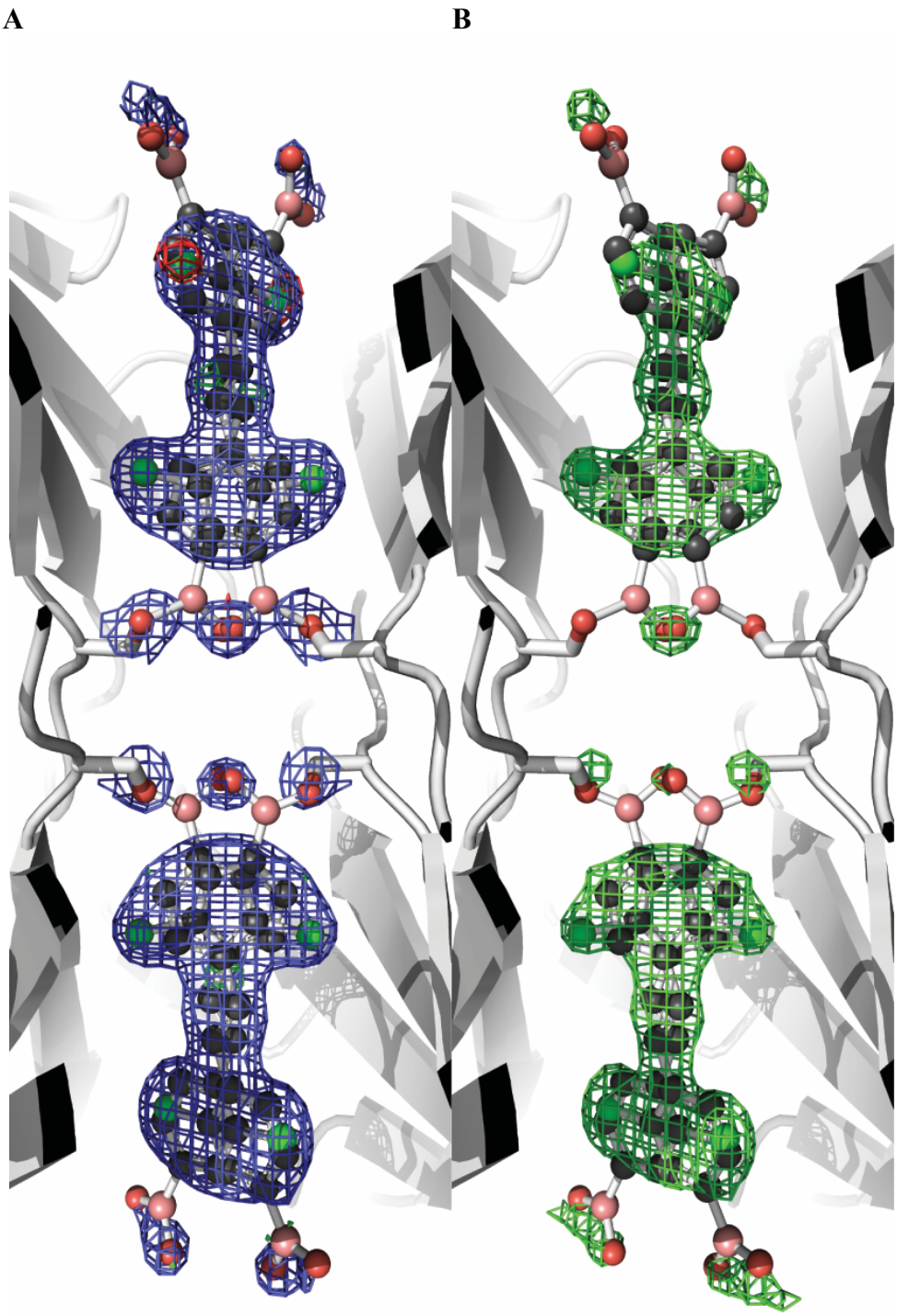

Figure 4.14 Electron density in the TTR·**4.10** complex. (A) Final structure. Blue: $2F_o - F_c$ contoured at 1.0σ; red and green: $F_o - F_c$ contoured at -3.0σ and 3.0σ, respectively. (B) Final structure after ligand removal and refinement by simulated annealing. Green: $F_o - F_c$ contoured at 3.0σ.

Table 4.13 Crystallographic data collection and refinement statistics for TTR in complex with **4.11**.

Complex	**4.11**
PDB Code	5u4g
Data Collection	
X-Ray Source	LS-CAT 21-ID-F
Detector	MAR 225 CCD
Wavelength (Å)	0.97872
Resolution, last shell (Å)	38.5-1.8 (1.86-1.80)
Space group	$P\ 2_1\ 2_1\ 2_1$
Unit cell, *a*, *b*, *c* (Å)	$a = 43.019$, $b = 85.118$ $c = 64.023$
Unit cell, α, β, γ (°)	$\alpha = \beta = \gamma = 90$
No. of Reflections	163190
No. of Unique Reflections	22450 (1087)
Redundancy (last shell)	7.3 (7.3)
Mean I/σ (last shell)	29.4 (3.1)
Completeness (last shell)	99.7 (99.4)
R-meas (last shell)	0.057 (0.513)
R-pim (last shell)	0.021 (0.187)
Wilson *B*-factor	22.8
Average Mosaicity (°)	0.6
Refinement	
Working Set (last shell)	20232 (1898)
Test Set (last shell)	2189 (199)
R_{work} (last shell)	0.188 (0.246)
R_{free} (last shell	0.223 (0.281)
RMSD of Bond Lengths (Å)	0.009
RMSD of Bond Angles (°)	1.207
Total Number of Atoms	1947
Protein Residues	231
Protein	1799
Ligand	40
Water	108
Average *B*-factor	27.6
Protein	27.3
Ligand	30.5
Water	32.6
Ramachandran Favored, Allowed, Outliers (%) from MolProbity	97.9, 1.7, 0.4

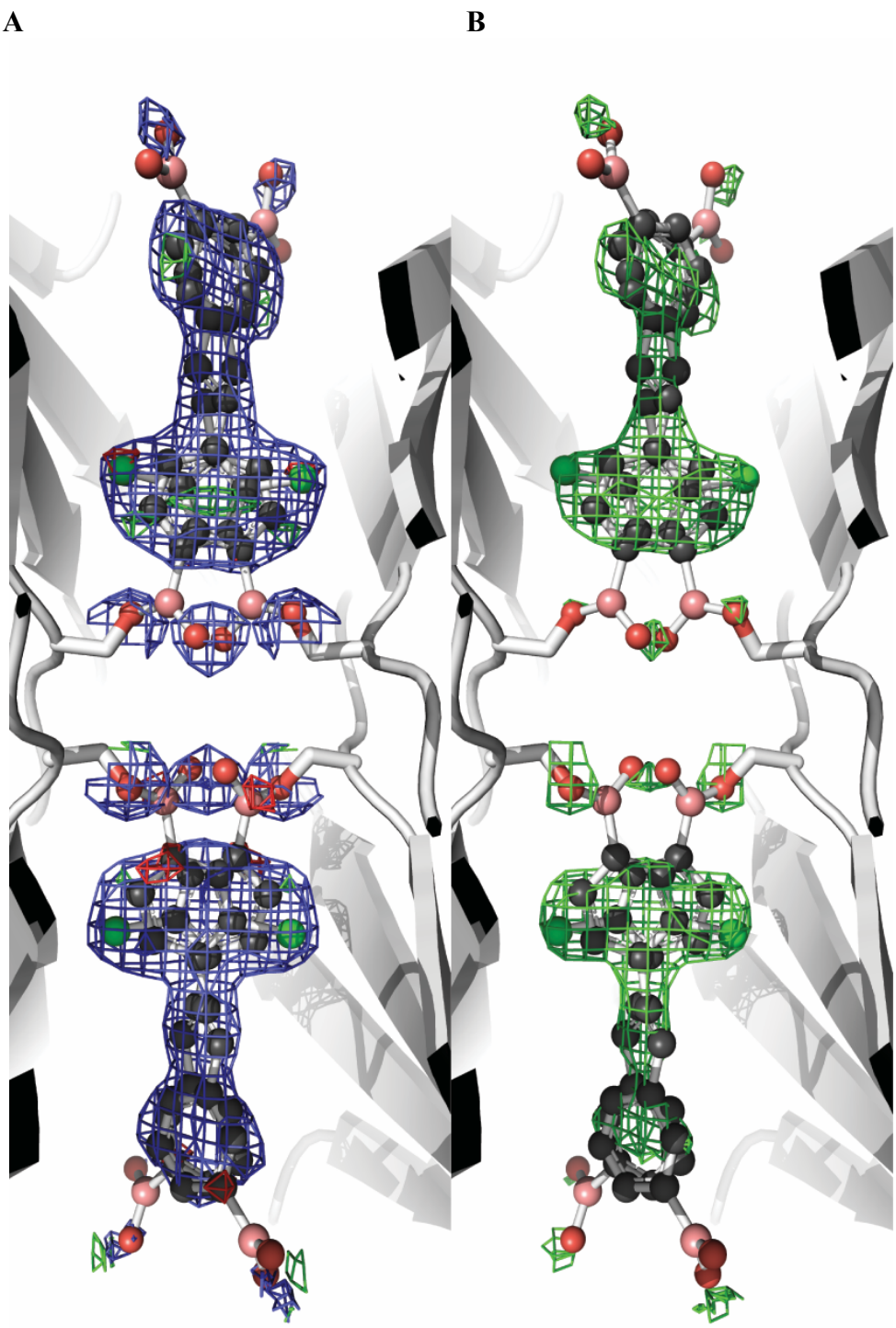

Figure 4.15 Electron density in the TTR·**4.11** complex. (A) Final structure. Blue: $2F_o - F_c$ contoured at 1.0σ; red and green: $F_o - F_c$ contoured at -3.0σ and 3.0σ, respectively. (B) Final structure after ligand removal and refinement by simulated annealing. Green: $F_o - F_c$ contoured at 3.0σ.

Table 4.14 Non-covalent interactions and distances in TTR·ligand complexes.

Ligand	Interaction type	Ligand atom	Protein atom	Distance (Å)
4.2	Dative	B01/A	NZ, A/15 Lys/A	2.8
4.2	Dative	B01/B	NZ, A/15 Lys/B	3.2
4.2	Dative	Average	—	3.0
4.2	Hydrogen bond	O04/A	NZ, A/15 Lys′/A	2.6
4.2	Hydrogen bond	O03/B	NZ, A/15 Lys′/B	2.2
4.2	Hydrogen bond	Average	—	2.4
4.2	Hydrogen bond	O02/A	OG,A/117 Ser/A	2.7
4.2	Hydrogen bond	O02/A	OG,B/117 Ser/A	3.0
4.2	Hydrogen bond	O01/A	OG,A/117 Ser′/A	2.7
4.2	Hydrogen bond	O01/A	OG,B/117 Ser′/A	2.7
4.2	Hydrogen bond	O02/A	OG,A/117 Ser/B	3.0
4.2	Hydrogen bond	O02/A	OG,B/117 Ser/B	2.7
4.2	Hydrogen bond	O01/A	OG,A/117 Ser′/B	2.9
4.2	Hydrogen bond	O01/A	OG,B/117 Ser′/B	2.6
4.2	Hydrogen bond	Average	—	2.8
4.3	Hydrogen bond	O02/A	OG,A/117 Ser/A	2.4
4.4	Dative	B01/A	NZ, A/15 Lys/A	3.4
4.4	Dative	B01/B	NZ, A/15 Lys/B	4.4
4.4	Dative	Average	—	3.9
4.4	Hydrogen bond	O03/A	NZ, A/15 Lys′/A	3.4
4.4	Hydrogen bond	O03/B	NZ, A/15 Lys′/B	3.0
4.4	Hydrogen bond	Average	—	3.2
4.4	Hydrogen bond	O01/A	OG,A/117 Ser/A	2.2
4.4	Hydrogen bond	O21/A	OG,A/117 Ser′/A	3.0
4.4	Hydrogen bond	O02/B	OG,A/117 Ser/B	2.1
4.4	Hydrogen bond	O01/B	OG,A/117 Ser′/B	2.8
4.4	Hydrogen bond	Average	—	2.5
4.5	Hydrogen bond	O01,A/A	OG,A/117 Ser′/B	2.7
4.5	Hydrogen bond	O01,A/A	OG,B/117 Ser′/B	2.9
4.5	Hydrogen bond	O01,B/A	OG,A/117 Ser′/B	2.4
4.5	Hydrogen bond	O01,B/A	OG,B/117 Ser′/B	2.5
4.5	Hydrogen bond	O01,A/B	OG,A/117 Ser′/A	3.0
4.5	Hydrogen bond	O01,A/B	OG,A/117 Ser′/A	2.6
4.5	Hydrogen bond	O01,B/B	OG,A/117 Ser′/A	3.3
4.5	Hydrogen bond	O01,B/B	OG,A/117 Ser′/A	2.8
4.5	Hydrogen bond	Average	—	2.8
4.5	Hydrogen bond	O03/B	NZ, A/15 Lys/A	2.5
4.5	Hydrogen bond	O02/B	NZ, A/15 Lys′/A	3.6
4.5	Hydrogen bond	Average	—	3.1
4.6	Dative	B01/A	NZ, A/15 Lys/A	2.9
4.6	Dative	B01/B	NZ, A/15 Lys′/B	3.0
4.6	Hydrogen bond	Average	—	3.0
4.6	Hydrogen bond	O02/A	NZ, A/15 Lys′/A	3.0

4.6	Hydrogen bond	O01/B	NZ, A/15 Lys/B	4.0
4.6	Hydrogen bond	Average	—	3.5
4.6	Hydrogen bond	O03/A	OG,A/117 Ser′/A	3.1
4.6	Hydrogen bond	O03/A	OG,B/117 Ser′/A	2.9
4.6	Hydrogen bond	O04/A	OG,A/117 Ser′/A	2.7
4.6	Hydrogen bond	O04/A	OG,B/117 Ser′/A	2.3
4.6	Hydrogen bond	O03/B	OG,A/117 Ser/B	3.0
4.6	Hydrogen bond	O03/B	OG,B/117 Ser/B	3.1
4.6	Hydrogen bond	O04/B	OG,A/117 Ser/B	2.4
4.6	Hydrogen bond	O04/B	OG,B/117 Ser/B	2.5
4.6	Hydrogen bond	Average	—	2.8
4.7	Hydrogen bond	O03/A	OG, A/117 Ser′/A	2.2
4.7	Hydrogen bond	O03/B	OG, A/117 Ser/B	2.3
4.7	Hydrogen bond	Average	—	2.3
4.7	Hydrogen bond	O01/A	NZ, A/15 Lys/A	2.7
4.7	Hydrogen bond	O02/A	NZ, A/15 Lys′/A	2.3
4.7	Hydrogen bond	Average	—	2.5
4.8	Dative	B01,A/A	NZ, A/15 Lys/A	2.9
4.8	Dative	B01,A/B	NZ, A/15 Lys′/B	2.9
4.8	Cative	Average	—	2.9
4.8	Hydrogen bond	O02,A/A	NZ, A/15 Lys′/A	3.0
4.8	Hydrogen bond	O01/B	NZ, A/15 Lys/B	3.0
4.8	Hydrogen bond	Average	—	3.0
4.8	Hydrogen bond	O03/A	OG,A/117 Ser′/A	2.9
4.8	Hydrogen bond	O03/A	OG,B/117 Ser′/A	2.6
4.8	Hydrogen bond	O04/A	OG,A/117 Ser′/A	2.7
4.8	Hydrogen bond	O04/A	OG,B/117 Ser′/A	3.0
4.8	Hydrogen bond	O03/B	OG,A/117 Ser/B	2.8
4.8	Hydrogen bond	O03/B	OG,B/117 Ser/B	3.0
4.8	Hydrogen bond	O04/B	OG,A/117 Ser/B	2.5
4.8	Hydrogen bond	O04/B	OG,B/117 Ser/B	2.7
4.8	Hydrogen bond	Average	—	2.8
4.10	Dative	B02/A	NZ, A/15 Lys/A	3.5
4.10	Hydrogen bond	O03/A	NZ, A/15 Lys′/A	3.6
4.10	Hydrogen bond	O02/A	NZ, A/15 Lys′/A	2.7
4.10	Hydrogen bond	O03/B	NZ, A/15 Lys′/B	2.6
4.10	Hydrogen bond	Average	—	2.7
4.11	Dative	B01/A	NZ, A/15 Lys/A	3.2
4.11	Hydrogen bond	O02/A	OG,B/117 Ser′/A	2.8
4.11	Hydrogen bond	O/04/B	OG,B/117 Ser′/B	3.0
4.11	Hydrogen bond	Average	—	2.9

Table 4.15 Observed sigma-hole bond lengths and bond angles in TTR·ligand complexes reported in this work.

Ligand	Ligand atom	Protein residue	Length	$\theta_{C–Cl–O}$	$\theta_{Cl–O–C}$
4.10	Cl02/A	108 Ala′/A	3.65	175.4	83.4
4.10	Cl02/B	108 Ala′/B	3.64	174.9	87.8
4.11	Cl01/A	108 Ala′/A	3.73	173.4	85.1
4.11	Cl01/B	108 Ala′/B	3.66	175.3	84.3
		Average	3.67	174.8	85.2

5

Future Directions

5.1 Stimuli-responsive boronic acids for protein delivery

The practical use of boronic acids to facilitate protein delivery is still in the early stages of development. With ongoing improvements in boronic acid-based cellular recognition, and binding to select glycans and antigens,[23,24,101] boronic acid-mediated delivery will undoubtedly continue to see a surge in interest and application. Although the idea of "smart", or stimuli responsive, carriers or materials for biomedical applications is well established,[264,265] this approach has yet to be significantly incorporated into boronic acid-based delivery.

With modular principles kept in mind, boronic acids with immolative linkers can be accessed easily by chemical synthesis. In chapter 2, I described an esterase-sensitive boronic acid for the release of a native protein. Selective removal of boronate appendages can be engineered into the molecule via alternative linkers. One such boronate, which incorporates a methyl maleic anhydride motif, could still access solvent exposed lysine residues but would be removed under acidic conditions (Figure 5.1, compound **5.1**).[266,267]

Acidic sensitivity is a good trigger for controlled release, especially for biopharmaceuticals, since the endosomal pathway is the most likely mechanism of uptake.[31] As the endosome matures into a lysosome, it becomes more acidic. Acid sensitive linkers could be developed to incorporate newly established borolectins, such as those developed by the Dennis

Hall and coworkers, for improved cell-recognition and multidentate binding (Figure 5.1, compound **5.2**).[105]

5.2 Investigation of boronic acids to increase protein serum retention

Boronic acids are well known to interact with biological polyols such as saccharides. I and others have exploited this interaction to facilitate cellular up-take of protein therapeutics by targeting the glycocalyx. Nevertheless, in the circulatory system, which is often a common route of entry for biopharmaceuticals, contains a number of glycoproteins as well as erythrocytes,[268] which possess complex saccharides that could coordinate with boronic acid-labeled proteins.

An open question is whether boronic acids could also be used as a way to increase retention time of macromolecules in serum by interacting with different components within the circulatory system. This goal could be accomplished by developing a boronic acid functionalized MRI or PET contrast agent such as compound **5.3** (Figure 5.2) and compare circulation times *in vivo* to that of the same agent lacking the boronic acid. If boronic acids prove to increase the circulation times of protein therapeutics, then this approach would allow for new design strategies to move away from the common PEGylated-based systems, which are known to be detrimental to enzymatic function.

5.3 Characterization of the mode of action for boronic acid stabilizers of TTR amyloidosis

In chapter 4, I described the synthesis of a small library of boronic acid–stilbene compounds for the stabilization of the quaternary structure of transthyretin (TTR). TTR is notorious for binding a wide variety of organic molecules without a clear structure–activity relationship (SAR).[242,269] One major observation from our studies was the preference for mono-

boronic acids to consistently bind in the "reverse" binding mode compared to the paired phenolic control molecule.

The observation that mono-boronated small molecules prefer to bind in one binding mode despite significant structural changes to the scaffold suggests that boronic acids may have a particular mode of action in the context of binding the T_4 pocket of TTR. Elucidating this mechanism is important for future small-molecule boronic acid-based inhibitors of TTR amyloidosis. There are a number of factors that could be perturbed. Alterations in the pK_a value of certain functional groups are known to affect the orientation of the binding mode.[247,270] Additionally, halogen bonding is known to play a role.[241] Both of these aspects can be investigated thoroughly.

Understanding the mode of action for boronic acid could also have an impact on the larger role of small-molecule boronic acid therapeutics. There is some recent evidence of boronic acid-containing compounds coordinating in unexpected ways with either active-site residues[271] or bulk solvent.[272] Careful structural studies might improve future therapeutic design, especially considering the growing interest in boronic acid-based therapeutics.[25,26,118]

Scheme 5.1

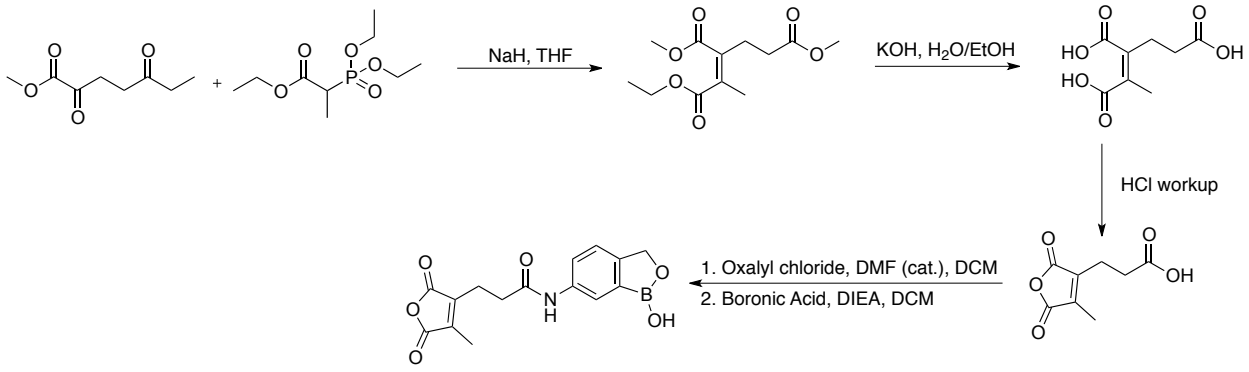
NaH, THF
KOH, H2O/EtOH
HCl workup
1. Oxalyl chloride, DMF (cat.), DCM
2. Boronic Acid, DIEA, DCM

5.1

Scheme 5.1 Proposed synthesis of acid-labile boronic acid **5.1** for protein delivery.

Figure 5.1

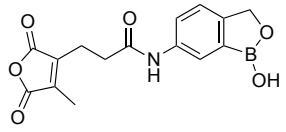

5.1

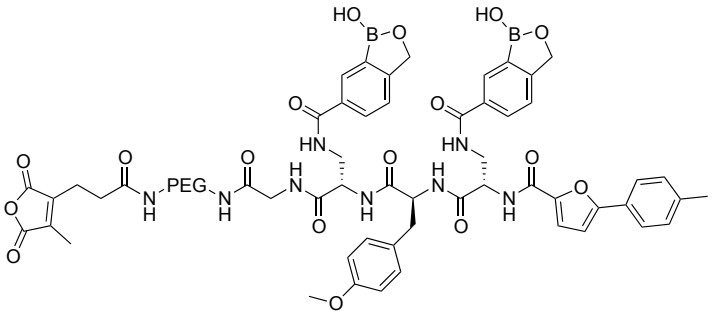

5.2

Figure 5.1 Proposed acid-labile boronic acids for protein delivery and cell-type specificity.

Figure 5.2

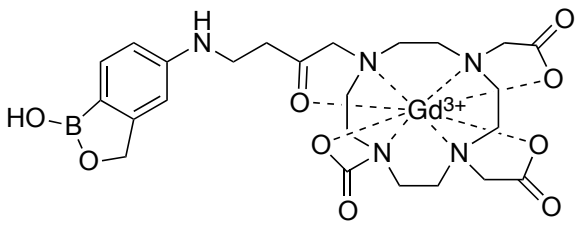

Figure 5.2 Proposed boronic acid–based MRI contrast agent for studying serum retention.

Appendix: Towards a boronic acid-based "pro/soft" drug strategy

A.1 Abstract

The unregulated increase of reactive oxygen species (ROS), resulting in oxidative damage, has been linked to several human disease states including neurodegeneration, diabetes, and cancer. Current small-molecule anti-oxidants have had limited clinical success as potential therapeutics, despite promising pre-clinical results. One potential pharmacokinetic issue could be a high rate of metabolism and excretion. We propose a general boronic acid-masking strategy that allows small-molecule anti-oxidants to be activated selectively in the presence of ROS while controlling the mechanism of inactivation and metabolism.

A.2 Author Contributions

T.P.S. proposed the use of boronic acids as a way to mask radical scavenging ability of dietary anti-oxidant molecules. A.A.P. synthesized and characterized a small library of anti-oxidant analogs containing boronic acids. T.P.S. and A.A.P. preformed preliminary *in vitro* and *in cellulo* studies.

A.3 Rational

Reactive oxygen species (ROS) have important roles in cellular function including cellular signaling, differentiation, and protection.[273-276] Under normal physiological conditions, mammalian cells utilize endogenous anti-oxidant enzymes, as well as small-molecule reducing agents, to tightly regulate the concentration of ROS within cells.[107] Nevertheless, the up-regulation of ROS, including the major ROS hydrogen peroxide (H_2O_2), has been correlated with oxidative stress that is causative in a variety of human diseases, such as neurodegeneration, diabetes, and cancer.[109-111,277] In addition, an interaction between free Cu^{+} or Fe^{2+} and H_2O_2 will generate hydroxide radicals (•OH) via a metal-catalyzed Fenton reaction (Figure A.1).[107,278,279] Hydroxide radicals are particularly damaging to cellular components because of their non-specific reactivity towards biomolecules such as DNA, proteins, and lipids. This reactively manifests with symptoms of hemochromatosis, overt copper toxicity, and inflammation.[276,280,281] More importantly, there are no known endogenous mechanisms to neutralize this particular ROS.[107]

Organisms rely on dietary-based small-molecule anti-oxidants as radical scavengers. These include flavin-containing compounds, whose anti-oxidant activity arises from conjugated nitrogen heterocycles, as well as phenolic molecules, such as vitamin C, vitamin E, and many types of carotenoids.[282,283] The latter examples possess phenolic substituents on highly conjugated scaffolds that can react with hydroxyl radicals, and subsequently delocalize an electron through a conjugated π-system to decrease its reactivity (Scheme A.1).[284]

Although poly-phenol anti-oxidants can be effective radical scavengers, they can be quickly metabolized and excreted from the body.[285] This rapid removal arises from the two phases of small-molecule metabolism.[286,287] Phase I metabolism employs the cytochrome P450

class of enzymes to oxidize organic molecules by placing reactive handles, such as phenols, on aryl rings or by unmasking nucleophilic functional groups, such as reducing an amide bond to an amine.[288] This process provides therapeutic organic molecules with a nucleophile for phase II metabolism.

Phase II involves multiple transferase enzymes to conjugate polar functional groups such as glucuronic acid, amino acids, sulfates, and glutathione to the products of phase I.[288] This process increases the hydrophilicity of the small molecule and accelerates its excretion from the body. One major limitation of poly-phenol anti-oxidants is that they already possess a nucleophilic handle poised for phase II modification. For these reasons, as well as many others, phenolic-based anti-oxidants have had limited clinical success, despite promising results in pre-clinical testing.[289-291]

Boronic acid can be used as a general masking agent for phenolic functional groups. As I described in chapters 2 and 3, boronic acids are physiologically benign and will chemoselectively oxidize to a phenol through a hydroboration-oxidation mechanism in the presence of H_2O_2. This strategy has been employed in both peroxide sensing technology[106] as well as a pro-drug meathod.[116]

There are a number of benefits for a boronic acid anti-oxidant. First, in the absence of H_2O_2, the boronate analogue remains in its inactive form, giving the small-molecule pro-drug like characteristics. Second, and more importantly, the boronic acid could potentially increase retention time by forcing the molecule through phase I metabolism and improve its therapeutic value.[292] Lastly, the active antioxidant will have a predictable and controlled route of metabolic inactivation, giving this analog soft-drug characteristics. Ideally, boronic acids will provide

small-molecule anti-oxidants with selective activation under oxidative stress as well as a protective mask from cellular metabolism while traveling to the site of action.

A.4 Preliminary Results and Discussion

Naturally derived phenolic anti-oxidants were chosen for their known radical scavenging ability and biological safety. Additionally, since oxidative damage can occur to both cytosolic and membrane components, molecules with varying log*P* values were selected (Figure A.2). With the exception of compounds **A.3** and **A.4**, each boronate was accessed directly from the commercially available phenol through triflate activation, followed by palladium-catalyzed cross-coupling of pinacol boronate, and subsequent deprotection.

The substitution with a boronic acid abolishes radical scavenging ability *in vitro*. A radical scavenging assay using 2,2-diphenyl-1-picrylhdrazyl (DPPH) indicated that for compounds **A.6** and **A.7**, the presence of the boronic acid did not lead to the reduction of DPPH (Figure A.2). In contrast, after exposure to an equivalent concentration of H_2O_2 for 1 h, the radical scavenging ability of **A.6** and **A.7** returned by approximately 50% and 30% respectively, relative to the positive controls (**A.2** and **A.3**).

Compounds **A.5** and **A.8** did not perform as well as expected. This underperformance could be due to steric interactions from the *ortho*-substituents leading to instability and protodeboronation of the boronic acid functionality.[293] Indeed, attempts to deprotect **A.8** to acquire the free boronic acid often resulted in the protodeboronated product. For these reasons, these molecules were not characterized further by studies *in cellulo*.

The boronated small molecules were not toxic towards HEPG2 hepatocytes. Compounds **A.6** and **A.7**, as well as their respective control molecules (**A.2** and **A.3**), did not show any

inherent toxicity in HEPG2 cells up to 100-μM range (Figure A.3). Interestingly, compound **A.7** and its control **A.3** showed *enhanced* toxicity at 100 μM relative to a vehicle control with increasing concentrations of H_2O_2 (Figure A.4). Although synergistic toxicity is known in the literature,[294,295] these experiments need to be repeated under more stringent experimental conditions to confirm this observation.

Compound **A.6** was found to decrease the observed concentration of ROS *in cellulo* relative to the parent control. In a fluorescent DCFH–DA assay for intracellular ROS, pre-treatment of HEPG2 cells with **A.6** showed a decrease in the rate of intracellular ROS generation over time compared to pre-treatment of either the vehicle control or with **A.2** (Figure A.5). There are two possible reasons for this observation. The boronic acid can interact with H_2O_2 to form water and boric acid, removing up to one stoichiometric equivalent of H_2O_2, or the boronic acid takes longer to be removed compared to the parent control, leading to sustained cellular protection. It is likely that both mechanisms are operating co-currently.

A.5 Conclusions and Future Directions

In summary, I have described preliminarily work towards the development of a potential pro/soft-drug strategy for phenolic-based anti-oxidants using boronic acid. Boronic acid has been used previously as a viable pro-drug strategy, but has not been explored as a method to specifically attenuate drug metabolism. A few examples exist in the literature describing the metabolic byproducts of boronic acid-containing small-molecules,[296-299] but future work in this area needs to characterize fully both the rate and the extent of boronic acid metabolism.

Future studies should focus on both cellular protection as well as cellular recovery. These studies require additional assays of both the levels of intracellular ROS and cellular viability.

Additional small-molecule boronic acids could also be explored for more effective radical-scavenging ability. These boronic acids could be based on either simple natural products or synthetic scaffolds with different physiological characteristics, such as CNS targeting or metal-chelating ability.[300,301] In addition, studies on how these molecules affect lipid peroxidation *in vitro* would be informative. Finally, the mechanism of boronic acid metabolism is not well defined, and it is important to determine experimentally how these molecules are processed physiologically.

A.6 Materials and Methods

A.6.1 General Information

All chemicals were from Sigma–Aldrich (Milwaukee, WI) and were used without further purification. All glassware was flame-dried and all reactions were performed under an inert nitrogen atmosphere. Reagent grade solvents; dichloromethane (DCM), tetrahydrofurane (THF), triethylamine (TEA), and dimethylformamide (DMF), were dried over a column of alumina and were removed from a dry still under inert atmosphere. Removal of solvents "under reduced pressure" refers to the use of a rotary evaporator water-aspirator pressure (<20 torr) and water bath of <40 °C. Flash column chromatography was performed with Silicycle 40–63 Å silica (230–400 mesh) and thin layer chromatography (TLC) was performed with EMD 250 μm silica gel 60-F254 plates.

^{1}H and ^{13}C NMR spectra were acquired at ambient temperature with a Bruker Avance III 500i spectrometer at the National Magnetic Resonance Facility at Madison (NMRFAM) and referenced to residual protic solvent. Mass spectrometry was performed with a Micromass LCT (electrospray ionization, ESI) in the Mass Spectrometry Facility in the Department of Chemistry at the University of Wisconsin–Madison. Absorbance measurements were made with an infinite M1000 plate reader from Tecan (Männedorf, Switzerland).

HEPG2 cell lines were obtained from ATCC and cultured in a 50-mL cell culture flask with Dulbecco's Modified Eagle Medium (DMEM). Cells were allowed to incubate at 37 °C in a 5% CO_2 atmosphere. Cells were split at 90% confluence by removing medium, washing with Dulbecco's Phosphate Buffered Saline (DPBS) and incubating with 0.25% Trypsin/EDTA for 5 minutes. After cell dissociation, DMEM was added to the flask and cells were split 1:4 into a new 50 mL Corning surface cell culture flask.

A.6.2 Chemical Synthesis

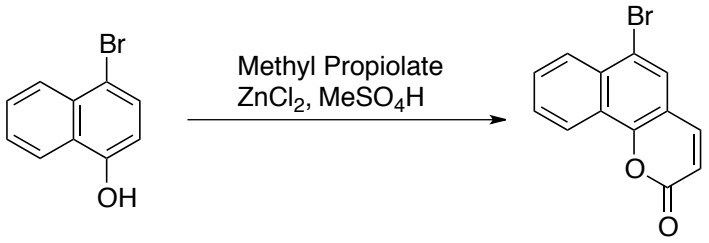

A.7.2

4-Bromo-1-napthol (1.000 g, 4.48 mmol) and $ZnCl_2$ (1.221 g, 8.96 mmol) were dissolved in methane sulfonic acid (22 mL). Methyl propionate (0.789 g, 8.96 mmol) was added, and the reaction mixture was heated to 70 °C and stirred overnight. The reaction mixture was then cooled to room temperature, and the solvent was removed under reduced pressure. The crude product was purified via flash column chromatography (50% v/v DCM:hexanes) to afford **A.7.2** as a white solid (0.510 g, 41%).

^{1}H NMR (500 MHz, $CDCl_3$ δ): 6.48–6.46 (d, J = 9.50, 1H), 7.39–7.41 (d, J = 8.53 Hz, 1H), 7.59–7.64 (m, 3H), 7.76–7.78 (d, J = 9.44Hz, 1H), 7.83–7.82 (d, J = 5.46 Hz, 1H), 8.49–8.46 (d, J = 5.21 Hz, 1H); **^{13}C NMR (125 MHz, $CDCl_3$, δ)**: 114.18, 115.84, 122.20, 122.95, 123.52, 124.37, 127.11, 127.74, 128.65, 134.75, 144.13, 151.20, 160.87; **HRMS–ESI (*m/z*)**: $[M + NH_4]^+$ calcd for $C_{13}H_7BrO_2$, 291.9968; found, 291.9959.

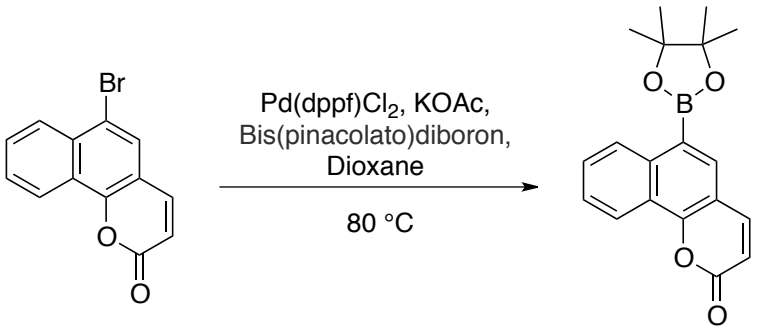

A.7.2 **A.7.3**

Compound **A.7.2** (0.250 g, 0.91 mmol), KOAc (0.268 g, 2.73 mmol), $Pd(dppf)Cl_2$ (0.067 g, 0.091 mmol), and bis(pinacolato)diboron (0.693g, 2.73mmol) were added to a Schlenk flask, which was then evacuated and backfilled with N_2(g). Dioxane (9.1 mL) was deoxygenated by sonication under high vacuum and backfilled with N_2(g). Deoxygenated dioxane was then cannulated into the reaction flask. The reaction mixture was heated to 80 °C and stirred overnight. The reaction mixture was filtered, and the solvent was removed under reduced pressure. The crude product was purified via flash column chromatography (15% v/v EtOAc:hexanes) to afford **A.7.3** as a white solid (0.11 g, 37%).

^{1}H NMR (500 MHz, CD_3OD, δ): 1.45 (s, 12H), 6.54–6.56 (d, J = 9.44, 1H), 7.67–7.72 (m, 2H), 8.10–8.12 (d, J = 9.47 Hz, 1H), 8.18 (s, 1H), 8.50–8.51 (d, J = 7.65 Hz, 1H), 8.85–8.84 (d, J = 7.75 Hz, 1H); **^{13}C NMR (125 MHz, CD_3OD, δ)**: 23.87, 83.98, 113.73, 115.13, 121.44, 122.52, 126.61, 128.39, 128.61, 134.13, 138.24, 145.06, 153.04, 161.24; **HRMS–ESI (*m/z*)**: $[M + H]^+$ calcd for $C_{19}H_{19}BO_4$, 322.1486; found, 322.1483.

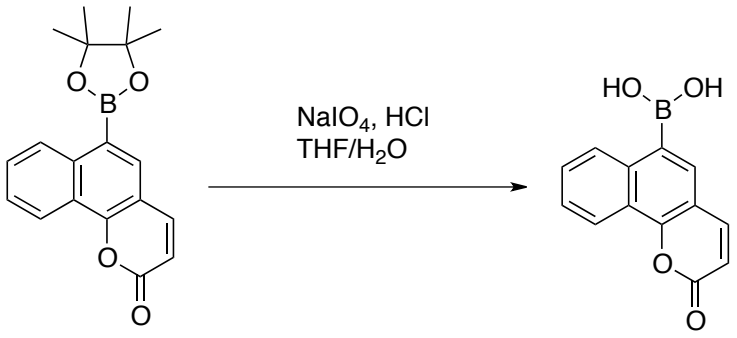

A.7.3 **A.7**

Compound **A.7.3** (0.1 g, 0.31 mmol) was dissolved in a 6.2-mL solution of 4:1 THF/H_2O. $NaIO_4$ (0.199 g, 0.93 mmol) was added, followed by 0.1 mL of 1 M HCl. The reaction mixture was then stirred overnight at room temperature. The crude mixture was filtered, and the solvent was removed under reduced pressure. The crude product was purified via flash column chromatography (2% v/v methanol:DCM) to afford **A.7** as a white solid (0.02 g, 27%).

^{1}H NMR (500 MHz, CD_3OD, δ): 6.54–6.56 (d, J = 9.43, 1H), 7.67–7.71 (m, 3H), 7.90–7.92 (d, J = 7.30 Hz, 1H), 8.09–8.11 (d, J = 9.47 Hz, 1H), 8.52–8.50 (d, J = 7.20 Hz, 1H); **^{13}C NMR (125 MHz, CD_3OD, δ)**: 104.96, 113.92, 115.15, 121.72, 122.42, 126.74, 128.04, 128.19, 128.54, 136.55, 145.01, 161.40; **HRMS–ESI (*m/z*)**: $[M + H]^+$ calcd for the dimethyl boronic ester $C_{15}H_{13}BO_4$, 268.1016; found, 268.1009.

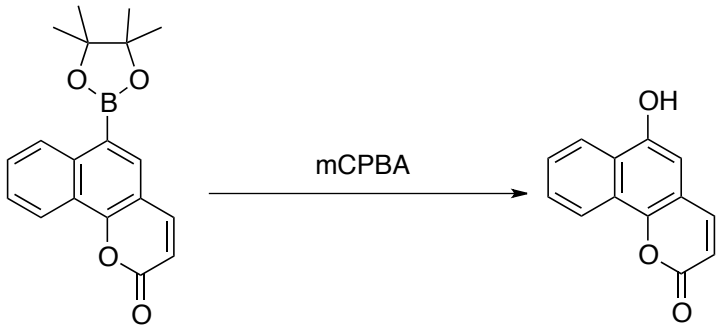

A.7.3 **A.3**

Compound **A.7.3** (0.050 g, 0.155 mmol) and mCPBA (0.032 g, 0.186 mmol) were dissolved in a 1.5-mL solution of 2:1 v/v ethanol:H_2O. The reaction mixture was then stirred overnight at room temperature. The solvent was removed under reduced pressure, and crude product was purified via flash column chromatography (50% v/v EtOAc:hexanes) to afford **A.3** as a yellow solid (0.017 g, 52%).

^{1}H NMR (500 MHz, $CDCl_3$, δ): 6.52–6.54 (d, J = 9.46 Hz, 1H), 7.46–7.48 (d, J = 8.49 Hz, 1H), 7.64–7.67 (m, 2H), 7.69–7.71 (d, J = 8.49 Hz, 1H), 7.84–7.86 (d, J = 9.45 Hz, 1H), 7.86–7.90 (m, 1H), 8.55–8.58 (m, 1H); **^{13}C NMR (125 MHz, $CDCl_3$, δ)**: 114.39, 116.08, 122.45, 123.20, 123.70, 124.59, 127.33, 127.93, 128.86, 134.96, 144.36, 151.45, 161.11; **HRMS–ESI (*m/z*)**: $[M + H]^+$ calcd for $C_{13}H_8O_3$, 213.0468; found, 213.0471.

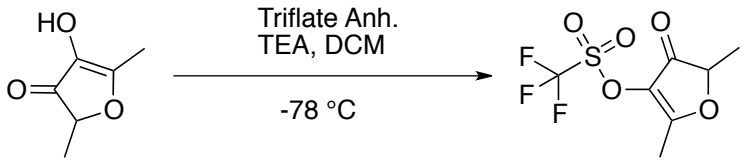

A.1 **A.1.2**

4-Hydroxy-2,5-dimethyl-3(2*H*)-furanone (**A.1**) (1.00 g, 7.80 mmol) was dissolved in DCM (78 mL), and the reaction was cooled to –78 °C in a dry ice bath. Pyridine (1.57 mL, 19.51 mmol) was then added, followed by drop-wise addition of trifluoromethansulfonic anhydride (1.57 mL, 9.36 mmol). The reaction mixture was warmed to room temperature and stirred for 4 h. The solvent was then removed under reduced pressure, and the crude product was purified via flash column chromatography (60% v/v DCM:hexanes) to afford **A.1.2** as a yellow oil (0.606 g, 30 %).

^{1}HNMR (500 MHz, $CDCl_3$, *δ*): 1.51–1.53 (d, *J* = 7.15 Hz, 3H), 2.36 (s, 3H), 4.62–4.68 (q, *J* = 7.21 Hz, 1H); **^{13}C NMR (125 MHz, $CDCl_3$, *δ*)**: 14.50, 16.32, 82.40, 117.02, 120.21, 129.41, 182.74, 192.40; **HRMS–ESI (*m/z*)**: $[M + H]^+$ calcd for $C_7H_7F_3O_5S$, 261.0040; found, 261.0045.

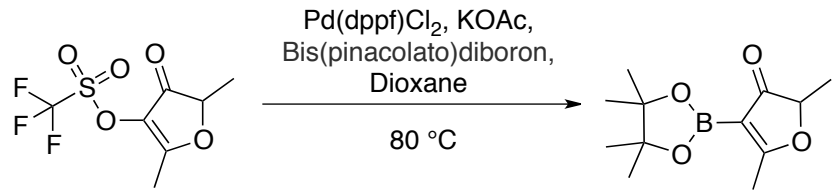

A.1.2 **A.1.3**

Compound **A.1.2** (0.30 g, 1.15 mmol), KOAc (0.339 g, 3.45 mmol), $Pd(dppf)Cl_2$ (0.084 g, 0.115 mmol), and bis(pinacolato)diboron (0.876 g, 3.45 mmol) were added to a Schlenk flask, which was then evacuated and backfilled with N_2(g). Dioxane (11 mL) was deoxygenated by sonication under high vacuum and backfilled with N_2(g). Deoxygenated dioxane was then cannulated into the reaction flask, and the reaction mixture was stirred overnight at 80 °C. The reaction mixture was filtered, and solvent was removed under reduced pressure. The crude product was purified by flash column chromatography (20%–50% v/v EtOAc:hexanes) to afford **A.1.3** as a white solid (0.086 g, 31%).

^{1}H NMR (500 MHz, CD_3OD *δ*): 1.29 (s, 12H), 1.39–1.40 (d, *J* = 7.15 Hz, 3H), 2.44 (s, 3H), 4.56–4.60 (q, *J* = 7.18 Hz, 1H); **^{13}C NMR (125 MHz, CD_3OD, *δ*)**: 16.45, 17.66, 25.05, 84.37, 84.57, 201.66, 210.18; **HRMS–ESI (*m/z*)**: $[M + H]^+$ calcd for $C_{12}H_{19}BO_4$, 238.1486; found, 238.1481.

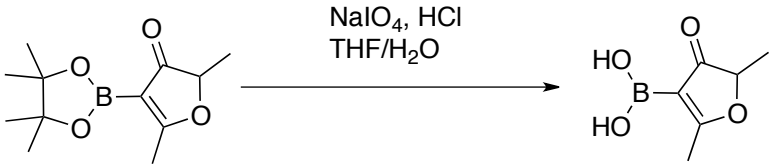

A.1.3 **A.5**

Compound **A.1.3** (0.050 g, 0.210 mmol) was dissolved in a 2-mL solution of 4:1 THF/H_2O. $NaIO_4$ (0.135 g, 0.630 mmol) was added, followed by 0.05 mL of 1 M HCl. The reaction mixture was then stirred at room temperature for 4 h. The reaction mixture was filtered, and the solvent was removed under reduced pressure. The crude product was purified by HPLC (20–90% H_2O:ACN gradient with 0.1% v/v TFA over 75 min). The product was recovered, frozen, and lyophilized overnight to afford **A.5** as a white powder (0.015 g, 46%).

^{1}HNMR (500 MHz, CD_3OD, δ): 1.39–1.40 (d, J = 7.12 Hz, 3H), 2.31 (s, 3H), 4.54–4.59 (q, J = 7.20 Hz, 1H); **^{13}C NMR (125 MHz, CD_3OD, δ)**: 16.58, 17.67, 83.76, 198.62, 210.64; **HRMS–ESI (*m/z*)**: $[M + H]^+$ calcd for the dimethyl boronate ester $C_8H_{13}BO_4$, 184.1016; found, 184.1018.

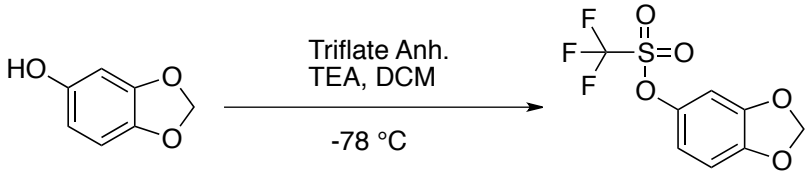

A.2 **A.2.1**

3,4-(Methylenedioxy)phenol (**A.2**) (0.50 g, 3.62 mmol) was dissolved in DCM (36 mL), and the reaction mixture was cooled to –78 °C in a dry ice/acetone bath. Pyridine (0.73 mL, 9.05 mmol) was added, followed by drop-wise addition of trifluoromethansulfonic anhydride (0.73 mL, 4.34 mmol). The reaction mixture was warmed to room temperature and stirred for 4 h. The solvent was removed under reduced pressure, and the crude product was purified via flash column chromatography (10%–20% v/v EtOAc:hexanes) to afford **A.2.1** as a yellow solid (0.90 g, 93%).

^{1}H NMR (500 MHz, $CDCl_3$, δ): 6.05 (s, 2H), 6.73–6.77 (m, 2H), 6.80–6.81 (d, J = 8.41, 1H); **^{13}C NMR (125 MHz, $CDCl_3$, δ)**: 102.61, 103.52, 108.34, 114.54, 143.60, 147.59, 148.66; **HRMS–ESI (*m/z*)**: $[M + H]^+$ calcd for $C_8H_6F_3O_5S$, 270.9883; found, 270.9874.

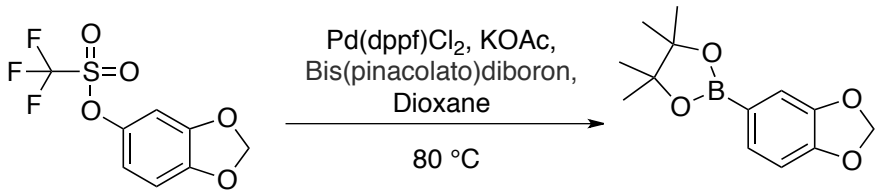

A.2.1 **A.2.2**

Compound **A.2.1** (0.50 g, 1.87 mmol), KOAc (0.550 g, 5.61 mmol), $Pd(dppf)Cl_2$, (0.137 g, 0.187 mmol) and bis(pinacolato)diboron (1.424 g, 5.61 mmol) were placed in a Schlenk flask, which was then evacuated and backfilled with N_2(g). Dioxane (19 mL) was deoxygenated by sonication under high vacuum and backfilled with N_2(g). Deoxygenated dioxane was then cannulated into the reaction flask. The reaction mixture was heated to 80 °C and stirred overnight. The reaction mixture was filtered, and the solvent was removed under reduced pressure. The crude product was purified by flash column chromatography (5% v/v EtOAc:hexanes) to afford **A.2.2** as a white solid (0.217 g, 47%).

^{1}HNMR (500 MHz, $CDCl_3$, δ): 1.33 (s, 12H), 5.95 (s, 2H), 6.82–6.84 (d, J = 7.73 Hz, 1H), 7.24 (s, 1H), 7.35–7.37 (d, J = 7.70 Hz, 1H); **^{13}C NMR (125 MHz, $CDCl_3$, δ)**: 24.98, 83.85, 100.88, 108.43, 114.07, 129.85, 147.31, 150.28; **HRMS–ESI (*m/z*)**: $[M + H]^+$ calcd for $C_{13}H_{17}BO_4$, 247.1251; found, 247.1243

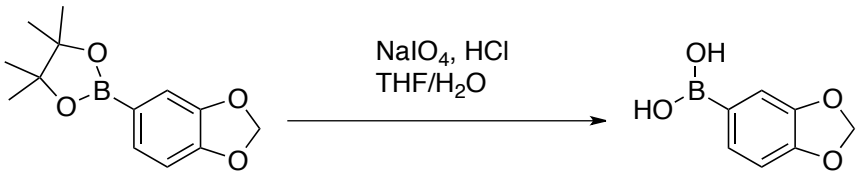

A.2.2 **A.6**

Compound **A.2.2** (0.100 g, 0.403 mmol) was dissolved in a 4-mL solution of 4:1 THF/H_2O. $NaIO_4$ (0.26 g, 1.21 mmol) was added, followed by 0.1 mL of 1 M HCl. The reaction was then stirred at room temperature for 4 h. The reaction mixture was filtered, and the solvent was removed under reduced pressure. The crude product was purified via HPLC (20–90% H_2O/ACN gradient with 0.1% v/v TFA over 75 min). The product peak was recovered, frozen, and lyophilized overnight to afford **A.6** as a white powder (0.011 g, 14 %).

^{1}HNMR (500 MHz, CD_3OD, δ): 5.92 (s, 2H), 6.82–6.84 (d, J = 7.74 Hz, 1H), 7.07 (s, 1H), 7.15–7.17 (d, J = 7.74 Hz, 1H); **^{13}C NMR (125 MHz, CD_3OD, δ)**: 103.24, 110.28, 115.45, 130.57, 149.87, 151.64; **HRMS–ESI (*m/z*)**: $[M - H]^-$ calcd for the methyl boronate ester $C_8H_9BO_4$, 178.0557; found, 178.0557.

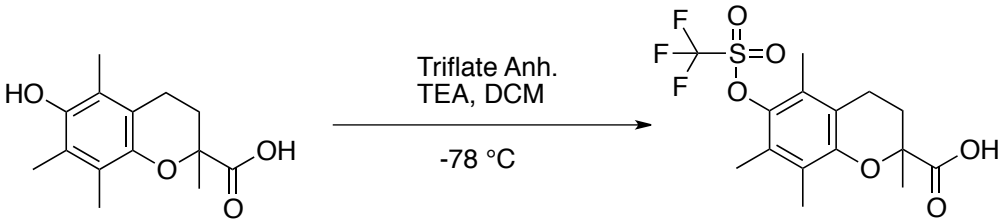

A.4 **A.4.1**

6-hydroxy-2,5,7,8-tetramethylchroman-2-carboxylic acid (**A.4**) (0.20 g, 0.799 mmol) was dissolved in DCM (8 mL) and cooled to –78 °C in a dry ice/acetone bath. Pyridine (0.16 mL, 2.00 mmol) was then added to the flask, followed by drop-wise addition of trifluoromethansulfonic anhydride (0.16 mL, 0.959 mmol). The reaction mixture was then washed with H_2O (3 x 4 mL), and the aqueous layers were combined and acidified to pH 4 with acetic acid. This solution was then extracted with DCM (3 x 10 mL). The organic layers were combined, and the solvent was removed under reduced pressure. The crude product was purified via flash column chromatography (20%–80% v/v EtOAc:hexanes) to afford **A.4.1** as a white solid (0.243g, 80%).

^{1}HNMR (500 MHz, CD_3OD, δ): 1.56 (s, 3H), 1.79–1.84 (m, 1H), 2.11 (s, 6H), 2.18 (s, 3H), 2.33–2.37 (m, 1H), 2.40–2.48 (m, 1H), 2.67–2.71 (m, 1H); **^{13}C NMR (125 MHz, CD_3OD δ)**: 12.29, 13.23, 14.09, 20.84, 25.35, 29.77, 77.55, 117.19, 119.31, 124.05, 126.71, 127.87, 140.11, 151.27, 178.61; **HRMS–ESI (*m/z*)**: $[M + NH_4]^+$ calcd for $C_{15}H_{17}F_3O_6S$, 400.1036; found, 400.1031.

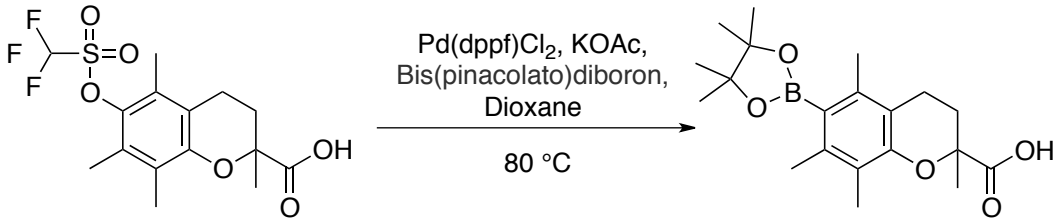

A.4.1 **A.8**

Compound **A.4.1** (0.100g, 0.261 mmol) KOAc (0.077 g, 0.784 mmol), $Pd(dppf)Cl_2$, (0.019 g, 0.026 mmol) and bis(pinacolato)diboron (0.199 g, 0.784 mmol) were placed in a Schlenk flask, which was evacuated and backfilled N_2(g). Dioxane (3 mL) was deoxygenated by sonication under high vacuum and backfilled with N_2(g). Deoxygenated dioxane was cannulated into the reaction flask and the reaction mixture was heated to 80 °C and stirred overnight. The reaction mixture was filtered, and the solvent was removed under reduced pressure. The crude product was purified by flash column chromatography (20%–80% v/v EtOAc:hexanes) to afford **A.8** as a yellow solid (0.058 g, 62%).

^{1}HNMR (500 MHz, $CDCl_3$, *δ*): 1.23 (s, 12H), 1.65 (s, 3H), 1.89–1.95 (m, 1H), 2.17 (s, 6H), 2.24 (s, 3H), 2.30–2.45 (m, 1H), 2.54–2.61 (m, 1H), 2.65-2.70 (m, 1H); **^{13}C NMR (125 MHz, $CDCl_3$, *δ*)**: 12.18, 13.38, 14.18, 20.93, 24.65, 24.90, 25.17, 29.85, 75.39, 118.38, 124.56, 127.00, 128.78, 140.48, 150.55, 177.88; **HRMS–ESI (*m/z*)**: $[M + H]^+$ calcd for the single methyl boronate ester $C_{20}H_{29}BO_5$, 361.2108; found, 361.2171.

A.6.3 DPPH radical scavenging assay

Each compound (50 μM) was dissolved in methanol and mixed with 1 equiv of H_2O_2 or vehicle control, and allowed to stir at room temperature for 1 h. The solvent was removed under reduced pressure, and the resulting residue was dissolved in 1.0 mL of methanol. A 150-μL aliquot of each reaction solution was then added to the wells of a 96-well plate in triplicate. DPPH (2,2-diphenyl-1-picrylhydrazyl) was then added to each well at a final concentration of 50 μM. Absorbance was measured at 520 nm with a Tecan Infinite M1000 microplate reader for a 0 h time point. The plate was then sealed and gently stirred at room temperature for 1 h. Another absorbance reading was taken at the 1 h. % Radical-scavenging was calculated by the following formula: % Scavenging = 100 x $(A_c–A_s)/A_c$ where A_c is the absorbance of the solvent blank and A_s is the absorbance of the sample. Each sample was normalized by the following formula: 100 x $(A_{final}\text{-}A_{initial})/(A_{F\text{-}blank}/A_{I\text{-}blank})$.

A.6.4 MTS cell cytotoxicity assay

HEPG2 cells were plated at 5,000 cells per well in a 96-well plate. Each boronate, or its paired phenolic control, was added to the cells at increasing concentration, and incubated for 12 h. The medium was removed and each well was washed with PBS. The cells were then incubated with CellTiter 96 MTS reagent from Promega (Madison, WI) for 2 h before detection at 490 nm in a Tecan Infinite M1000 microplate reader.

A.6.5 MTS assay for cellular protection

HEPG2 cells were plated at 5,000 cells per well in a 96-well plate. Each boronate, or its phenolic control, was added to the cells at a final concentration of 100 μM and incubated for 2 h.

The medium was removed, and each well was washed with PBS and replaced with new DMEM containing 10% v/v FBS. Cells were then treated with H_2O_2 (80 μM) for 12 h. The medium was removed, and the cells were washed with PBS. The cells were then incubated with CellTiter 96 MTS reagent from Promega for 2 h before detection at 490 nm in a Tecan Infinite M1000 microplate reader.

A.6.6 DCFH-DA assay for intracellular ROS

Intracellular ROS levels were measured in HEPG2 hepatocyte cells exposed to H_2O_2 using the ROS sensitive reporter chloromethyl-2',7'-dichlorofluorescein (DCFH–DA). Briefly, HEPG2 cells were plated at 5,000 cells per well in a 96-well plate. After 12 h, the cells were treated with DCFH–DA for 20 min at a final concentration of 10 μM. The medium was then removed from each well, the cells were washed with PBS, and suspended with new DMEM medium containing 10% v/v FBS. Cells were then treated with vehicle control, boronate, or parent molecule at a final concentration of 100 μM for 1 h. Medium was removed, the cells were washed with PBS and suspended with new DMEM. Cells were then treated with hydrogen peroxide (80 μM final concentration), and the fluorescence intensity was recorded with excitation at 492 nm and emission detection at 520 nm every 30 min for 3 h. Between measurements, the plate was incubated at 37 °C in a 5% CO_2 atmosphere.

A.7 NMR Spectra

^{1}H NMR ($CDCl_3$) and ^{13}C NMR ($CDCl_3$) of Compound **A.7.2**

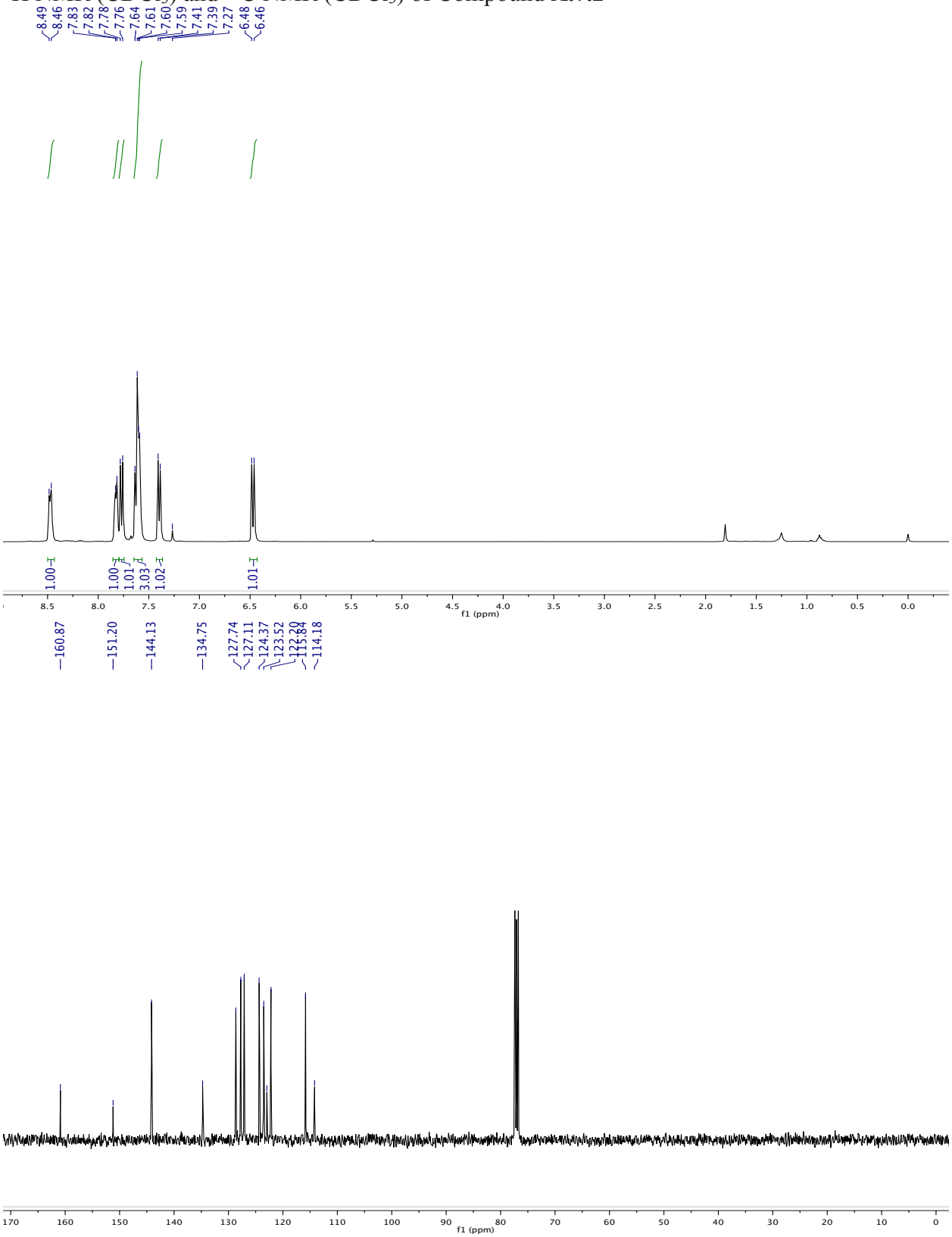

^{1}H NMR (CD_3OD) and ^{13}C NMR (CD_3OD) of Compound **A.7.3**

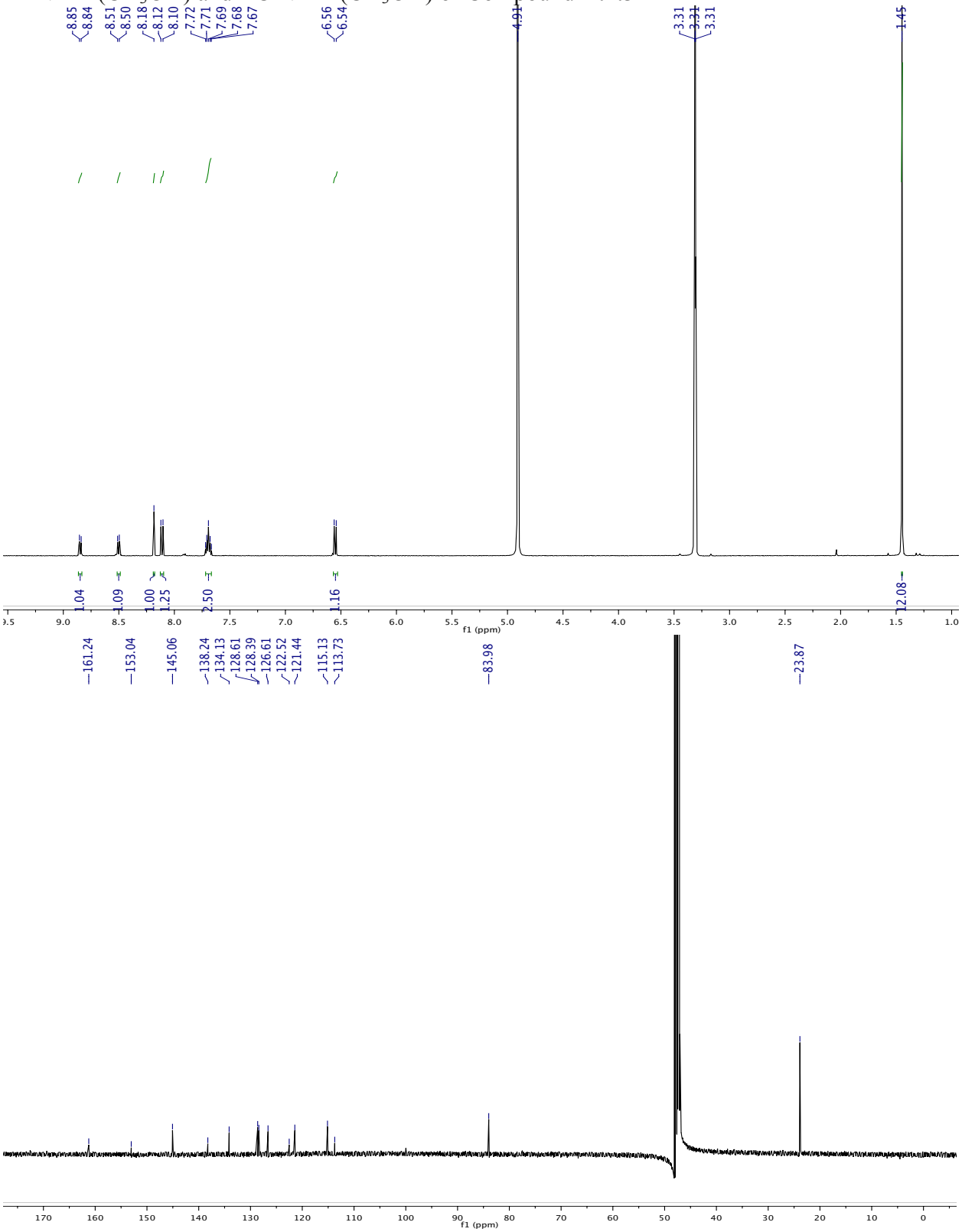

^{1}H NMR (CD_3OD) and ^{13}C NMR (CD_3OD) of Compound **A.7**

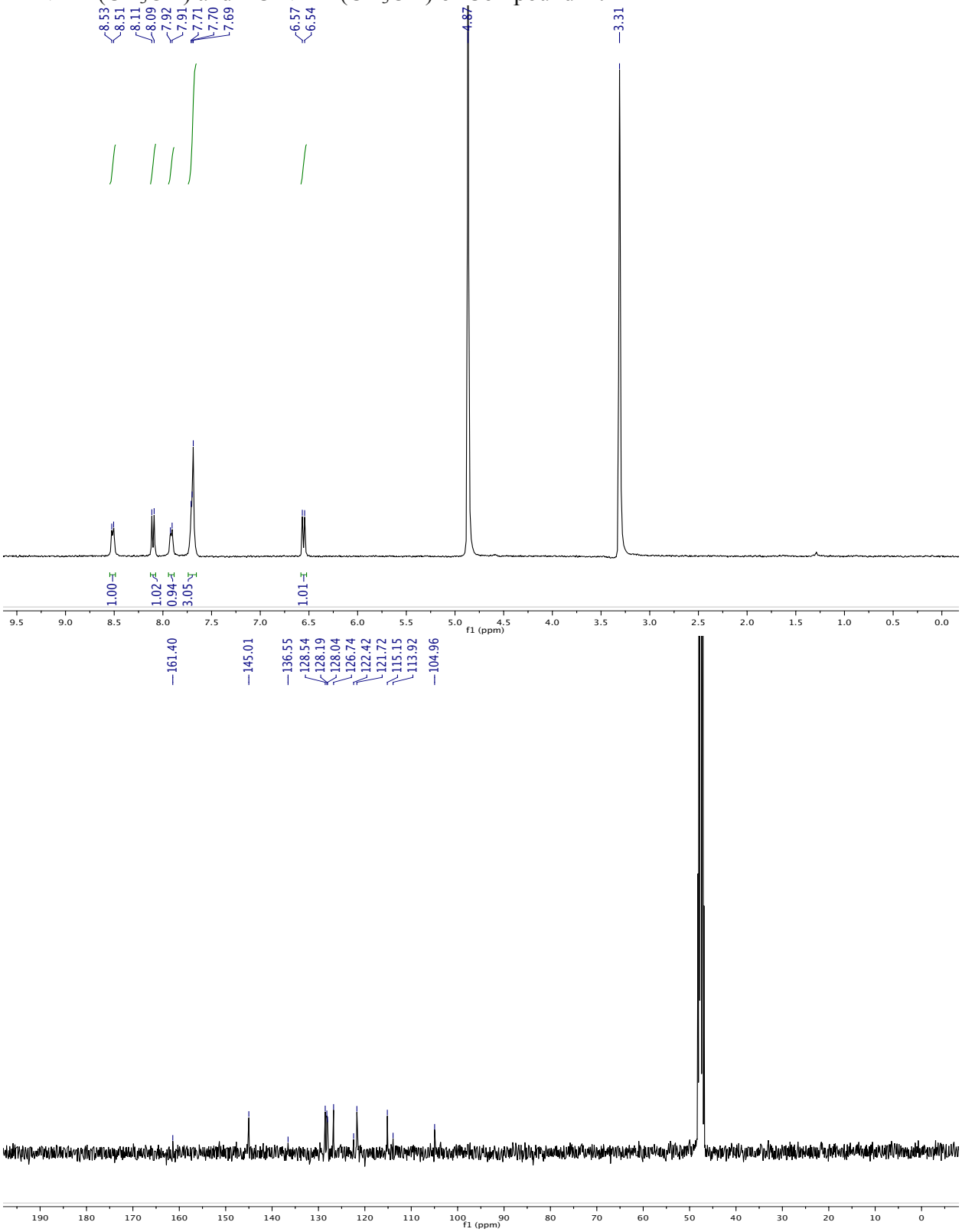

^{1}H NMR ($CDCl_3$) and ^{13}C NMR ($CDCl_3$) of Compound **A.3**

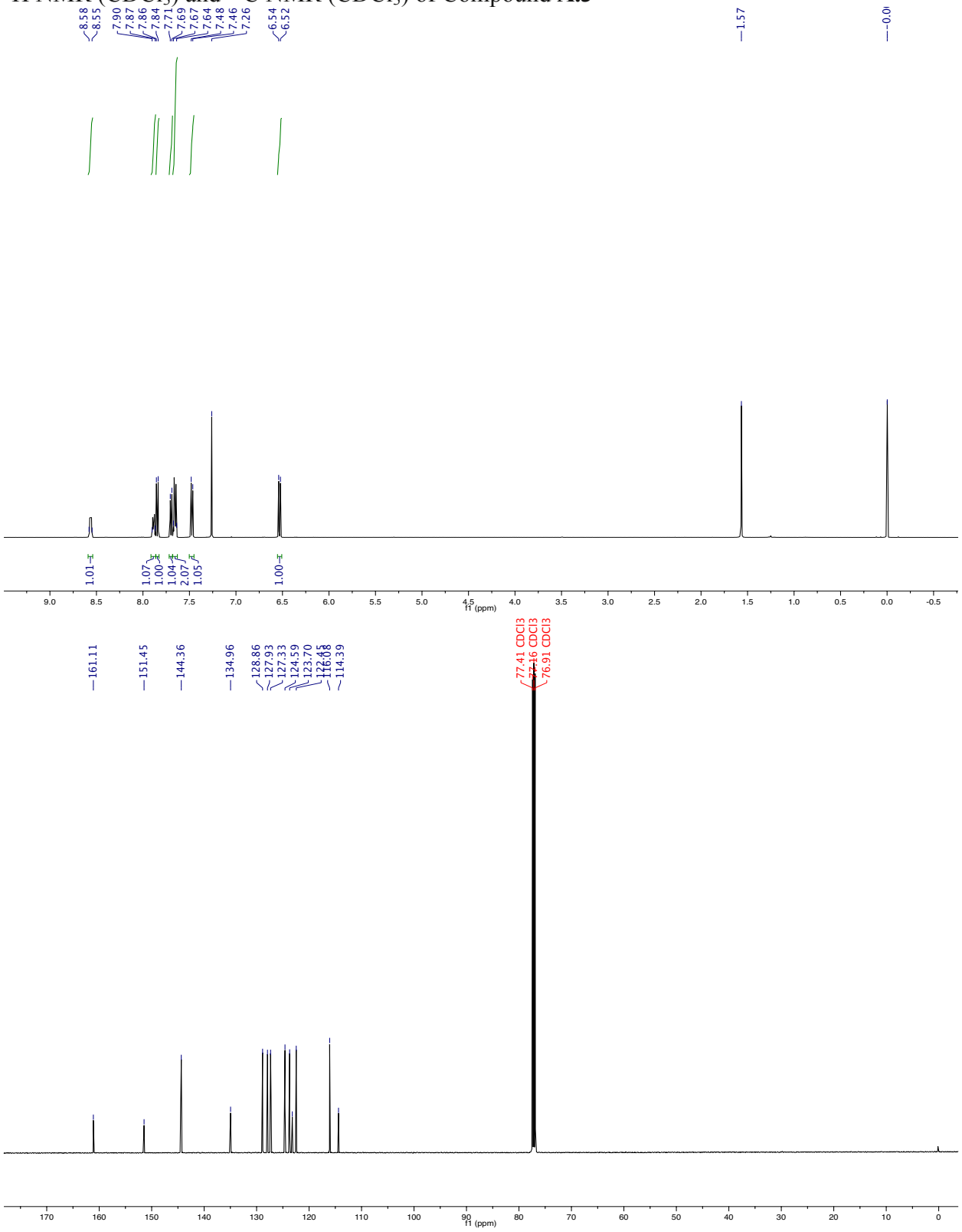

^{1}H NMR ($CDCl_3$) and ^{13}C NMR ($CDCl_3$) of Compound **A.1.2**

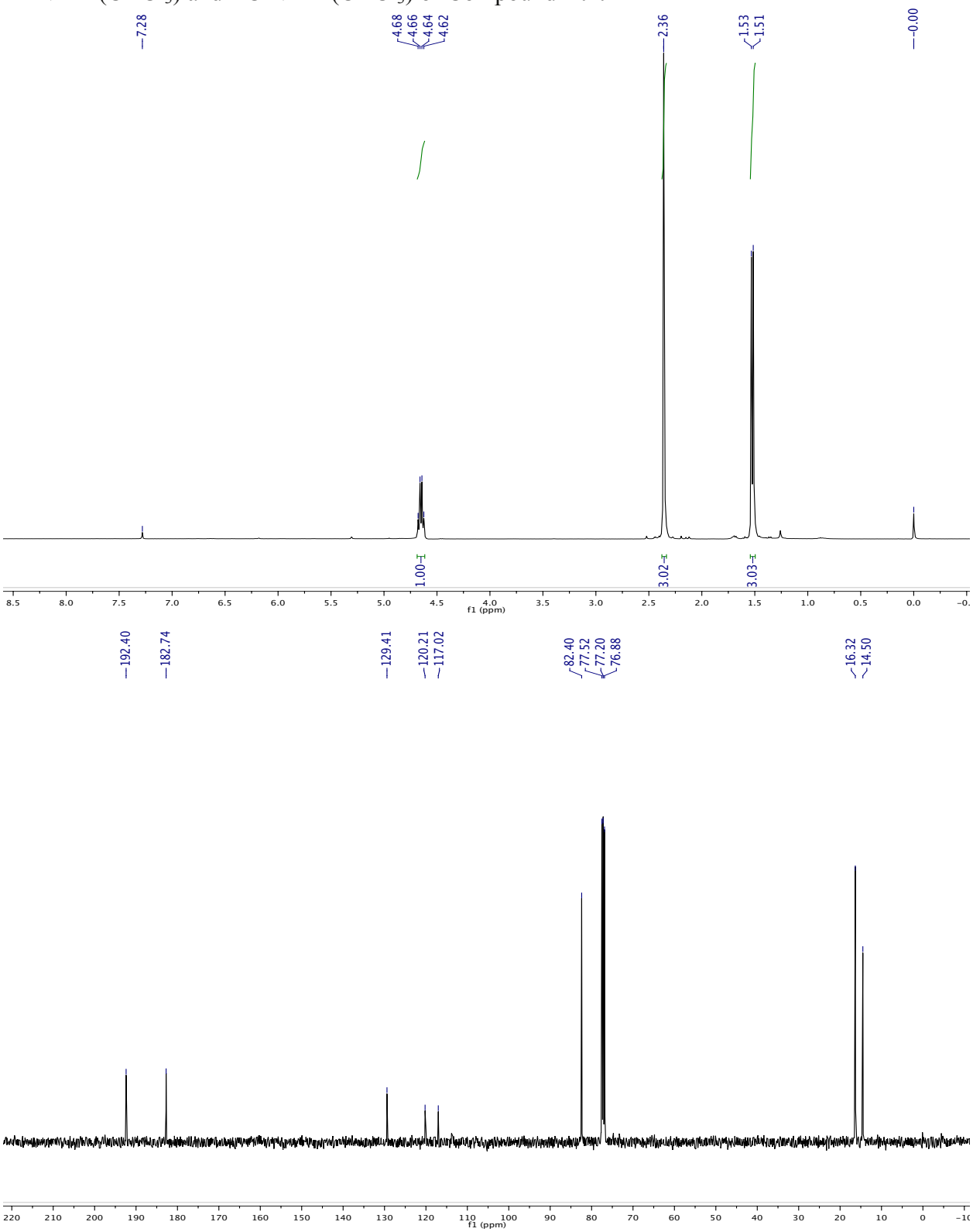

^{1}H NMR (CD_3OD) and ^{13}C NMR (CD_3OD) of Compound **A.1.3**

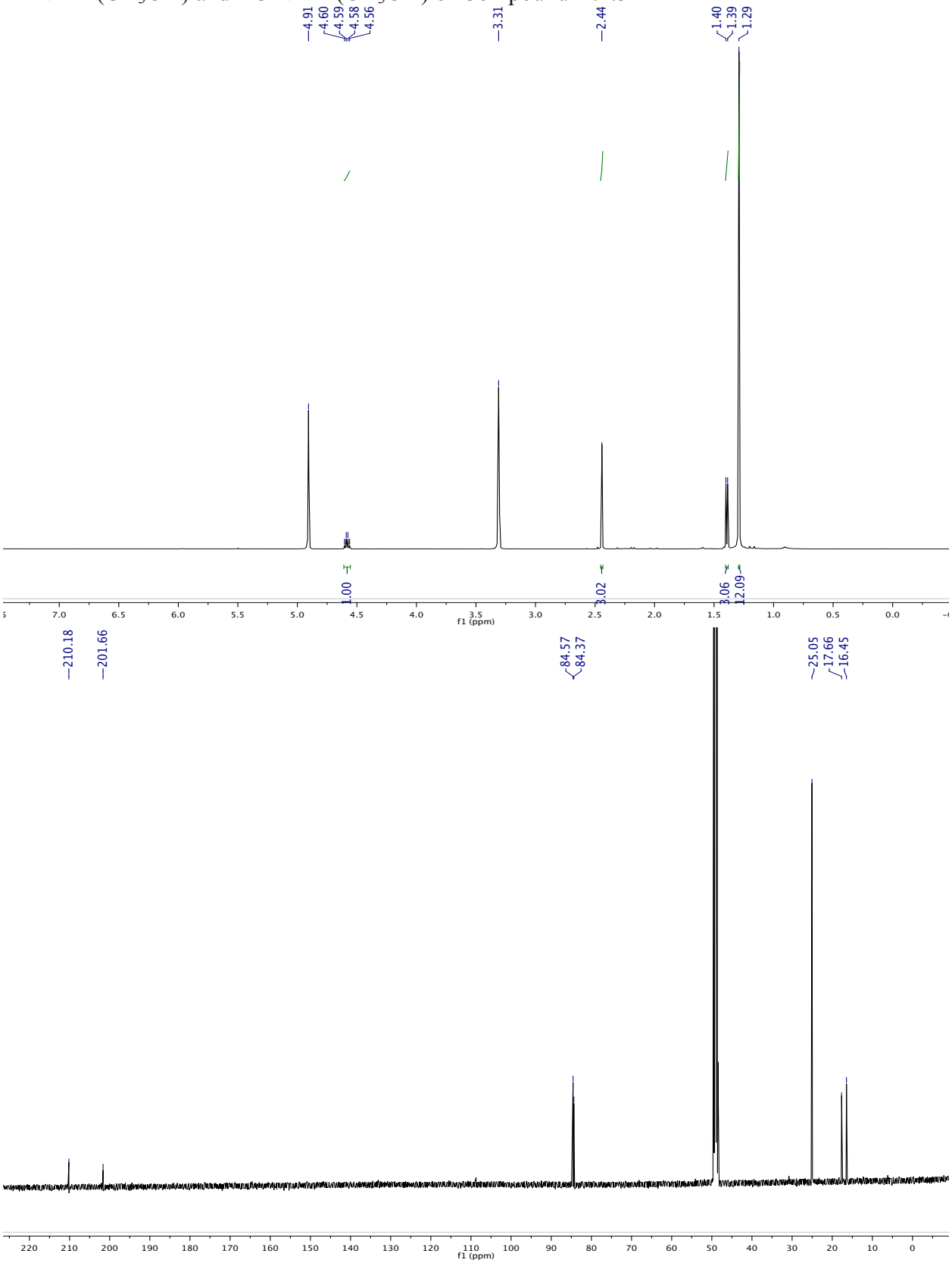

^{1}H NMR (CD_3OD) and ^{13}C NMR (CD_3OD) of Compound **A.5**

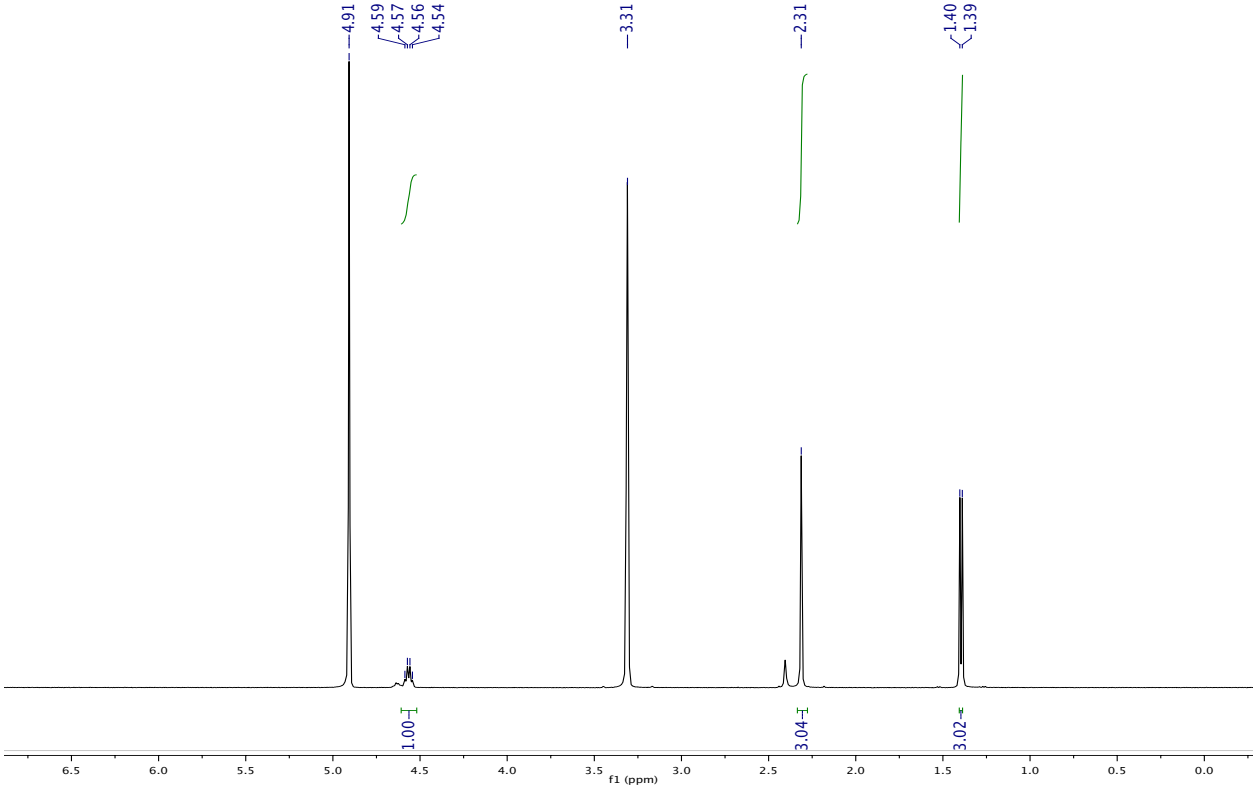

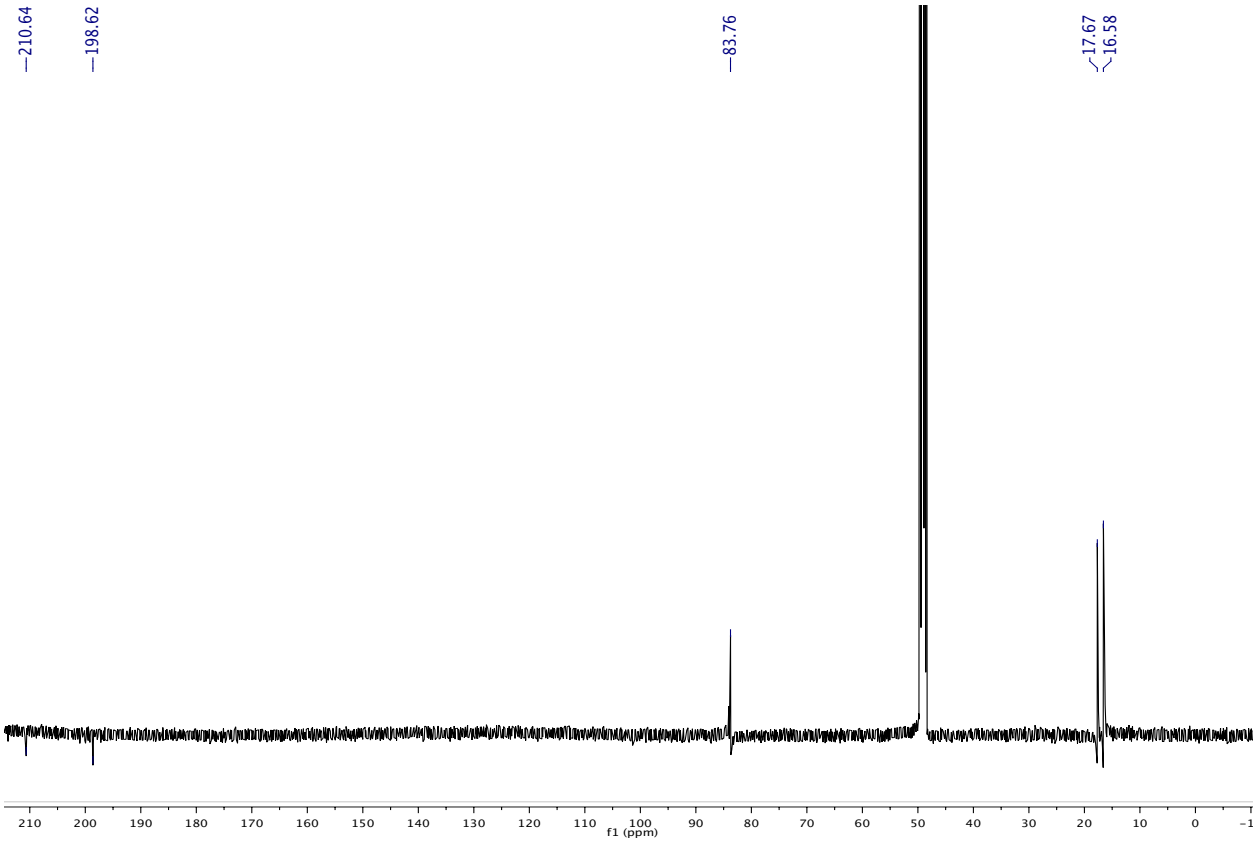

^{1}H NMR ($CDCl_3$) and ^{13}C NMR ($CDCl_3$) of Compound **A.2.1**

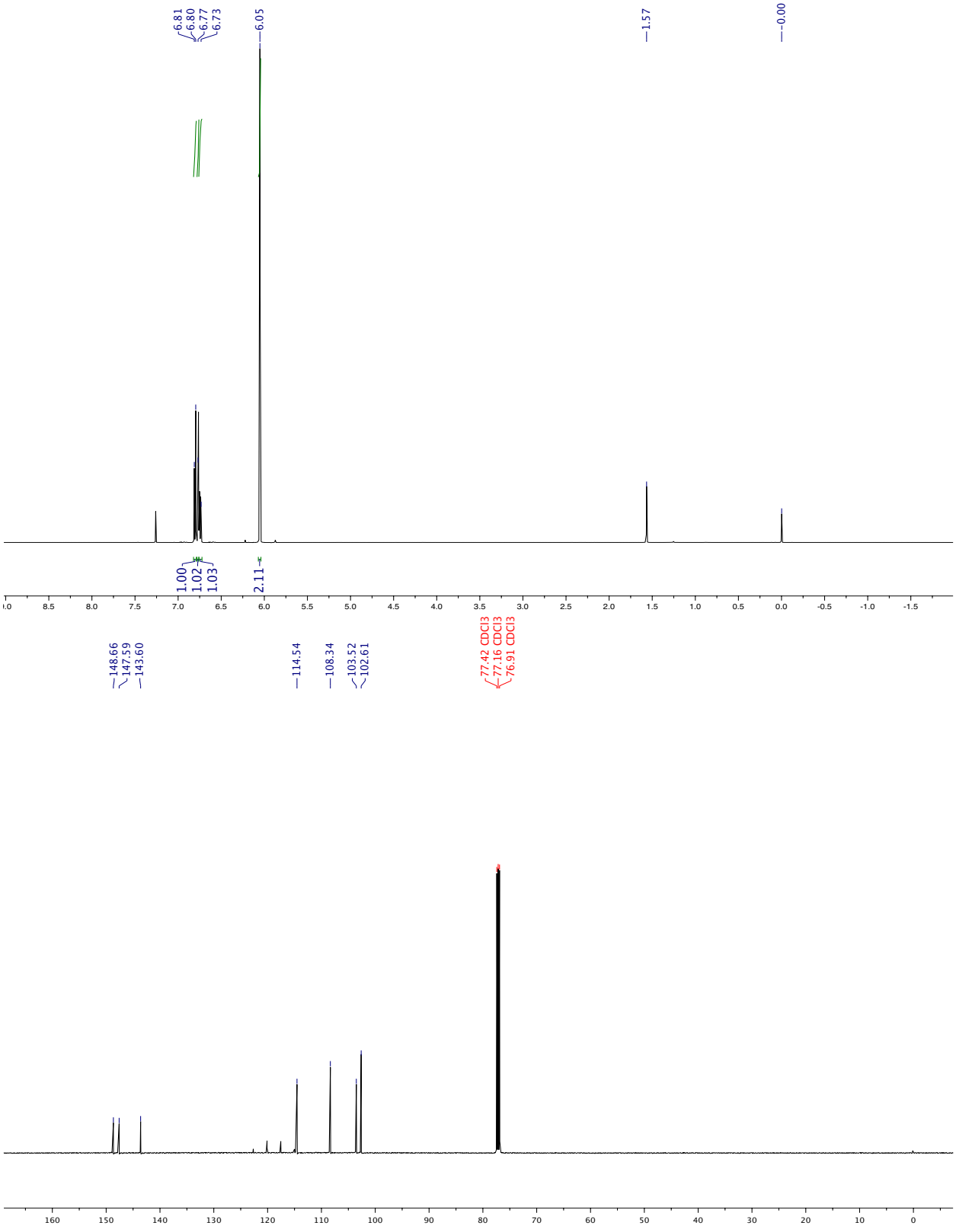

^{1}H NMR ($CDCl_3$) and ^{13}C NMR ($CDCl_3$) of Compound **A.2.2**

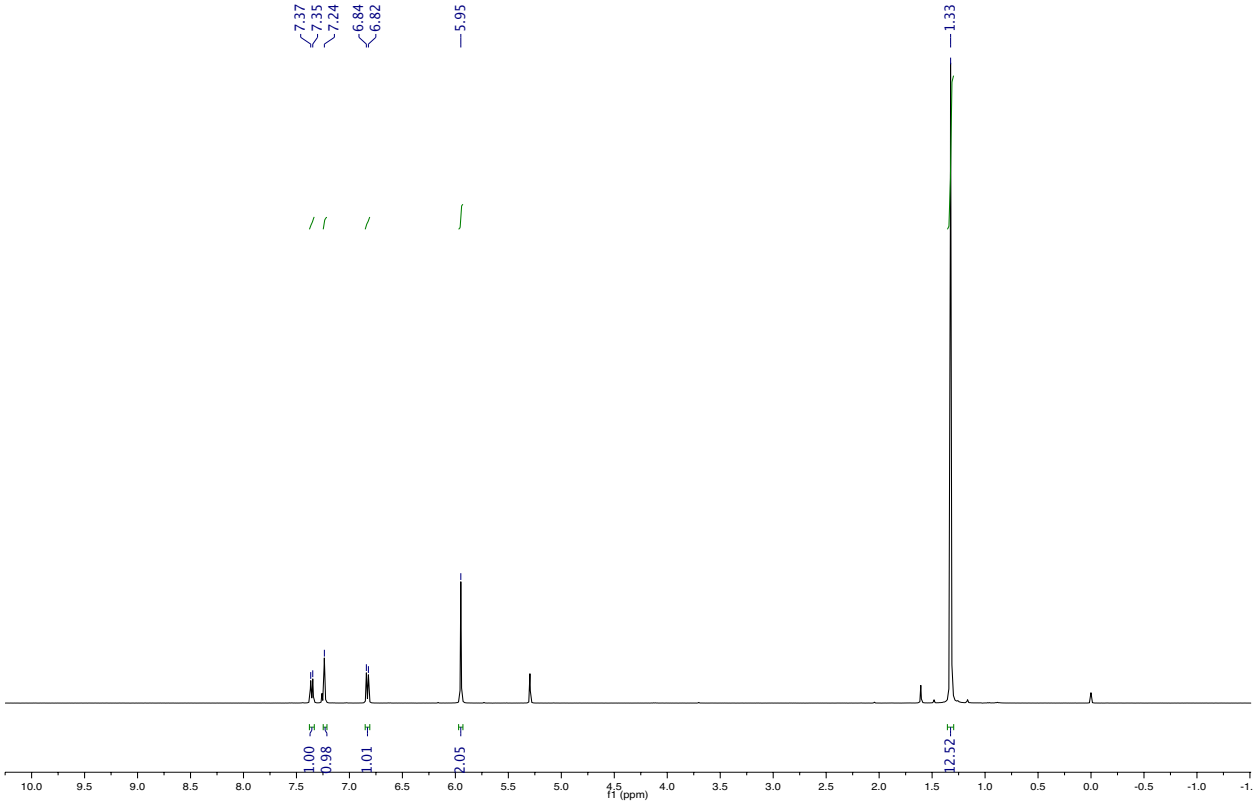

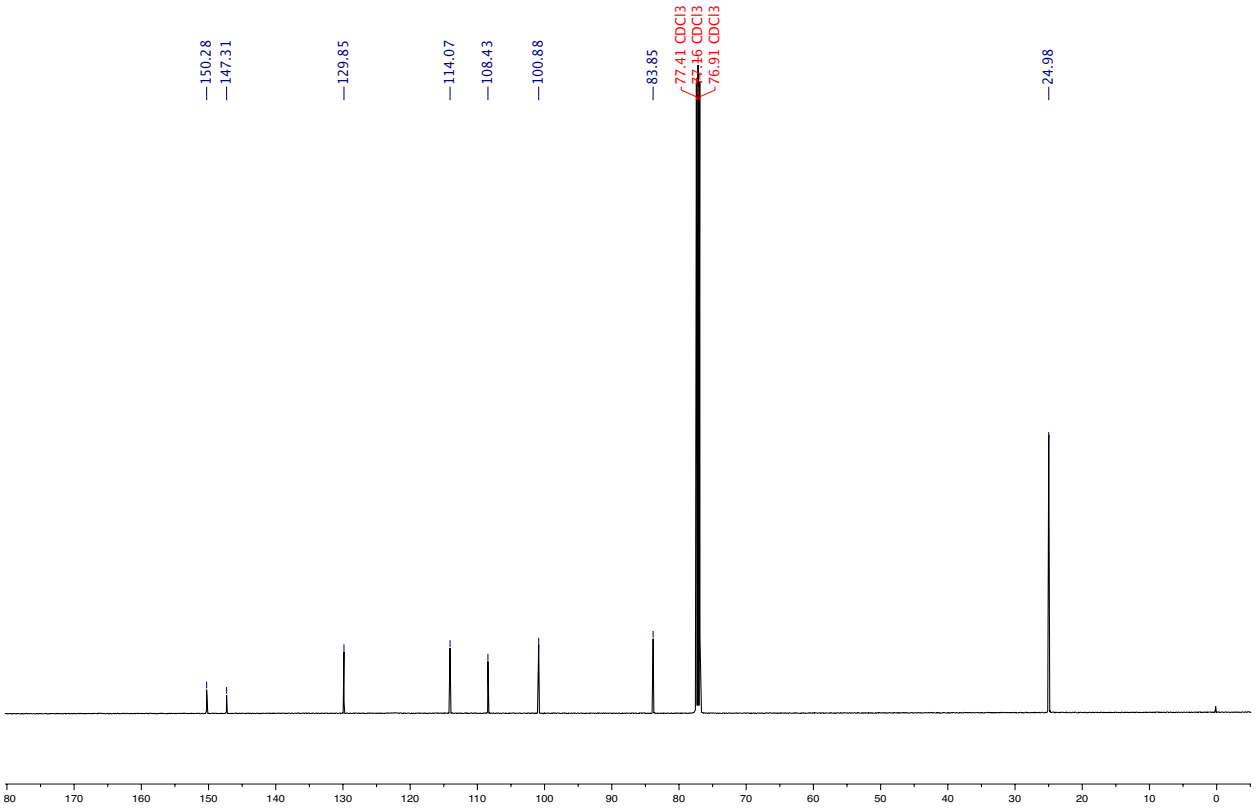

^{1}H NMR (CD_3OD) and ^{13}C NMR (CD_3OD) of Compound **A.6**

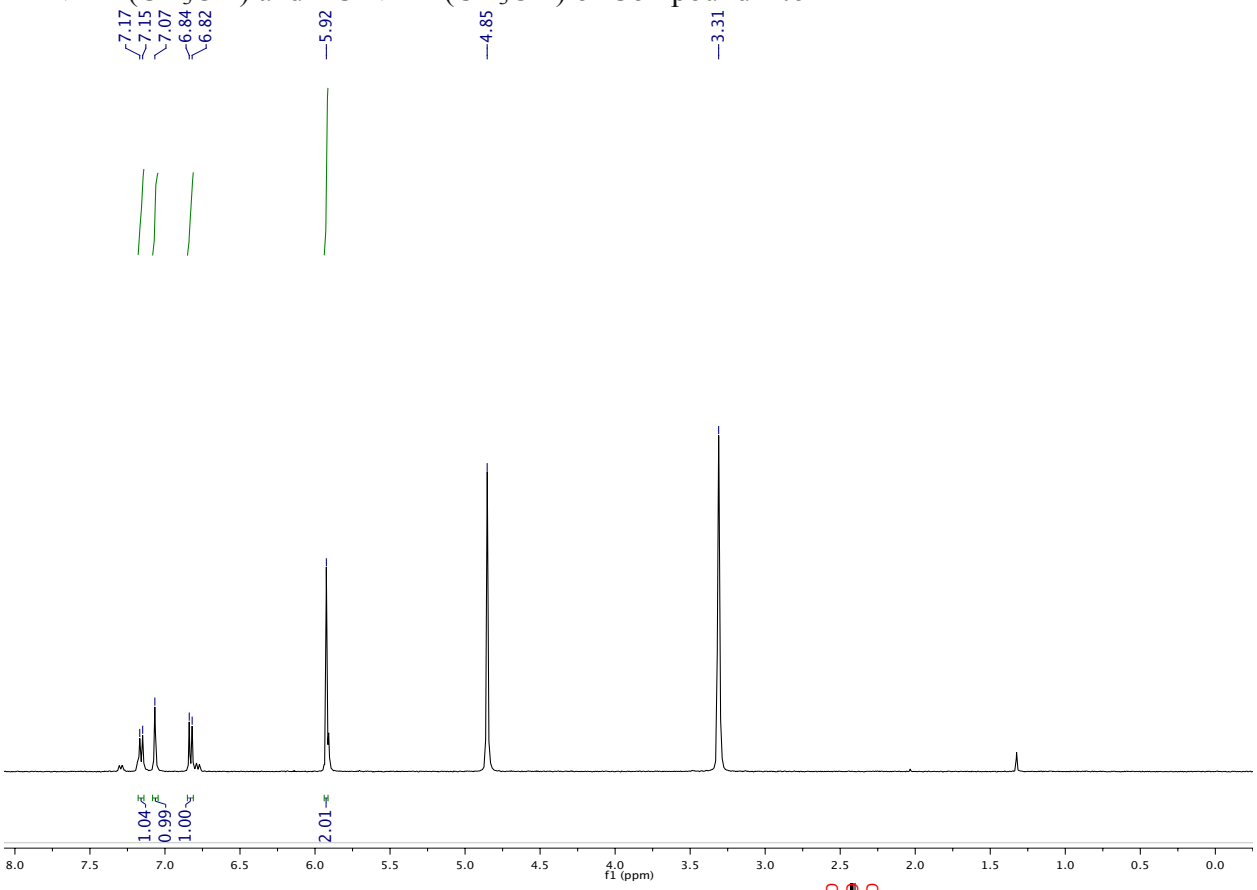

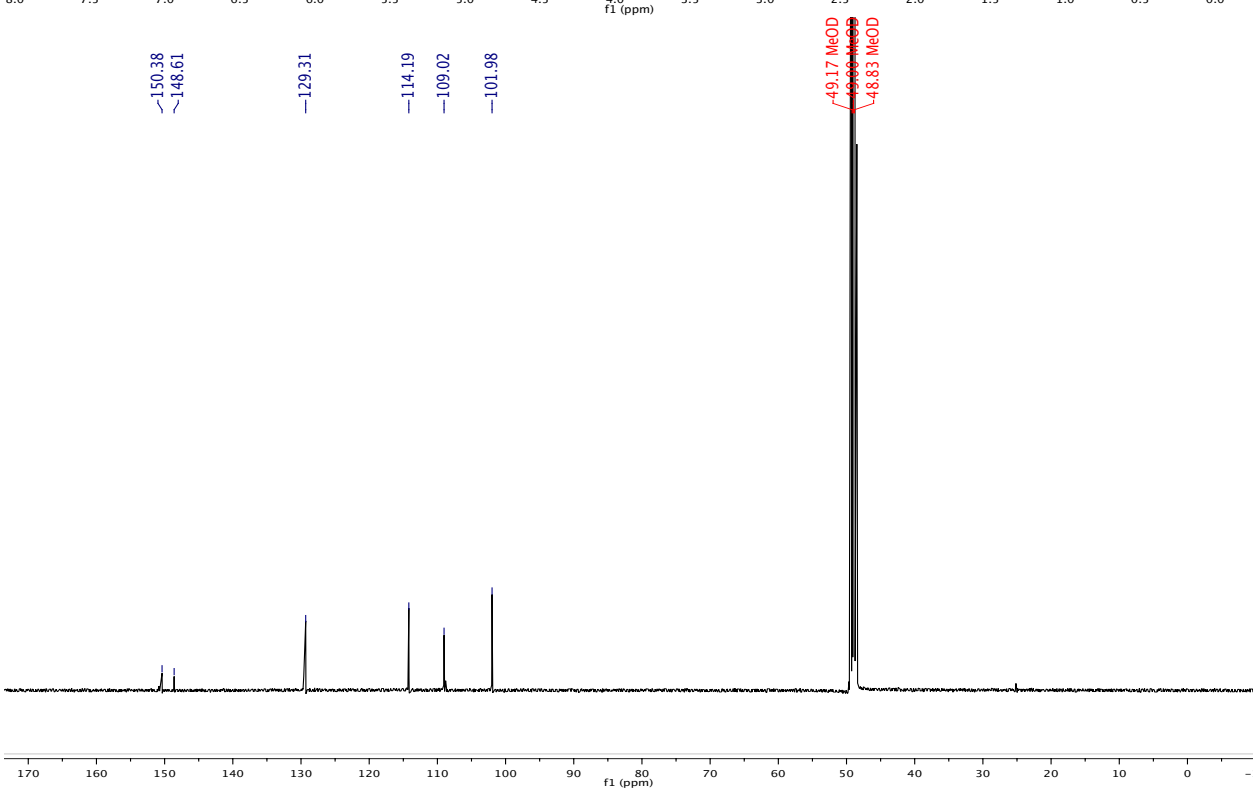

^{1}H NMR ($CDCl_3$) and ^{13}C NMR ($CDCl_3$) of Compound **A.4.1**

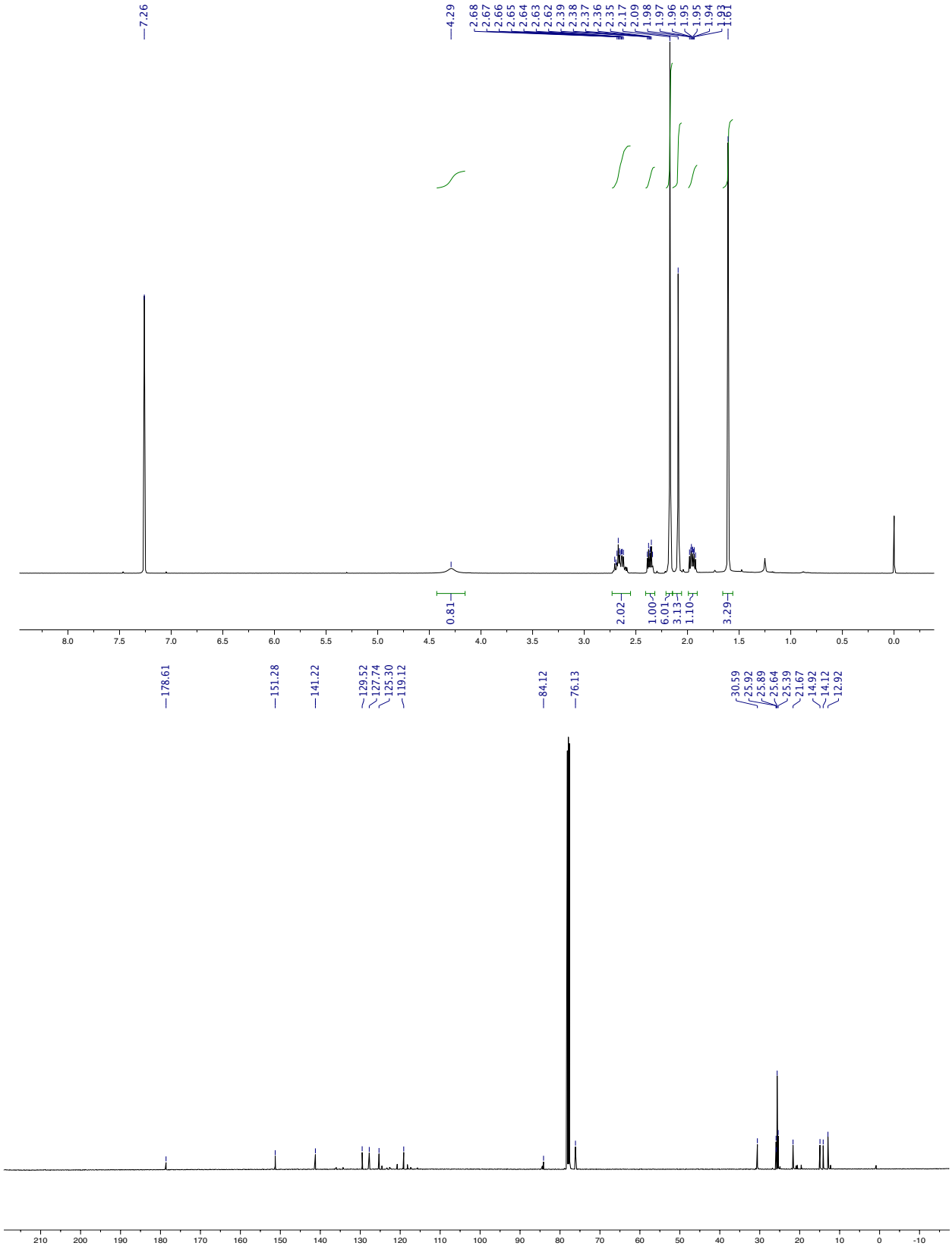

^{1}H NMR ($CDCl_3$) and ^{13}C NMR ($CDCl_3$) of Compound **A.8**

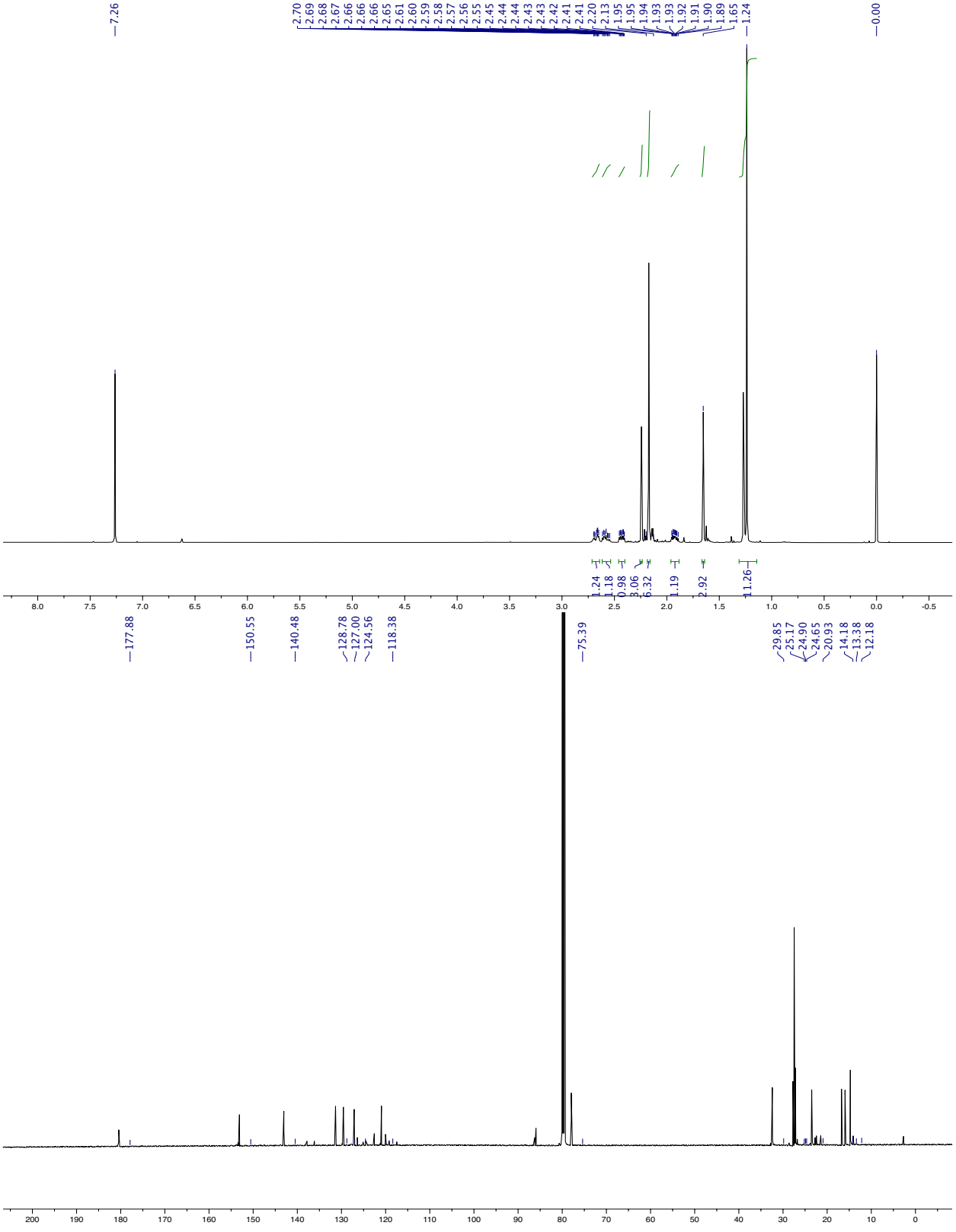

Scheme A.1

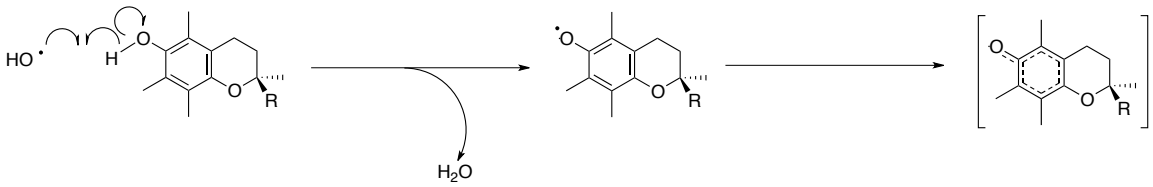

Scheme A.1 Proposed mechansim of radical scavenging by a phenol-contaning small-molecule.

Figure A.1

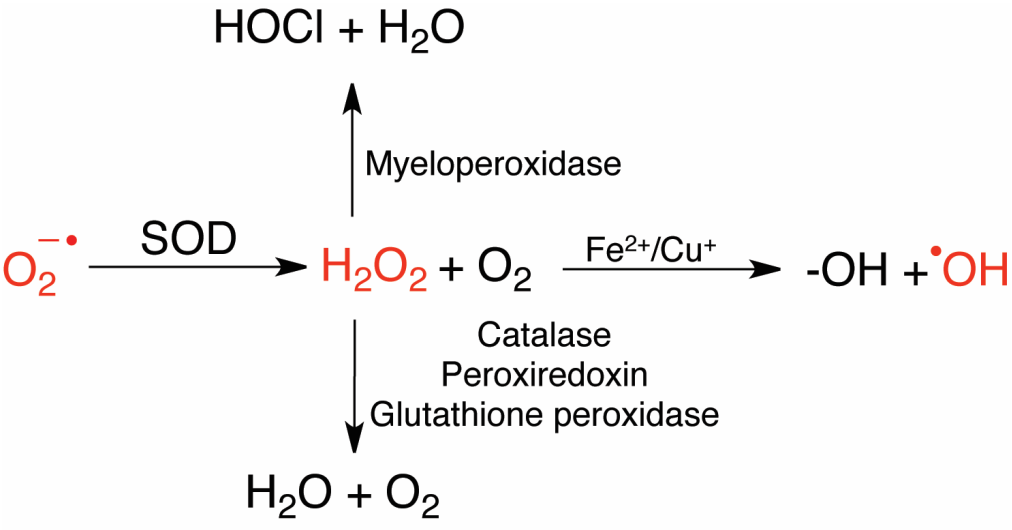
HOCl + H2O
Myeloperoxidase
O2−•
SOD
H2O2 + O2
Fe2+/Cu+
-OH + •OH
Catalase
Peroxiredoxin
Glutathione peroxidase
H2O + O2

Figure A.1 Endogenous production of intracellular reactive oxygen species (ROS). Superoxide is generated from the electron transport chain and with quickly converted to H_2O_2 by Cu/Zn superoxide dismutase 1 (SOD1). Different enzymes then break down H_2O_2 further into more benign species. Interaction of H_2O_2 with free Cu^{+} or Fe^{2+} will generate a reactive hydroxyl radical that has no known process of neutralization.

Figure A.2

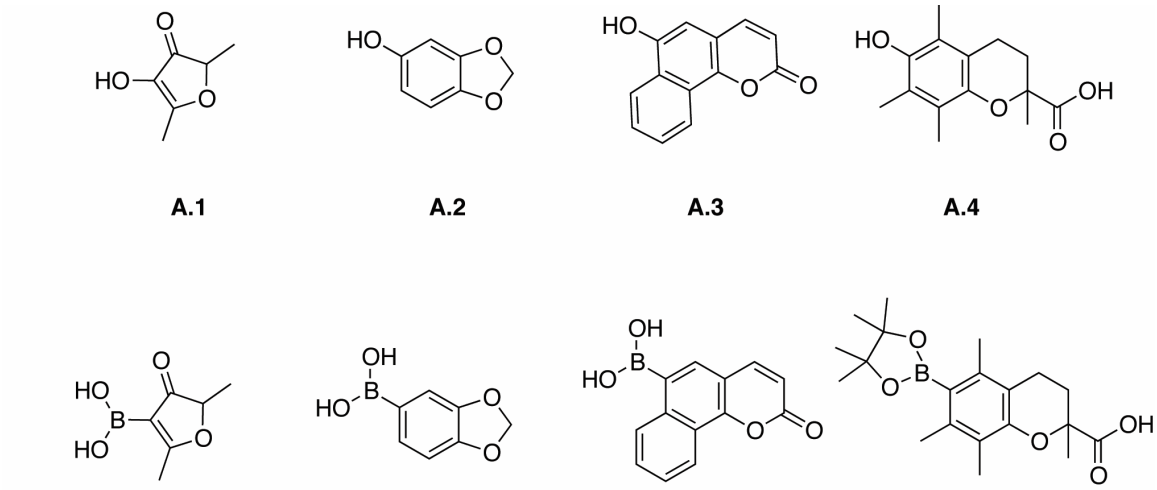

log*P*	~0.55	1.29	2.79	3.66

Figure A.2 Proposed small-molecule boronates and the active anti-oxidant products. The log*P* values were obtained from the literature and refer to the phenolic species.

Figure A.3

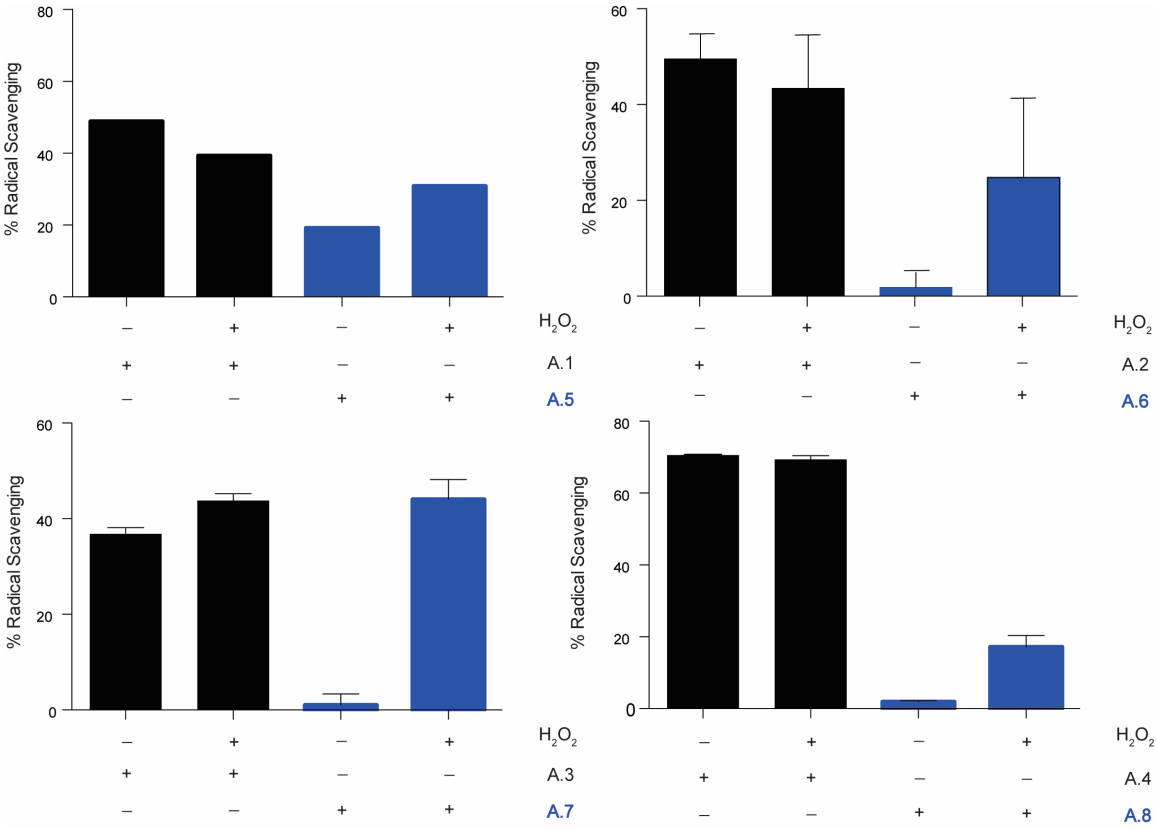
% Radical Scavenging
80
60
40
20
0
H_2O_2
A.1
A.5
% Radical Scavenging
60
40
20
0
H_2O_2
A.2
A.6
% Radical Scavenging
60
40
20
0
H_2O_2
A.3
A.7
% Radical Scavenging
80
60
40
20
0
H_2O_2
A.4
A.8

Figure A.3 DPPH radical scavenging activity for masked antioxidants. With the exception of compound **A.5**, all boronates (blue) lacked radical-scavenging ability. Pre-exposure to H_2O_2 led to the active phenol and a return of radical-scavenging ability *in vitro*.

Figure A.4

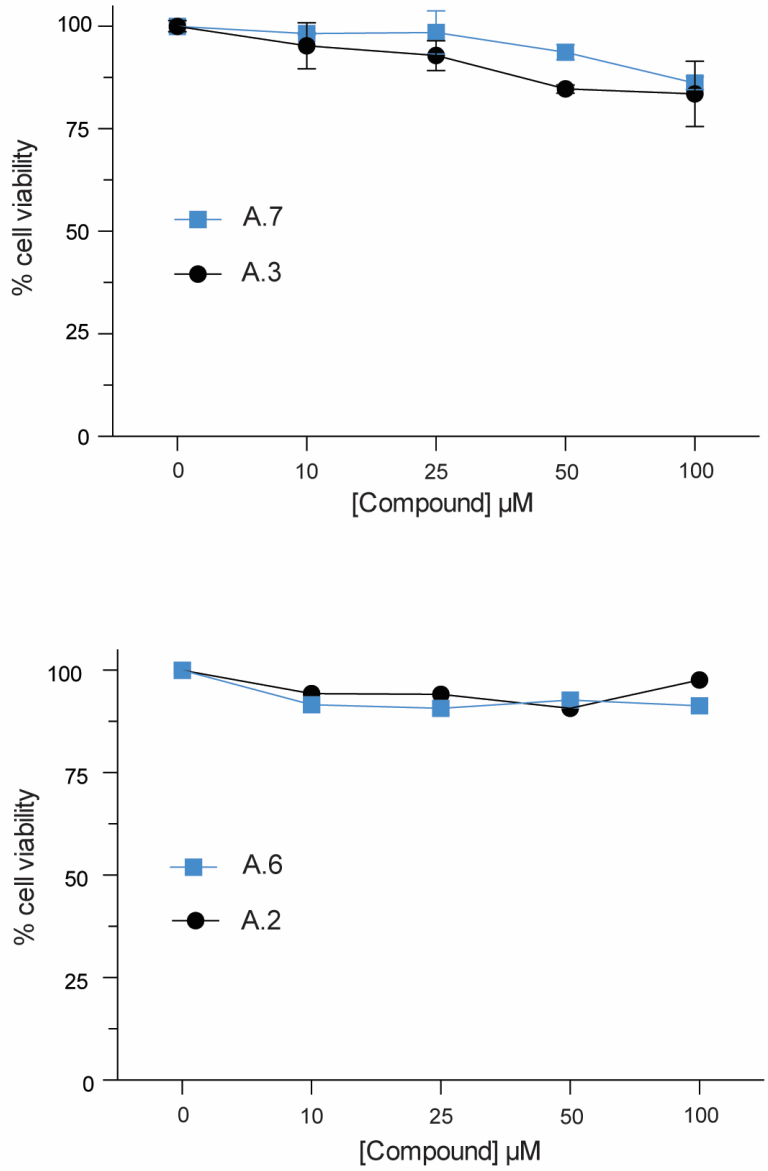
100
75
50
25
0
% cell viability
A.7
A.3
0
10
25
50
100
[Compound] µM
100
75
50
25
0
% cell viability
A.6
A.2
0
10
25
50
100
[Compound] µM

Figure A.4 Graph of cell viability indicating that boronates **A.7** and **A.6**, as well as the paired phenolic species (**A.3** and **A.2**), were not cytotoxic up to 100 μM when treated to HEPG2 cells over 24 h.

Figure A.5

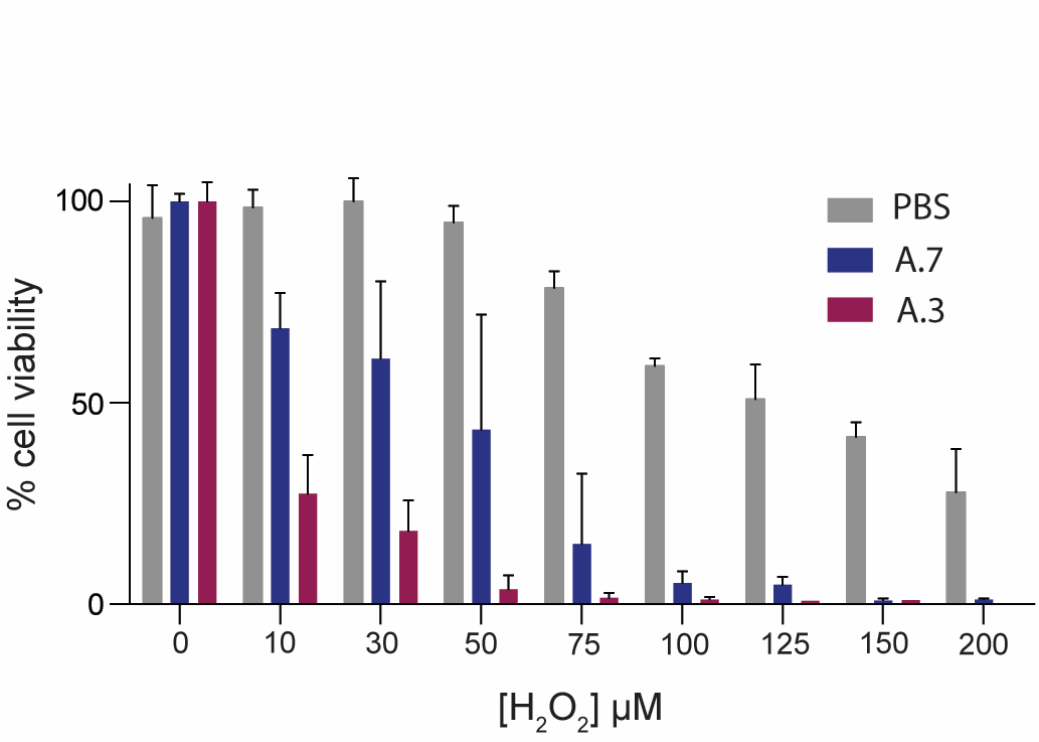
100
50
0
% cell viability
PBS
A.7
A.3
0
10
30
50
75
100
125
150
200
[H2O2] µM

Figure A.5 Boronate **A.7** and the paired phenol **A.3**, showed enhanced cytotoxicity when treated to HEPG2 cells in the presence of H_2O_2 relative to a vehicle control, even at sub-toxic levels of H_2O_2.

Figure A.6

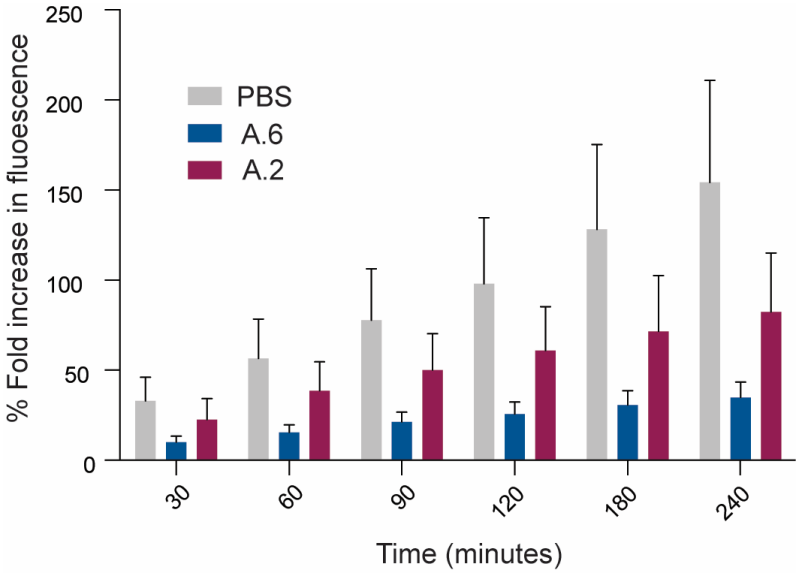
250
200
150
100
50
0
% Fold increase in fluoescence
PBS
A.6
A.2
30
60
90
120
180
240
Time (minutes)

Figure A.6 DCFH-DA assay for intracellular ROS. Treatment of HEPG2 cells with boronate **A.6** led to less ROS accumulation over time compared to the paired phenol.

References

(1) Frankland, E. On a new series of organic compounds containing boron. *J Chem Soc* **1862**, *15*, 363-381.

(2) Lorand, J. P.; Edwards, J. O. Polyol complexes and structure of the benzeneboronate ion. *J Org Chem.* **1958**, *24*, 769-774.

(3) Kuivila, H. G.; Keough, A. H.; Soboczenski, E. D. Areneboronates from diols and polyols. *Inorg Chem.* **1953**.

(4) Edwards, J. O.; Morrison, G. C.; Ross, V. F.; Schultz, J. W. The structure of the aqueous borate ion. *J Am Chem Soc.* **1954**, *77*, 266-268.

(5) Peters, J. A. Interactions between boric acid derivatives and saccharides in aqueous media: Structures and stabilities of resulting esters. *Coord Chem Rev.* **2014**, *268*, 1-22.

(6) Barker, S. A.; Chopra, A. K.; Hatt, B. W.; Somers, P. J. The interaction of areneboronic acids with monosaccharides. *Carbohydr Res.* **1973**, *26*, 33-40.

(7) Springsteen, G.; Wang, B. A detailed explanation of boronic acid-diol complexation. *Tetrahedron.* **2002**, *58*, 5291-5300.

(8) Yan, J.; Springsteen, G.; Deeter, S.; Wang, B. The relationship among pKa, pH, and binding constants in the interactions between boronic acids and diols—it is not as simple as it appears. *Tetrahedron.* **2004**, *60*, 11205-11209.

(9) Tomsho, J. W.; Benkovic, S. J. Elucidation of the mechanism of the reaction between phenylboronic acid and a model diol, Alizarin Red S. *J Org Chem.* **2012**, *77*, 2098-2106.

(10) Martinez-Aguirre, M. A.; Villamil-Ramos, R.; Guerrero-Alvarez, J. A.; Yatsimirsky, A. K. Substituent effects and pH profiles for stability constants of arylboronic acid diol esters. *J Org Chem.* **2013**, *78*, 4674-4684.

(11) Iwatsuki, S.; Nakajima, S.; Inamo, M.; Takagi, H. D.; Ishihara, K. Which is reactive in alkaline solution, boronate ion of boronic acid? Kinetic evidence for reactive trigonal boronic acid in an alkaline solution. *Inorg Chem.* **2007**, *46*, 354-356.

(12) Rietjens, M.; Steenbergen, P. A. Crosslinking mechanism of boric acid with diols revisited. *Eur J Inorg Chem.* **2005**, 1162-1174.

(13) Bull, S. D.; Davidson, M. G.; Van Den Elsen, J. M. H.; Fossey, J. S.; Jenkins, A. T. A.; Jiang, Y.-B.; Kubo, Y.; Marken, F.; Sakurai, K.; Zhao, J.; James, T. D. Exploiting the reversible covalent bonding of boronic acids—Recognition, sensing, and assembly. *Acc Chem Res.* **2012**, *46*, 312-326.

(14) Fujita, N.; Shinkai, S.; James, T. D. Boronic acids in molecular self-assembly. *Chem Asian J.* **2008**, *3*, 1076-1091.

(15) Whyte, G. F.; Vilar, R.; Woscholski, R. Molecular recognition with boronic acids-applications in chemical biology. *J Chem Biol.* **2013**, *6*, 161-174.

(16) Wu, X.; Li, Z.; Chen, X. X.; Fossey, J. S.; James, T. D.; Jiang, Y. B. Selective sensing of saccharides using simple boronic acids and their aggregates. *Chem Soc Rev.* **2013**, *42*, 8032-8048.

(17) Duggan, P. J. Fructose-permeable liquid membranes containing boronic acid carriers. *Aust J Chem.* **2004**, *57*, 291-299.

(18) Uziel, M.; Smith, L. H.; Taylor, S. A. Modified nucleosides in urine: Selective removal and analysis. *Clin Chem.* **1976**, *22*, 1451-1455.

(19) Habtu, M. M.; Bourne, S. A.; Koch, K. R.; Luckay, R. C. Competitive bulk liquid membrane transport and solvent extraction of some transition and post-transition metal ions using acylthiourea ligands as ionophores. *New J Chem.* **2006**, *30*, 1155-1162.

(20) Piest, M.; Engbersen, J. F. Role of boronic acid moieties in poly(amido amine)s for gene delivery. *J Control Release.* **2011**, *155*, 331-340.

(21) Ma, R.; Shi, L. Phenylboronic acid-based glucose-responsive polymeric nanoparticles: synthesis and applications in drug delivery. *Polym Chem.* **2014**, *5*, 1503-1518.

(22) Guan, Y.; Zhang, Y. Boronic acid-containing hydrogels: Synthesis and their applications. *Chem Soc Rev.* **2013**, *42*, 8106-8121.

(23) Jin, S.; Cheng, Y.; Reid, S.; Li, M.; Wang, B. Carbohydrate recognition by boronolectins, small molecules, and lectins. *Med Res Rev.* **2010**, *30*, 171-257.

(24) Nakagawa, Y.; Yukishige, I. Molecular architecture and therapeutic potential of lectin mimics. *Adv Carbohydr Chem Biochem.* **2012**, *68*, 1-58.

(25) Smoum, R.; Rubinstein, A.; Dembitsky, V. M.; Srebnik, M. Boron containing compounds as protease inhibitors. *Chem Rev.* **2012**, *112*, 4156-4220.

(26) Ban, H. S.; Nakamura, H. Boron-based drug design. *Chem Rec.* **2015**, *15*, 616-635.

(27) Adamczyk-Wozniak, A.; Borys, K. M.; Sporzynski, A. Recent developments in the chemistry and biological applications of benzoxaboroles. *Chem Rev.* **2015**, *115*, 5224-5247.

(28) Trippier, P. C.; McGuigan, C. Boronic acids in medicinal chemistry: anticancer, antibacterial and antiviral applications. *MedChemComm.* **2010**, *1*, 183-198.

(29) Mukherjee, S.; Ghosh, R. N.; Maxfield, F. R. Endocytosis. *Physiol Rev.* **1997**, *77*, 759-803.

(30) Scalise, M.; Pochini, L.; Giangregorio, N.; Tonazzi, A.; Indiveri, C. Proteoliposomes as tool for assaying membrane transporter functions and interactions with xenobiotics. *Pharmaceutics* **2013**, *5*, 472-497.

(31) Sahay, G.; Alakhova, D. Y.; Kabanov, A. V. Endocytosis of nanomedicines. *J Control Release.* **2010**, *145*, 182-195.

(32) Fu, A.; Tang, R.; Hardie, J.; Farkas, M. E.; Rotello, V. M. Promises and pitfalls of intracellular delivery of proteins. *Bioconjug Chem.* **2014**, *25*, 1602-1608.

(33) Pisal, D. S.; Kosloski, M. P.; Balu-Iyer, S. V. Delivery of therapeutic proteins. *J Pharm Sci.* **2010**, *99*, 2557-2575.

(34) Wilson, C. J. Rational protein design: developing next-generation biological therapeutics and nanobiotechnological tools. *Wiley Interdiscip Rev Nanomed Nanobiotechnol.* **2015**, *7*, 330-341.

(35) Pachioni-Vasconcelos Jde, A.; Lopes, A. M.; Apolinario, A. C.; Valenzuela-Oses, J. K.; Costa, J. S.; Nascimento Lde, O.; Pessoa, A.; Barbosa, L. R.; Rangel-Yagui Cde, O. Nanostructures for protein drug delivery. *Biomater Sci.* **2016**, *4*, 205-218.

(36) Brock, R. The uptake of arginine-rich cell-penetrating peptides: Putting the puzzle together. *Bioconjug Chem.* **2014**, *25*, 863-868.

(37) Torchilin, V. P. Recent advances with liposomes as pharmaceutical carriers. *Nat Rev Drug Discov.* **2005**, *4*, 145-160.

(38) Zheng, Y.; Li, S.; Weng, Z.; Gao, C. Hyperbranched polymers: advances from synthesis to applications. *Chem Soc Rev.* **2015**, *44*, 4091-4130.

(39) Blanco, E.; Shen, H.; Ferrari, M. Principles of nanoparticle design for overcoming biological barriers to drug delivery. *Nat Biotechnol.* **2015**, *33*, 941-951.

(40) Cloninger, M. J. Biological applications of dendrimers. *Curr Opin Chem Biol.* **2002**, *6*, 742-748.

(41) Yang, J.; Zhang, Q.; Chang, H.; Cheng, Y. Surface-engineered dendrimers in gene delivery. *Chem Rev.* **2015**, *115*, 5274-5300.

(42) Alley, S. C.; Okeley, N. M.; Senter, P. D. Antibody-drug conjugates: targeted drug delivery for cancer. *Curr Opin Chem Biol.* **2010**, *14*, 529-537.

(43) Russell, S. J.; Peng, K. W.; Bell, J. C. Oncolytic virotherapy. *Nat Biotechnol.* **2012**, *30*, 658-670.

(44) Onoue, S.; Yamada, S.; Chan, H. K. Nanodrugs: Pharmacokinetics and safety. *Int J Nanomed.* **2014**, *9*, 1025-1037.

(45) Svenson, S. The dendrimer paradox - high medical expectations but poor clinical translation. *Chem Soc Rev.* **2015**, *44*, 4131-4144.

(46) Gallop, P. M.; Paz, M. A.; Henson, E. Boradeption- A new procedure for transferring water-insoluble agents across cell membranes. *Science* **1982**, *217*, 166-169.

(47) Gallop, P. M.; Paz, M. A.; Henson, E.; Latt, S. A. Dynamic approches to the delivery of reporter reagents into living cells. *Biotechniques* **1984**, *2*, 32-36.

(48) Goldberger, G.; Paz, M. A.; Torrelio, B. M.; Okamoto, Y.; Gallop, P. M. Effect of hydroxyorganoboranes of synthesis, transport and N-linked glycosylation of plasma proteins. *Biochem Biophys Res Commun.* **1987**, *148*, 493-499.

(49) Smith, B. D. Liquid membrane transport using boronic acid carriers. *Supramol Chem.* **1996**, *7*, 55-60.

(50) Shinbo, T.; Nishimura, K.; Yamaguchi, T.; Sugiura, M. Uphill transport of monosaccharides across an organic liquid membrane. *J Chem Soc, Chem Commun.* **1986**, 349-351.

(51) van den Berg, R.; Peters, A. J.; van Bekkum, H. The structure and (local) stability constants of borate esters of mono- and di-saccharides as studied by ^{10}B and ^{13}C NMR spectroscopy. *Carbohydr Res.* **1994**, *253*, 1-12.

(52) Chapelle, S.; Verchere, J.-F. A 11B and 13C NMR determination of the structures of boronate complexes of pentoses and related sugars. *Tetrahedron* **1988**, *44*, 4469-4482.

(53) Morin, G. T.; Paugam, M.-F.; Hughes, M. P.; Smith, B. D. Boronic acids mediate glycoside transport through a liquid organic membrane via reversible formation of trigonal boronate esters. *J Org Chem.* **1994**, *59*, 2724-2728.

(54) Grotjohn, B. F.; Czarnik, A. W. Selective transport of ribonucleosides through a liquid membrane. *Tetrahedron Lett.* **1989**, *30*, 2325-2328.

(55) Mohler, L. K.; Czarnic, A. W. Ribonucleoside membrane transport by a new class of synthetic carrier. *J Am Chem Soc.* **1993**, *115*, 2998-2999.

(56) Paugam, M.-F.; Smith, B. D. Active transport of uridine through a liquid organic membane by phenylboronic acid and driven by a fluoride ion gradient. *Tetrahedron lett.* **1993**, *34*, 3723-3726.

(57) Paugam, M.-F.; Valencia, L. S.; Boggess, B.; Smith, B. D. Dopamine transport using a crown boronic acid. *J Am Chem Soc.* **1994**, *116*, 11203-11204.

(58) Paugam, M.-F.; Bien, J. T.; Smith, B. D.; Chrisstoffels, L. A. J.; de Jong, F.; Reinhoudt, D. N. Facilitated catecholamine transport though bulk and polymer-supported liquid membranes. *J Am Chem Soc.* **1996**, *118*, 9820-9825.

(59) Altamore, T. M.; Duggan, P. J.; Krippner, G. Y. Improving the membrane permeability of sialic acid derivatives. *Bioorg Med Chem.* **2006**, *14*, 1126-1133.

(60) Mohler, L. K.; Czarnic, A. W. α-amino acid chelative complexation by an arylboronic acid. *J Am Chem Soc.* **1993**, *115*, 7037-7038.

(61) Reetz, M. T.; Huff, J.; Rudolph, J.; Tollner, K.; Deege, A.; Goddard, R. Highly efficient transport of amino acids through liquid membranes via three-component supromolecules. *J Am Chem Soc.* **1994**, *116*, 11588-11589.

(62) Paugam, M.-F.; Morin, G. T.; Smith, B. D. Metal cation:glucopyranoside co-transport through a liquid organic membrane. *Tetrahedron lett.* **1993**, *34*, 7841-7844.

(63) Bien, J. T.; Shang, M.; Smith, B. D. Modification of a boronic acid cleft produces a sodium- saccharide cotransportert. *J Org Chem.* **1995**, *60*, 2147-2152.

(64) Morin, G. T.; Hughes, M. P.; Paugam, M.-F.; Smith, B. D. Transport of glycosides through liquid organic membranes mediated by reversible boronate formation Is a diffusion-controlled process. *J Am Chem Soc.* **1994**, *116*, 8895-8901.

(65) Riggs, J. A.; Litchfield, R. K.; Smith, B. D. Molecular recognition and membrane transport with mixed-ligand borates. *J Org Chem.* **1996**, *61*, 1148-1150.

(66) Westmark, P. R.; Smith, B. D. Boronic acids selectively facilitate glucose transport through a lipid bilayer. *J Am Chem Soc.* **1994**, *116*, 9343-9344.

(67) Westmark, P. R.; Smith, B. D. Boronic acids facilitate the transport of ribonucleosides through lipid bilayers. *J Pharm Sci.* **1995**, *85*, 266-269.

(68) Westmark, P. R.; Gardiner, S. J.; Smith, B. D. Selective monosaccharide transport through lipid bilayers using boronic acid carriers. *J Am Chem Soc.* **1996**, *118*, 11093-11100.

(69) Jia, H. Z.; Zhu, J. Y.; Wang, X. L.; Cheng, H.; Chen, G.; Zhao, Y. F.; Zeng, X.; Feng, J.; Zhang, X. Z.; Zhuo, R. X. A boronate-linked linear-hyperbranched polymeric nanovehicle for pH-dependent tumor-targeted drug delivery. *Biomaterials* **2014**, *35*, 5240-5249.

(70) Li, Y.; Xiao, W.; Xiao, K.; Berti, L.; Luo, J.; Tseng, H. P.; Fung, G.; Lam, K. S. Well-defined, reversible boronate crosslinked nanocarriers for targeted drug delivery in response to acidic pH values and cis-diols. *Angew Chem Int Ed.* **2012**, *51*, 2864-2869.

(71) Murthy, N.; Campbell, J.; Fausto, N.; Hoffman, A. S.; Stayton, P. S. Bioinspired pH-responsive polymers for the intracellular delivery of biomolecular drugs. *Bioconjug Chem.* **2003**, *13*, 412-419.

(72) Cal, P. M.; Frade, R. F.; Cordeiro, C.; Gois, P. M. Reversible lysine modification on proteins by using functionalized boronic acids. *Chem Eur J.* **2015**, *21*, 8182-8187.

(73) Zhao, Y.; B. G. Trewyn; I. I. Slowing; Lin, V. S.-Y. Mesoporous silica nanoparticle-based double drug delivery system for glucose-responsive controlled release of insulin and cyclic AMP. *J Am Chem Soc.* **2009**, *131*, 8398-8400.

(74) Roy, D.; Sumerlin, B. S. Glucose-sensitivity of boronic acid block copolymers at physiological pH. *ACS Macro Letters.* **2012**, *1*, 529-532.

(75) Sinha, A.; Chakraborty, A.; Jana, N. R. Dextran-gated, multifunctional mesoporous nanoparticle for glucose-responsive and targeted drug delivery. *ACS Appl Mater Interfaces.* **2014**, *6*, 22183-22191.

(76) Wang, M.; Sun, S.; Neufeld, C. I.; Perez-Ramirez, B.; Xu, Q. Reactive oxygen species-Responsive protein modification and its intracellular delivery for targeted cancer therapy. *Angew Chem Int Ed.* **2014**, *53*, 4131-4144.

(77) Ng, D. Y.; Arzt, M.; Wu, Y.; Kuan, S. L.; Lamla, M.; Weil, T. Constructing hybrid protein zymogens through protective dendritic assembly. *Angew Chem Int Ed Engl.* **2014**, *53*, 324-328.

(78) Zhao, Z.; Yao, X.; Zhang, Z.; Chen, L.; He, C.; Chen, X. Boronic acid shell-crosslinked dextran-*b*-PLA micelles for acid-responsive drug delivery. *Macromol Biosci.* **2014**, *14*, 1609-1618.

(79) Bapat, A. P.; Roy, D.; Ray, J. G.; Savin, D. A.; Sumerlin, B. S. Dynamic-covalent macromolecular stars with boronic ester linkages. *J Am Chem Soc.* **2011**, *133*, 19832-19838.

(80) Chen, W.; Cheng, Y.; Wang, B. Dual-responsive boronate crosslinked micelles for targeted drug delivery. *Angew Chem Int Ed Engl.* **2012**, *51*, 5293-5295.

(81) Wang, J.; Zhang, Z.; Wang, X.; Wu, W.; Jiang, X. Size- and pathotropism-driven targeting and washout-resistant effects of boronic acid-rich protein nanoparticles for liver cancer regression. *J Control Release.* **2013**, *168*, 1-9.

(82) Aguirre-Chagala, Y. E.; Santos, J. L.; Huang, Y.; Herrera-Alonso, M. Phenylboronic acid-installed polycarbonates for the pH-dependent release of diol-containing molecules. *ACS Macro Lett.* **2014**, *3*, 1249-1253.

(83) Yang, B.; Lv, Y.; Zhu, J. Y.; Han, Y. T.; Jia, H. Z.; Chen, W. H.; Feng, J.; Zhang, X. Z.; Zhuo, R. X. A pH-responsive drug nanovehicle constructed by reversible attachment of cholesterol to PEGylated poly(L-lysine) via catechol-boronic acid ester formation. *Acta Biomater.* **2014**, *10*, 3686-3695.

(84) Xu, Y.; Lu, Y.; Wang, L.; Lu, W.; Huang, J.; Muir, B.; Yu, J. Nanomicelles based on a boronate ester-linked diblock copolymer as the carrier of doxorubicin with enhanced cellular uptake. *Colloids Surf B Biointerfaces.* **2016**, *141*, 318-326.

(85) Cal, P. M.; Frade, R. F.; Chudasama, V.; Cordeiro, C.; Caddick, S.; Gois, P. M. Targeting cancer cells with folic acid-iminoboronate fluorescent conjugates. *Chem Comm.* **2014**, *50*, 5261-5263.

(86) Pillay, T. L.; Ariatti, M. Protein bound phenylboronic acid forms boronic acid-DNA complexes. *Med Sci Res.* **1992**, *20*, 285-286.

(87) Boutureira, O.; Bernardes, G. J. Advances in chemical protein modification. *Chem Rev.* **2015**, *115*, 2174-2195.

(88) Baslé, E.; Joubert, N.; Pucheault, M. Protein chemical modification on endogenous amino acids. *Chem Biol.* **2010**, *17*, 213-227.

(89) Bandyopadhyay, A.; Gao, J. Iminoboronate formation leads to fast and reversible conjugation chemistry of α-nucleophiles at neutral pH. *Chem Eur J.* **2015**, *21*, 14748-14752.

(90) Bandyopadhyay, A.; Cambray, S.; Gao, J. Fast and selective labeling of N-terminal cysteines at neutral pH via thiazolidino boronate formation. *Chem Sci.* **2016**, *7*, 4589-4593.

(91) Andersen, K. A.; Smith, T. P.; Lomax, J. E.; Raines, R. T. *ACS Chem Biol.* **2016**, *11*, 319-323.

(92) Biswas, S.; Kinbara, K.; Niwa, T.; Taguchi, H.; Ishii, N.; Watanabe, S.; Miyata, K.; Kataoka, K.; Aida, T. Biomolecular robotics for chemomechanically driven guest delivery fuelled by intracellular ATP. *Nat Chem.* **2013**, *5*, 613-620.

(93) Ellis, G. A.; Palte, M. J.; Raines, R. T. Boronate-mediated biologic delivery. *J Am Chem Soc.* **2012**, *134*, 3631-3634.

(94) Burnett, T. J.; Peebles, H. C.; Hageman, J. H. Synthesis of a flouorecent boronic acid which reversibly binds to cell walls and a diboronic acid which agglutinates erythrocytes. *Biochem Biophys Res Commun.* **1980**, *96*, 157-162.

(95) Vandenburg, Y. R.; Zhang, Z.-Y.; Fishkind, D. J.; Smith, B. D. Enhanced cell binding using liposomes containing an artificial carbohydrate-binding receptor. *Chem Comm.* **2000**, 149-150.

(96) Kashiwada, A.; Tsuboi, M.; Mizuno, T.; Nagasaki, T.; Matsuda, K. Target-selective vesicle fusion system with pH-selectivity and responsiveness. *Soft Matter* **2009**, *5*, 4719-4725.

(97) Kashiwada, A.; Tsuboi, M.; Matsuda, K. Target-selective one-way membrane fusion system based on a pH-responsive coiled coil assembly at the interface of liposomal vesicles. *Langmuir* **2011**, *27*, 1403-1408.

(98) Bérubé, M.; Dowlut, M.; Hall, D. G. Benzoboroxoles as efficient glycopyranoside-binding agents in physiological conditions: Structure and selectivity of complex formation. *J Org Chem.* **2008**, *73*, 6471-6479.

(99) Dowlut, M.; Hall, D. G. An Improved class of sugar-binding boronic acids, soluble and capable of complexing glycosides in neutral water. *J Am Chem Soc.* **2006**, *128*, 4226-4227.

(100) Dai, C.; Sagwal, A.; Cheng, Y.; Peng, H.; Chen, W.; Wang, B. Carbohydrate biomarker recognition using synthetic lectin mimics. *Pure Appl Chem.* **2012**, *84*, 2479-2498.

(101) Yan, J.; Fang, H.; Wang, B. Boronolectins and fluorescent boronolectins: An examination of the detailed chemistry issues important for the design. *Med Res Rev.* **2005**, *25*, 490-520.

(102) Levonis, S. M.; Kiefel, M. J.; Houston, T. A. Boronolectin with divergent fluorescent response specific for free sialic acid. *Chem Commun.* **2009**, 2278-2280.

(103) Chu, Y.; Wang, D.; Wang, K.; Liu, Z. L.; Weston, B.; Wang, B. Fluorescent conjugate of sLe(x)-selective bisboronic acid for imaging application. *Bioorg Med Chem Lett.* **2013**, *23*, 6307-6309.

(104) Burroughs, S.; Wang, B. Boronic acid-based lectin mimics (boronolectins) that can recognize cancer biomarker, the Thomsen–Friedenrich antigen. *ChemBioChem.* **2010**, *11*, 2245-2246.

(105) Pal, A.; Berube, M.; Hall, D. G. Design, synthesis, and screening of a library of peptidyl bis(boroxoles) as oligosaccharide receptors in water: identification of a receptor for the tumor marker TF-antigen disaccharide. *Angew Chem Int Ed.* **2010**, *49*, 1492-1495.

(106) Lippert, A. R.; Van de Bittner, G. C.; Chang, C. J. Boronate oxidation as a bioorthogonal reaction approach for studying the chemistry of hydrogen peroxide in living systems. *Acc Chem Res.* **2011**, *44*, 793-804.

(107) Paulsen, C. E.; Carroll, K. S. Cysteine-mediated redox signaling: Chemistry, biology, and tools for discovery. *Chem Rev.* **2013**, *113*, 4633-4679.

(108) Halliwell, B. Oxidative stress and cancer: have we moved forward? *Biochem J.* **2007**, *401*, 1-11.

(109) Jimenez-Del-Rio, M.; Velez-Pardo, C. The bad, the good, and the ugly about oxidative stress. *Oxid Med Cell Longev.* **2012**, *2012*, 1-13.

(110) Emerit, J.; Edeas, M.; Bricaire, F. Neurodegenerative diseases and oxidative stress. *Biomed Pharmacother.* **2004**, *58*, 39-46.

(111) Valko, M.; Leibfritz, D.; Moncol, J.; Cronin, M. T.; Mazur, M.; Telser, J. Free radicals and antioxidants in normal physiological functions and human disease. *Int J Biochem Cell Biol.* **2007**, *39*, 44-84.

(112) Cornelius, C.; Crupi, R.; Calabrese, V.; Graziano, A.; Milone, P.; Pennisi, G.; Radak, Z.; Calabrese, E. J.; Cuzzocrea, S. Traumatic brain injury: Oxidative stress and neuroprotection. *Antioxid redox signal.* **2013**, *19*, 836-853.

(113) Major Jourden, J. L.; Cohen, S. M. Hydrogen peroxide activated matrix metalloproteinase inhibitors: a prodrug approach. *Angew Chem Int Ed.* **2010**, *49*, 6795-6797.

(114) Jourden, J. L.; Daniel, K. B.; Cohen, S. M. Investigation of self-immolative linkers in the design of hydrogen peroxide activated metalloprotein inhibitors. *Chem Commun* **2011**, *47*, 7968-7970.

(115) Chen, W.; Balakrishnan, K.; Kuang, Y.; Han, Y.; Fu, M.; Gandhi, V.; Peng, X. Reactive oxygen species (ROS) inducible DNA cross-linking agents and their effect on cancer cells and normal lymphocytes. *J Med Chem.* **2014**, *57*, 4498-4510.

(116) Zhong, Q.; Zhang, C.; Zhang, Q.; Miele, L.; Zheng, S.; Wang, G. Boronic prodrug of 4-hydroxytamoxifen is more efficacious than tamoxifen with enhanced bioavailability independent of CYP2D6 status. *BMC Cancer.* **2015**, *15*, 625.

(117) Wang, L.; Xie, S.; Ma, L.; Chen, Y.; Lu, W. 10-Boronic acid substituted camptothecin as prodrug of SN-38. *Eur J Med Chem.* **2016**, *116*, 84-89.

(118) Fu, H.; Fang, H.; Sun, J.; Wang, H.; Liu, A.; Sun, J.; Wu, Z. Boronic acid-based enzyme inhibitors: A review of recent progress. *Curr Med Chem.* **2014**, *21*, 3271-3280.

(119) Teicher, B. A.; Ara, G.; Herbst, R.; Palombella, V. J.; Adams, J. The proteasome inhibitor PS-341 in cancer therapy. *Clin Cancer Res.* **1999**, *5*, 2638-2645.

(120) Adams, J.; Palombella, V. J.; Sausville, E. A.; Johnson, J. A.; Destree, A.; Lazarus, D. D.; Maas, J.; Pien, C. S.; Prakash, S.; Elliott, P. J. Proteasome inhibittors: A novel class of potent and effective antitumor agents. *Cancer Res.* **1999**, *59*, 2615-2622.

(121) Adams, J. The development of proteasome inhibitiors as anticancer drugs. *Cancer Cell.* **2003**, *5*, 417-421.

(122) Ke, W.; Sampson, J. M.; Ori, C.; Prati, F.; Drawz, S. M.; Bethel, C. R.; Bonomo, R. A.; van den Akker, F. Novel insights into the mode of inhibition of class A SHV-1 β-lactamases revealed by boronic acid transition state inhibitors. *Antimicrob Agents Chemother.* **2011**, *55*, 174-183.

(123) Rojas, L. J.; Taracila, M. A.; Papp-Wallace, K. M.; Bethel, C. R.; Caselli, E.; Romagnoli, C.; Winkler, M. L.; Spellberg, B.; Prati, F.; Bonomo, R. A. Boronic acid transition state inhibitors active against KPC and other class A β-Lactamases: Structure-activity relationships as a guide to inhibitor design. *Antimicrob Agents Chemother.* **2016**, *60*, 1751-1759.

(124) Bechara, C.; Sagan, S. Cell-penetrating peptides: 20 Years later, where do we stand? *FEBS Lett.* **2013**, *587*, 1693-1702.

(125) Milletti, F. Cell-penetrating peptides: Classes, origin, and current landscape. *Drug Discov Today.* **2012**, *17*, 850-860.

(126) Fonesca, S. B.; Pereira, M. P.; Kelley, S. O. Recent advances in the use of cell-penetrating peptides for medical and biological applications. *Adv Drug Deliv Rev.* **2009**, *61*, 953-964.

(127) Di Pisa, M.; Chassaing, G.; Swiecicki, J.-M. When cationic cell-penetrating peptides meet hydrocarbons to enhance in-cell cargo delivery. *Peptide Sci.* **2015**, *21*, 356-369.

(128) Sievers, E. L.; Senter, P. D. Antibody–drug conjugates in cancer therapy. *Annu Rev Med.* **2013**, *64*, 15-29.

(129) Srinivasarao, M.; Galliford, C. V.; Low, P. S. Principles in the design of ligand-targeted cancer therapeutics and imaging agents. *Nat Rev Drug Discov.* **2015**, *14*, 203-219.

(130) Gong, Y.; Leroux, J. C.; Gauthier, M. A. Releasable conjugation of polymers to proteins. *Bioconjugate Chem.* **2015**, *26*, 1172-1181.

(131) Chu, D. S. H.; Schellinger, J. G.; Shi, J.; Convertine, A. J.; Stayton, P. S.; Pun, S. H. Application of living free radical polymerization for nucleic acid delivery. *Acc Chem Res.* **2012**, *45*, 1089-1099.

(132) Allen, T. M.; Cullis, P. R. Liposomal drug delivery systems: From concept to clinical applications. *Adv Drug Deliv Rev.* **2013**, *65*, 36-48.

(133) Kumari, P.; Ghosh, B.; Biswas, S. Nanocarriers for cancer-targeted drug delivery. *J Drug Target.* **2015**, *10*, 1-13.

(134) Chou, L. Y. T.; Ming, K.; Chan, W. C. W. Strategies for the intracellular delivery of nanoparticles. *Chem Soc Rev.* **2011**, *40*, 233-245.

(135) Field, L. D.; Delehanty, J. B.; Chen, Y. C.; Medintz, I. L. Peptides for specifically targeting nanoparticles to cellular organelles: Quo vadis? *Acc Chem Res.* **2015**, *48*, 1380-1390.

(136) Rin Jean, S.; Tulumello, D. V.; Wisnovsky, S. P.; Lei, E. K.; Pereira, M. P.; Kelley, S. O. Molecular vehicles for mitochondrial chemical biology and drug delivery. *ACS Chem Biol.* **2014**, *9*, 323-333.

(137) Fuchs, S. M.; Raines, R. T. Polyarginine as a multifunctional fusion tag. *Protein Sci.* **2005**, *14*, 1538-1544.

(138) Fuchs, S. M.; Rutkoski, T. J.; Kung, V. M.; Groeschl, R. T.; Raines, R. T. Increasing the potency of a cytotoxin with an arginine graft. *Protein Eng Design Select.* **2007**, *20*, 505-509.

(139) De Groot, A. S.; Scott, D. W. Immunogenicity of protein therapeutics. *Trends Immunol.* **2007**, *28*, 482-490.

(140) Pisal, D. S.; Kosloski, M. P.; Balu-Iyer, S. V. Delivery of therapeutic proteins. *J Pharm Sci.* **2010**, *99*, 2557-2575.

(141) Bosch, L. I.; Fyles, T. M.; James, T. D. Binary and ternary phenylboronic acid complexes with saccharides and Lewis bases. *Tetrahedron* **2004**, *60*, 11175-11190.

(142) Wang, B.; Nicolaou, M. G.; Liu, S.; Borchard, R. T. Structural analysis of a facile lactonization system facilitated by a “trimethyl lock”. *Bioorg Chem.* **1996**, *5*, 39-49.

(143) Milstien, S.; Cohen, L. A. Concurrent general-acid and general-base catalysis of esterfication. *J Am Chem Soc.* **1970**, *92*, 4377-4382.

(144) Danforth, C.; Nicholson, A. W.; James, J. C.; Loudon, G. M. Steric acceleration of lactonization reactions: An analysis of “stereopopulation control”. *J Am Chem Soc.* **1976**, *98*, 4275-4281.

(145) Nicolaou, M. G.; Wolfe, J. L.; Schowen, R. L.; Borchard, R. T. Facilitated intramolecular conjugate addition of amides of 3-(3″,6″-dioxo-2″,4″-dimethyl-1″,4″-cyclohexadienyl)-

3,3-dimethylpropionic acid. 2. Kinetics of degradation. *J Org Chem.* **1996**, *61*, 6633-6638.

(146) Jung, M. E.; Piizzi, G. *gem*-Disubstituent effect: Theoretical basis and synthetic applications. *Chem Rev.* **2005**, *105*, 1735-1766.

(147) Levine, M. N.; Raines, R. T. Trimethyl lock: A trigger for molecular release in chemistry, biology, and pharmacology. *Chem Sci.* **2012**, *3*, 2412-2420.

(148) Fukami, T.; Yokoi, T. The emerging role of human esterases. *Drug Metab Pharmacokinet.* **2012**, *27*, 466-477.

(149) Liederer, B. M.; Borchardt, R. T. Enzymes involved in the bioconversion of ester-based prodrugs. *J Pharm Sci.* **2006**, *95*, 1177-1195.

(150) Lavis, L. D. Ester bonds in prodrugs. *ACS Chem Biol.* **2008**, *3*, 203-206.

(151) Testa, B.; Mayer, J. M. *Hydrolysis in Drug and Prodrug Metabolism: Chemistry, Biochemistry, and Enzymology*; Verlag Helvetica Chimica Acta: Zürich, Switzerland, 2003.

(152) McCaldon, P.; Argos, P. Oligopeptide biases in protein sequences and their use in predicting protein coding regions in nucleotide sequences. *Proteins.* **1988**, *4*, 99-122.

(153) Greenwald, R. B.; Choe, Y. H.; Conover, C. D.; Shum, K.; Wu, D.; Royzen, M. Drug delivery systems based on trimethyl lock lactonization: Poly(ethylene glycol) prodrugs of amino-containing compounds. *J Med Chem.* **2000**, *43*, 475-487.

(154) Fuchs, S. M.; Raines, R. T. Arginine grafting to endow cell permeability. *ACS Chem Biol.* **2007**, *2*, 167-170.

(155) Turcotte, R. F.; Lavis, L. D.; Raines, R. T. Onconase cytotoxicity relies on the distribution of its positive charge. *FEBS J.* **2009**, *276*, 4270-4281.

(156) Johnson, R. J.; Chao, T.-Y.; Lavis, L. D.; Raines, R. T. Cytotoxic ribonucleases: The dichotomy of Coulombic forces. *Biochemistery* **2007**, *46*, 10308-10316.

(157) Lavis, L. D.; Chao, T.-Y.; Raines, R. T. Fluorogenic label for biomolecular imaging. *ACS Chem Biol.* **2006**, *1*, 252-260.

(158) Leland, P. A.; Schultz, L. W.; Kim, B.-M.; Raines, R. T. Ribonuclease A variants with potent cytotoxic activity. *Proc Natl Acad Sci USA*. **1998**, *95*, 10407-10412.

(159) Lomax, J. E.; Eller, C. H.; Raines, R. T. Rational design and evaluation of mammalian ribonuclease cytotoxins. *Methods Enzymol.* **2012**, *502*, 273-290.

(160) Gilbert, H. F. Molecular and cellular aspects of thiol–disulfide exchange. *Adv Enzymol.***1990**, *63*, 69-172.

(161) Robbins, P. B.; Oliver, S. F.; Sheu, S. M.; Goodnough, J. B.; Wender, P.; Khavari, P. A. Peptide delivery to tissues via reversibly linked protein transduction sequence. *BioTechniques* **2002**, *33*, 190-194.

(162) Mix, K. A.; Raines, R. T. Optimized diazo scaffold for protein esterification. *Org Lett.* **2015**, *17*, 2358-2361.

(163) McGrath, N. A.; Andersen, K. A.; Davis, A. K. F.; Lomax, J. E.; Raines, R. T. Diazo compounds for the bioreversible esterification of proteins. *Chem Sci.* **2015**, *6*, 752-755.

(164) Dixon, H. B. F.; Perham, R. N. Reversible blocking of amino groups with citraconic anhydride. *Biochem J.* **1968**, *109*, 312-314.

(165) Cabantous, S.; Terwilliger, T. C.; Waldo, G. S. Protein tagging and detection with engineered self-assembling fragments of green fluorescent protein. *Nat Biotechnol.* **2005**, *23*, 102-107.

(166) Crameri, A.; Whitehorn, E. A.; Tate, E.; Stemmer, W. P. C. Improved green fluorescent protein by molecular evolution using DNA shuffling. *Nat Biotechnol.* **1996**, *14*, 315-319.

(167) Patterson, G. H.; Knobel, S. M.; Sharif, W. D.; Kain, S. R.; Piston, D. W. Use of the green fluorescent protein and its mutants in quantitative fluorescence microscopy. *Biophys J.* **1997**, *73*, 2782-2790.

(168) Pedelacq, J.-D.; Cabantous, S.; Tran, T.; Terwilliger, T. C.; Waldo, G. S. Engineering and characterization of a superfolder green fluorescent protein. *Nat Biotechnol.* **2006**, *24*, 79-88.

(169) Waldo, G. S.; Standish, B. M.; Berendzen, J.; Terwilliger, T. C. Rapid protein-folding assay using green fluorescent protein. *Nat Biotechnol.* **1999**, *17*, 691-695.

(170) Endo, F.; Komine, O.; Yamanaka, K. Neuroinflamation in motor neuron disease. *Clin Exp Neuroimmunol.* **2016**, *7*, 126-138.

(171) Hayashi, Y.; Homma, K.; Ichijo, H. SOD1 in neurotoxicity and its controversial roles in SOD1 mutation-negative ALS. *Adv Biol Regul.* **2016**, *60*, 95-104.

(172) Bensimon, G.; Lacomblez, L.; Meininger, V. A controlled trial of riluzole in amyotrophic lateral sclerosis. *N Engl J Med.* **1994**, *330*, 585-591.

(173) Lacomblez, L.; Bensimon, G.; Leigh, P. N.; Guillet, P.; Meininger, Z. Dose-ranging study of riluzole in amyotrophic lateral sclerosis. *Lancet* **1996**, *347*, 1425-1431.

(174) Padhi, A. K.; Kumar, H.; Vasaikar, S. V.; Jayaram, B.; Gomes, J. Mechanisms of loss of functions of human angiogenin variants implicated in amyotrophic lateral sclerosis. *PLoS One.* **2012**, *7*, e32479.

(175) Greenway, M. J.; Andersen, P. M.; Russ, C.; Ennis, S.; Cashman, S.; Donaghy, C.; Patterson, V.; Swingler, R.; Kieran, K.; Prehn, J.; Morrison, K. E.; Green, A.; Acharya,

K. R.; Brown, R. H., Jr.; Hardiman, O. ANG mutations segregate with familial and 'sporadic' amyotrophic lateral sclerosis. *Nat Genet.* **2006**, *38*, 411-413.

(176) Kieran, D.; Sebastia, J.; Greenway, M. J.; King, M. A.; Connaughton, D.; Concannon, C. G.; Fenner, B.; Hardiman, O.; Prehn, J. H. Control of motoneuron survival by angiogenin. *J Neurosci.* **2008**, *28*, 14056-14061.

(177) Li, S.; Hu, G.-F. Angiogenin-mediated rRNA transcription in cancer and neurodegeneration. *Int J Biochem Mol Biol.* **2010**, *1*, 26-35.

(178) Li, S.; Hu, G.-F. Emerging role of angiogenin in stress response and cell survival under adverse conditions. *J Cell Physiol.* **2012**, *227*, 2822-2826.

(179) Yoshioka, N.; Wang, L.; Kishimoto, K.; Tsuji, T.; Hu, G.-f. A therapeutic target for prostate cancer based on angiogenin-stimulated angiogenesis and cancer cell proliferation. *Proc Natl Acad Sci USA.* **2006**, *103*, 14519-14524.

(180) Di Matteo, V.; Esposito, E. Biochemical and therapeutic effects of entioxidants in the treatment of Alzheimer's disease, Parkinson's disease, and Amyotrophic Lateral Sclerosis. *CNS Neurol Disord Drug Targets.* **2003**, *2*, 95-107.

(181) Ilieva, H.; Polymenidou, M.; Cleveland, D. W. Non-cell autonomous toxicity in neurodegenerative disorders: ALS and beyond. *J Cell Biol.* **2009**, *187*, 761-772.

(182) Rosen, D. R.; Siddique, T.; Patterson, D.; Figlewicz, D. A.; Sapp, P.; Hentati, A.; Donaldson, D.; Goto, J.; O'Regan, J. P.; Deng, H.-X.; Rahmani, Z.; Krizus, A.; McKenna-Yasek, D.; Cayabyab, A.; Gaston, S. M.; Berger, R.; Tanzi, R. E.; Halperin, J. J.; Herzfeldt, B.; Van den Bergh, R.; Hung, W.-Y.; Bird, T.; Deng, G.; Mulder, D. W.; Smyth, C.; Laing, N. G.; Soriano, E.; Pericak-Vance, M. A.; Rouleau, J. H. G. A.;

Gusella, J. S.; Horvitz, H. R.; Brown, R. H., Jr. Mutations in Cu/Zn superoxide dismutase gene are associated with familial amyotrophic lateral sclerosis. *Nature* **1993**, *362*, 59-62.

(183) Ainley, A. D.; Challenger, F. CCLXXX.—Studies of the boron–carbon linkage. Part I. The oxidation and nitration of phenylboric acid. *J Chem Soc.* **1930**, 2171-2180.

(184) Peng, X.; Gandhi, V. ROS-activated anticancer prodrugs: A new strategy for tumor-specific damage. *Ther Deliv.* **2012**, *3*, 823-833.

(185) Lin, V. S.; Dickinson, B. C.; Chang, C. J. Boronate-based fluorescent probes: Imaging hydrogen peroxide in living systems. *Methods Enzymol.* **2013**, *526*, 19-43.

(186) Subramanian, V.; Crabtree, B.; Acharya, K. R. Human angiogenin is a neuroprotective factor and amyotrophic lateral sclerosis associated angiogenin variants affect neurite extension/pathfinding and survival of motor neurons. *Hum Mol Genet.* **2008**, *17*, 130-149.

(187) Shapiro, R.; Fox, E. A.; Riordan, J. F. Role of lysines in human angiogenin: Chemical modification and site-directed mutagenesis. *Biochemistry* **1989**, *29*, 1726-1732.

(188) Crabtree, B.; Thiyagarajan, N.; Prior, S. H.; Wilson, P.; Iyer, S.; Ferns, T.; Shapiro, R.; Brew, K.; Subramanian, V.; Acharya, K. R. Characterization of human angiogenin variants implicated in amyotrophic lateral sclerosis. *Biochemistry* **2007**, *46*, 11810-11818.

(189) Gunnoo, S. B.; Madder, A. Chemical protein modification through cysteine. *ChemBioChem.* **2016**, *17*, 529-553.

(190) Valkevich, E. M.; Guenette, R. G.; Sanchez, N. A.; Chen, Y.-c.; Ge, Y.; Strieter, E. R. Forging isopeptide bonds using thiol-ene chemistry: Site-specific coupling of ubiquitin

molecules for studying the activity of isopeptidases. *J Am Chem Soc.* **2012**, *134*, 6916-6919.

(191) Messmore, J. M.; Fuchs, D. N.; Raines, R. T. Ribonuclease A: Revealing structure–function relationships with semisynthesis. *J Am Chem Soc.* **1995**, *117*, 8057-8060.

(192) Leland, P. A.; Staniszewski, K. E.; Park, C.; Kelemen, B. R.; Raines, R. T. The ribonucleolytic activity of angiogenin. *Biochemistry* **2002**, *41*, 1343-1350.

(193) Acharya, K. R.; Shapiro, R.; Allen, S. C.; Riordan, J. F.; Vallee, B. L. Crystal structure of human angiogenin reveals the structural basis for its functional divergence from ribonuclease. *Proc Natl Acad Sci USA.* **1994**, *91*, 2915-2919.

(194) Russo, N.; Shapiro, R.; Acharya, K. R.; Riordan, J. F.; Vallee, B. L. Role of glutamine-117 in the ribonucleolytic activity of human angiogenin. *Proc Natl Acad Sci USA.* **1994**, *91*, 2920-2924.

(195) Ridet, J. L.; Malhotra, S. K.; Privat, A.; Gage, F. H. Reactive astrocytes—cellular and molecular cues to biological function. *Trends Neurosci.* **1997**, *20*, 570-577.

(196) Sofroniew, M. V.; Vinters, H. V. Astrocytes: Biology and pathology. *Acta Neuropathol.* **2010**, *119*, 7-35.

(197) Vargas, M. R.; Johnson, D. A.; Sirkis, D. W.; Messing, A.; Johnson, J. A. Nrf2 activation in astrocytes protects against neurodegeneration in mouse models of familial amyotrophic lateral sclerosis. *J Neurosci.* **2008**, *28*, 13574-13581.

(198) Skorupa, A.; King, M. A.; Aparicio, I. M.; Dussmann, H.; Coughlan, K.; Breen, B.; Kieran, D.; Concannon, C. G.; Marin, P.; Prehn, J. H. Motoneurons secrete angiogenin to induce RNA cleavage in astroglia. *J Neurosci.* **2012**, *32*, 5024-5038.

(199) Skorupa, A.; Urbach, S.; Vigy, O.; King, M. A.; Chaumont-Dubel, S.; Prehn, J. H.; Marin, P. Angiogenin induces modifications in the astrocyte secretome: relevance to amyotrophic lateral sclerosis. *J Proteomics.* **2013**, *91*, 274-285.

(200) Abramov, A. Y.; Jacobson, J.; Wientjes, F.; Hothersall, J.; Canevari, L.; Duchen, M. R. Expression and modulation of an NADPH oxidase in mammalian astrocytes. *J Neurosci.* **2005**, *25*, 9176-9184.

(201) Dobson, C. M. Protein folding and misfolding. *Science* **2003**, *426*, 884-890.

(202) Chiti, F.; Dobson, C. M. Protein misfolding, functional amyloid, and human disease. *Annu Rev Biochem.* **2006**, *75*, 333-366.

(203) Knowles, T. P.; Vendruscolo, M.; Dobson, C. M. The amyloid state and its association with protein misfolding diseases. *Nat Rev Mol Cell Biol.* **2014**, *15*, 384-396.

(204) Richardson, S. J. Cell and molecular biology of transthyretin and thyroid hormones. *Int Rev Cytol.* **2007**, *258*, 137-193.

(205) Klabunde, T.; Petrassi, H. M.; Oza, V. B.; Raman, P.; Kelly, J. W.; Sacchettini, J. C. Rational design of potent human transthyretin amyloid disease inhibitors. *Nat Struct Biol.* **2000**, *7*, 312-321.

(206) Hamilton, J. A.; Benson, M. D. *Cell Mol Life Sci.* **2001**, *58*, 1491-1521.

(207) Hund, E. Familial amyloidotic polyneuropathy: current and emerging treatment options for transthyretin-mediated amyloidosis. *Appl Clin Genet.* **2012**, *5*, 37-41.

(208) Yang, D. T.; Joshi, G.; Cho, P. Y.; Johnson, J. A.; Murphy, R. M. Transthyretin as both a sensor and a scavenger of β-amyloid oligomers. *Biochemistry* **2013**, *52*, 2849-2861.

(209) Li, X.; Zhang, X.; Ladiwala, A. R. A.; Du, D.; Yadav, J. K.; Tessier, P. M.; Wright, P. E.; Kelly, J. W.; Buxbaum, J. N. Mechanisms of transthyretin inhibition of β-amyloid aggregation *in vitro*. *J Neurosci.* **2013**, *33*, 19423-19433.

(210) Stein, T. D.; Anders, N. J.; DeCarli, C.; Chan, S. L.; Mattson, M. P.; Johnson, J. A. *J Neurosci.* **2004**, *24*, 7707-7717.

(211) Miller, D. W.; Dill, K. A. Ligand binding to proteins: The binding landscape model. *Protein Sci.* **1997**, *6*, 2166-2179.

(212) Celej, M. S. Protein stability induced by ligand binding correlates with changes in protein flexibility. *Protein Sci.* **2003**, *12*, 1496-1506.

(213) O'Sullivan, C.; Tompson, F. W. LX.—Invertase: A contribution to the history of an enzyme or unorganised ferment. *J Chem Soc.* **1890**, *57*, 834-931.

(214) Obici, L.; Merlini, G. An overview of drugs currently under investigation for the treatment of transthyretin-related hereditary amyloidosis. *Expert Opin Investig Drugs.* **2014**, *23*, 1239-1251.

(215) Nencetti, S.; Orlandini, E. TTR Fibril Formation Inhibition: Is there a SAR. *Curr Med Chem.* **2012**, *19*, 2356-2379.

(216) Johnson, S. M.; Wiseman, R. L.; Sekijima, Y.; Green, N. S.; Adamski-Werner, S. L.; Kelly, J. W. Native state kinetic stabilization as a strategy to ameliorate protein misfolding diseases: A focus on the transthyretin amyloidoses. *Acc Chem Res.* **2005**, *38*, 911-921.

(217) Adamski-Werner, S. L.; Palaninathan, S. K.; Sacchettini, J. C.; Kelly, J. W. Diflunisal analogs stabilize the native state of transthyretin. Potent inhibition of amyloidogenesis. *J Med Chem.* **2004**, *47*, 355-374.

(218) Castano, A.; Helmke, S.; Alvarez, J.; Delisle, S.; Maurer, M. S. Diflunisal for ATTR cardiac amyloidosis. *Congest Heart Fail.* **2012**, *18*, 315-319.

(219) Scott, L. J. Tafamidis: A Review of Its Use in Familial Amyloid Polyneuropathy. *Drugs* **2014**, *74*, 1371-1378.

(220) Bulawa, C. E.; Connelly, S.; Devit, M.; Wang, L.; Weigel, C.; Fleming, J. A.; Packman, J.; Powers, E. T.; Wiseman, R. L.; Foss, T. R.; Wilson, I. A.; Kelly, J. W.; Labaudiniere, R. Tafamidis, a potent and selective transthyretin kinetic stabilizer that inhibits the amyloid cascade. *Proc Natl Acad Sci USA.* **2012**, *109*, 9629-9634.

(221) Sekijima, Y. Recent progress in the understanding and treatment of transthyretin amyloidosis. *J Clin Pharm Ther.* **2014**, *39*, 225-233.

(222) Johnson, D. S.; Weerapana, E.; Cravatt, B. F. Stategies for discovering and derisking covalent, irreversible ezyme inhibitors. *Future Med Chem.* **2010**, *2*, 949-964.

(223) Baillie, T. A. Targeted covalent inhibitors for drug design. *Angew Chem, Int Ed.* **2016**, *55*, 2-17.

(224) Johnson, S. M.; Connelly, S.; Fearns, C.; Powers, E. T.; Kelly, J. W. The transthyretin amyloidoses: from delineating the molecular mechanism of aggregation linked to pathology to a regulatory-agency-approved drug. *J Mol Biol.* **2012**, *421*, 185-203.

(225) Choi, S.; Connelly, S.; Reixach, N.; Wilson, I. A.; Kelly, J. W. Chemoselective small molecules that covalently modify one lysine in a non-enzyme protein in plasma. *Nat Chem Biol.* **2010**, *6*, 133-139.

(226) Choi, S.; Ton Ong, D. S.; Kelly, J. W. A stilbene that binds selectively to transthyretin in cells and remains dark until it undergoes a chemoselective reaction to create a bright blue fluorescent conjugate. *J Am Chem Soc.* **2010**, *132*, 16043-16051.

(227) Suh, E. H.; Liu, Y.; Connelly, S.; Genereux, J. C.; Wilson, I. A.; Kelly, J. W. Stilbene vinyl sulfonamides as fluorogenic sensors of and traceless covalent kinetic stabilizers of transthyretin that prevent amyloidogenesis. *J Am Chem Soc.* **2013**, *135*, 17869-17880.

(228) Grimster, N. P.; Connelly, S.; Baranczak, A.; Dong, J.; Krasnova, L. B.; Sharpless, K. B.; Powers, E. T.; Wilson, I. A.; Kelly, J. W. Aromatic sulfonyl fluorides covalently kinetically stabilize transthyretin to prevent amyloidogenesis while affording a fluorescent conjugate. *J Am Chem Soc.* **2013**, *135*, 5656-5668.

(229) Baranczak, A.; Liu, Y.; Connelly, S.; Han Du, W.-G.; Greiner, E. R.; Genereux, J. C.; Wiseman, R. L.; Eisele, Y. S.; Bradbury, N. C.; Dong, J.; Noodleman, L.; Sharpless, K. B.; Wilson, I. A.; Encalada, S. E.; Kelly, J. W. A fluorogenic aryl fluorosulfate for intraorganellar transthyretin imaging in living cells and in *Caenorhabditis elegans*. *J Am Chem Soc.* **2015**, *137*, 7404-7414.

(230) Antonov, V. K.; Ivanina, T. V.; Berezin, I. V.; Martinek, K. *FEBS Lett.* **1970**, *7*, 23-25.

(231) Kettner, C.; Shenvi, A. *J Biol Chem.* **1984**, *259*, 15106-15114.

(232) Koehler, K. A.; Lienhard, G. E. *Biochemistry* **1971**, *10*, 2477-2483.

(233) Wang, B.; Chen, L.; Sun, Y.; Zhu, Y.; Sun, Z.; An, T.; Li, Y.; Lin, Y.; Fan, D.; Wang, Q. Development of phenylboronic acid-functionalized nanoparticles for emodin delivery. *J Mater Chem B.* **2015**, *3*, 3840-3847.

(234) Wu, X.; Li, Z.; Chen, X. X.; Fossey, J. S.; James, T. D.; Jiang, Y. B. Selective sensing of saccharides using simple boronic acids and their aggregates. *Chem Soc Rev.* **2013**, *42*, 8032-8048.

(235) Hoang, T. T.; Smith, T. P.; Raines, R. T. Angiogenin–boronic acid conjugate with selective neuroprotection activity. *Angew Chem, Int Ed.* **2017**, *56*, In Press.

(236) *Boronic acids: Preparation and applications in organic synthesis, medicine and materials*; Hall, D. G., Ed.; Wiley–VCH Verlag: Weinheim, Germany, 2011.

(237) Services, U. S. D. o. H. a. H. *Toxicology Profile for Boron*; Agency for Toxic Substances and Disease Registry: Atlanta, GA, 2010.

(238) Baures, P. W.; Peterson, S. A.; Kelly, J. W. Discovering transthyretin amyloid fibril inhibitors by limited screening. *Bioorg Med Chem.* **1998**, *6*, 1389-1401.

(239) Bourgault, S.; Choi, S.; Buxbaum, J. N.; Kelly, J. W.; Price, J. L.; Reixach, N. Mechanisms of transthyretin cardiomyocyte toxicity inhibition by resveratrol analogs. *Biochem Biophys Res Commun.* **2011**, *410*, 707-713.

(240) Johnson, S. M.; Cohen, S. M.; Wilson, I. A.; Kelly, J. W. Toward optimization of the linker substructure common to transthyretin amyloidogenesis inhibitors using biochemical and structural studies. *J Med Chem.* **2008**, *51*, 6348-6358.

(241) Cotrina, E. Y.; Pinto, M.; Bosch, L.; Vila, M.; Blasi, D.; Quintana, J.; Centeno, N. B.; Arsequell, G.; Planas, A.; Valencia, G. Modulation of the fibrillogenesis inhibition properties of two transthyretin ligands by halogenation. *J Med Chem.* **2013**, *56*, 9110-9121.

(242) Palaninathan, S. K. Nearly 200 X-Ray crystal structures of transthyretin- What do they tell us about this protein and the design of drugs for TTR amyloidoses? *Curr Med Chem.* **2012**, *19*, 2324-2342.

(243) Oza, V. B.; Smith, C.; Raman, P.; Koepf, E. K.; Lashuel, H. A.; Petrassi, H. M.; Chiang, K. P.; Powers, E. T.; Sacchettini, J. C.; Kelly, J. W. Synthesis, structure, and activity of diclofenac analogues as transthyretin amyloid fibril formation inhibitors. *J Med Chem.* **2002**, *45*, 321-332.

(244) Palaninathan, S. K.; Mohamedmohaideen, N. N.; Orlandini, E.; Ortore, G.; Nencetti, S.; Lapucci, A.; Rossello, A.; Freundlich, J. S.; Sacchettini, J. C. Novel transthyretin amyloid fibril formation inhibitors: synthesis, biological evaluation, and X-ray structural analysis. *PLoS ONE.* **2009**, *4*, e6290.

(245) Neumann, P.; Cody, V.; Wojtczak, A. Ligand binding at the transthyretin dimer–dimer interface- structure of the transthyretin–T4Ac complex at 2.2 A˚ resolution. *Acta Cryst.* **2005**, *D61*, 1313-1319.

(246) Muzio, T.; Cody, V.; Luft, J. R.; Pangborn, W.; Wojtczak, A. Complex of rat transthyretin with tetraiodothyroacetic acid refined at 2.1 and 1.8 Å resolution. *Acta Biochim Polonica.* **2001**, *48*, 877-884.

(247) Johnson, S. M.; Cohen, S. M.; Wilson, I. A.; Kelly, J. W. Toward optimization of the linker substructure common to transthyretin amyloidogenesis inhibitors using biochemical and structural studies. *J Med Chem.* **2008**, *51*, 6348-6358.

(248) www.chemspider.com, Society of Chemistry, London, UK; accessed December 7, 2016.

(249) Groll, M.; Berkers, C. R.; Ploegh, H. L.; Ovaa, H. Crystal structure of the boronic acid-based proteasome inhibitor bortezomib in complex with the yeast 20S proteasome. *Structure* **2006**, *14*, 451-456.

(250) Bone, R.; Frank, D.; Kettner, C. A.; Agard, D. A. Structural analysis of specificity: alpha-lytic protease complexes with analogues of reaction intermediates. *Biochemistry* **1989**, *28*, 7600-7609.

(251) Kawasaki, Y.; Chufan, E. E.; Lafont, V.; Hidaka, K.; Kiso, Y.; Mario Amzel, L.; Freire, E. How much binding affinity can be gained by filling a cavity? *Chem Biol Drug Des.* **2010**, *75*, 143-151.

(252) Eriksson, A. E.; Baase, W. A.; Zhang, X.-J.; Heinz, D. W.; Blaber, M.; Baldwin, E. P.; Matthews, B. W. *Science* **1992**, *255*, 178-183.

(253) Voth, A. R.; Khuu, P.; Oishi, K.; Ho, P. S. Halogen bonds as orthogonal molecular interactions to hydrogen bonds. *Nat Chem.* **2009**, *1*, 74-79.

(254) Riley, K. E.; Merz, K. M., Jr. Insights into the strength and origin of halogen bonding: the halobenzene-formaldehyde dimer. *J Phys Chem A.* **2007**, *111*, 1688-1694.

(255) Zhu, C.; Wang, R.; Falck, J. R. Mild and rapid hydroxylation of aryl/heteroaryl boronic acids and boronate esters with N-oxides. *Org Lett.* **2012**, *14*, 3494-3497.

(256) Windsor, I. W.; Raines, R. T. Fluorogenic assay for inhibitors of HIV-1 protease with sub-picomolar affinity. *Sci Rep.* **2015**, *5*, 11286.

(257) McCutchen, S. L.; Colon, W.; Kelly, J. W. Transthyretin mutation Leu-55-Pro significantly alters tetramer stability and increases amyloidogenicity. *Biochemistry.* **1993**, *32*, 12119-12127.

(258) Grimm, F. A.; Lehmler, H. J.; He, X.; Robertson, L. W.; Duffel, M. W. Sulfated metabolites of polychlorinated biphenyls are high-affinity ligands for the thyroid hormone transport protein transthyretin. *Environ Health Perspect.* **2013**, *121*, 657-662.

(259) Giraldo, J.; Vivas, N. M.; Vila, E.; Badia, A. Assessing the (a)symmetry of concentration-effect curves: empirical versus mechanistic models. *Pharmacol Ther.* **2002**, *95*, 21-45.

(260) Miroy, G. J.; Lai, Z.; Lashuel, H. A.; Peterson, S. A.; Strang, C.; Kelly, J. W. Inhibiting transthyretin amyloid fibril formation via protein stabilization. *Proc Natl Acad Sci USA.* **1996**, *93*, 15051-15056.

(261) Otwinowski, Z.; Minor, W. Processing of X-ray diffraction data collected in oscillation mode. *Methods Enzymol.* **1997**, *276*, 307-326.

(262) Adams, P. D.; Afonine, P. V.; Bunkoczi, G.; Chen, V. B.; Davis, I. W.; Echols, N.; Headd, J. J.; Hung, L. W.; Kapral, G. J.; Grosse-Kunstleve, R. W.; McCoy, A. J.; Moriarty, N. W.; Oeffner, R.; Read, R. J.; Richardson, D. C.; Richardson, J. S.; Terwilliger, T. C.; Zwart, P. H. PHENIX: a comprehensive Python-based system for macromolecular structure solution. *Acta Crystallogr D, Biol Crystallogr.* **2010**, *66*, 213-221.

(263) Emsley, P.; Lohkamp, B.; Scott, W. G.; Cowtan, K. Features and development of Coot. *Acta Crystallogr D, Biol Crystallogr.* **2010**, *66*, 486-501.

(264) Blum, A. P.; Kammeyer, J. K.; Rush, A. M.; Callmann, C. E.; Hahn, M. E.; Gianneschi, N. C. Stimuli-responsive nanomaterials for biomedical applications. *J Am Chem Soc.* **2015**, *137*, 2140-2154.

(265) Wong, P. T.; Choi, S. K. Mechanisms of drug release in nanotherapeutic delivery systems. *Chem Rev.* **2015**, *115*, 3388-3432.

(266) Maier, K.; Wagner, E. Acid-labile traceless click linker for protein transduction. *J Am Chem Soc.* **2012**, *134*, 10169-10173.

(267) Meyer, M.; Philipp, A.; Oskuee, R.; Schmidt, C.; Wagner, E. Breathing life into polycations- functionalization with pH-responsive endosomolytic peptides and polyethylene glycol enables siRNA delivery. *J Am Chem Soc.* **2008**, *130*, 3272-3273.

(268) Sorensen, A. L.; Clausen, H.; Wandall, H. H. Carbohydrate clearance receptors in transfusion medicine. *Biochim Biophys Acta.* **2012**, *1820*, 1797-1808.

(269) Nencetti, S.; Orlandini, E. TTR fibril formation inhibition: Is there a SAR? *Curr Med Chem.* **2012**, *19*, 2356-2379.

(270) Johnson, S. M.; Connelly, S.; Wilson, I. A.; Kelly, J. W. Biochemical and structural evaluation of highly selective 2-Arylbenzoxazole-based transthyretin amyloidogenesis inhibitors. *J Med Chem.* **2008**, *51*, 260-270.

(271) Zervosen, A.; Herman, R.; Kerff, F.; Herman, A.; Bouillez, A.; Prati, F.; Pratt, R. F.; Frere, J. M.; Joris, B.; Luxen, A.; Charlier, P.; Sauvage, E. Unexpected tricovalent binding mode of boronic acids within the active site of a penicillin-binding protein. *J Am Chem Soc.* **2011**, *133*, 10839-10848.

(272) Lei, J.; Hansen, G.; Nitsche, C.; Klein, C. D.; Zhang, L.; Hilgenfeld, R. Crystal structure of Zika virus NS2B-NS3 protease in complex with a boronate inhibitor. *Science* **2016**, *353*, 503-505.

(273) Rhee, S. G.; Chang, T.-S.; Bae, Y. S.; Lee, S.-R.; Kang, S. W. Cellular regulation by hydrogen peroxide. *J Am Soc Nephrol.* **2003**, *14*, 211-215.

(274) Miller, E. W.; Tulyathan, O.; Isacoff, E. Y.; Chang, C. J. Molecular imaging of hydrogen peroxide produced for cell signaling. *Nat Chem Biol.* **2007**, *3*, 263-267.

(275) Bae, Y. S.; Kang, S. W.; Seo, M. S.; Baines, I. C.; Tekle, E.; Chock, P. B.; Rhee, S. G. Epidermal growth factor (EGF)-induced generation of hydrogen peroxide. *J Biol Chem.* **1997**, *272*, 217-221.

(276) Schieber, M.; Chandel, N. S. ROS function in redox signaling and oxidative stress. *Curr Biol.* **2014**, *24*, R453-462.

(277) Aykin-Burns, N.; Ahmad, I. M.; Zhu, Y.; Oberley, L. W.; Spitz, D. R. Increased levels of superoxide and H2O2 mediate the differential susceptability of cancer cells versus normal cells to glucose deprivation. *Biochem J.* **2009**, *418*, 29-37.

(278) Prousek, J. Fenton chemistry in biology and medicine. *Pure Appl Chem.* **2007**, *79*, 2325-2338.

(279) Winterbourn, C. C. Toxicity of iron and hydrogen peroxide: The Fenton reaction. *Toxicology Letters* **1995**, *82*, 969-974.

(280) Figueiredo, M. S.; Baffa, O.; Neto, J. B.; Zago, M. A. Liver injury and generation of hydroxyl free radicals in experimental secondary hemochromatosis. *Res Exp Med.* **1993**, *193*, 27-37.

(281) Gaetke, L. Copper toxicity, oxidative stress, and antioxidant nutrients. *Toxicology* **2003**, *189*, 147-163.

(282) Okoh, S.; Asekun, O.; Familoni, O.; Afolayan, A. Antioxidant and free radical scavenging capacity of seed and shell essential oils extracted from *Abrus precatorius* (L). *Antioxidants.* **2014**, *3*, 278-287.

(283) Iqbal, T.; Hussain, A. I.; Chatha, S. A.; Naqvi, S. A.; Bokhari, T. H. Antioxidant activity and volatile and phenolic profiles of essential oil and different extracts of wild mint (*Mentha longifolia*) from the Pakistani flora. *J Anal Methods Chem.* **2013**, *2013*, 1-6.

(284) Foti, M. C.; Amorati, R. Non-phenolic radical-trapping antioxidants. *J Pharm Pharmacol.* **2009**, *61*, 1435-1448.

(285) Yallapu, M. M.; Nagesh, P. K.; Jaggi, M.; Chauhan, S. C. Therapeutic applications of curcumin nanoformulations. *AAPS J.* **2015**, *17*, 1341-1356.

(286) Tukey, R. H.; Strassburg, C. P. Genetic multiplicity of the human UDP-glucuronosyltransferases and regulation in the gastrointestinal tract. *Mol Pharmacol.* **2001**, *50*, 405-414.

(287) Xu, C.; Li, C. Y.-T.; Kong, A.-N. Induction of Phase I, II, and III drug metabolism/transport by xenobiotics. *Arch Pharm Res.* **2005**, *28*, 249-268.

(288) Guengerich, F. P. Cytochrome P450s and other enzymes in drug metabolism and toxicity. *AAPS J.* **2006**, *8*, E101-E111.

(289) Greenberg, E. R.; Baron, J. A.; Tosteson, T. D.; Freeman, D. H.; Beck, G. J.; Bond, J. H.; Colacchio, T. A.; Coller, J. A.; Frankl, H. D.; Haile, R. W.; Mandel, J. S.; Nierenberg, D. W.; Rothstein, R.; Snover, D. C.; Stevens, M. M.; Summer, R. W.; van Stolk, R. U. A clinical trail of antioxidant vitamins to prevent colorectal adenoma. *N Engl J Med.* **1994**, *331*, 141-147.

(290) Vivekananthan, D. P.; Penn, M. S.; Sapp, S. K.; Hsu, A.; Topol, E. J. Use of antioxidant vitamins for the prevention of cardiovascular disease: meta-analysis of randomised trials. *The Lancet* **2003**, *361*, 2017-2023.

(291) Steinhubl, S. R. Why have antioxidants failed in clinical trials? *Am J Cardiol.* **2008**, *101*, 14D-19D.

(292) Khdour, O. M.; Lu, J.; Hecht, S. M. An acetate prodrug of a pyridinol-based vitamin E analogue. *Pharm Res.* **2011**, *28*, 2896-2909.

(293) Lozada, J.; Liu, Z.; Perrin, D. M. Base-promoted protodeboronation of 2,6-disubstituted arylboronic acids. *J Org Chem.* **2014**, *79*, 5365-5368.

(294) Solovieva, M. E.; Solovyev, V. V.; Kudryavtsev, A. A.; Trizna, Y. A.; Akatov, V. S. Vitamin B12b enhances the cytotoxicity of dithiothreitol. *Free Radic Biol Med.* **2008**, *44*, 1846-1856.

(295) Rota, C.; Tomasi, A.; Iannone, A. Alpha-tocopherol amplifies benzoyl peroxide free radical decomposition in a chemical system. *Free Radic Res.* **2006**, *40*, 637-645.

(296) Gibson, C. R.; Staubus, A. E.; Barth, R. F.; Yang, W.; Kleinholz, N. M.; Jones, R. B.; Green-Church, K.; Tjarks, W.; Soloway, A. H. Boron neutron capture therapy of brain tumors: Investigation of urinary metabolites and oxidation products of sodium borocaptate by electronspray ionization mass spectrometry. *Drug Metab Dispos.* **2001**, *29*, 1588-1598.

(297) Labutti, J.; Parsons, I.; Huang, R.; Miwa, G.; Gan, L.-S.; Daniels, J. S. Oxidative deboronation of the peptide boronic acid proteasome inhibitor bortezomib: Contributions from reactive oxygen species in this novel Cytochrome P450 reaction. *Chem Res Toxicol.* **2006**, *19*, 539-546.

(298) Li, A. C.; Yu, E.; Ring, S. C.; Chovan, J. P. Boronic acid-containing proteasome inhibitors: alert to potential pharmaceutical bioactivation. *Chem Res Toxicol.* **2013**, *26*, 608-615.

(299) Pekol, T.; Daniels, J. S.; Labutti, J.; Parsons, I.; Nix, D.; Baronas, E.; Hsieh, F.; Gan, L. S.; Miwa, G. Human metabolism of the proteasome inhibitor bortezomib: identification of circulating metabolites. *Drug Metab Dispos.* **2005**, *33*, 771-777.

(300) Charkoudian, L. K.; Pham, D. M.; Frade, R. F. A pro-chelator triggered by hydrogen peroxide inhibits iron-promoted hydroxyl radical formation. *J Amer Chem Soc.* **2006**, *128*, 12424-12425.

(301) Charkoudian, L. K.; Pham, D. M.; Kwon, A. M.; Vangeloff, A. D.; Franz, K. J. Modifications of boronic ester pro-chelators triggered by hydrogen peroxide tune reactivity to inhibit metal-promoted oxidative stress. *Dalton Trans.* **2007**, 5031-5042.